



THE HONG KONG
POLYTECHNIC UNIVERSITY

香港理工大學

Pao Yue-kong Library

包玉剛圖書館

Copyright Undertaking

This thesis is protected by copyright, with all rights reserved.

By reading and using the thesis, the reader understands and agrees to the following terms:

1. The reader will abide by the rules and legal ordinances governing copyright regarding the use of the thesis.
2. The reader will use the thesis for the purpose of research or private study only and not for distribution or further reproduction or any other purpose.
3. The reader agrees to indemnify and hold the University harmless from and against any loss, damage, cost, liability or expenses arising from copyright infringement or unauthorized usage.

IMPORTANT

If you have reasons to believe that any materials in this thesis are deemed not suitable to be distributed in this form, or a copyright owner having difficulty with the material being included in our database, please contact lbsys@polyu.edu.hk providing details. The Library will look into your claim and consider taking remedial action upon receipt of the written requests.

**STUDY ON HEAT TRANSFER SURROUNDING
PILE FOUNDATION GROUND HEAT EXCHANGERS
WITH GROUNDWATER ADVECTION**

ZHANG WENKE

Ph.D

The Hong Kong Polytechnic University

2015

The Hong Kong Polytechnic University
Department of Building Services Engineering

**Study on Heat Transfer Surrounding Pile
Foundation Ground Heat Exchangers with
Groundwater Advection**

Zhang Wenke

A thesis submitted in partial fulfillment of the requirements for
the Degree of Doctor of Philosophy

January, 2015

CERTIFICATE OF ORIGINALITY

I hereby declare that this thesis is my own work and that, to the best of my knowledge and belief, it reproduces no material previously published or written, nor material that has been accepted for the award of any other degree or diploma, except where due acknowledgement has been made in the text.

_____ (Signed)

Zhang Wenke (Name of student)

Department of Building Services Engineering

The Hong Kong Polytechnic University

Hong Kong, China

January, 2015

ABSTRACT

Abstract of thesis entitled: Study on Heat Transfer Surrounding Pile Foundation

Ground Heat Exchangers with Groundwater Advection

Submitted by: Zhang Wenke

For the degree of: Doctor of Philosophy

At The Hong Kong Polytechnic University in January, 2015.

Currently, the ground-coupled heat pump (GCHP) technology has gained more and more attentions due to its outstanding high performance characteristics in energy saving, environmental protection and associated benefits. The development of investigations have led to a new type of ground heat exchanger (GHE) entitled “energy pile”. In brief, it is proposed for spiral heat exchange tubs to be enclosed in the pile foundation of buildings, thus integrating the bearing structure of buildings with a heat transfer component. A certain proportion of the heating load or cooling load can be met in this way; thereby reducing the initial cost of the whole cooling and heating system.

A range of research studies have been conducted on the pure conduction of pile foundation GHE, however, little references or documentation exists in the literature concerning the influence exerted by groundwater flow. It should be recognized that varying degrees of groundwater seepage phenomena exist below ground. As the depth of

the pile is usually more than ten meters or even many more meters, the underground hydraulic gradient inevitably leads to the groundwater flow. Accordingly the heat transfer involving conduction and groundwater advection should be taken into account when considering the role of seepage. The study presented in this thesis includes corresponding studies on simulation models for an energy pile with groundwater advection, and each type of model consists of both infinite and finite length sources. Heat transfer experiments were then conducted to indirectly verify the seepage models. In addition, a reasonable methodology to obtain the groundwater velocity is also proposed.

The models were investigated and then further developed to be more advanced from some classical models such as line and hollow cylindrical heat sources. Firstly, a new model, referred to as the “solid” cylindrical source model, is initially proposed. In this model, the pile diameter is much thicker and the depth is usually shorter than in the case of the borehole, and the spiral coils are disposed in the vicinity of the pile circumference. The cylinder is filled with medium identical to that out of it; thus, the interior heat capacity of the pile cannot be ignored. Analytical solutions for the solid cylindrical models while groundwater flows through it were obtained.

Secondly, the ring-coil model is put forward to represent the configuration of spiral coils set inside the pile by a more appropriate method. The solid cylindrical model only regards the pile foundation GHE as a uniform surface heat source and thus the coil intervals are not considered. Compared to the solid cylindrical model, the ring-coil model is relatively advanced because it takes into consideration the discontinuity of the heat source along the depth. This heat source is deemed as a series of separated coils

arranged along the z-direction so that focus is on the impacts of the coil pitch. If groundwater goes through the energy pile with spiral coils, the temperature response induced by conduction and groundwater advection at any point except the heat source can be achieved.

Thirdly, focus is on comparing the solid cylindrical and ring-coil models with an improved model. An attempt is made to reduce the deficiencies of the former two by introducing a spiral line, hence proposing the spiral heat source model. The improvement is the fact that a spiral line replaces the separated coils and thus a succession of connected coils with a certain diameter are distributed down the depth of pile. Accordingly, not only the coil pitch but also the helix angles are dealt with. Thereby, the spiral heat source seepage model efficiently shows the thermal transfusions with greater accuracy and precision at the time of the combined contributions of both conduction and groundwater advection.

However and regrettably the on-site heat exchange experiments of energy pile have not yet been conducted to validate the theoretical models. Next, the significant experiments based on the actual engineering projects were conducted to check the heat transfer ability and verify the conduction model of the pile foundation GHE. The experiments conducted in this study focused on the pure conduction of energy piles, and two groups of trials were conducted and the heat transfer superiority of the energy pile is shown by comparing pile foundation GHE with borehole GHE. The pure conduction model can then be validated by the experimental results. The combined heat transfer models including pure conduction and groundwater advection are indirectly proven because it derives from the pure conduction case. Thus, the combined model could be

certificated indirectly in the event of the pure conduction model being confirmed.

Lastly, the groundwater velocity is a vital parameter embodying the influence degrees of seepage, the comprehension of both value and orientation of velocity is becomingly increasingly important. To avoid the huge difficulties of directly measuring the velocity by means of the test equipments, a significant methodology named “back calculation” is suggested. The conditional extreme values of the sum of the variance and the corresponding derivatives combined with the theoretical models were put to use when the target functions had been established. By this means, the groundwater velocity can be obtained based on the temperature responses at different points around a borehole GHE.

In summary, all models involving both energy pile and groundwater advection developed and presented in the thesis are introduced one by one on the simple to complex principle. The spiral heat source model is the optimum case from the perspective of academic study as it most approximately simulates the energy pile with groundwater advection. However, other models can still be employed to provide theoretical basis for some situations such as engineering projects and so on, because in these cases the requirements for calculation accuracy are not too high. The application of energy piles can reduce the initial cost of meeting a building’s need for heating and cooling. Groundwater advection does improve the heat transfer performance of energy piles as it enables heat accumulation around the pile to be alleviated, therefore the temperature difference between GHE and the surrounding underground medium is maintained or even increased. Thermal transmission is further promoted and accordingly heat exchange quantity is enlarged. The flow velocity including its value and orientation

can be deduced when the back calculation method is employed. The pure conduction experiments have produced satisfactory effects, and an aim of the future work is the implementation of the heat transfer experiments with groundwater advection to directly validate the groundwater seepage models. Full understanding of groundwater advection is helpful to emphasize not only the significance but also the popularization of energy pile technology.

Keywords: Ground-coupled heat pump; Ground heat exchangers; Pile foundation; Spiral heat exchange tubes; Groundwater flow; advection; Seepage; Heat transfer; Solid cylindrical heat source; Ring-coil heat source; Spiral heat source; Green function; Sum of variance; Derivative; Extreme value; Back calculation; Temperature response; Analytical solution; Virtual heat source method; Infinite length; Finite length; Conduction experiment; Velocity; Value and orientation; Hydraulic gradient; Moving heat source; Dimensionless parameter

PUBLICATIONS ARISING FROM THE THESIS

Journal Papers:

[1] W.K. Zhang, H.X. Yang, L.Lu and Z.H. Fang, Investigation on heat transfer around buried coils of pile foundation heat exchangers for ground-coupled heat pump applications, *International Journal of Heat and Mass Transfer*, 55(2012) 6023-6031.

[2] W.K. Zhang, H.X. Yang, L.Lu and Z.H. Fang, The analysis on solid cylindrical heat source model of foundation pile ground heat exchangers with groundwater flow, *Energy*, 55(2013) 417-425.

[3] W.K. Zhang, H.X. Yang, L.Lu, P. Cui and Z.H. Fang, The research on ring-coil heat transfer models of pile foundation ground heat exchangers in the case of groundwater seepage. *Energy and Buildings*, 71(2014) 115-128.

[4] W.K. Zhang, H.X. Yang, L.L. Sun, N.F. Han and Z.H. Fang, Heat transfer model of ground heat exchangers with groundwater seepage. *Journal of HV&AC*, 42(2012) 129-134.

[5] P. Cui, W.K. Zhang, N.R. Diao and Z.H. Fang, Heat transfer of spiral coils buried in the medium with uniform groundwater advection, *Acta Energiae Solaris Sinica*, 2014 (Accepted).

[6] W.K. Zhang, H.X. Yang, L. Lu, N.R. Diao and Z.H. Fang, Study on spiral source models revealing groundwater transfusion effects on pile foundation ground heat

exchangers, International Journal of Heat and Mass Transfer, 84(2015) 119-129.

[7] W.K. Zhang, H.X. Yang, L.Lu and Z.H. Fang, The Investigation on Thermal Exchange and Influencing Factors for Borehole Ground Heat Exchangers, Applied Thermal Engineering, 84 (2015) 310-319.

[8] W.K. Zhang, Q. Zhao, H.X. Yang, L. Lu. and Z.H. Fang, Analysis on the Heat Exchange Experiments and the Simulation Models of Energy Pile, Geothermics (Revised).

[9] W.K. Zhang, H.X. Yang, N.R. Diao, L. Lu and Z.H. Fang, Exploration on the Reverse Calculation Method of Groundwater Velocity By Means of the Moving Line Heat Source, International Journal of Thermal Science (Revised).

[10] W.K. Zhang, H.X. Yang, N.R. Diao, L. Lu, P. Cui and Z.H. Fang, The Analysis on Groundwater Velocity Based on the Finite Line Heat Source Seepage Model, International Journal of Heat and Mass Transfer (Under review).

[11] D.Q. Wang, L. Lu, W.K. Zhang and P. Cui, Numerical and analytical analysis of groundwater influence on the pile geothermal heat exchanger with cast-in spiral coils. Applied Energy (In Press), 2015.

Conference Papers:

[1] W.K. Zhang, H.X. Yang, Z.H. Fang and N.R. Diao, Analytical Solutions of Combined Heat Transfer on Spiral Tubes in Energy Piles, The 12th International Conference on Sustainable Energy Technologies, 2013, Hong Kong, China.

[2] Z.H. Fang, N.R. Diao, W.K. Zhang and H.X. Yang, Combined conduction and

advection transfer around a buried coil. Proceedings of the 8th International Symposium on Heat Transfer, 2012, Beijing, China.

[3] W.K. Zhang, H.X. Yang, L. Lu and Z.H. Fang, The study on heat transfer case of pile foundation ground heat exchangers. The 12th International Conference on Sustainable Energy Technologies, 2013, Hong Kong, China.

[4] W.K. Zhang, H.X. Yang, L. Lu and Z.H. Fang. The heat transfer analysis and optimal design of borehole ground heat exchangers. The 6th International Conference on Applied Energy, Taiwan, 2014.

ACKNOWLEDGEMENTS

This Thesis is the harvest of my Ph. D research consisting of three-year hard work. During the period of study in The Hong Kong Polytechnic University (PolyU), a number of people have given me unforgettable encouragement and help to overcome difficulties and make progress. It is my honor to avail myself of this opportunity to give thankful expressions to these kind-hearted and responsible people.

First of all, I would like to show my deep gratitude to my supervisor, Professor Yang Hongxing. He sedulously instructs my research work and follows with interest the development of this thesis; not only takes care of study but also pays attention to my living. His constant solicitude and guidance helped me finish my Ph.D project successfully and achieve valuable new knowledge.

My truehearted appreciation is dedicated to Professor Fang Zhaohong as he helped me a lot to solve academic problems in the process of the simulation. In addition, he pointed out directions about new research domain for my project, and he always concerned with my progress.

An unusually sincere gratitude from me is devoted to my Co-supervisor, Dr. Lu Lin, as the outstanding young teachers, she gives a succession of significant advices to help me complete my research work. Thank all the members of the Renewable Energy Research Group (RERG), and I will remember the time when I studied and worked with

them all my life.

My particular appreciation also goes to Professors Adrian Bejan and S. Lorente. They taught me a lot and gave me many valuable instructions on my research when I studied with them in Duke University for a research student attachment programme.

I conveyed earnest thankfulness to my dear parents, Mr. Zhang Xiuliang and Ms. Wang Suqin, as they provided me favorable family environment which is helpful to my growth and advancement. Meanwhile, I would like to thank my wife Ms Liu Xin. She always supports and encourages me.

In conclusion, thousands and thousands of words are amalgamated into a sentence, i.e. I acknowledge all the people who directly or indirectly have provided help to my study and work.

TABLE OF CONTENTS

CERTIFICATE OF ORIGINALITY	I
ABSTRACT	II
ACKNOWLEDGEMENTS	X
TABLE OF CONTENTS	XII
LIST OF FIGURES	XXII
CHAPTER 1 INTRODUCTION	1
1.1 The introduction about GCHP system.....	2
1.2 The conventional GHEs	3
1.3 Pile foundation GHEs.....	5
1.4 The significance of investigating groundwater flow	8
1.5 Aims and objectives of the thesis	9
1.6 Organization of the thesis.....	11
CHAPTER 2 ITERATURE REVIEW	13
2.1 Introduction	13
2.2 Theoretical investigations on pure conduction of pile foundation GHEs	14
2.2.1 Analytical solutions of mathematical models	14

2.2.1.1 Line heat source.....	14
2.2.1.2 Hollow cylindrical heat source.....	17
2.2.1.3 Solid cylindrical heat source	18
2.2.1.4 Ring-coil heat source.....	20
2.2.1.5 Spiral heat source	23
2.2.2 Numerical methods for simulation.....	24
2.2.2.1 Finite difference model	24
2.2.2.1.1 Heat transfer outside pipe.....	25
2.2.2.1.2 Heat transfer inside pipe.....	26
2.2.2.2 Comsol Multiphysics package.....	27
2.2.2.3 Coupled multi-physical finite element modeling.....	28
2.3 Studies on heat transfer experiments of pile foundation GHEs	29
2.3.1 The heat transfer comparisons of energy piles with different types of tubes	29
2.3.2 The thermo-mechanical behavior of energy pile.....	31
2.3.3 Heat exchange capacity of CFG pile geothermal exchangers.....	34
2.3.4 Heat transfer performance of the spiral GHEs	36
2.3.5 Field performance of an energy pile system	38
2.4 Theoretical research on borehole GHEs with groundwater advection.....	39

2.4.1 The analytical methods.....	39
2.4.2 The numerical methods	42
2.5 Studies on groundwater advection experiments of borehole GHEs	44
2.6 Studies on impacts which groundwater exerts on pile foundation GHEs	46
2.7 Study on obtaining the velocity of groundwater	47
2.8 Summary	49
 CHAPTER 3 SOLID CYLINDRICAL HEAT SOURCE MODELS WITH GROUNDWATER FLOW	 52
3.1 Introduction	52
3.2 Basic principles for acquiring analytical solutions.....	54
3.2.1 The Green's function.....	54
3.2.2 Moving heat source	56
3.2.3 Advection in porous medium	58
3.3 Line heat source models with groundwater advection	59
3.4 The solid cylindrical heat source models	61
3.4.1 The relevant preconditions	61
3.4.2 Pure conduction models	62
3.4.2.1 Infinite cylindrical source model.....	62
3.4.2.2 Finite cylindrical source model	63

3.4.2.3	The characteristics of pure conduction models	63
3.4.2.3.1	The schematic diagram of temperature distribution.....	63
3.4.2.3.2	The temperature response trend	65
3.4.3	Combined heat transfer models.....	66
3.4.3.1	Infinite cylindrical source model.....	67
3.4.3.2	Finite cylindrical source model	68
3.4.3.3	The characteristics of combined heat transfer models	69
3.4.3.3.1	The schematic diagram of temperature distribution.....	69
3.4.3.3.2	The temperature response trend	71
3.4.3.3.3	Comparisons of temperature responses of representative locations	76
3.5	Comparisons between pure conduction models and combined models	78
3.6	Summary	82
 CHAPTER 4 COMBINED THERMAL EXCHANGE MODLS WHILE GROUNDWATER FLOWS THROUGH RING-COIL HEAT SOURCES		84
4.1	Introduction	84
4.2	Pure conduction of ring-coil models	86
4.2.1	The methodology adopted.....	86
4.2.2	Infinite ring-coil heat source model	87
4.2.3	Finite ring-coil heat source model.....	88

4.2.4 The presentation for temperature responses	89
4.2.4.1 The trends of temperature responses with the time	89
4.2.4.2 Temperature distribution around the ring-coil heat source	91
4.3 Combined thermal exchange of ring-coil models	92
4.3.1 The methodology adopted.....	92
4.3.2 Infinite ring-coil heat source model	93
4.3.3 Finite ring-coil heat source model.....	95
4.3.4 The presentation for temperature responses	96
4.3.4.1 The trends of temperature responses with the time	96
4.3.4.2 The temperature distribution around ring-coil heat source	98
4.3.5 The characteristics of finite ring-coil seepage model.....	98
4.3.5.1 The thermal responses at locations with different radial distances from ring-coil heat source	99
4.3.5.2 The role of groundwater velocity	101
4.3.5.3 The effects of coil pitch.....	102
4.3.5.4 Comparisons of temperature responses at different distances along z- axis from ring-coils	104
4.3.5.5 The alternative method for simplifying calculation	106
4.4 Comparisons between pure conduction and combined heat transfer	108
4.5 Summary	110

CHAPTER 5 SPIRAL HEAT SOURCE MODELS WITH GROUNDWATER FLOW

..... 112

5.1 Introduction 112

5.2 The spiral-coil models without considering groundwater seepage 113

 5.2.1 The research technique 114

 5.2.2 Infinite spiral heat source model 115

 5.2.3 Finite spiral heat source model..... 116

5.3 Heat transfer comparisons between pile foundation GHE and borehole GHE
..... 117

5.4 New models with groundwater seepage..... 120

 5.4.1 The research technique 120

 5.4.2 Infinite spiral heat source model 121

 5.4.3 Finite spiral heat source model..... 122

5.5 Characteristics of spiral heat source seepage models..... 123

 5.5.1 The regular pattern of temperature responses 123

 5.5.1.1 The temperature responses with the time 123

 5.5.1.1.1 Pure conduction models 124

 5.5.1.1.2 Heat transfer models with groundwater seepage..... 124

 5.5.1.2 The temperature distribution around spiral coils..... 127

 5.5.1.2.1 Pure conduction models 127

5.5.1.2.2 Heat transfer models with groundwater seepage.....	128
5.5.2 The temperature responses of locations with different radial distances from the heat source.....	129
5.5.3 The role of groundwater velocity	130
5.5.4 Influence of pitch B of spiral coils	131
5.5.5 The alternative simplified calculation method	133
5.5.6 Comparison between the temperature responses of $\varphi = 0$ and $\varphi = \pi$	135
5.5.7 The influence which groundwater seepage exerts on a pile group.....	136
5.6 Comparisons between models without and with groundwater seepage	139
5.7 Summary	141
CHAPTER 6 THERMAL TRANSMISSION EXPERIMENTS OF ENERGY PILES	143
6.1 Introduction	143
6.2 Presentation on energy piles of building employing the GCHP system	144
6.2.1 Characteristics of pile foundation GHE	144
6.2.2 The local underground thermal properties	145
6.3 Description and analysis about experiments	146
6.3.1 Experimental procedures.....	146
6.3.2 The analysis on recorded data	149
6.3.2.1 The first experiment	149

6.3.2.2 The second experiment.....	152
6.4 The comparisons between mathematical model results and experimental findings.....	155
6.5 Summary	158
 CHAPTER 7 BACK CALCULATION METHOD BASED ON THE LINE HEAT SOURCE SEEPAGE MODELS TO OBTAIN GROUNDWATER VELOCITY	160
7.1 Introduction	160
7.2 The influence that groundwater seepage exerts on a borehole GHE	162
7.2.1 The analytical solutions of line heat source models with groundwater advection	162
7.2.1.1 Infinite line heat source seepage model	162
7.2.1.2 Finite line heat source seepage model.....	163
7.2.2 Comparisons between temperature responses of with and without groundwater seepage.....	163
7.2.3 The temperature field while groundwater seepage exists	164
7.2.3.1 The influence of seepage angles.....	164
7.2.3.2 The influences of seepage's intensity and time.....	165
7.2.3.3 The change regulation of mean temperature	167
7.3 Description of the back calculation method	169
7.3.1 The arrangement of test points on the horizontal plane	169

7.3.2 The depth location of distributed points.....	171
7.3.3 The principles of back calculation.....	172
7.3.3.1 The objective function.....	172
7.3.3.2 The partial derivatives	175
7.3.3.2.1 Derivative formulas of infinite line heat source seepage model	176
7.3.3.2.2 Derivative formulae for finite line heat source seepage model..	176
7.3.3.2.3 Determine the velocity after using partial derivatives.....	177
7.4 Characteristics involved in the infinite line heat source seepage model	178
7.4.1 The relationship between points' radius and velocity value	178
7.4.2 The research on inflection points of the temperature response curves.....	179
7.4.3 The relationship between the time needed for reaching half of the stable temperature response and the velocity value	182
7.4.4 Preliminary judgment on orientation of groundwater flow.....	183
7.4.5 The estimation of velocity value based on the ratio of the maximal response to the minimal response	184
7.5 Characteristics involved in the finite line heat source seepage model	185
7.5.1 The influence that orientation exerts on the comparisons of three points' temperature responses	185
7.5.2 The slopes of the temperature responses with the time.....	187
7.6 The trials of back calculation	189

7.6.1 Trials based on the infinite line heat source seepage model	190
7.6.2 Trials based on the finite line heat source seepage model	192
7.7 Summary	193
CHAPTER 8 CONCLUSIONS AND RECOMMENDATIONS FOR FUTURE WORK	195
8.1 The existing research work.....	196
8.2 The simulation models of pile foundation GHE with groundwater advection	197
8.3 The heat transfer experiments of pile foundation GHEs	199
8.4 The back calculation method for obtaining groundwater velocity	199
8.5 Recommendations for future work.....	200
REFERENCES.....	202

LIST OF FIGURES

Figure 1.1 The schematic diagram of ground-coupled heat pump system.....	3
Figure 1.2 The schematic diagram of two types of GHE.....	4
Figure 1.3 Previous common types of heat transfer tubes inside pile.....	5
Figure 1.4 The configuration of pile foundation GHE.....	7
Figure 1.5 GCHP system with energy piles.....	7
Figure 2.1 The construction drawing of on-site pile foundation GHEs.....	29
Figure 2.2 The thermal-mechanical behavior of energy pile.....	33
Figure 2.3 The profile and layout of the CFG energy piles and sensors.....	34
Figure 2.4 The installation types of spiral coils.....	37
Figure 2.5 Temperature distribution around borehole GHE while infinite line heat source with groundwater advection is employed.....	40
Figure 2.6 Isothermals of both infinite and finite moving line heat source models....	41
Figure 2.7 The schematic diagram of experiment rig of groundwater flow.....	46
Figure 3.1 Geometry of solid cylindrical heat source model.....	53
Figure 3.2 Isothermals of finite line heat source seepage model.....	61
Figure 3.3 Isothermals of pure conduction model of solid cylindrical heat source....	65

Figure 3.4 Temperature responses of solid cylindrical heat source pure conduction models with the time66

Figure 3.5 Isothermals of solid cylindrical source model with groundwater advection71

Figure 3.6 Temperature responses of solid cylindrical heat source seepage models with the time.....73

Figure 3.7 The differences of temperature responses with the velocity.....74

Figure 3.8 The temperature responses with the time while different velocities are adopted75

Figure 3.9 Isothermals down z-axis at different time and velocities respectively when $\varphi=0$ 77

Figure 3.10 Isothermals down z-axis at different time and velocities respectively when $\varphi = \pi$77

Figure 3.11 The ratios of temperature responses of two heat transfer modes with the time.....79

Figure 3.12 The ratios of heat exchange rates of two heat transfer modes with the time.....80

Figure 3.13 The ratios of temperature responses of two heat transfer modes with the velocity.....81

Figure 3.14 The ratios of heat exchange rates of two heat transfer modes with the velocity81

Figure 4.1 Schematic diagram of ring-coil heat source model.....	85
Figure 4.2 The temperature responses of ring-coil pure conduction models	90
Figure 4.3 The isothermals of ring-coil pure conduction model	91
Figure 4.4 The temperature responses of ring-coil combined heat transfer models ..	97
Figure 4.5 The isothermals of ring-coil combined heat transfer model	98
Figure 4.6 The temperature responses of positions with different R values	99
Figure 4.7 Temperature profiles along z -axis when φ adopts 0 and π respectively .	100
Figure 4.8 The temperature responses with the time when velocity adopts different values.....	102
Figure 4.9 The temperature responses with the time when coils pitch adopts different values.....	103
Figure 4.10 The temperature responses with the velocity when coil pitch adopts different values.....	104
Figure 4.11 Two adjacent coils and different positions between them	105
Figure 4.12 The temperature responses of different positions between adjacent coils	106
Figure 4.13 The errors of two calculation methods while H adopts different values	107
Figure 4.14 The errors of two calculation methods when B takes different values .	108

Figure 4.15 The temperature responses ratios and heat transfer rates' ratios with the time while the velocity is constant	109
Figure 4.16 The temperature responses ratios and heat transfer rates' ratios with the velocity while the time is constant	110
Figure 5.1 The geometry of the spiral heat source inside the pile foundation GHE .	113
Figure 5.2 The temperature response ratios of pile foundation GHE to borehole GHE	119
Figure 5.3 The heat transfer rates' ratios of pile foundation GHE to borehole GHE	120
Figure 5.4 The temperature responses of spiral pure conduction models with the time	124
Figure 5.5 The temperature responses of spiral combined heat transfer models with the time.....	126
Figure 5.6 The temperature responses of different combined models with the time	127
Figure 5.7 Isothermals induced by spiral pure conduction model	128
Figure 5.8 Isothermals of the spiral combined heat transfer model	128
Figure 5.9 The temperature responses with the time when R adopts different values	129
Figure 5.10 The temperature responses with the time while S adopts three different values.....	130

Figure 5.11 Temperature fields with different velocities of groundwater flow	131
Figure 5.12 The temperature responses with the time while B adopts different values	132
Figure 5.13 The temperature fields when B adopts different values.....	133
Figure 5.14 The temperature responses of two calculation methods with the time and with the velocity respectively.....	134
Figure 5.15 The temperature responses of the sides $\varphi = 0$ and $\varphi = \pi$	136
Figure 5.16 The distribution pattern of pile group	137
Figure 5.17 The temperature distribution of pile group with groundwater advection	138
Figure 5.18 The temperature responses of places near pile 1# and pile 10#.....	138
Figure 5.19 The temperature responses of pure conduction and combined heat transfer.....	140
Figure 5.20 The heat transfer rates' ratios of two heat transfer modes with the time and with the velocity	141
Figure 6.1 Schematic diagram of on-site energy pile.....	145
Figure 6.2 The photo of thermophysical tester.....	146
Figure 6.3 Schematic diagram of heat transfer experiment of pile foundation GHEs	147
Figure 6.4 The on-site photos of heat transfer experiments of energy piles	148

Figure 6.5 The inlet and outlet temperatures of the circulating liquid in the first experiment.....	149
Figure 6.6 The flow rate of the circulating liquid in the first experiment.....	150
Figure 6.7 The heating power of the No.1 instrument in the first experiment.....	151
Figure 6.8 The heat transfer rates according to two different methods in the first experiment.....	151
Figure 6.9 The inlet and outlet temperatures of the circulating liquid in the second experiment.....	153
Figure 6.10 The flow rate of the circulating liquid in the second experiment	153
Figure 6.11 The total heating power of the No.1 and the No.2 instruments in the second experiment.....	154
Figure 6.12 The heat transfer rates according to two different methods in the second experiment.....	154
Figure 6.13 Comparisons between calculated results and experimental findings of the first experiment	157
Figure 6.14 Comparisons between calculated results and experimental findings of the second experiment.....	157
Figure 7.1 The groundwater flowing through borehole GHE	160
Figure 7.2 Temperature responses of with and without groundwater seepage	164
Figure 7.3 The diagram of different groundwater orientations	165

Figure 7.4 The temperature fields when groundwater orientation takes different angles.....	165
Figure 7.5 The isothermals with the increase of S	166
Figure 7.6 The isothermals with the increase of Fo	167
Figure 7.7 The mean temperature responses with the time when φ adopts different angles.....	168
Figure 7.8 The mean temperature responses with S when φ adopts different values	169
Figure 7.9 The schematic diagram of three evenly-distributed points around borehole GHE	170
Figure 7.10 Some other distributing modes for three points around borehole GHE	171
Figure 7.11 The distributing diagram while there are different numbers of points .	171
Figure 7.12 The mean temperature responses of the finite model along Z-axis	172
Figure 7.13 The flow chart of the iteration process for obtaining groundwater velocity	175
Figure 7.14 The temperature responses of three points when S adopts two extreme values.....	179
Figure 7.15 The changing trend that Fo is along with $Lg (S)$	181
Figure 7.16 The curve which product of S and Fo changes with $Lg (S)$	181
Figure 7.17 The change trend of Fo of reaching the half stable temperature response with S	183

Figure 7.18 The influence that groundwater orientation exerts on temperature difference of every two points.....	184
Figure 7.19 The ratios of the maximum to the minimal responses with S	185
Figure 7.20 The temperature responses of three points with the time	186
Figure 7.21 The temperature responses of three points with the seepage orientation	187
Figure 7.22 The variation trends of slopes of three points while S and φ remain changeless	188
Figure 7.23 The slopes with the time when orientation and velocity value respectively change	189
Figure 7.24 The theoretical temperature responses versus simulated experimental data	190
Figure 7.25 The temperature responses of theoretical results and simulated experimental data	191
Figure 7.26 The temperature responses of theoretical results and simulated experimental data	192
Figure 7.27 The temperature responses of theoretical results and simulated experimental data	193

LIST OF TABLES

Table 2.1	The symbols and the corresponding meanings outside pipe	25
Table 2.2	The symbols and the corresponding meanings inside pipe	26
Table 2.3	The symbols and the corresponding meanings of energy pile with U-tube	28
Table 2.4	Heat transfer comparisons of different types of tubes.....	30
Table 2.5	The symbols of THM model and the corresponding meanings	32
Table 2.6	The heat transfer capacity of single pile and grouped piles by means of TRT	35
Table 2.7	The heat transfer capacity of single pile and grouped piles by means of TPT.....	35
Table 2.8	The heat transfer capacity during the whole process	36
Table 2.9	The operating result of the heating period of the energy pile system	38
Table 2.10	Values of various parameters used for model	42
Table 2.11	Annual maximum drop of mean fluid temperature	43
Table 6.1	Introduction of underground medium	146
Table 6.2	The actual parameters and corresponding dimensionless values	156

NOMENCLATURE

Abbreviations

h_1, h_2	depth of spiral coils (m)
h_3	depth of pile (m)
h	length of heat source (m)
x, y, z	rectangular coordinate (m)
X, Y, Z	dimensionless rectangular coordinate
t_0	initial temperature (K)
T	temperature (K)
t	temperature (K)
a	thermal diffusivity ($\text{m}^2 \text{s}^{-1}$)
c_p	specific heat ($\text{J kg}^{-1} \text{K}^{-1}$)
k	thermal conductivity ($\text{W m}^{-1} \text{K}^{-1}$)
H	dimensionless depth

r_0	coil or pile radius (m)
r_b	borehole or pile radius (m)
r	radial coordinate (m)
q	heating rate of point heat source
q_l	heating rate per length source (W m^{-1})
u	speed in x-direction (m s^{-1})
v	speed in x-direction (m s^{-1})
b	coil pitch
m	mass flow rate (kg s^{-1})
R_s	distance to the point heat source (m)
R_m	dimensionless distance to the point heat source
R	dimensionless radius
R_D	dimensionless radius
B	dimensionless coil pitch
U	equivalent velocity
V	dimensionless velocity

S	dimensionless velocity
Fo	dimensionless time
P	electric heating power (kW)
T	objective function
L	product
M	Green function of groundwater seepage
Pr	ratio

Greek symbols

τ	time
φ	angular coordinate (rad)
β	angular coordinate (rad)
ϕ	angular coordinate (rad)
Θ	dimensionless excess temperature
θ	excess temperature
ξ, η, ζ	rectangular coordinate (m)

ψ integration variable

Superscript

' integration parameter

Δ first-order partial derivative

$\Delta\Delta$ second-order partial derivative

Subscripts

a advection

p pure conduction

i infinite model

f finite model

l line heat source

c solid cylindrical heat source

r ring-coil heat source

<i>s</i>	spiral heat source
<i>w</i>	water
<i>ave</i>	average
<i>be</i>	the mean of two values
<i>co</i>	coil
<i>cal</i>	calculation result
<i>rec</i>	simulative recorded data
<i>to</i>	total
<i>out</i>	outlet
<i>in</i>	inlet
<i>li</i>	liquid
<i>st</i>	spiral tube
<i>j</i>	the order number of data
<i>max</i>	the maximal value
<i>min</i>	the minimal value

CHAPTER 1 INTRODUCTION

Small and medium sized thermal coal boilers have been gradually prohibited in cities and towns as a result of the increased attentions paid on air environment protection by the international community. Consequently focus has been turned to the development of heating modes other than district heating. Heat pump technology achieves reasonable heating and air conditioning in line with the recommended air pollution reduction (GB50155, 2003). From the perspective of the characteristics of heating or cooling sources, the heat pump system can be divided into two types: air-source and ground-source.

Air-source heat pumps (ASHP) avails themselves of outdoor air as both cooling and heating sources. The system is simple and has low initial cost, but the performance is relatively poor due to the fact that it is easily impacted by the influence of outdoor environment (Zheng, 1998); periodical defrosting has to be carried out to avoid loss of heat (Miller W.A, 1987). Ground-source heat pump (GSHP) takes advantage of heat energy stored within 200m below ground to fulfill heat supply and cooling for buildings. In recent years this technology has been widely-adopted day by day and its heating or cooling performance has been considered satisfactory. The GSHP system can be classified into ground-coupled heat pump (GCHP), surface water source heat pump (SWSHP) and groundwater source heat pump (GWSHP) in accordance with the ways of geothermal energy acquisition system (Langley, 1989. Healy and Ugursal, 1997).

The SWSHP system regards the water existing in rivers, lakes and seas as sources

required to conduct heating and cooling, and the GWSHP system makes full use of energy obtained via extracted underground water which is then recharged into the phreatic zone. The services achieved from these two types of systems are not widespread because their applications are obviously limited by natural conditions and water source. With this contrast, GCHP technology has gained more and more all-pervading application, because the ground distribution is broad and the other advantages including high energy efficiency and environmental protection are evident (Lund, 2006).

1.1 The introduction about GCHP system

The GCHP system utilizes underground mediums including soil, sand and so on as cooling source or heating sources (Eckert, 1976). Underground temperature in the deeper stratum fluctuates a little all the year round, with the temperatures respectively higher and lower than outdoor temperatures in winter and in summer, thus the GCHP system can overcome the technical obstacles of the ASHP system, meaning that the operation performance of the system can be improved. To be more specific, the temperature of the underground can be elevated temperature by means of heat pump to warm the indoor spaces of buildings in winter. Conversely, heat can be abstracted from buildings in summer and then kept in reserve below ground with the help of heat pump. Hence, not only is there a drop in the building temperature, but also thermal energy is stored in underground medium for serving in winter. Currently, the total area that employs ground source heat pump is nearly 3.5 hundred million square meters. The applications in some regions such as Beijing, Shanghai, Tianjing, Shandong, Hebei and Henan are more popular as the air condition systems of these areas are responsible for not only cooling but also heating, therefore it is not easy to induce the imbalance

between heat adsorption and release in underground medium.

In this way, underground medium acts as an energy accumulator when the GCHP system is employed. Thus, the energy utilization efficiency of air-conditioning system is further improved as underground medium is an ideal heating or cooling source, not only the heating efficiency but also the cooling performance can be advantageously improved. In addition, the domestic hot water can be either produced by way of the GCHP system. Giving a multi-use system and the corresponding diagram is shown in Figure 1.1. Thus the ground heat exchangers (GHEs) play a significant role in the employment of underground energy, enabling the production of cooling, heating and domestic hot water.

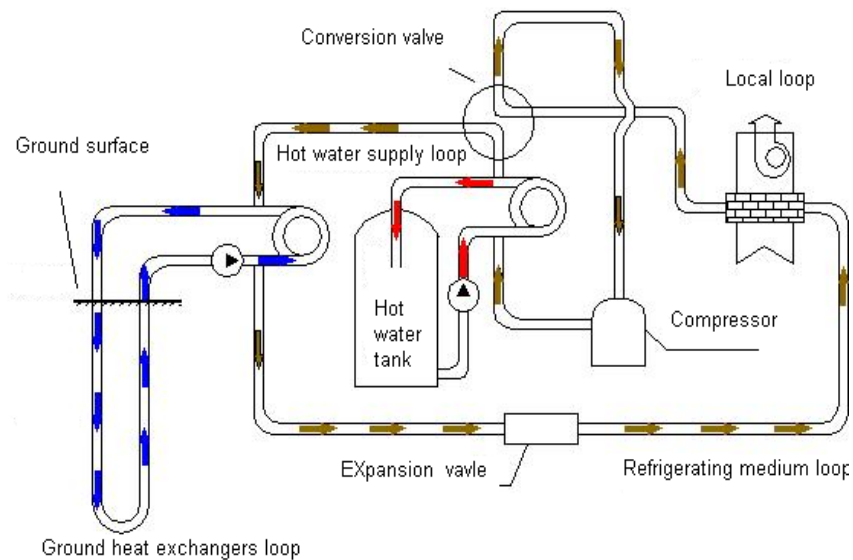


Figure 1.1 The schematic diagram of ground-coupled heat pump system

1.2 The conventional GHEs

A GCHP system also consists of GHEs, heat pump units and indoor end equipments; GHE is the significant component that embodies the vital difference between GCHP and other heat pump systems. Currently, there are two GHE types employed for releasing or

abstracting heat, that is, horizontal and borehole GHEs are defined according to the arrangement pattern.

Horizontal GHE, i.e. heat exchange tubes are buried in ditches or shallow depth trenching (Mei, 1986), the cost of the system is low but the heat transfer performance is susceptiblely influenced by outside climate. The main defect is that a large area is needed for the distribution of heat exchange tubes; consequently horizontal GHE is less suitable for Chinese condition i.e. a large population with relatively little land. Borehole GHE is defined as that single U-tube or double U-tubes are installed into a borehole (Deerman and Kavanaugh, 1991). The depth of borehole is usually between 50m and 150m meanwhile the diameter is from 130mm to 150mm. Thus, the advantages of the employment of borehole GHEs are obvious because the less land area and stable working performance can be achieved. Accordingly, the vertical borehole GHE is the mainstream especially when GHEs are used in the engineering projects. The diagrams of these two GHEs' types are shown in Figure 1.2.

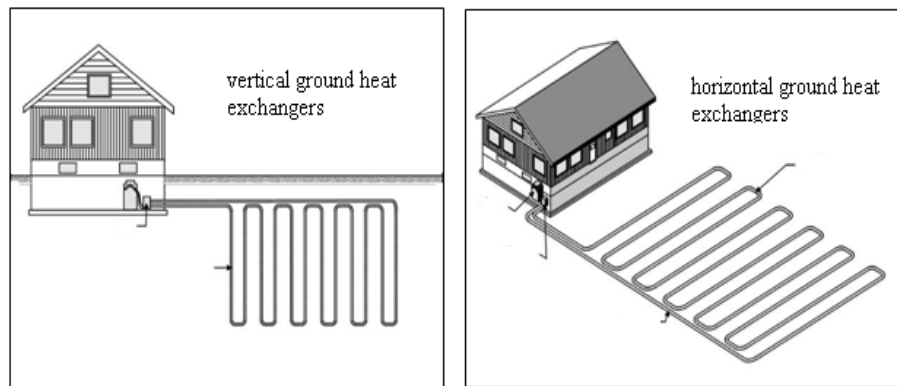


Figure 1.2 The schematic diagram of two types of GHE

Although borehole GHEs are given priority for application in GCHP system, the initial cost is high since a great amount of money must be spent on drilling boreholes

and burying U-tubes, a large investment is the primary factor hindering the development of GCHP technology (Ramamoorthy et al., 2001).

1.3 Pile foundation GHEs

With the development of GHE technology, people begin to realize that the bearing structure of buildings can be used, i.e. pile foundation can be utilized to bury heat transfer tubes, therefore a certain proportion of air-conditioning load can be undertaken and the rest of the load is charged with conventional GHEs, thus reducing the initial cost of the whole system. GHE and pile foundation are thus integrated and this new GHE is also entitled “energy pile” (Sanner, 2001). With regard to the energy pile with spiral coils, the geometry is quite different from that of the borehole, that is, the pile diameter is much thicker and depth usually shorter than in the case of boreholes; the heat transfer coils are disposed in the proximity of the pile circumference. Several types of heat transfer pipes can be located inside the pile and the corresponding configurations are shown in Figure 1.3 (Liu et al., 2009).

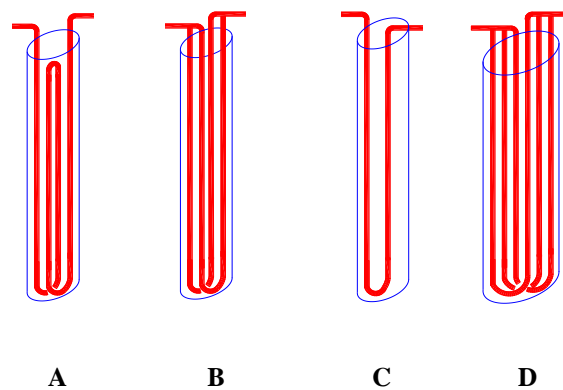


Figure 1.3 Previous common types of heat transfer tubes inside pile

A and B stand for W tube and double U-tubes in parallel, respectively, C denotes

single U tube and D is the shunt-wound triple U-tubes; but some problems must be noted when these types of tube are put to use. Firstly, the heat transfer area is small and therefore full use cannot be made of pile space if single U-tube is buried. Secondly, it is easy for air to accumulate at the top of the pipe when the W-tube is considered. The accumulation of air will lead to the obstruction of circulating solution. Thirdly, the shunt-wound double U-tubes or treble U-tubes have been installed in Europe and have been in operation with success, and high heat transfer efficiency can be achieved; however, the total heat transfer area was greater, causing the flow area to be larger, thus the difference of inlet and outlet temperatures of circulating liquid began to drop and was lower than hoped. This heat transfer process was thus unfavorably affected because the circulating pump power and running cost were increased.

The heat transmission coefficient of spiral tubes is comparatively higher than that of straight tubes. It is undeniable that on the one hand, spiral tubes are complicated and the cost is also higher than that of U-tubes or W-tube, however, on the other hand, a greater heat transfer area is attained in the same space because of the longer tube. The construction process consists of several steps. To be more specific, 1, spiral coils are fixed in the prefabricated hollow steel cage; 2, both the coils and steel cage are lowered into the pile foundation (Zhong and Tang, 2007); 3, the concrete is cast into the pile and the energy pile formed. The configuration of pile foundation GHE is displayed in Figure 1.4.

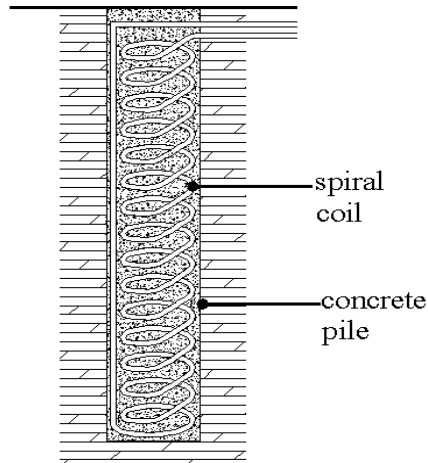
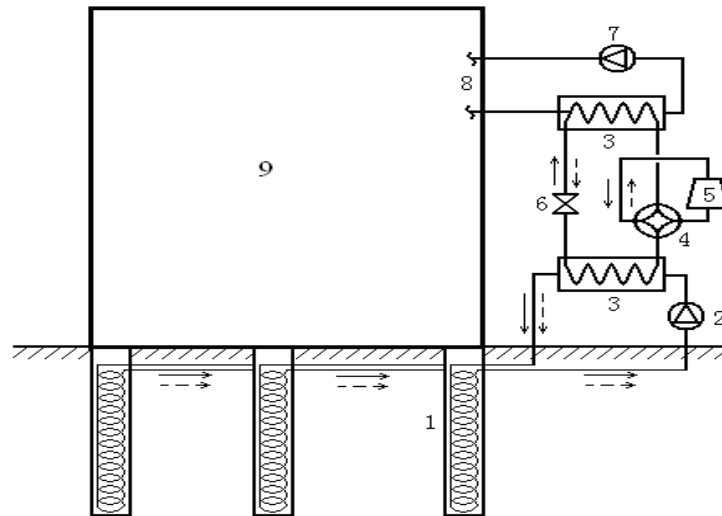


Figure 1.4 The configuration of pile foundation GHE

As a general rule, pile foundations are divided into precast and driven cast-in-place piles (Tang, 2000), the former is prefabricated at the construction site and then is sunk into the ground; the hole has to be drilled at the pile location for the latter method before concrete is poured; the spiral coils can be placed in any of drilled holes. The GCHP system including pile foundation with spiral heat exchange tubes is shown in Figure 1.5.



- 1. pile-foundation ground heat exchangers 2. circulating pump 3. heat exchanger
- 4. four-way directional control valve 5. compressor 6. flow regulating valve
- 7. circulating pump 8. heat exchanger 9. building

Figure 1.5 GCHP system with energy piles

1.4 The significance of investigating groundwater flow

The length of piles is generally more than ten meters and even reaches dozens of meters, which means piles may penetrate several geologic strata and pass through any existing water tables. Water is held and moves between the grains of geologic formations in response to hydraulic gradients (Neuman and Witherspoon, 1970). The heat transfer between pile GHEs and the surrounding medium becomes more sophisticated due to the groundwater flow; this is a coupled process which comprises conduction through the solid matrix and water in its pores and heat advection by moving groundwater. Groundwater sources are in abundance in some regions, such as the middle and lower reaches of the Yangtze River, where the groundwater level can be as little as 1.5 meters deep, thus groundwater seepage should be taken into account in the system design, in addition, the regions closed to the lakes and rivers have favorable hydraulic gradient, such as some cities in Jiangsu, Zhejiang, Fujian and so on of China, thus these areas should consider the influence of groundwater advection while local hydraulic gradient attains a certain level. During the operating period of the GCHP system with pile foundation GHEs, heat accumulation around GHEs inevitably occurs because heat is emitted from GHEs to the surrounding medium, therefore the temperature difference between them decreases with the proceeding of heat transfer. When groundwater flows through piles, a certain proportion of the accumulated heat is taken away owing to the convection, the temperature difference is increased again to guarantee successful thermal exchange and thus the heat transfer rates are improved. The application of pile foundation GHEs essentially improves the economic performance of the GCHP system as the expense on developing borehole GHEs is reduced. With reference to the influence

that groundwater seepage has on energy pile, it looks like that a beautiful thing is added to a contrasting beautiful thing. Accordingly, energy piles can be responsible for more heating or cooling load and therefore initial cost can be further dropped.

Investigation on pure conduction of energy pile has made progress in recent years, the relevant mathematical models simulating the heat transfer process and the corresponding analytical solutions expressing thermal response have been respectively established and obtained. A substantial number of studies on borehole GHEs with groundwater flow have been conducted, however, the exploration about the heat transfer of pile foundation GHEs with groundwater flow is little, in other words, the theoretical models describing the details of the whole heat transfer process including conduction and groundwater advection have not been proposed. Energy pile is a new type of GHE that involves the combination of structure technology and heat exchange knowledge. To further promote the development of GCHP, a novel study of energy piles with groundwater flow is necessary. The potentials of this investigation merit such further scrutiny.

1.5 Aims and objectives of the thesis

The development of models describing the combined heat transfer of pile foundation GHE with groundwater advection is an urgent task. Energy equations and moving heat sources and other mathematical knowledge are necessary to obtain the analytical solutions of temperature response.

The aims of this study are to establish different simulation models from the simple to the complex and to acquire the corresponding analytical solutions. Thus several models of pile foundation GHE with groundwater seepage will be put forward in the light of the

simplification degrees. The most accurate model, i.e. the one which is approximate to the actual configuration of the energy pile in the case of groundwater seepage, is pointed out. Secondly, an on-site experiment is conducted to indirectly prove the availability of these seepage models. Thirdly, a back calculation method to acquire the groundwater velocity including orientation and value is proposed, thereby a firm foundation can be laid for giving expression to the impact degree of seepage phenomenon. The specific objectives of the thesis are as follows:

(1) To establish solid cylindrical seepage model. This model is the simplest one because pile foundation GHE is deemed as a cylindrical surface heat source ignoring the configuration of spiral coils, and groundwater flows through its surface. By means of this model, heat transfer can be roughly calculated and a basis is provided for later more complicated models.

(2) To establish ring-coil seepage model, the spiral heat exchange tubes is considered as a series of separated coils arranged one by one along the z-axis, and these coils are passed by groundwater. The GHE structure is not sufficiently accurate because the simplification conditions still exist. This model, however, is more advanced than the solid cylindrical seepage model.

(3) To establish spiral seepage model regarding buried spiral tubes as a string of spiral coils rather than separated coils. This model is the most accurate case from the research perspective. The other models, however, are valid choices when the calculation requirement is not too high or strict.

(4) To develop the computer program based on the simulation models to present the temperature response at any point except the heat source in the underground medium,

and also to explore the trends of the temperature response with the time or with the groundwater velocity.

(5) To obtain the mean temperature response while groundwater flows through energy piles, and then to compare the differences of infinite and finite models. Afterwards two heat transfer modes, i.e. pure conduction and combined heat transfer including conduction and groundwater advection, will be compared in terms of heat transfer performance.

(6) It should be noted that there are no seepage experiments for pile foundation GHE, but the analytical solutions of seepage models are derived from pure conduction, if the pure conduction model is validated, the seepage models can then be indirectly proven.

(7) To suggest a new methodology to acquire the local groundwater velocity. The line heat source seepage models are chosen as the basis for back calculation.

1.6 Organization of the thesis

The investigation work finished by experts and scholars can indicate the next academic direction of the research area presented in this thesis. The comprehensive and critical literature review presented in chapter 2 gives the existing achievements of the study on pile foundation GHEs, and followed by the research purpose of the thesis. The mathematical model of solid heat source with groundwater advection is described in chapter 3, analytical solutions of two-dimensional and three-dimensional models are respectively obtained, and the corresponding heat transfer analysis is conducted. Based on the solid model, the ring-coil heat source seepage models are presented and discussed in chapter 4; the pitch between adjacent coils is an important parameter because the

discontinuity of surface heat source is taken into consideration. This chapter presents an in-depth discussion on the characteristics involved in this seepage model. In addition, the most accurate model which can depict the configuration of energy pile with groundwater flow in a relatively analogical manner is the spiral heat source seepage model; chapter 5 summarizes the significant properties of the spiral model. Afterwards, the heat exchange experiments of pile foundation GHEs are demonstrated and the corresponding description is given in chapter 6, the on-site experiments are completed based on the engineering project which employs the GCHP system with energy piles. The experimental effects are satisfactory and the pure conduction model is validated. The seepage experiments are difficult to be conducted because the order of magnitude of groundwater velocity is too small, thus the experimental period may attain several months even years provided that the trials are conducted. As a consequence, the actual seepage experiments of energy piles have not been developed. Seepage models can be indirectly verified if only the pure conduction model is validated by means of experiments, due to the fact that the former is derived from the latter. A novel back calculation method for obtaining the groundwater velocity is proposed in chapter 7. The infinite and finite line heat source seepage models are respectively made full use to achieve the value and orientation of velocity. Conclusions are drawn in chapter 8, together with recommendations of future work. One important task is to establish a new experimental rig for groundwater seepage, in such a way the seepage models can be directly verified. Other points for consideration are generalized either. It is felt that there is no doubt that future investigations can promote the further application of energy pile technology.

CHAPTER 2 ITERATURE REVIEW

2.1 Introduction

Civil engineering and heat transfer academics have completed much investigative work on energy piles. The mechanical behavior of pile foundation is inevitably influenced because heat travels through its surface. Thus, different professions need to be incorporated; the better heat transfer performance qualifies energy pile to take on a certain proportion of air conditioning load. Accordingly, this novel technology is receiving growing attentions. A series of mathematical models have been proposed based on an in-depth understanding of energy piles with spiral coils, and the corresponding analytical solutions obtained. In this way, the heat transfer between pile and its surrounding underground medium can be revealed while only pure conduction actually exists. Meanwhile, numerical methods have been employed to analyze the temperature variation in the area around pile foundation GHE. It should be noted that academic research studies including both analytical analyses and numerical discussions have brought the theoretical investigations of the energy pile to a certain level. However, the studies aiming to investigate heat transfer related to groundwater flowing through energy piles is little, in that simulation models or other expressions have not been proposed. Hence, the contributions of this current study are significant.

In addition, on-site experiments on energy piles have been conducted by researchers and the persuasive data obtained, which has revealed the heat exchange superiority of energy pile. The temperature response and the heat transfer rate with the time are able to

be recorded during the use of energy piles. The corresponding groundwater seepage research has been conducted in recent years, but most revolves around the influence that groundwater advection exerts on borehole GHE. In view of this, it is particularly important to launch the studies on heat transfer of pile foundation GHE with groundwater seepage. The study presented in this thesis centers on this research area.

2.2 Theoretical investigations on pure conduction of pile foundation GHEs

2.2.1 Analytical solutions of mathematical models

During the evolution of heat transfer models of the pile foundation GHE, fundamental models were studied first and others were then proposed with focus on models' difficulty levels. To understand the heat dissipation process from a single pile to its surrounding medium is an important first step; a second step is to obtain heat transfers of multiple piles, Eskilson (1987) and Hellstrom (1991) employed superposition principle to conduct analysis of these procedures. Models and their analytical expressions with different sophistications and precisions have been presented.

2.2.1.1 Line heat source

It is well known that the classical models of borehole GHE are usually dependent on one-dimensional analytical solutions. A most-widely-used one-dimensional (1-D) model for this purpose is the Kelvin's line source model (Kelvin, 1882), because the borehole diameter is usually from 130mm to 150mm and the depth lies in the range of between 50m and 150m. Thus the line heat source is a reasonable choice and some design methods were based on the Kelvin's heat source theory (Bose et al., 1985). The 1-D

model cannot take the ground boundary into account and therefore the deviation from normal temperature response comes into being. With the aim of expressing the effect of the ground boundary, the virtual method was employed by Zeng et al.(2002) to obtain the analytical solution of the finite-depth borehole GHEs.

It should be highlighted that the Green function is the basis of achieving the analytical solutions (Chang et al., 1973), in particular, it shows the temperature response at a point (x, y, z) at time τ in the medium to the instantaneous point heat source that is located at (x', y', z') and begin to emit heat from the time τ' , and the corresponding expression is given in Equation (2.1)

$$G(x, y, z, \tau; x', y', z', \tau') = \frac{1}{8[\sqrt{\pi a(\tau - \tau')}]^3} \exp\left[-\frac{(x - x')^2 + (y - y')^2 + (z - z')^2}{4a(\tau - \tau')}\right] \quad (2.1)$$

Equation (2.1) can then be expressed as Equation (2.2) in cylindrical coordinate.

$$G = \frac{1}{8[\pi a(\tau - \tau')]^{3/2}} \cdot \exp\left[-\frac{r^2 + r'^2 - 2rr' \cos(\varphi - \varphi') + (z - z')^2}{4a(\tau - \tau')}\right] \quad (2.2)$$

The mathematical model and the corresponding conditions for 1-D line heat source are summarized in Equation (2.3).

$$\left. \begin{aligned} \frac{\partial \theta}{\partial \tau} &= a \left(\frac{\partial^2 \theta}{\partial r^2} + \frac{1}{r} \frac{\partial \theta}{\partial r} \right), \text{ for } 0 < r < \infty \text{ and } \tau > 0 \\ \theta &= 0, \quad \text{for } 0 < r < \infty \text{ and } \tau = 0 \\ \theta &\rightarrow 0, \quad \text{for } r \rightarrow \infty \text{ and } \tau \geq 0 \\ -\frac{\partial \theta}{\partial \tau} &= \frac{q_l}{2\pi r} \quad \text{for } r \rightarrow 0 \text{ and } \tau \geq 0 \end{aligned} \right\} \quad (2.3)$$

According to the Green function, the temperature response of the infinite model is listed as follows:

$$\theta_{l,i} = \frac{q_l}{\rho c} \int_0^\tau d\tau' \int_{-\infty}^{\infty} G dz' = -\frac{q_l}{4\pi k} Ei\left(-\frac{r^2}{4a\tau}\right) \quad (2.4)$$

where $Ei(m) = \int_{-\infty}^m \frac{e^u}{u} du = \gamma + \ln(-m) + \sum_{k=1}^{\infty} \frac{m^k}{k!k}$ is the exponential integral function, and $\gamma \approx 0.577216$ is the Euler-Mascheroni constant (Brent, 1977)

The two-dimensional (2-D) line heat source model was proposed by Eskilson (1987), the line heat source with finite length stretches from the ground surface to a certain depth along z-axis. The analytical solution of temperature response is derived by means of the images expressing the boundary conditions (Cui et al., 2006), and the corresponding analytical expression is described as:

$$\theta_{l,f} = \frac{q_l}{\rho c} \int_0^\tau d\tau' \left[\int_{h_1}^{h_2} G dz' - \int_{-h_2}^{-h_1} G dz' \right] = \frac{q_l}{4\pi k} \int_{h_1}^{h_2} \left\{ \frac{\operatorname{erfc}\left[\frac{\sqrt{r^2 + (z-z')^2}}{2\sqrt{a\tau}}\right]}{\sqrt{r^2 + (z-z')^2}} - \frac{\operatorname{erfc}\left[\frac{\sqrt{r^2 + (z-z')^2}}{2\sqrt{a\tau}}\right]}{\sqrt{r^2 + (z-z')^2}} \right\} dz' \quad (2.5)$$

In addition, a new infinite line heat source in a composite medium has been established (Li and Lai, 2012), and the source emits heat continuously at a rate q_l per unit time and per unit length (W/m). Borehole or pile GHE can be divided into two parts, that is, the backfilling material inside the GHE and the underground medium outside the GHE. The temperature response induced by this line source can be obtained by means of integration with respect to the time τ , thus the corresponding expressions inside and outside GHE are respectively acquired in Equation (2.6) and (2.7).

$$T_{l,i,1}(\tau, r, \varphi) = \frac{q_l}{2\rho_1 c_1 \pi} \sum_{n=-\infty}^{+\infty} \cos n(\varphi - \varphi') \times \int_0^\tau \int_0^{+\infty} \frac{\exp[-a_1 u^2 (\tau - \tau')] J_n(ur) J_n(ur') (\beta' g' - \psi' f')}{\beta'^2 + \psi'^2} u du d\tau' \quad (2.6)$$

$$T_{l,i,2}(\tau, r, \varphi) = \frac{q_l a_1}{\pi^2 r_b} \sum_{n=-\infty}^{+\infty} \cos n(\varphi - \varphi') \times \int_0^\tau \int_0^{+\infty} \frac{\exp[-a_1 u^2 (\tau - \tau')] J_n(ur') [\psi' J_n(aur) - \beta' Y_n(aur)]}{\beta'^2 + \psi'^2} u du d\tau' \quad (2.7)$$

where r_b is the radius of GHE, and J_n and Y_n are respectively the Bessel functions of the first and the second kinds of order n ; u is the integral variable ($1/m$). The subscribes 1 and 2 mean the regions $r < r_b$ and $r > r_b$ respectively; k , ρ and c in turn delegates the thermal conductivity, the density and the specific heat of the backfilling material or the underground medium. a is the dimensionless variable and $a = \sqrt{a_1/a_2}$, where a_1 and a_2 are thermal diffusivities of these two different mediums.

2.2.1.2 Hollow cylindrical heat source

For pile foundation GHE with spiral coils, the geometry of the pile is quite different from that of the borehole. Its diameter is much thicker and depth usually shorter than in the case of boreholes. The spiral coils are disposed in the proximity of the pile's internal surface. Thus, the line heat source is no longer reasonable as the heat capacity of the GHE should be taken into consideration. For this reason, a new model, i.e. "hollow" cylindrical heat source is suggested to preliminarily reveal the pile structure (Carslaw and Jaeger, 1959). Supposing that the radius of the pile is r_b whereby the domain $r_b < r < \infty$ is considered, and the heating flux is directly exposed to the cylinder surface, which means the heat capacity of the "hot rod" is totally ignored. As a result, this model is

referred as “hollow” cylindrical source model (Kavanaugh and Rafferty, 1997) and its formulation becomes:

$$\left. \begin{aligned} \frac{\partial \theta}{\partial \tau} &= a \left(\frac{\partial^2 \theta}{\partial r^2} + \frac{1}{r} \frac{\partial \theta}{\partial r} \right), \text{ for } r_b < r < \infty \text{ and } \tau > 0 \\ \theta &= 0, \text{ for } r_b < r < \infty \text{ and } \tau = 0 \\ \theta &\rightarrow 0, \text{ for } r \rightarrow \infty \text{ and } \tau \geq 0 \\ -\frac{\partial \theta}{\partial \tau} &= \frac{q_l}{2\pi r} \text{ for } r = r_b \text{ and } \tau \geq 0 \end{aligned} \right\} \quad (2.8)$$

On the basis of Equation (2.8), the temperature response of any point except the surface heat source can be achieved, and the expression of analytical solution is shown in Equation (2.9).

$$\theta(r, \tau) = \frac{q_l}{2\pi\lambda} \left[-\frac{1}{r_0} \frac{2}{\pi} \int_0^\infty \left(1 - e^{-au^2\tau} \right) \frac{J_0(ur)Y_1(ur_0) - Y_0(ur)J_1(ur_0)}{u^2 [J_1^2(ur_0) + Y_1^2(ur_0)]} du \right] \quad (2.9)$$

where J_0 and J_1 are the zero order Bessel functions of the first and the second kinds, respectively, and Y_0 and Y_1 are the first order Bessel functions of the first and the second kinds, respectively.

2.2.1.3 Solid cylindrical heat source

Because the interior heat capacity is disregarded in hollow cylindrical heat source model, significant improvements must be made based on this model. A new model referred to as the “solid” cylindrical source model was then proposed (Man et al., 2010), and it takes the pile GHE characteristics into proper consideration. This model supposes that the cylinder is no longer a cavity but filled with the medium identical to that out of the cylinder; thereby the whole infinite domain is composed of a homogeneous medium. The pile radius is r_o and the Green function is then employed, only the radial heat

conduction is considered in the infinite model and therefore the energy equation being with the conditions are demonstrated as follows:

$$\left. \begin{aligned} \frac{\partial \theta}{\partial \tau} &= a \left(\frac{\partial^2 \theta}{\partial r^2} + \frac{1}{r} \frac{\partial \theta}{\partial r} \right) + \frac{q_l \delta(r-r_0)}{2\pi r_0 \rho c}, \text{ for } 0 < r < \infty \text{ and } \tau > 0 \\ \theta &= 0, \text{ for } 0 < r < \infty \text{ and } \tau = 0 \\ \frac{\partial \theta}{\partial r} &= 0, \text{ for } r = 0 \text{ and } \tau > 0 \\ \theta &\rightarrow 0 \text{ for } r \rightarrow \infty \text{ and } \tau \geq 0 \end{aligned} \right\} \quad (2.10)$$

where r_0 is the pile radius and $\delta(r-r_0)$ is the Dirac δ -function.

Thus, the expression of temperature response induced by 1-D solid cylindrical heat source is described in Equation (2.11).

$$\theta_{c,i} = -\frac{q_l}{2\pi^2 k} \int_0^\pi Ei \left(-\frac{r^2 + r_0^2 - 2rr_0 \cos \varphi'}{4a\tau} \right) d\varphi' \quad (2.11)$$

It is desirable to consider heat conduction not only along the radial but also follow the z-axis directions because the depth-to-diameter ratio of pile is smaller, the ground boundary cannot be ignored with the result that a 2-D model needs to be studied. Given that the distances from the boundary to the start position and to the end position along the depth direction are respectively h_1 and h_2 , the virtual method is used once again to obtain the expression of temperature response for the finite solid cylindrical heat source model.

$$\theta_{c,f} = \frac{q_l}{8\pi k} \int_0^\tau \frac{1}{(\tau-\tau')} I_0 \left[\frac{rr_0}{2a(\tau-\tau')} \right] \exp \left[-\frac{r^2 + r_0^2}{4a(\tau-\tau')} \right] \left\{ erf \left[\frac{z-h_1}{2\sqrt{a(\tau-\tau')}} \right] - erf \left[\frac{z-h_2}{2\sqrt{a(\tau-\tau')}} \right] + erf \left[\frac{z+h_1}{2\sqrt{a(\tau-\tau')}} \right] - erf \left[\frac{z+h_2}{2\sqrt{a(\tau-\tau')}} \right] \right\} d\tau' \quad (2.12)$$

where $I_0(x) = \frac{1}{\pi} \int_0^\pi \exp(x \cos \varphi') d\varphi'$ is the zero order modified Bessel function.

In addition, Li et al.(2012) suggested a solid cylindrical model in a composite medium, an infinite cylindrical surface source with the radius $r' < r_b$ is installed in the energy pile, and the whole domain is divided into two parts, which means the thermophysical properties inside and outside the pile are different. The temperature responses of the medium inside and outside the pile are shown in Equations (2.13) and (2.14) respectively.

$$T_{c,i,1}(\tau, r) = \frac{q_l}{2\pi k_1} \int_0^{+\infty} [1 - \exp(-a_1 u^2 \tau)] \cdot \frac{J_0(ur) J_0(ur') (\beta' g' - \psi' f')}{u(\beta'^2 + \psi'^2)} du \quad (2.13)$$

$$T_{c,i,2}(\tau, r) = \frac{q_l}{\pi^2 r_b} \int_0^{+\infty} [1 - \exp(-a_1 u^2 \tau)] \cdot \frac{J_0(ur') [\psi' J_0(aur) - \beta' Y_0(aur)]}{u^2 (\beta'^2 + \psi'^2)} du \quad (2.14)$$

where all the parameters or variables have the same meanings as those shown in section 2.2.1.1.

2.2.1.4 Ring-coil heat source

The solid cylindrical heat source model is more advanced compared with the classical line or “hollow” cylindrical heat source models, however, this model fails to distinguish the effect of the coil pitch because the spiral coils are simplified as a continuous cylindrical surface. The temperature distribution fluctuates along the axial direction in the vicinity of the cylindrical surface due to the non-integrity of the heat source. This feature is of great importance in the analysis of the temperature rise of the buried pipe containing the circulating fluid when GCHP system is employed. Consequently, more sophisticated models are needed for better understanding and analysis of the heat

transfer around the buried spiral coils.

Cui et al. (2011) investigated a transient ring-coil heat source model; the spiral coils installed in the pile were regarded as a series of separated coils, meaning that every two adjacent coils have no connection. The explicit analytical solutions of the temperature response were achieved by using both the Green's function theory and the image method. The influences of both the coil pitch and the locations were evaluated and discussed according to the solution. Assuming that every coil maintains the radius r_0 and heat begins to be emitted from $\tau = \tau'$, with the constant heat intensity $q_l b$, the simulation model and the corresponding conditions for every coil heat source in infinite medium is summarized as follows:

$$\left. \begin{aligned} \frac{\partial \theta}{\partial \tau} &= a \left(\frac{\partial^2 \theta}{\partial r^2} + \frac{1}{r} \frac{\partial \theta}{\partial r} \right) + \frac{q_l b \delta(r - r_0)}{2\pi r_0 \rho c}, \text{ for } 0 < r < \infty \text{ and } \tau > \tau' \\ \theta &= 0, \text{ for } 0 < r < \infty \text{ and } \tau = \tau' \\ \frac{\partial \theta}{\partial r} &= 0, \text{ for } r = 0 \text{ and } \tau > 0 \\ \theta &\rightarrow \infty \text{ for } r \rightarrow r_0 \text{ and } \tau \geq 0 \end{aligned} \right\} \quad (2.15)$$

In accordance with the Green function, the temperature response that one coil induces at any point except the heat source in the infinite medium is revealed in Equation (2.16).

$$\theta_{co} = \frac{q_l b}{2\pi \rho c} \int_0^{\tau} d\tau' \int_0^{2\pi} G d\varphi' = \frac{q_l b}{8\rho c} \int_0^{\tau} \frac{1}{[\pi a(\tau - \tau')]^{3/2}} \exp\left[-\frac{r^2 + r_0^2 + (z - z')^2}{4a(\tau - \tau')}\right] I_0\left[\frac{rr_0}{2a(\tau - \tau')}\right] d\tau' \quad (2.16)$$

As for the infinite model, the z -coordinates of the rings are defined as $z' = \pm(n+0.5)b$, $n=0, 1, 2, 3, \dots$. Accordingly, the temperature response in the medium to all the ring sources is founded to be:

$$\theta_{r,i} = \frac{q_l b}{2\pi\rho c} \sum_{n=-\infty}^{\infty} \int_0^{\tau} d\tau' \int_0^{2\pi} G(z' = nb + 0.5b) d\phi' = \quad (2.17)$$

$$\frac{q_l b}{8\rho c} \sum_{n=-\infty}^{\infty} \int_0^{\tau} \frac{1}{[\pi a(\tau - \tau')]^{3/2}} \exp\left[-\frac{r^2 + r_0^2 + (z - nb - 0.5b)^2}{4a(\tau - \tau')}\right] I_0\left[\frac{rr_0}{2a(\tau - \tau')}\right] d\tau'$$

While keeping the ring source simplification, the heat source is considered to be buried in a semi-infinite medium with limited length, stretching from h_1 to h_2 from the ground boundary. The coils may then be approximated as $m = \text{int} [(h_2 - h_1)/b]$ ring pieces. Again, the images are set symmetrical to the boundary, and the solution for the finite-length ring-coil heat source model is achieved as:

$$\theta_{r,f} = \frac{q_l b}{2\pi\rho c} \int_0^{\tau} d\tau' \left[\sum_{n=1}^m \int_0^{2\pi} G(z' = h_1 + nb - 0.5b) d\phi' - \sum_{n=0}^m \int_0^{2\pi} G(z' = -h_1 - nb + 0.5b) d\phi' \right] \quad (2.18)$$

$$= \frac{q_l b}{8\rho c} \int_0^{\tau} \frac{1}{[\pi a(\tau - \tau')]^{3/2}} I_0\left[\frac{rr_0}{2a(\tau - \tau')}\right] \cdot \exp\left[-\frac{r^2 + r_0^2}{4a(\tau - \tau')}\right] \cdot \sum_{n=1}^m \left\{ \exp\left[-\frac{(z - h_1 - nb + 0.5b)^2}{4a(\tau - \tau')}\right] - \exp\left[-\frac{(z + h_1 + nb - 0.5b)^2}{4a(\tau - \tau')}\right] \right\} d\tau'$$

In addition, a ring-coil heat source model is established and the analytical solutions of temperature responses induced by a spiral heat exchanger are obtained (Li et al., 2012). The spiral coils are distributed horizontally rather than vertically and thereby all coils are on the same plane. The virtual ring tube surface temperature response of the unit ring circle is calculated by a superposition of the contributions of the ring source itself and adjacent ring sources. The formula is then obtained to calculate the average tube surface temperature resulting from the dimensionless temperature responses rise at a point far from the ring source that maintains constant place. Firstly, the ring source model in an infinite medium is explored and the analytical solution of a single ring source is shown in Equation (2.19).

$$\begin{cases} \theta_{\text{inf}} = \frac{q}{4\pi k} \int_0^{2\pi} \frac{1}{r^*} \text{erfc}\left(\frac{r^*}{\sqrt{4a\tau}}\right) d\sigma \\ r^* = \sqrt{(r_0 \cos \sigma - r \cos \varphi)^2 + (r_0 \sin \sigma - r \sin \varphi)^2 + z^2} \end{cases} \quad (2.19)$$

Therefore, the total contribution of all spiral coils at the same horizontal plane is:

$$\theta_{\text{inf},P} = \frac{kr_0}{q} \sum_{i=0}^{n-1} \theta_{\text{inf}}(r_i, \varphi_i, z_i) \quad (2.20)$$

Secondly, the virtual method is used to get the temperature response of a single ring source in the finite medium and the corresponding formula is exhibited in Equation (2.21).

$$\begin{cases} \theta_f = \frac{q}{4\pi k} \int_0^{2\pi} \left[\frac{1}{r_+^*} \text{erfc}\left(\frac{r_+^*}{\sqrt{4a\tau}}\right) - \frac{1}{r_-^*} \text{erfc}\left(\frac{r_-^*}{\sqrt{4a\tau}}\right) \right] d\sigma \\ r_+^* = \sqrt{(r_0 \cos \sigma - r \cos \varphi)^2 + (r_0 \sin \sigma - r \sin \varphi)^2 + (-z' - z)^2} \\ r_-^* = \sqrt{(r_0 \cos \sigma - r \cos \varphi)^2 + (r_0 \sin \sigma - r \sin \varphi)^2 + (z' - z)^2} \end{cases} \quad (2.21)$$

Accordingly, the result of the total ring sources is as follows:

$$\theta_{f,P} = \frac{kr_0}{q} \sum_{i=0}^{n-1} \theta_f(r_i, \varphi_i, z_i) \quad (2.22)$$

2.2.1.5 Spiral heat source

In this model, spiral coils are represented by a spiral line, which means the connection of every two adjacent coils are taken into consideration. The spiral line with coil pitch b emits heat at the rate of $q_1 b$ and the coils are no longer symmetric with respect to the z -axis, the temperature distribution caused by the heat source is three-dimensional (3-D). The ground is regarded as a homogeneous medium, that is, the thermophysical properties inside and outside the cylindrical circumference of the spiral

coils are identical. The spiral line can be deemed as the sum of numerous point heat sources located at the spiral line, every point source emits heat at the intensity of $q_1 b d\phi' d\tau' / (2\pi)$ and the corresponding coordinates are $r = r_0$, $z' = b\phi' / (2\pi)$.

As a consequence, the temperature response of any point except the heat source induced by the infinite spiral heat source model is displayed as:

$$\begin{aligned}\theta_{s,i}(r, \phi, z, \tau) &= \frac{q_1 b}{2\pi\rho c} \int_0^\tau d\tau' \int_{-\infty}^{\infty} G(z' = b\phi' / 2\pi) d\phi' \\ &= \frac{q_1 b}{16\pi\rho c} \int_0^\tau d\tau' \int_{-\infty}^{\infty} \frac{1}{[\pi a(\tau - \tau')]^{3/2}} \cdot \exp\left[-\frac{r^2 + r_0^2 - 2rr_0 \cos(\phi - \phi') + (z - b\phi' / 2\pi)^2}{4a(\tau - \tau')}\right] d\phi'\end{aligned}\quad (2.23)$$

With regard to the finite spiral model, the source stretches from h_1 to h_2 below the ground surface, the virtual method is employed again to obtain the temperature response:

$$\begin{aligned}\theta_{s,f} &= \frac{q_1 b}{2\pi\rho c} \int_0^\tau d\tau' \left[\int_{2\pi h_1/b}^{2\pi h_2/b} G(z' = b\phi' / 2\pi) d\phi' - \int_{2\pi h_1/b}^{2\pi h_2/b} G(z' = -b\phi' / 2\pi) d\phi' \right] \\ &= \frac{q_1 b}{16\pi\rho c} \int_0^\tau \frac{d\tau'}{[\pi a(\tau - \tau')]^{3/2}} \cdot \exp\left[-\frac{r^2 + r_0^2}{4a(\tau - \tau')}\right] \\ &\quad \int_{2\pi h_1/b}^{2\pi h_2/b} \exp\left[\frac{2rr_0 \cos(\phi - \phi')}{4a(\tau - \tau')}\right] \left\{ \exp\left[-\frac{(z - b\phi' / 2\pi)^2}{4a(\tau - \tau')}\right] - \exp\left[-\frac{(z + b\phi' / 2\pi)^2}{4a(\tau - \tau')}\right] \right\} d\phi'\end{aligned}\quad (2.24)$$

2.2.2 Numerical methods for simulation

2.2.2.1 Finite difference model

For a single cylindrical energy pile, a simplified three-dimensional finite difference model was employed (Lee and Lam, 2013). The heat exchange pipes were installed into pile and all the pipes were identical, they have the same distance from the center of the pile. The end connection and the thermal capacitance of pipes were ignored, and the temperature of ground boundary was constant. In addition, the fluid kept the same rate in

every pipe and no groundwater flow existed.

2.2.2.1.1 Heat transfer outside pipe

A sector column was used to represent one pipe and the sector was circumscribed by the pile radius. Along the circumferential direction, the measurements were relative to the first pipe in the counter-clockwise direction. Thus, this heat transfer style was pure conduction and the corresponding energy equation is provided as:

$$\frac{T_{g,i,j,m}^{d+1} - T_{g,i,j,m}^d}{\Delta t} = \left(\frac{Q_{r_+} + Q_{r_-} + Q_{\theta_+} + Q_{\theta_-} + Q_{z_+} + Q_{z_-} + Q_{so} q_{\text{fact}}}{\rho c_{g,eq} \Delta A_{j,m} \Delta z_i} \right) \quad (2.25)$$

where the meanings of relevant parameters are listed in Table 2.1

Table 2.1 The symbols and the corresponding meanings outside pipe

Symbols	Meanings
T	Temperature (K)
Δt	Discretization time step (s)
d	Discretization step designation in time
g	Ground including all the regions outside the pipes
i, j, m	Ground discretization step designations in the z -, r - and θ -
z_-, z_+	Upstream z -direction, downstream z -direction
r_-, r_+	Upstream r -direction, downstream r -direction
θ_-, θ_+	Upstream θ -direction, downstream θ -direction
Q	Heat transferred into control volume of ground (W)
eq	Equivalent properties of control volume of ground
s, ρ, c	Soil, density (kg m^{-3}), specific heat capacity ($\text{J kg}^{-1} \text{K}^{-1}$)
q_{fact}	Load factor to be multiplied in calculating the source term
ΔA	Cross-sectional area of control volume of ground (m^2)
Δz	Length of control volume of ground in z -direction (m)

2.2.2.1.2 Heat transfer inside pipe

Because fluid flows along the pipe and its temperatures become strongly coupled, the fluid temperature for each control volume should be determined sequentially in an iterative manner, the pipe connection configuration based on a specified temperature profile along each pipe surface must be taken into account. Considering that the cross-sectional area of the pipes is much smaller than that of the surface, the heat conduction in the axial direction is neglected. The corresponding energy equation is given as:

$$q_{p,u,i} = \frac{m_f c_f (T_{f,u,i}^{n+1} - T_{f,u,i+1}^{n+1})}{dz_i} \quad (2.26)$$

$$T_{f,u,i}^{n+1} = \frac{1}{8} (T_{g,i,j,m}^{n+1} + T_{g,i,j,m+1}^{n+1} + T_{g,i,j+1,m}^{n+1} + T_{g,i,j+1,m+1}^{n+1} + T_{g,i+1,j,m}^{n+1} + T_{g,i+1,j,m+1}^{n+1} + T_{g,i+1,j+1,m}^{n+1} + T_{g,i+1,j+1,m+1}^{n+1}) \quad (2.27)$$

where the meanings of relevant parameters are listed in Table 2.2

Table 2.2 The symbols and the corresponding meanings inside pipe

Symbols	Meanings
T	Temperature (K)
n	Discretization step designation in time
g	Ground including all the regions outside the pipes
i, j, m	Ground discretization step designations in the z -, r - and
m	Mass flow rate (kg s^{-1})
f	Circulating fluid around the pipes in the energy pile
q_p	Pipe load (W m^{-1})
u	Pipe designation
c	Specific heat capacity ($\text{J kg}^{-1} \text{K}^{-1}$)
dz	Ground grid spacing in z -direction (m)

2.2.2.2 Comsol Multiphysics package

Hassani Nezhad Gashti et al. (2013) proposed a numerical modeling of thermal regimes in steel energy pile foundations, and this 3-D model employs Comsol Multiphysics package. By means of comparisons between numerical model and experimental results, the agreement can be acceptable and therefore the model is proven reasonable. The actual depth of the pile is approximately 30m in the case study, the domain extension $10\text{m} \times 10\text{m}$ is selected for the finite volume mesh and the height of soil domain is 30m.

For the types of heat exchange tubes inside the pile, one is a single U-tube and another is a double U-tubes. There are about 230, 000 tetrahedral elements chosen for modeling single U-tube pile and nearly 260,000 tetrahedral elements for the double U-tube pile. The meshing of domains is continuously refined to achieve constant output of the model.

The power output of the pile foundation GHEs can be calculated by way of the following equation:

$$W = q_l \cdot \rho \cdot c_p \cdot \Delta T_t \quad (2.28)$$

And the total energy output is:

$$Q = \int_{t_1}^{t_2} W \cdot dt \quad (2.29)$$

The heat energy equation of the whole heat transfer is obtained in Equation (2.30)

$$(\rho c_p)_{eq} \frac{\partial T}{\partial t} + \rho c_p \cdot u \cdot \nabla T = \nabla \cdot (k_{eq} \nabla T) + Q \quad (2.30)$$

where the meanings of relevant parameters are shown in Table 2.3.

Table 2.3 The symbols and the corresponding meanings of energy pile with U-tube

Symbols	Meanings
ρ	Density of heat-carrier-fluid (kg / m ³)
c_p	Fluid heat capacity at constant pressure (J / kg · K)
u	Heat-carrier-fluid velocity vector (m / s)
Q	Heat sources other than viscous heating (W / m ³)
$(\rho c_p)_{eq}$	Equivalent heat capacity at constant pressure (J / kg · K)
T	Absolute temperature (K)
t	Time (s)
k_{eq}	Equivalent thermal conductivity (W / m K)
q	Heat flux by conduction (W / m ²)
l	Pile length (m)

2.2.2.3 Coupled multi-physical finite element modeling

A thermo-hydro-mechanical two dimensional (2-D) solution to the three-dimensional (3-D) problem has been proposed (Dupray et al., 2014). It can be employed for not only studying the thermal behavior of the energy pile but also evaluating the structural consequences. The coupled multi-physical finite element modeling is conducted. The energy balance equation of the saturated soil is given as follows:

$$\frac{\partial((\rho c_p)(T - T_0))}{\partial t} + \text{div}(f_T) - Q_T = 0 \quad (2.31)$$

where f_T and Q_T are respectively the heat flow and a volume heat source, and ρ and c_p are respectively the density and specific heat of the mixture (solid matrix with voids filled by liquid). In addition, T means the temperature and T_0 delegates the initial temperature.

2.3 Studies on heat transfer experiments of pile foundation GHEs

2.3.1 The heat transfer comparisons of energy piles with different types of tubes

The pile foundation GHEs are employed in the GCHP system for achieving district heating and cooling. Several types of heat exchange tubes are installed into vertical piles and the running performances can then be compared with each other, the most efficient one can be determined by this way (Gao et al., 2008). The view of on-site energy piles is shown in Figure 2.1.



Figure 2.1 The construction drawing of on-site pile foundation GHEs

By means of a series of performance tests, the experimental data of heat exchange abilities are obtained. These types include U-tube, double U-tubes, W-tube and triple U-tubes. The thermophysical properties of the underground medium and backfilling materials inside the piles are constant, and the materials of different types of tubes are the same. To emulate the circulating pumps, a water tank of constant temperature and two electric heaters are put to use, water flows through the tubes and keeps its

temperature stable at about 35°C. The supply and return temperatures are measured by platinum resistance thermometers with A-class PT100 sensors; the volumetric flow rate is measured by a turbine flow meter. To observe the heat transfer performance of the four types of GHEs, dynamic measurements are conducted and the results are then obtained when all parameters attain stable states. The performances of these types of GHEs are listed in Table 2.4 and the comparisons can be made.

Table 2.4 Heat transfer comparisons of different types of tubes

Types	Water flow (m³/h)	Energy output (W / m)	Heat transfer coefficient (W / m °C)
W-shaped	0.342	83.05	5.840
W-shaped and double flow rate	0.342×2	94.25	6.230
Single U-shaped	0.342	57.84	3.891
Double U-shaped	0.342×2	89.53	5.780
Triple U-shaped	0.342×3	108.07	6.947

Energy outputs and heat transfer coefficients of different types of heat exchange tubes are calculated, the temperature of the soil under 5 m depth stays almost constant at about 18.2°C. By way of comparisons, the heat transfer ability of every type of tube can be displayed.

In addition, Jalaluddin (2011) conducted an experimental study about several types of steel pile foundation GHEs, U-tube, double-tube and multi-tube are each installed into different piles. The cooling modes are employed to investigate the heat transfer performance of piles with different tubes, and the water passes tubes for releasing heat to the ground. The flow rates of water are respectively set as 2, 4, and 8 liters / min. Some

thermal resistances are installed into different positions along the depth direction of the pile so that temperatures can be measured.

The water temperatures of both the inlet and the outlet are also recorded at set time interval to enable the heat exchange rate to be acquired. The final argument is that the double-tube has the highest heat exchange rate, an multi-tube and U-tube respectively occupy the second and the third places. Afterwards, the flow rates are increased to observe the change of heat transfer abilities of the different tubes; the results show that the heat transfer rates of double-tube and multi-tube can continue to increase with the flow rates, however, the U-tube tends to be constant. Accordingly, the double-tube and multi-tube can be operated in a wide range, and the double-tube is the most attractive choice.

2.3.2 The thermo-mechanical behavior of energy pile

There is no doubt that the combination of pile and heat exchange tubes is a novel technology, because the supporting parts of buildings are fully utilized to share cooling load or heating load. However, the interrelationship between mechanical performance and thermal performance is a significant issue that requires further attention. At present, the understanding about mechanical behavior of energy piles under heat exchange condition is a little.

Firstly, Laloui et al. (2006) presented a model which is named as “thermo-hydro-mechanical” (THM), and it was derived from homogenization theory (Modaressi et al, 1991). The influences that thermal behaviour and thermal effects exert on the mechanical behaviour of piles are discussed based on the THM model, which involves some equations that are listed in Equation (2.32).

$$\left\{ \begin{array}{l}
\text{div } \sigma + \rho g = 0, \rho = n\rho_f + (1-n)\rho_s \\
\frac{\partial P}{Q} - \frac{\partial T}{Q} + \text{div} \partial u_{rf} + \text{div} \partial u_s = 0 \\
Q = \frac{1}{[n\beta_f + (1-n)\beta_s]} \\
Q' = \frac{1}{[n\beta'_f + (1-n)\beta'_s]} \\
\rho c \partial T / \partial t + \rho_f c_f \text{grad} T \partial u_{rf} / \partial t + \rho c T \text{div} \partial u_s / \partial t + \rho_f c_f T \text{div} \partial u_{rf} / \partial t \\
- \left[\frac{\beta'_f}{\beta_f} \text{div}(n \partial u_s / \partial t + \partial u_{rf} / \partial t) + \frac{(1-n) \partial \sigma' / \partial T}{d\varepsilon_s / dt} \right] T - \text{div}[\Lambda \text{grad} T] = 0 \\
\dot{\varepsilon} = \dot{\varepsilon}^{Te} + \dot{\varepsilon}^P
\end{array} \right. \quad (2.32)$$

And the parameters and the corresponding meanings are shown in Table 2.5.

Table 2.5 The symbols of THM model and the corresponding meanings

Symbols	Meanings
σ, σ'	Total stress tensor, effective stress tensor
ρ	Total average mass density
ρ_s, ρ_f	Mass density of solid and fluid, respectively
n, g	Porosity, gravity vector
P, T	Pore water pressure, temperature
u_{rf}	Relative fluid velocity
u_s	Solid displacement
c	Total equivalent specific heat
c_f	Fluid specific heat
t	Time (s)
β_f, β'_f	Compressibility of solid, effective compressibility of solid
β_s, β'_s	Compressibility of fluid, effective compressibility of fluid
$\dot{\varepsilon}$	Total strain
$\dot{\varepsilon}^{Te}, \dot{\varepsilon}^P$	Linear thermo-elastic strain rate, plastic strain rate

Secondly, Gashti et al. (2014) finished significant experiments to check the thermo-mechanical behaviour of energy piles, because this behaviour in structural and geotechnical terms is influenced by temperature variations in the pile shaft induced by heat exchange. Energy piles release heat in summer and abstract heat in winter, and the corresponding operation modes are divided into cooling and heating under which the behaviour is analyzed. The schematic diagrams of energy piles in the running states are depicted in Figure 2.2

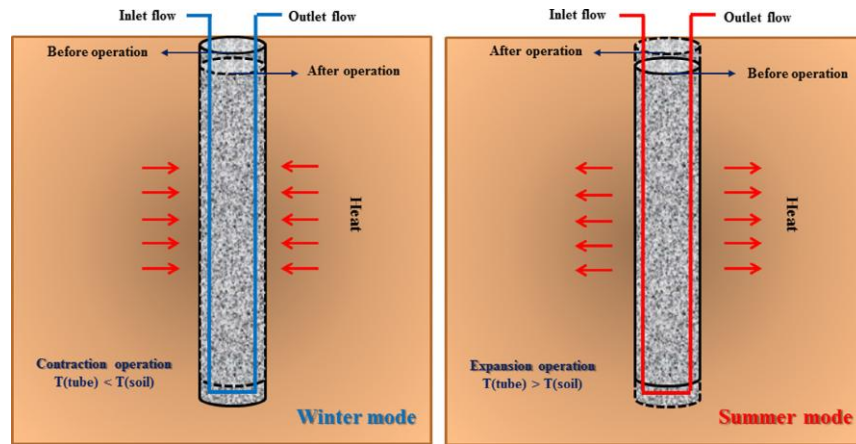


Figure 2.2 The thermal-mechanical behavior of energy pile

The U-tubes are installed into composite piles to enable both the structural and geotechnical resistances to be calculated. The pile and the surrounding soil are assumed to behave within a linear thermo-elastic range, and the soil–pile interface is assumed to make perfect contact. It is clear that the pile respectively presents contraction and expanding trends in the heating and cooling conditions. Accordingly, the pile shaft is in expansion mode in summer and with compressive stress added in winter. After the total contribution of the cooling and the heating, the stresses are about 20% of the ultimate compressive strength of typical concrete. Whether the expansion result or compressive effect is dominant depends on the comparison between the heating load and the cooling

load. When the cooling load is larger than the heating load, the expansion degree is stronger than the compressive level, and vice versa.

2.3.3 Heat exchange capacity of CFG pile geothermal exchangers

The heat exchange capacities of the cement-fly-ash-gravel (CFG) piles are investigated by means of the thermal response test (TRT) and thermal performance test (TPT) (You et al., 2014). The design method of borehole GHEs is usually adopted for that of pile foundation GHEs (NHBC, 2010) and therefore the obvious errors inevitably occur. Thus, Shuang You et al. propose that the innovative way of obtaining the heat transfer capacity of energy pile can be achieved based on an in-situ full-scale test. Additionally, all the influential factors of the heat exchange capacity are researched. These tests are conducted not only for single pile but also for grouped piles. The constant heat flux and the constant inlet temperature are respectively tested by TRTs and TPTs. The profiles and layout of CFG pile and the corresponding sensors are shown in Figure 2.3.

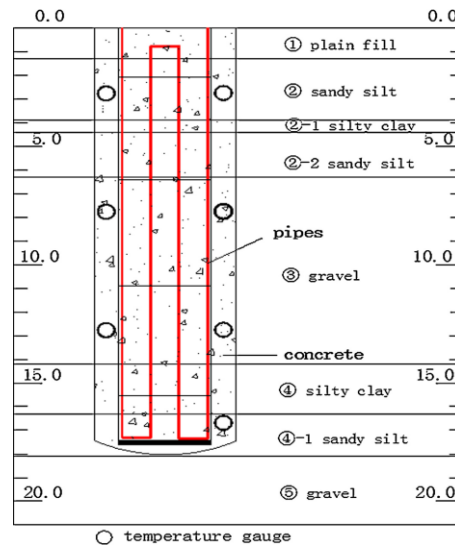


Figure 2.3 The profile and layout of the CFG energy piles and sensors

The piles are drilled and filled with concrete and reinforcement cage bounded with W-tubes is then immediately installed. The pile is then back-filled with gravel. The material of the tube is high-density polyethylene (HDPE) which keeps the diameter at 25mm and the depth at 72 m. Thermal sensors are set at four sections, that is, 3 m, 8 m, 13 m, and 18 m from the pile top to the bottom. The temperature variations along the pile are monitored section by section.

The heat transfer capacity of single pile and grouped piles obtained by means of TRT are given in Table 2.6.

Table 2.6 The heat transfer capacity of single pile and grouped piles by means of TRT

Pile type	Heating power of every pile (W)	Thermal conductivity (W/m°C)	Thermal resistance (m/°C/W)	Average temperature of inlet and outlet water (°C)
Single	1750	2.78	0.33	34.35
Grouped	1750	2.13	0.39	34.90

By using TPT, the following results are produced.

Table 2.7 The heat transfer capacity of single pile and grouped piles by means of TPT

Condition	Pile type	Inlet water temperature (°C)	Total heat exchange rate (W)	Heat exchange rate per meter (W/m)
Cooling	Single	5	-939	-58
	Grouped	5	-838	-46
Heating	Single	35	2160	116
	Grouped	35	2070	111

In addition, Morino made use of soil as heat sink and heat source (1994); a steel pile

is employed as a heat exchanger to exchange thermal energy with the surrounding soil. The external diameter of the steel pile is 400mm and the vertical depth is 20 m. The heat transfer quantity from pile to the soil is recorded and the variations of the water temperature in a steel pile are also studied. The heat exchanged with the soil per day is 210 MJ as a heat sink; and 113–150 MJ as a heat source during a short-term experiment. The average heat transfer capacity of energy pile during the whole operating period i.e. the sum of cooling and heating stages, is shown in Table 2.8.

Table 2.8 The heat transfer capacity during the whole process

Parameter	Value
total amount of heat collection	5.6GJ
heat collection rate	628kJ/m/h
average heat collection rate (including the “off ” time)	97 kJ/m/h
the minimal water temperature in the pile	4.2°C
total operation time	443h

2.3.4 Heat transfer performance of the spiral GHEs

Lee et al. (2015) investigated the thermal performance of spiral GHEs that are respectively installed vertically and horizontally. The pre-stressed high-strength piles are employed for vertically burying spiral heat exchange coils, and all coils are set along the pile’s depth direction and they locate at the central area of the space. The horizontal GHEs are those spiral coils that are installed at the bottom of the building foundation. Figure 2.4 shows the structural shapes of both vertical and horizontal spiral coils.

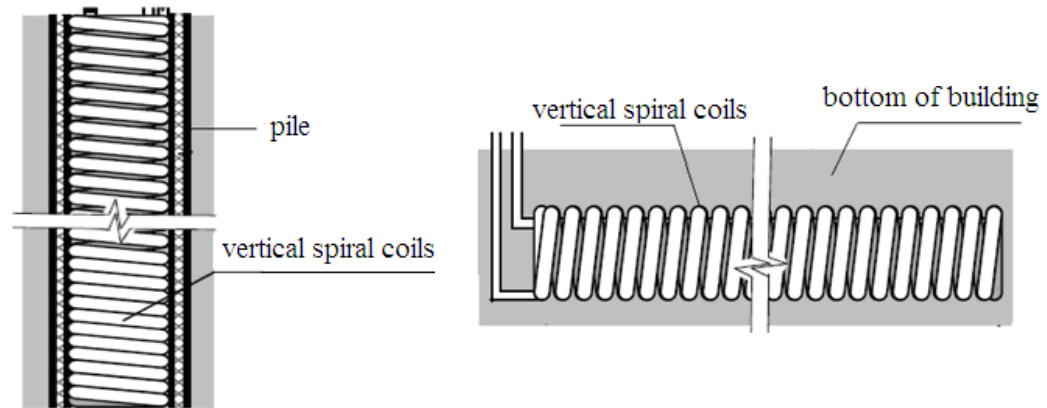


Figure 2.4 The installation types of spiral coils

The coefficients of performance, that is, COP of vertical and horizontal spiral coils, are both obtained; the heat transfer rate of vertical case is higher than that of horizontal case. In the short term, the vertical and horizontal cases have the same initial payback period, but the vertical case has larger savings (28%) than the horizontal case in the long term.

In addition, Park et al. (2015) studied the heat transfer performance of energy pile with spiral coils while the coil pitches respectively employ tight and loose values. The corresponding researches show that the spiral coils with tight pitch can provide more heat transfer quantity; however, the relative heat transfer performance is not directly in proportion to the length of spiral coils because the tight pitch may cause thermal interference between each coils of the spiral tube. The optimum configuration of spiral coils installed in the piles should be determined based on comprehensive factors, including the heat exchange efficiency, the increased material cost, the construction difficulties in case of an exceedingly longer spiral coils and the thermal performance of spiral coils.

2.3.5 Field performance of an energy pile system

The field performance of GCHP is tested by experiment while energy piles are employed for space heating (Hamada et al., 2000), and the heat exchange tubes are buried into piles of an actual building locating in Sapporo. As is well known, piles can be divided into bearing and friction cases according to the mechanism, in this system friction piles are taken into account for acting as GHEs, because the predetermined lengths can make them highly advantageous for use in air conditioning design.

A single U-tube is installed into every pile and then three tests are carried out to specify the design of pile foundation GHEs, because this type of tube has advantages as regards the economic efficiency and workability. The period of heating operation is from mid-December 2000 to late-April 2001. After such a long-term space heating operation, the corresponding measurements show that the seasonal average temperatures of circulating liquid returning from the underground and pile surfaces are respectively 2.4°C and 6.7 °C. The average operating results of the whole heating period are provided in Table 2.9 which lists the field performance of the energy pile system.

Table 2.9 The operating result of the heating period of the energy pile system

Parameter	Value
Room temperature	23.3°C
Relativity	38.9%
Fluid supply temperature to underground	-0.6°C
Fluid return temperature from underground	2.4°C
Surface temperature of friction pile	6.4°C

Fluid supply temperature to building	30.4°C
Fluid return temperature from building	28.4°C
Space heating amount	503.8MJ / day
Power consumption	173.3 MJ / day
COP	3.9

It is seen that the data given in Table 2.9 indicates that the field performance of the energy pile system is satisfactory.

2.4 Theoretical research on borehole GHEs with groundwater advection

Groundwater flows along a certain orientation under the role of the local hydraulic gradient, and considering that the borehole GHEs have been the mainstream in recent years, the corresponding research on impacts exerted by groundwater on heat transfer is more deserving. It is seen that borehole GHEs are usually taken into consideration for most of the engineering projects, the heat transfer and economic performances can be improved in the event of groundwater advection. The investigations including analytical and numerical methods are demonstrated in the following sections.

2.4.1 The analytical methods

Firstly, an equation including both conduction and groundwater advection has been established to estimate the groundwater impact on the heat transfer of borehole GHEs (Diao et al., 2004). The Green function is adopted to obtain the analytical transient solution of the temperature response induced by a line heat source in an infinite medium.

The two-dimensional expressions and the corresponding dimensionless forms are obtained, and authors' computations explain that the groundwater advection can change the underground conductive temperature distribution. The temperature response rise can be suppressed and all response can reach stable states finally. Thus there is a belief that the research provides theoretical basis for the design of borehole GHEs.

The temperature response is denoted as: $\theta = t - t_0$, where t and t_0 are respectively the actual temperature and the initial temperature, and Equation (2.33) gives the expression of θ .

$$\theta(x, y, \tau) = \frac{q_l}{4\pi k_0} \int_0^\tau \frac{1}{(\tau - \tau')} \cdot \exp\left[-\frac{[x - u(\tau - \tau')]^2 + y^2}{4a(\tau - \tau')}\right] d\tau' \quad (2.33)$$

The temperature distribution around borehole GHE changes with the time and the isothermal of different time are depicted in Figure 2.5, where $Fo = a \tau / r_0^2$.

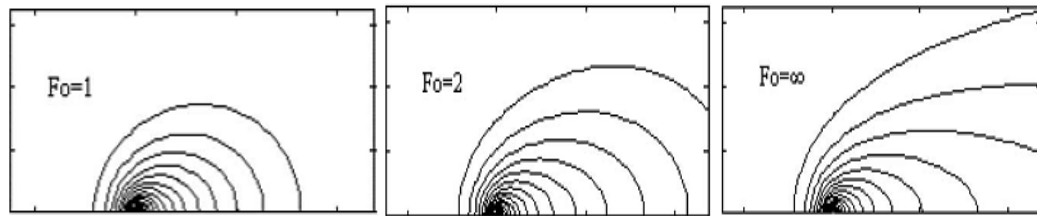


Figure 2.5 Temperature distribution around borehole GHE while infinite line heat source with groundwater advection is employed

Secondly, Molina-Giraldo et al. (2011) proposed a moving finite line heat source model and the ground boundary effect is considered in this model. Accordingly, the research related to groundwater seepage extends from two-dimensional (2-D) to three-dimensional (3-D) model, which means the heat transfer along three directions i.e. x , y , and z directions are all analyzed while groundwater flows through the borehole GHE.

The analytical expression of temperature response is given in Equation (2.34).

$$\theta(x, y, z, t) = \frac{q_l}{2\pi\lambda} \exp\left(\frac{ux}{2a}\right) \left[\int_0^H f(x, y, z, t) dz - \int_{-H}^0 f(x, y, z, t) dz \right] \quad (2.34)$$

where

$$f(x, y, z, t) = \frac{1}{4r} \left[\exp\left(-\frac{ur}{2a}\right) \operatorname{erfc}\left(\frac{r-ut}{2\sqrt{at}}\right) + \exp\left(\frac{ur}{2a}\right) \operatorname{erfc}\left(\frac{r+ut}{2\sqrt{at}}\right) \right] \quad (2.35)$$

The investigations into the finite moving line heat source can once again prove that the heat transfer around borehole GHE is affected by groundwater advection. Compared with the infinite moving line heat source model, the finite case is more important especially when the heat transfer time is long. In addition, the temperature response caused by the infinite model is always larger than that of the finite model while other conditions are the same. The temperature distributions of infinite and finite cases are shown in Figure 2.6, and it is clear that the temperature response of the latter is weaker.

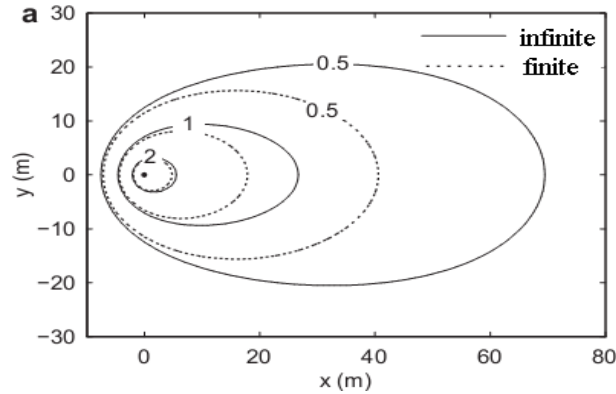


Figure 2.6 Isothermals of both infinite and finite moving line heat source models

Fujii et al. (2005) developed a mass and heat transport model to simulate the behaviour of a large-scale GSHP system in the Akita Plain, northern Japan. This model is used to study different operational schemes and to maximize the heat extraction rate

of the GCHP system. The heat transfer performance of GHE is simulated by means of this 3-D well model, and the horizontal area is $5\text{m} \times 5\text{m}$ and the depth that is equal to GHE length is 50m, and includes five layers. Groundwater flows from the east to the west, and its velocity keeps stable at about 1.4×10^{-4} m/day and this value can be put into the simulation model that is validated by the cylindrical source function G (Ingersoll, 1954). After detailed simulation and calculation, the results indicate that the heat extraction rates of GHE are enhanced if ground flow attains a certain degree, in other words, if the Peclet number is equal to or higher than 0.1, the effect of groundwater flow becomes obvious.

2.4.2 The numerical methods

Firstly, Lee and Lam (2012) explored a modified three-dimensional difference model for borehole GHEs located in multi-layers with inhomogeneous groundwater flow, and the model is validated by the simulation software FLUENT. The model is then used to study the effect of groundwater table on the performance of borehole GHE under the condition of various groundwater velocities. Research on the influence that velocity has on the table effect in a full-groundwater-flow is conducted; afterwards the trends of the fluid temperature leaving a borehole are investigated. The most significant aspect is that the performance of a single borehole GHE is studied based on different groundwater tables. Some parameters involved in the model simulation are introduced in Table 2.10.

Table 2.10 Values of various parameters used for model

Parameter	Value
Borehole radius (m)	0.055

Insulated length of borehole(m)	5
Effective length of borehole(m)	110
Thermal conductivity of pure soil ($\text{W m}^{-1} \text{K}^{-1}$)	3.5
Volumetric heat capacity of pure soil ($\text{kJ m}^{-3} \text{K}^{-1}$)	2160
Thermal conductivity of groundwater ($\text{W m}^{-1} \text{K}^{-1}$)	0.614
Volumetric heat capacity of groundwater ($\text{kJ m}^{-3} \text{K}^{-1}$)	4190
Porosity of soil	0.1
Applied borehole load (W)	3300

Secondly, numerical evaluations on heat transfer of different types of borehole GHEs arrays were conducted while groundwater advection exists (Choi et al., 2012). The 2-D heat transfer model containing conduction and advection is utilized to explore the effects of both the direction and the rate of groundwater flow. Three types of arrays including rectangular, L-type and single line are used in the research process; this model is based on the finite element method and the significant conclusion is that the mean temperature of circulating fluid drops with the time as a result of the groundwater advection. The maximum drop of this temperature is illustrated in Table 2.11.

Table 2.11 Annual maximum drop of mean fluid temperature

Time (year)	Single line-type (finite element)	L-type (finite element)	Rectangular (finite element)
1	-5.4°C	-5.5°C	-5.5°C
2	-5.9°C	-5.9°C	-6.1°C
5	-6.6°C	-6.7°C	-7.3°C
10	-7.3°C	-7.5°C	-8.4°C
15	-7.8°C	-8.0°C	-9.1°C

According to Table 2.11, no matter what type of the borehole GHEs arrays is adopted, the advection influence is inevitable only if the groundwater seepage phenomenon exists, and also if the impact degrees exerted by different types of arrays on the mean fluid temperatures are nearly equal.

Thirdly, Zanchini et al. (2012) carried out an analysis for the long-term impact which groundwater advection imposes on borehole GHEs, the COMSOL Multiphysics were implemented based on the finite element simulation. A certain range of Peclet numbers was selected and two regular time periodic heat loads were considered. The ground was modeled as a Darcy porous medium while the heating load in winter and cooling load in summer were both taken into account. The results indicate that the groundwater flow does not reduce the effects of hourly peak load but yields an important improvement of the long-term performance in case the Peclet numbers lie in a certain range.

Lastly, another outstanding numerical method is to employ physical and mathematical models of single tube cylindrical models with equivalent diameter (Liu et al., 2012), the aim was to determine the influence of groundwater seepage on underground temperature fields. The differences are caused because both different thermal conductivities and different porosities are respectively compared, and the domain factors are determined.

2.5 Studies on groundwater advection experiments of borehole GHEs

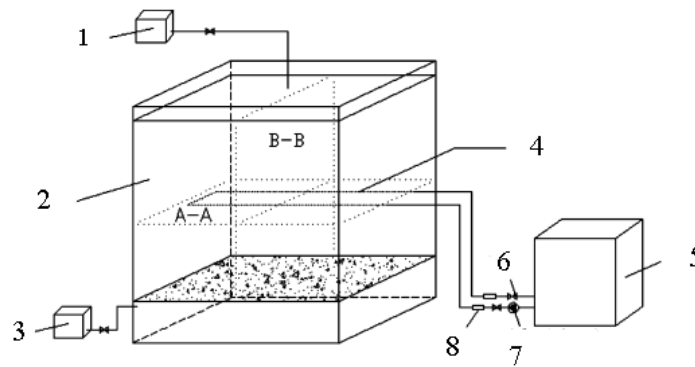
A number of groundwater seepage experiments have been conducted to check the groundwater's influence. The aim in this regard was to enable the simulation results of theoretical research to be validated by experimental findings.

Firstly, Fan et al. (2007a) coupled soil conduction and advection experiments. These experiments were implemented in saturated soil without seepage and soil with seepage. To better understand their influences on the heat transfer, the heat load of GHE, initial temperature of soil and the groundwater flow rate were all investigated. A sandbox was established and an electric heater was set along its center line for simulating the line heat source, the fixed water tank and mobile water tank were installed on the sandbox in order to create stable heat pressure, to enable the different seepage velocities to be achieved. The power of electric heater could be adjusted to enable the seepage experiments to be simulated under the condition of different heating loads.

Secondly, a thermal performance experiment of a borehole GHE in Baoding of China was conducted when the groundwater flow exists (Wang et al., 2009). The influence of groundwater flow on the heat transfer performance of borehole GHE was analyzed. The experimental setup is composed of heat source and cool source, a measuring system, a borehole GHE, water tank and so on. The circulating fluid was stored in an insulated water tank before it flows through the GHE, and the main role of this tank is to keep the water temperature stable. The measuring system includes Pt1000-type temperature sensors, electronic magnetic flow meters and other auxiliary instruments, thus both the temperature responses of some locations and the flow meter of groundwater can be obtained. This experiment is successfully and fully studied the impact of groundwater seepage. It was found that the heat transfer effect of borehole GHE with groundwater advection was better than that of pure conduction, and the stronger the velocity, the better the heat transfer performance.

Thirdly, Feng (2011) established an experimental rig with a sandbox; the U-tube was

installed into sandbox to simulate a borehole GHE. These scholars wanted to check the improvement of heat transfer capacity in case groundwater seepage is not ignored. For this reason, the high level cistern was set and therefore the water was able to drop and pass U-tube inside the sandbox under the role of gravity. The aim was to simulate the groundwater seepage and a lower water box was installed to retrieve the water leaking from the sandbox. In addition, an electric heating water tank was applied to heat the circulating water of U-tube. By this method, the water is able to circulate under the role of water pump, the diagram of the experiment rig is shown in Figure 2.7.



1. high level cistern 2. sandbox 3. lower water box 4. U-tube 5. heating water tank
6. valve 7. water pump 8. PT100 temperature sensor

Figure 2.7 The schematic diagram of experiment rig of groundwater flow

2.6 Studies on impacts which groundwater exerts on pile foundation GHEs

Go et al. (2014) conducted an experimental research on the temperature rise around pile foundation GHEs. Spiral coils were installed into a precast high-strength concrete pile and temperature response tests were then implemented to evaluate the heat transfer performance. The long-term effect yielded by groundwater advection on underground

temperature was examined. The energy pile was operated for a long period of time and the results show that the average temperature rise is weakened by groundwater advection. Comparisons between the groundwater advection's existence and absence were made, and the corresponding calculations were conducted while groundwater with various velocities passed through the pile arrays.

On the whole, the investigations into the influences exerted by groundwater on energy pile system are a little not only in theoretical methods but also in experiments; therefore the significance of this thesis is obvious.

2.7 Study on obtaining the velocity of groundwater

The seepage degree of groundwater is determined by its velocity and therefore how to obtain this parameter is vital, it is of the essence to realize the value and orientation of groundwater velocity for calculating the heat transfer. The references reveal that some instruments such as groundwater flow meters are put to use for directly testing the velocity. However, it is undoubtedly hard to obtain the velocity in such a way as the installation and operation have presented many difficulties. As a consequence, a number of methods have been being explored in recent years.

Firstly, the unsteady moving line heat source model is usually adopted to study heat transfer between borehole GHE and the surrounding medium when groundwater flows along the positive direction of x -axis. Regarding this, the model is made use for optimization involving the nonlinear simplex method, and then the velocity can be obtained (Yu et al., 2007). The key step of optimization is to employ the parameter estimation method because the groundwater velocity is difficult to be acquired. Explain

in detail, the circulating liquid extracts or releases heat when it flows through borehole GHE, its inlet temperature, outlet temperature and flow meter with the time are recorded. As is well known, thermal conductivity and volumetric specific heat capacity of underground medium as well as the groundwater velocity are three unknown parameters; the functions of the sum of variance are established to respectively estimate the values of these three parameters in the light of optimization techniques (Wei, 1987).

Secondly, despite the direct simulation for random field of groundwater velocity located in aquifers of spatially variable has been developed in recent years, homogeneous hydraulic conductivity is still stochastic. Then, the stream functions are taken into consideration to make a dual description of groundwater flow (Konecny and Fürst, 2010). The flow with the steady state is a necessary assumption, there have far boundaries and have no sources and sinks. A first-order approximation of the spectra of the random stream function and the random velocity field are obtained by means of a perturbation approach. In view of the parsimony in the use of parameters, the study on the generation of random velocity field with the help of stream functions is worthwhile. Accordingly, it is certain that only a scalar random field is generated. Therefore, the Mikhailov's method, that is, the partitioning and randomization of the spectrum, is employed to simulate the homogeneous Gaussian field (Mikhailov, 1978). In addition, the problems of conditional simulation of random velocity fields honoring measured velocity values at several locations are tackled. In a word, this generation method is demonstrated based on the comparison between the empirical and theoretical spectra. Admittedly, this is a significant progress during the period of studying groundwater velocity.

Thirdly, the velocity of the groundwater which is in a screened well can be rapidly measured by an automated on-line instrument (Patterson et al., 2010). A carbon dioxide gas tracer is an indispensable element of the vital instrument which is applied for measuring. The tracer can be periodically delivered to the permeable chamber that is within the well.

The diffusion's rate is fast while the gas tracer passes the wall of the permeable chamber. One aspect of the groundwater/chamber interface is that the gas entrainment is proportional to the velocity of groundwater flowing through the chamber. A second aspect relates to the ability of mass transfer passing this interface to control the effective diffusion entering the groundwater. The gas tracer is delivered periodically and the reduction in concentration of the tracer can be monitored from the permeable chamber, hence the groundwater velocity is determined multiple times every day.

In addition, the laboratory experiments are conducted in a calibrated flow chamber, and the corresponding results explain that the instrument can be used to accurately and reliably obtain the groundwater velocities while the interval is 3 hours and the flow rates are from 25m/year to 300 m/year. Furthermore, the velocity field testing by way of the velocity probes at multiple well locations in a sandy aquifer can provide velocities consistent with another monitoring technique and site modeling.

2.8 Summary

According to the descriptions above, the researches about the heat transfer of GHEs and groundwater advection have made progress not only academically but also experimentally. The application of pile foundation GHEs is a significant development of

GCHP technology because both heat transfer and civil structure have been effectively combined. Investigation into pure conduction of energy pile has been being carried out until nowadays. However, of further interest is the association of the groundwater flow and the energy, which is a novel research field that worth paying attention.

The employment of pile foundation GHEs has obvious advantages in terms of reducing initial cost and saving land area. Consideration of the groundwater seepage phenomenon provides an encouraging mean to enable further improvement of the heat transfer performance of pile foundation GHEs. As such the original conduction could be converted to the combined heat transfer including conduction and groundwater advection, enabling the heat accumulation around pile to be alleviated. The improvement degrees that groundwater seepage yields on the heat transfer performance are determined by the groundwater velocity. On the basis of the research work conducted by scholars or experts, the valuable study on the influence exerted by groundwater on pile foundation GHEs can be implemented.

The novel investigations presented in this thesis focuses on the analytical models of pile foundation GHEs with groundwater advection. The corresponding models will be proposed according to the principles of “from simple to complex” or “from abstract to concrete”. The exploration on heat transfer under the condition of combined heat transfer is to be conducted. The on-site experiments of energy pile should be conducted to check the heat transfer ability and verify the corresponding simulation models. At the same time, how to obtain the velocity including its value and orientation is a vital problem because this parameter reflects the intensity of groundwater advection. For this reason, the study presented in this thesis proposes a significant and feasible methodology

to achieve the groundwater velocity. It is hoped that a firm foundation will be laid for further research into exploring the influence of groundwater advection on pile foundation GHEs.

CHAPTER 3 SOLID CYLINDRICAL HEAT SOURCE

MODELS WITH GROUNDWATER FLOW

3.1 Introduction

Since the pile's interior is a considerable volume filled with the concrete or other mediums, the corresponding heat capacity cannot be ignored. Spiral coils are arranged close to the internal surface of the pile, creating an integrated system of pile with interior medium and coils. The filling material is regarded identical as that of the outside; it is inadvisable to still model the GHE as a line or hollow cylindrical heat source. It is a challenge to investigate the heat transfer of energy pile being passed by groundwater, and the research procedure starts with simple cases and move to more complex ones. Thus, to explore the advection influence that groundwater exerts on the energy pile, solid cylindrical heat source seepage models are first proposed.

This model treats the energy pile as a solid cylindrical surface heat source with its own interior heat capacity, and disregards the detailed configuration of the spiral coils. The surface of this model is deemed as evenly-distributed heat source emitting heat at a uniform rate (Kavanaugh and Rafferty, 1997). The geometry of the model is shown in Figure 3.1.

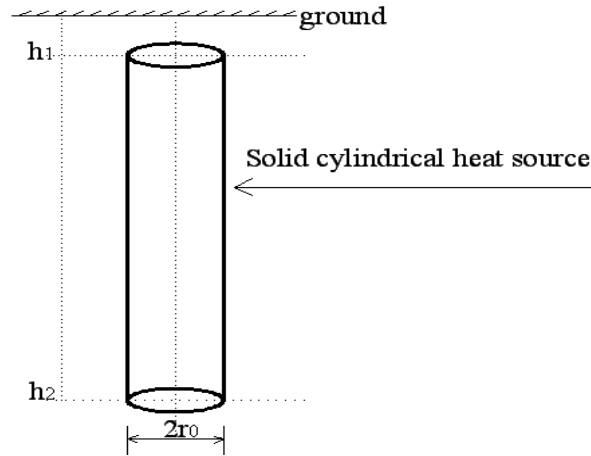


Figure 3.1 Geometry of solid cylindrical heat source model

Figure 3.1 illustrates the configuration of the solid cylindrical heat source model, with both heat transfer inside and outside the pile considered. This model cannot describe the structural characteristics of the energy pile in the most accurate way, but still represents a significant progress in the process of exploring the characteristics of pile foundation GHEs. The solid cylindrical model can provide theoretical guidelines with respect to calculated engineering projects provided that not too high an expectation is placed on the results. When groundwater flows through an energy pile, the heat exchange mode of the solid cylindrical heat source is converted from pure conduction to one including conduction and groundwater advection (KAYANE et al., 1985).

In fact, this model is even applicable for a borehole GHE with groundwater advection, because the borehole is filled with backfilling material and thus a certain degree of interior heat capacity still exists. This chapter describes the line heat source seepage models, the solid cylindrical heat source conduction model and the corresponding seepage models. This is because the investigations aiming at groundwater advection's influences on a GHE begins with the heat transfer of the borehole GHE with

groundwater advection, for which the line heat source model is widely used. Discussions on the heat transfer characteristics of the borehole GHE with groundwater advection can provide a valuable basis for study of the similar problem of pile foundation GHE.

3.2 Basic principles for acquiring analytical solutions

3.2.1 The Green's function

In order to investigate the heat transfer of a borehole or a pile foundation GHE based either on a pure conduction model or on a one taking account of the water flow in the porous medium, the Green's function theory is employed in this study, which has been proven to be a very potent and straightforward method of obtaining analytical solutions for various models studied (Carslaw and Jeager, 1959). The Green's function is the temperature response to an instantaneous point heat source, that is, a point lying in a given location emits a finite quantity of heat instantaneously at a given time, and in a certain domain with zero initial and boundary conditions. The Green's function for an infinite homogenous medium is the most essential and most useful in the heat conduction theory, its expression is shown in Equation (3.1).

$$G(x, y, z, \tau; x', y', z', \tau') = \frac{1}{8 \left[\sqrt{\pi a (\tau - \tau')} \right]^3} \exp \left[-\frac{(x-x')^2 + (y-y')^2 + (z-z')^2}{4a(\tau - \tau')} \right] \quad (3.1)$$

Equation (3.1) gives the temperature response of a point (x, y, z) at time τ in the medium to the instantaneous point heat source which lies in (x', y', z') and begins to emit heat from the time τ' . The Green's function may be regarded as the temperature rise in an infinite medium as a result of a quantity of heat. Thus, any heat source with complex shape can be regarded as the spatial gathering of a great multitude of points. The heat

source which provides continuous heating can be deemed as the collection of a large number of instantaneous heat sources according to the time sequence, and which can be expressed by integration of time or space. This approach can be utilized to solve the problems of heat conduction around buried coils. A point (x, y, z) in the Cartesian coordinate can be denoted (r, ϕ, z) in the cylindrical coordinate, allowing coordinates to be used interchangeably, and the expressions are listed as: $x = r \cos\phi$, $y = r \sin\phi$, $z = z$. The distance between the points (x, y, z) and (x', y', z') is given by:

$$R_s = \sqrt{(x-x')^2 + (y-y')^2 + (z-z')^2} = \sqrt{r^2 + r'^2 - 2rr' \cos(\phi - \phi') + (z-z')^2} \quad (3.2)$$

The Green's function becomes Equation (3.3) in the cylindrical coordinate.

$$G(r, \phi, z, \tau, r', \phi', z', \tau') = \frac{1}{8[\pi a(\tau - \tau')]^{3/2}} \cdot \exp\left[-\frac{r^2 + r'^2 - 2rr' \cos(\phi - \phi') + (z - z')^2}{4a(\tau - \tau')}\right] \quad (3.3)$$

For example, given that a point heat source lies in infinite medium and is located at (x', y', z') , and an amount of heat ρc is emitted instantaneously at the rate q (W) per unit time from $\tau' = 0$ to $\tau' = \tau$, the temperature response is achieved by integrating Equation (3.1) or (3.2) with respect to τ' , i.e.:

$$\theta = \frac{q}{\rho c} \int_0^\tau G d\tau' = \frac{q}{4\pi kR} \operatorname{erfc}\left(\frac{R_s}{2\sqrt{a\tau}}\right) \quad (3.4)$$

where R_s is given in Equation (3.2).

In case a semi-infinite medium has its surface kept at zero temperature, and is heated by a buried heat source with heating rate q , the solution may be obtained by the virtual heat source method (Zeng et al, 2003). To be more specific, a virtual heat sink with a negative heating rate $-q$ is positioned symmetrically with regard to the boundary. The

temperature of boundary, that is, t , is initially zero due to the symmetry of the source and the virtual sink. The temperature response in the medium can be obtained by summing up the contributions of all the heat sources and sinks in the infinite medium with the help of the Green's function.

3.2.2 Moving heat source

A series of problems can be regarded either as cases in which heat sources move through a fixed medium, or as cases that the medium flows past a fixed heat sources producing heat. In the following study, the medium flows along the x -direction with a uniform speed u while the heat source is deemed as motionless. The motionless coordinates are defined as (x, y, z) , at the same time the coordinates moving together with the medium are set as (ξ, η, ζ) . For the temperature $T(\xi, \eta, \zeta, \tau)$ in the coordinates moving with the medium, the traditional heat conduction equation holds, excluding the domain where the heat sources itself is located at, that is:

$$\frac{\partial T}{\partial \tau} = a \left(\frac{\partial^2 T}{\partial \xi^2} + \frac{\partial^2 T}{\partial \eta^2} + \frac{\partial^2 T}{\partial \zeta^2} \right) \quad (3.5)$$

As $T(\xi, \eta, \zeta, \tau) = t(x, y, z, \tau) = t(\xi + u\tau, \eta, \zeta, \tau)$ and the conversion between the two coordinate systems are $x = \xi + u\tau, y = \eta, z = \zeta$, thus energy conservation equation is acquired in Equation (3.6).

$$\frac{\partial T}{\partial \tau} = \frac{\partial t}{\partial x} \frac{\partial x}{\partial \tau} + \frac{\partial t}{\partial \tau} \frac{\partial \tau}{\partial \tau} = \frac{\partial t}{\partial \tau} + u \frac{\partial t}{\partial x} \quad (3.6)$$

This equation can later be expressed in the fixed coordinates and it is given as:

$$\frac{\partial t}{\partial \tau} + u \frac{\partial t}{\partial x} = a \left(\frac{\partial^2 t}{\partial x^2} + \frac{\partial^2 t}{\partial y^2} + \frac{\partial^2 t}{\partial z^2} \right) \quad (3.7)$$

The heat conduction caused by moving heat sources (or the flowing medium here) can also be solved by the Green's function theory, i.e. by integrating of the solutions of instantaneous point sources. In the case of an amount of heat $Q = \rho c$ emitted at the point (x', y', z') at time τ' , the point in the moving medium, which is at (x, y, z) at time τ , was at $[x - u(\tau - \tau'), y, z]$ at time τ' . Accordingly, the Green's function theory can be used to obtain the temperature response at the point (x, y, z) in the motionless coordinates at time τ to an instantaneous point source emitting heat at (x', y', z') at τ' . This temperature response is shown in Equation (3.8).

$$M(x, y, z, \tau; x', y', z', \tau') = \frac{1}{8[\pi a(\tau - \tau')]^{3/2}} \exp\left\{-\frac{[x - x' - u(\tau - \tau')]^2 + (y - y')^2 + (z - z')^2}{4a(\tau - \tau')}\right\} \quad (3.8)$$

The temperature response above can be defined as M function, with reference to a continuous point source emitting heat at the rate q (W) for times $\tau > 0$. The temperature response to the point source emitting heat continuously from 0 to τ is:

$$\begin{aligned} \theta &= \frac{q}{\rho c} \int_0^\tau M d\tau' = \frac{q}{2\pi^{3/2} k R} \exp\left[\frac{u(x - x')}{2a}\right] \cdot \int_{R/2\sqrt{a\tau}}^\infty \exp\left[-\psi^2 - \frac{u^2 R^2}{16a^2 \psi^2}\right] d\psi \\ &= \frac{q}{2\pi^{3/2} k} \exp\left[\frac{u(x - x')}{2a}\right] \cdot f(x, y, z, \tau; x', y', z') \end{aligned} \quad (3.9)$$

where

$$\begin{aligned} f(x, y, z, \tau; x', y', z') &= \frac{1}{R} \int_{R/2\sqrt{a\tau}}^\infty \exp\left[-\psi^2 - \frac{U^2 R^2}{16a^2 \psi^2}\right] d\psi \\ &= \frac{\sqrt{\pi}}{4R} \left[\exp\left(-\frac{UR}{2a}\right) \operatorname{erfc}\left(\frac{R - U\tau}{2\sqrt{a\tau}}\right) + \exp\left(\frac{UR}{2a}\right) \operatorname{erfc}\left(\frac{R + U\tau}{2\sqrt{a\tau}}\right) \right] \end{aligned} \quad (3.10)$$

In Equation (3.10), $R = \sqrt{(x - x')^2 + (y - y')^2 + (z - z')^2}$ in the Cartesian coordinate or

$R = \sqrt{r^2 + r'^2 - 2rr' \cos(\varphi - \varphi') + (z - z')^2}$ in the cylindrical coordinate.

When $u = 0$, that means the source (medium) is motionless and the temperature response is shown in Equation (3.4). For more complicated heat sources, such as line and cylindrical surfaces, of either the instantaneous or continuous nature, the temperature responses can be obtained directly by integration of the contributions made by all individual point sources.

3.2.3 Advection in porous medium

In the saturated porous medium, heat is transmitted in a combined mechanism, that is, by conduction through its solid matrix and liquid (water) in its pores as well as by convection of the moving liquid (Chiasson et al., 2000). The energy equation which describes heat transfer in the saturated porous medium containing heat advection and conduction is shown in Equation (3.11).

$$\rho c \frac{\partial t}{\partial \tau} + \rho_w c_w (\mathbf{v} \cdot \nabla t) = \nabla \cdot (k \nabla t) \quad (3.11)$$

where \mathbf{v} indicates the Darcy velocity in the porous medium, k and ρc are respectively the effective thermal conductivity and the volumetric specific heat of the bulk porous medium, weighted according to the proportions of saturated water and solid matrix.

The Darcy velocity is regarded as uniform in the whole domain concerned and parallel to the ground surface, this assumption is approved in the following discussions. The velocity u is defined to be in the direction of the x -coordinate. Accordingly, Equation (3.11) reduces to Equation (3.12) while the thermal properties are constant (Diao and Fang, 2006).

$$\frac{\partial t}{\partial \tau} + U \frac{\partial t}{\partial x} = a \nabla^2 t \quad (3.12)$$

where $U = u\rho_w c_w / (\rho c)$, can be referred to as the effective heat transport velocity, and $a = k / (\rho c)$ is the effective thermal diffusivity (Yuill and Mikler, 1995).

A comparison of Equations (3.7) and (3.12) shows that the advection problems can be formulated in the same expression as that of the moving source problem if $U = u\rho_w c_w / (\rho c)$ is substituted for u . Therefore, analytical solutions for the advection problems may also be obtained by using the Green's function theory.

3.3 Line heat source models with groundwater advection

In the past studies, line heat source models were usually employed for borehole GHE because of the borehole's size characteristics. When groundwater flows through a borehole GHE, the line source turns into a combined mechanism involving the emission of heat and groundwater advection. If heat is emitted at the rate of q_l along the z -axis, the line source may be looked on as a collection of innumerable point sources with a heating rate of $q_l dz'$. The excess temperature $\theta = t - t_0$ and parameters t and t_0 are respectively actual temperature and initial temperature of any point except heat source in the underground medium (Diao et al, 2004). Thus, the temperature response to the line source can be achieved by the integration of Equation (3.8), that is:

$$\theta_{a,l,i} = \frac{q_l}{\rho c} \int_0^\tau d\tau' \int_{-\infty}^{\infty} M(x' = y' = 0) dz' = \frac{q_l}{4\pi k} \exp\left(\frac{Ux}{2a}\right) \int_0^{\frac{4a\tau'}{R^2}} \frac{1}{\psi} \exp\left(-\frac{1}{\psi} - \frac{U^2 R^2 \psi}{16a^2}\right) d\psi \quad (3.13)$$

where $R = \sqrt{x^2 + y^2}$, the generalized incomplete gamma function is shown in Equation (3.14) and it can be utilized to obtain another form of Equation (3.13).

$$\Gamma(a, x; b) = \int_x^\infty \psi^{a-1} \exp\left(-\psi - \frac{b}{\psi}\right) d\psi \quad (3.14)$$

Equation (3.13) can also be expressed as:

$$\theta_{a,l,i} = \frac{q_l}{4\pi k} \exp\left(\frac{Ux}{2a}\right) \cdot \int_{R^2/(4a\tau)}^\infty \frac{1}{\psi} \exp\left(-\psi - \frac{U^2 R^2}{16a^2 \psi}\right) d\psi = \frac{q_l}{4\pi k} \exp\left(\frac{Ux}{2a}\right) \cdot \Gamma\left(0, \frac{R^2}{4a\tau}, \frac{U^2 R^2}{16a^2}\right) \quad (3.15)$$

For the line heat source of finite length in a semi-infinite medium, stretching from $z' = h_1$ to $z' = h_2$ along the z -axis, the temperature response can be formulated by the mirror method. The solution is also written as:

$$\theta_{a,l,f} = \frac{q_l}{\rho c} \int_0^\tau d\tau' \left[\int_{h_1}^{h_2} M(x' = y' = 0) dz' - \int_{-h_2}^{-h_1} M(x' = y' = 0) dz' \right] \quad (3.16)$$

Equation (3.16) can be given detailed expression as follows:

$$\begin{aligned} \theta_{a,l,f} &= \frac{q_l}{8\rho c} \int_0^\tau \frac{d\tau'}{[\pi a(\tau - \tau')]^{3/2}} \cdot \exp\left[-\frac{[x - U(\tau - \tau')]^2 + y^2}{4a(\tau - \tau')}\right] \cdot \\ &\left\{ \int_{h_1}^{h_2} \exp\left[-\frac{(z - z')^2}{4a(\tau - \tau')}\right] dz' - \int_{-h_2}^{-h_1} \exp\left[-\frac{(z - z')^2}{4a(\tau - \tau')}\right] dz' \right\} \\ &= \frac{q_l}{8\pi k} \int_0^\tau \frac{d\tau'}{\tau - \tau'} \cdot \exp\left[-\frac{[x - U(\tau - \tau')]^2 + y^2}{4a(\tau - \tau')}\right] \cdot \\ &\left\{ \operatorname{erfc}\left[\frac{z - h_1}{2\sqrt{a(\tau - \tau')}}\right] - \operatorname{erfc}\left[\frac{z - h_2}{2\sqrt{a(\tau - \tau')}}\right] - \operatorname{erfc}\left[\frac{z + h_1}{2\sqrt{a(\tau - \tau')}}\right] + \operatorname{erfc}\left[\frac{z + h_2}{2\sqrt{a(\tau - \tau')}}\right] \right\} \end{aligned} \quad (3.17)$$

The analytical solution of finite line heat source with groundwater advection is the aim because any real GHE has finite length. The temperature fields around a borehole GHE are shown in Figure 3.2; the isothermals of the vertical and horizontal cross sections are both shown. No matter at the XOY or at the XOZ plane, temperature distributions on both sides of the axis are different with those of pure conduction model,

in other words, the isotherm are now asymmetrical as a result of groundwater seepage.

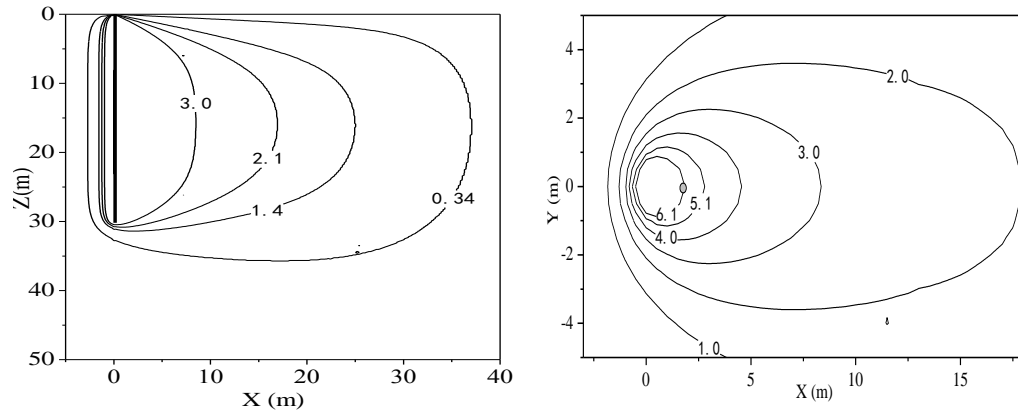


Figure 3.2 Isotherms of finite line heat source seepage model

3.4 The solid cylindrical heat source models

3.4.1 The relevant preconditions

With reference to the solid cylindrical heat source, the buried coils are simplified as a continuous circular cylindrical surface. When it comes to the radial dimension of the coil, the discontinuity of the source in the longitudinal direction was not considered. As a result, the temperature difference along the pitches of the coils on the cylindrical surface is blurred. It is assumed that the domain studied is a homogeneous saturated porous medium, either infinite or semi-infinite, with k , ρc and a denoting its effective properties. It is also assumed that water moves in the porous medium with a uniform Darcy u , parallel to the x -axis. Defining $U = u\rho_w c_w / (\rho c)$ as discussed in section 3.2.3, because Equation (3.3) provides the expression of Green function of pure conduction, the analytical solutions of temperature responses induced by a solid cylindrical conduction model can be achieved. The analytical solutions can then be extended to deal with the advection situations by substituting the M function for the Green's function in the

relevant expressions. The thermophysical properties of the medium do not change with the temperature. The supply of heat starts at $\tau = 0$ when the medium is at zero temperature and the heating rate per unit length of the source, q_l , is constant. For the models of heat sources with the finite length, the ground is assumed to be a semi-infinite medium, and its boundary, i.e. the ground surface, keeps a constant zero temperature throughout the period concerned. As for finite models, the heat source which is simplified as finite-length solid cylinder surface are buried perpendicular to the boundary, stretching from depth h_1 to depth h_2 .

3.4.2 Pure conduction models

3.4.2.1 Infinite cylindrical source model

In this model, the axis of the cylindrical surface with radius r_0 is coincident with z -axis. The heat source with a step heating rate q_l per length of the cylinder, can be regarded as a combination of numerous point sources located at the cylindrical surface with instantaneous intensity of $q_l d\phi' dz' d\tau' / (2\pi)$. This problem is one-dimensional in its nature and therefore the expression should be independent of the coordinates ϕ and z . $z=0$ and $\phi=0$ are set for convenience in the evaluation, and the expression of the temperature response in the medium can be written straightforwardly as:

$$\theta_{p,c,i} = \frac{q_l}{2\pi\rho c} \int_0^\tau d\tau' \int_{-\infty}^{\infty} dz' \int_0^{2\pi} G(r, \phi=0, z=0, \tau; r'=r_0, \phi', z', \tau') d\phi' \quad (3.18)$$

The triple integrals can first be performed with respect to either z' or ϕ' . When Equation (3.18) is integrated with respect to z' first, the following is obtained:

$$\theta_{p,c,i} = -\frac{q_l}{2\pi^2 k} \int_0^\tau Ei \left(-\frac{r^2 + r_0^2 - 2rr_0 \cos \phi'}{4a\tau} \right) d\phi' \quad (3.19)$$

If the integration is carried out with respect to ϕ' first, another expression is resulted in:

$$\theta_{p,c,i} = \frac{q_l}{4\pi k} \int_0^\tau \frac{1}{\tau - \tau'} \exp\left[-\frac{r^2 + r_0^2}{4a(\tau - \tau')}\right] \cdot I_0\left[\frac{rr_0}{2a(\tau - \tau')}\right] d\tau' \quad (3.20)$$

where $I_0(x) = \frac{1}{\pi} \int_0^\pi \exp(x \cos \phi') d\phi'$ is the modified Bessel function of the zero order.

3.4.2.2 Finite cylindrical source model

In the two-dimensional (2-D) model, the cylindrical heat source is considered as a one with limited length, stretching from h_1 to h_2 in the z -direction (Man et al., 2011). There is a suppositional solid cylindrical heat sink symmetrical to heat source with ground boundary as in-between interface, the mirror method is again used to obtain the solution and the expression is demonstrated as:

$$\theta_{p,c,f} = \frac{q_l}{2\pi\rho c} \int_0^\tau d\tau' \int_0^{2\pi} d\phi' \left(\int_{h_1}^{h_2} G dz' - \int_{-h_2}^{-h_1} G dz' \right) \quad (3.21)$$

Integrating with respect to ϕ' and z' results in:

$$\theta_{p,c,f} = \frac{q_l}{8\pi k} \int_0^\tau \frac{d\tau'}{(\tau - \tau')} I_0\left[\frac{rr_0}{2a(\tau - \tau')}\right] \exp\left[-\frac{r^2 + r_0^2}{4a(\tau - \tau')}\right] \cdot \left\{ \operatorname{erfc}\left[\frac{z - h_2}{2\sqrt{a(\tau - \tau')}}\right] - \operatorname{erfc}\left[\frac{z - h_1}{2\sqrt{a(\tau - \tau')}}\right] + \operatorname{erfc}\left[\frac{z + h_2}{2\sqrt{a(\tau - \tau')}}\right] - \operatorname{erfc}\left[\frac{z + h_1}{2\sqrt{a(\tau - \tau')}}\right] \right\} \quad (3.22)$$

3.4.2.3 The characteristics of pure conduction models

3.4.2.3.1 The schematic diagram of temperature distribution

The expressions in section 3.4.2.1 and 3.4.2.2 contain a number of parameters, which

are inconvenient to the study of the characteristics of solid cylindrical models with diameter r_0 . Thus, non-dimensional parameters are introduced and the corresponding expressions are: $\Theta = k \theta / q_1$, $H_1 = h_1 / r_0$, $H_2 = h_2 / r_0$, $Z = z / r_0$, $Fo = a \tau / r_0^2$ and $R = r / r_0$. Accordingly, Θ , H_1 , H_2 , Z , Fo and R are respectively dimensionless variables for temperature response, starting depth point, end depth point, z coordinate, time and radial distance. Dimensionless expressions of infinite and finite models are respectively shown in Equations (3.23) and (3.24).

$$\Theta_{p,c,i} = \frac{1}{4\pi} \int_0^{Fo} \frac{1}{Fo - Fo'} \exp \left[-\frac{R^2 + 1}{4(Fo - Fo')} \right] \cdot I_0 \left[\frac{R}{2(Fo - Fo')} \right] dFo' \quad (3.23)$$

$$\Theta_{p,c,f} = \frac{1}{8\pi} \int_0^{Fo} \frac{dFo'}{(Fo - Fo')} I_0 \left[\frac{R}{2(Fo - Fo')} \right] \exp \left[-\frac{R^2 + 1}{4(Fo - Fo')} \right] \cdot \left\{ \operatorname{erfc} \left[\frac{Z - H_2}{2\sqrt{Fo - Fo'}} \right] - \operatorname{erfc} \left[\frac{Z - H_1}{2\sqrt{Fo - Fo'}} \right] + \operatorname{erfc} \left[\frac{Z + H_2}{2\sqrt{Fo - Fo'}} \right] - \operatorname{erfc} \left[\frac{Z + H_1}{2\sqrt{Fo - Fo'}} \right] \right\} \quad (3.24)$$

Analytical solutions of pure conduction models are given above. Because an infinite model has no length limitation along the z -axis, the temperature field of longitudinal sectional view cannot be shown. Any actual energy pile has a finite length, the corresponding temperature distributions of a finite solid cylindrical model at both longitudinal and horizontal sections are shown in Figure 3.3.

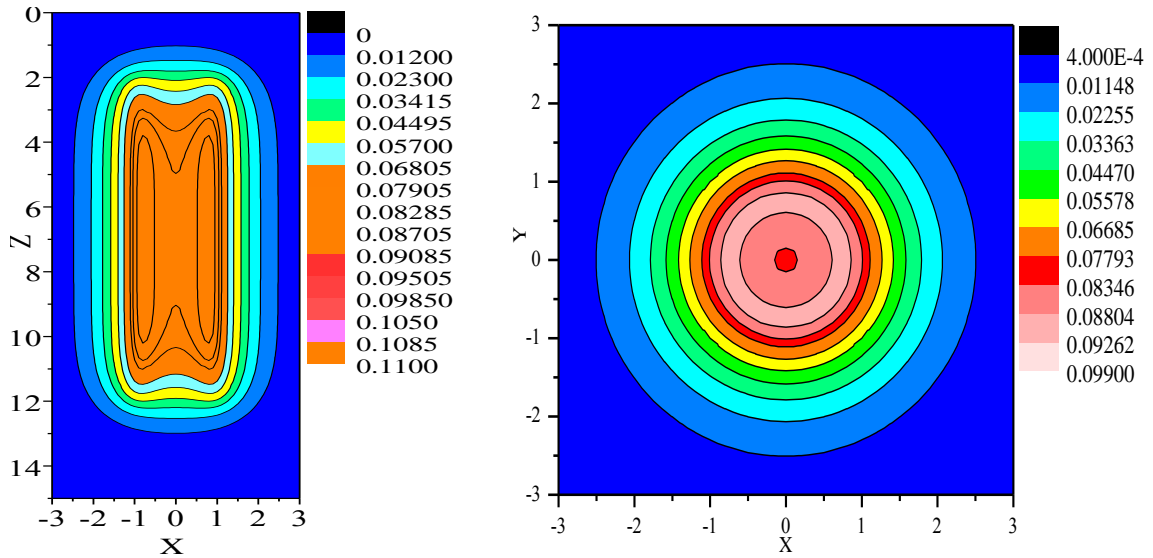


Figure 3.3 Isothermals of pure conduction model of solid cylindrical heat source

It follows that the isothermals are symmetrical on both sides of the axis when only pure conduction applies.

3.4.2.3.2 The temperature response trend

The heat emitted from the energy pile during the process of heat transfer produces temperature response at all points except at heat source itself. The responses increase with the time, and the sizes of a pile has obvious impacts on the response degrees at the same point if other conditions are equal. Some examples of pure conduction are chosen, including the infinite and the finite models with different ratios of length to radius. All temperature responses that increase with the time are shown in Figure 3.4. For the infinite model, the points at the cylindrical surface can be selected, and any value for Z can be set because the heat transfer along Z -axis is not considered. The finite model, disposed perpendicular to the boundary from h_1 to h_2 , has the length of $h = h_2 - h_1$. It is suggested that the mid height of pile foundation GHE, that is, $h_{mid} = h_1 + h / 2$, is chosen, and the corresponding non-dimensional alteration is $H_{mid} = H_1 + H / 2$.

For pure conduction, the temperature response caused by infinite model increases indefinitely, but all temperature responses of finite model must reach stable values. These final temperatures and the time taken to reach them are determined by the ratios of length to radius. The larger the ratios, the higher the final response values and the longer it takes to reach them (Zhang et al., 2013a). There is no doubt that the temperature response of the infinite model is stronger than those of the finite models at any time.

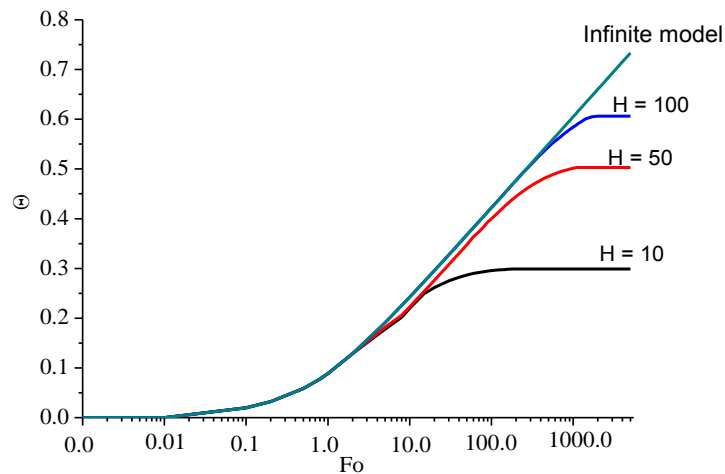


Figure 3.4 Temperature responses of solid cylindrical heat source pure conduction models with the time

3.4.3 Combined heat transfer models

Section 3.4.1 gives the relevant preconditions for both the pure conduction and the combined heat transfer models; the latter can convert itself into the former if the groundwater velocity is zero. As for pile foundation GHE, the cylindrical heat source models reported in the literature only targets pure conduction, and the research in the thesis takes the combined heat transfer including conduction and groundwater advection into consideration, which means the influence of groundwater advection is explored. The

expressions of seepage models and the corresponding characteristics are demonstrated below.

3.4.3.1 Infinite cylindrical source model

For the infinite cylindrical source buried in the infinite medium with groundwater advection, energy pile emits heat from zero to a certain time while groundwater flows through it, the heat source keeps constant heat transfer rate and has the infinite depth, accordingly only x and y directions are taken into account. The energy equation and the corresponding conditions are listed in Equation (3.25).

$$\left. \begin{aligned} \frac{\partial \theta}{\partial \tau} + u \frac{\partial \theta}{\partial r \cos \varphi} &= a \left(\frac{\partial^2 \theta}{\partial r^2} + \frac{1}{r} \frac{\partial \theta}{\partial r} \right) + \frac{q \delta(r - r_0, z - z')}{2\pi r_0 \rho c}, \text{ for } 0 < r < \infty, -\infty < z' < +\infty, \tau > 0, \\ \theta &= 0, \text{ for } 0 < r < \infty, \tau = 0 \\ \frac{\partial \theta}{\partial r} &= 0, \text{ for } r = 0, \tau > 0 \\ -k \frac{\partial \theta}{\partial r} 2\pi r &= q_l, \text{ for } r \rightarrow r_0, \tau > 0 \end{aligned} \right\} \quad (3.25)$$

where the $\delta (r - r_0)$ is the Dirac δ function.

The M function can be appropriately used for obtaining the analytical solutions and the corresponding expression of temperature responses in the medium are written concisely as Equation (3.26). In this way the solid cylindrical heat source can be deemed to consist of an infinite number of coil heat sources each with the heating rate q_l .

$$\theta_{a, c, i} = \frac{q_l}{2\pi \rho c} \int_0^\tau d\tau' \int_{-\infty}^{\infty} dz' \int_0^{2\pi} M (r' = r_0) d\phi' \quad (3.26)$$

For the cylinder with both radius r_0 lying along the z -axis, the expressions $x' = r_0 \cos \varphi'$ and $y' = r_0 \sin \varphi'$ can be achieved. If the integration is first conducted with respect to τ' first, the temperature response to a continuous point source, i.e. Equation (3.9), may be used,

and the expression becomes:

$$\begin{aligned}\theta_{a,c,i} &= \frac{q_l}{4\pi^{5/2}k} \int_0^{2\pi} \exp\left[\frac{U(x-r_0 \cos \phi')}{2a}\right] d\phi' \cdot \int_{-\infty}^{\infty} dz' \frac{1}{R} \cdot \int_{R/(2\sqrt{a\tau})}^{\infty} \exp\left(-\psi^2 - \frac{U^2 R^2}{16a^2 \psi^2}\right) d\psi \\ &= \frac{q_l}{4\pi^{5/2}k} \int_0^{2\pi} \exp\left[\frac{U(x-r_0 \cos \phi')}{2a}\right] d\phi' \cdot \int_{-\infty}^{\infty} f(\phi', z') dz'\end{aligned}\quad (3.27)$$

where f is defined as Equation (3.10), and $R = \sqrt{(x-r_0 \cos \phi')^2 + (y-r_0 \sin \phi')^2 + (z-z')^2}$.

From another perspective, if the integration is implemented first with respect with z' , which means the cylinder is deemed to consist of an infinite number of line sources, another expression is generated in Equation (3.28):

$$\theta_{a,c,i} = \frac{q_l}{4\pi^2 k} \int_0^{2\pi} d\phi' \exp\left[\frac{U(x-r_0 \cos \phi')}{2a}\right] \cdot \int_0^{4a\tau/R^2} \frac{1}{\psi} \exp\left[-\frac{1}{\psi} - \frac{U^2 R^2 \psi}{16a^2}\right] d\psi \quad (3.28)$$

where $R = \sqrt{(x-r_0 \cos \phi')^2 + (y-r_0 \sin \phi')^2}$.

3.4.3.2 Finite cylindrical source model

The finite cylindrical heat source has a limited length from h_1 to h_2 along the z -direction, the underground space is three dimensional, that is, x , y and z directions are all considered if groundwater exerts seepage effects on energy pile. The mirror method is again used to obtain the solution of the heat transfer problem with the boundary temperature of the semi-infinite medium kept constant i.e. $\theta = 0$. The heat sink with intensity $-q_l$ is set on the location symmetrical to the heat source with intensity q_l , and the boundary is considered to be the middle interface. The corresponding energy equations are given as:

$$\left. \begin{aligned}
\frac{\partial \theta}{\partial \tau} + u \frac{\partial \theta}{\partial (r \cos \phi)} &= a \left(\frac{\partial^2 \theta}{\partial r^2} + \frac{1}{r} \frac{\partial \theta}{\partial r} + \frac{\partial^2 \theta}{\partial z^2} \right) + \frac{q \delta(r-r_0, z-z')}{2\pi r_0 \rho c}, \text{ for } 0 < r < \infty, h_1 < z < h_2, \tau > 0 \\
\theta &= 0, \text{ for } z = 0, \tau \geq 0 \\
\frac{\partial \theta}{\partial r} &= 0, \text{ for } r = 0, \tau > 0 \\
-k \frac{\partial \theta}{\partial r} 2\pi r &= q_l, \text{ for } r \rightarrow r_0, \tau > 0
\end{aligned} \right\} \quad (3.29)$$

The temperature response for the problem is then achieved as:

$$\begin{aligned}
\theta_{a,c,f} &= \frac{q_l}{2\pi \rho c} \int_0^\tau d\tau' \int_0^{2\pi} d\phi' \left(\int_{h_1}^{h_2} M(r'=r_0) dz' - \int_{-h_2}^{-h_1} M(r'=r_0) dz' \right) \\
&= \frac{q_l}{4\pi^{5/2} k} \int_0^{2\pi} \exp \left[\frac{U(x-r_0 \cos \phi')}{2a} \right] d\phi' \cdot \left[\int_{h_1}^{h_2} f(\phi', z') dz' - \int_{-h_2}^{-h_1} f(\phi', z') dz' \right]
\end{aligned} \quad (3.30)$$

Integrating with respect to z' first results in:

$$\begin{aligned}
\theta_{a,c,f} &= \frac{q_l}{16\pi^2 k} \int_0^{2\pi} d\phi' \int_0^\tau \frac{d\tau'}{(\tau-\tau')} \cdot \exp \left[-\frac{[x-r_0 \cos \phi' - U(\tau-\tau')]^2 + (y-r_0 \sin \phi')^2}{4a(\tau-\tau')} \right] \\
&\quad \left\{ \operatorname{erfc} \left[\frac{z-h_1}{2\sqrt{a(\tau-\tau')}} \right] - \operatorname{erfc} \left[\frac{z-h_2}{2\sqrt{a(\tau-\tau')}} \right] - \operatorname{erfc} \left[\frac{z+h_1}{2\sqrt{a(\tau-\tau')}} \right] + \operatorname{erfc} \left[\frac{z+h_2}{2\sqrt{a(\tau-\tau')}} \right] \right\}
\end{aligned} \quad (3.31)$$

3.4.3.3 The characteristics of combined heat transfer models

3.4.3.3.1 The schematic diagram of temperature distribution

As the troubles appeared in pure conduction models, the parameters are so many that the difficulty in analyzing the expressions must be increased; this is unfavorable for exploring the characteristics of combined models. Non-dimensional parameters are put into use again and the expressions are almost the same as those shown in 3.4.2.3.1. In addition, the non-dimensional velocity is $V = u r_0 / a$ (Bear, 1983). Accordingly, non-dimensional analytical solutions of Equation (3.28) and (3.31) are respectively converted

into Equation (3.32) and (3.33).

$$\Theta_{a,c,i} = \frac{1}{4\pi^2} \int_0^{2\pi} d\phi' \exp\left[\frac{V(X - \cos\phi')}{2}\right] \int_0^{4Fo/[(X - \cos\phi')^2 + (Y - \sin\phi')^2]} \frac{1}{\eta} \exp\left[-\frac{1}{\eta} - \frac{V^2[(X - \cos\phi')^2 + (Y - \sin\phi')^2]\eta}{16}\right] d\eta \quad (3.32)$$

$$\Theta_{a,c,f} = \frac{1}{16\pi^2} \int_0^{2\pi} d\phi' \int_0^{Fo} \frac{dFo'}{(Fo - Fo')} \exp\left\{-\frac{[X - \cos\phi' - V(Fo - Fo')]^2 + (Y - \sin\phi')^2}{4(Fo - Fo')}\right\} \left\{ \operatorname{erfc}\left(\frac{Z - H_2}{2\sqrt{Fo - Fo'}}\right) - \operatorname{erfc}\left(\frac{Z - H_1}{2\sqrt{Fo - Fo'}}\right) - \operatorname{erfc}\left(\frac{Z + H_1}{2\sqrt{Fo - Fo'}}\right) + \operatorname{erfc}\left(\frac{Z + H_2}{2\sqrt{Fo - Fo'}}\right) \right\} \quad (3.33)$$

The finite seepage model is a research focus as any real energy pile has a limited length. Based on Equation (3.32), the temperature distributions of energy pile with groundwater advection are shown in Figure 3.5. Temperature fields in the XOZ and XOY planes are given, and the isothermals are asymmetrical on both sides of axis due to groundwater advection. Since the direction of seepage is defined to be along the positive direction of the X-axis, groundwater flows into the left hand side and then passes through the right hand side. Figure 3.5 shows that the temperature responses at the right hand side are higher than those at the left, demonstrating that groundwater flow alleviates heat accumulation on the left and then carries heat to the right. The response degrees of the right hand side are stronger after a short time, but the whole responses must be mitigated with the time no matter for the right or for the left. Comparing Figure 3.5 with Figure 3.3, it seems that a heat shift of the isothermals occurs when groundwater advection exists.

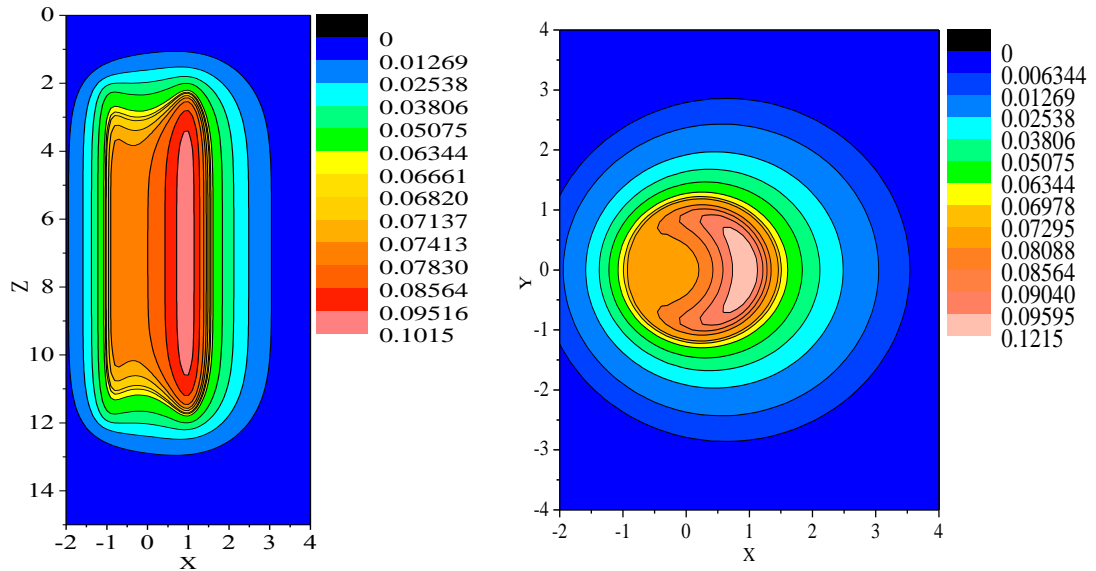


Figure 3.5 Isotherms of solid cylindrical source model with groundwater advection

3.4.3.3.2 The temperature response trend

For the pure conduction model, the discussions in section 3.4.2.3.2 prove that temperature response of the infinite model increases for ever while those induced by the finite model are certain to be stable finally. It is significant to discuss the trends and the degrees of models' temperature responses when conduction and groundwater advection constitute heat transfer mode. The role of groundwater seepage, as it affects temperature responses induced by energy pile, can be seen by comparing the temperature responses of two different modes including pure conduction and combined heat transfer. Equations (3.32) and (3.33) give the analytical solutions of thermal responses at any point except the heat source itself. However, unlike the case of pure conduction, the temperature distributions along different radial directions are not equal even though the same value is set for radius at the same horizontal plane. To show the response trends with the time at any horizontal circle, the definite integral along the circumference should be adopted to obtain the mean value. Using such mean value to represent the temperature response is

feasible in the cases of the infinite and finite models.

For the infinite model, heat transfer along Z direction is not taken into consideration and therefore the value for Z can be set as 0, and the mid depth along the Z -axis can be chosen for the finite model because the temperature response at this location is strong enough according to the isothermals in Figure 3.5, that is, the value of $H_{\text{mid}} = H_1 + H / 2$ is selected for Z . Another integral is added to Equations (3.28) and (3.31) and they are then respectively transformed into Equations (3.34) and (3.35):

$$\overline{\theta_{a,c,i}} = \frac{q_i}{4\pi^2 k \cdot 2\pi} \int_0^{2\pi} d\phi' \int_0^{2\pi} \exp\left[\frac{U(r \cos \phi - r_0 \cos \phi')}{2a}\right] \int_0^{4a\tau / [(r \cos \phi - r_0 \cos \phi')^2 + (r \sin \phi - r_0 \sin \phi')^2]} \frac{1}{\eta} \exp\left[-\frac{1}{\eta} - \frac{U^2[(r \cos \phi - r_0 \cos \phi')^2 + (r \sin \phi - r_0 \sin \phi')^2]\eta}{16a^2}\right] d\phi d\eta \quad (3.34)$$

$$\overline{\theta_{a,c,f}} = \frac{q_i}{16\pi^2 k \cdot 2\pi} \int_0^{2\pi} d\phi' \int_0^{2\pi} \int_0^{\tau} \frac{d\phi d\tau'}{(\tau - \tau')} \cdot \exp\left[-\frac{[r \cos \phi - r_0 \cos \phi' - U(\tau - \tau')]^2 + (r \sin \phi - r_0 \sin \phi')^2}{4a(\tau - \tau')}\right] \left\{ \operatorname{erfc}\left[\frac{z - h_1}{2\sqrt{a(\tau - \tau')}}\right] - \operatorname{erfc}\left[\frac{z - h_2}{2\sqrt{a(\tau - \tau')}}\right] - \operatorname{erfc}\left[\frac{z + h_1}{2\sqrt{a(\tau - \tau')}}\right] + \operatorname{erfc}\left[\frac{z + h_2}{2\sqrt{a(\tau - \tau')}}\right] \right\} \quad (3.35)$$

The integral is conducted along circumference direction of pile and the circle's radius is $r = r_0$. For Equation (3.34) and (3.35), the corresponding dimensionless expressions are respectively obtained in Equations (3.36) and (3.37).

$$\overline{\Theta_{a,c,i}} = \frac{1}{8\pi^3} \int_0^{2\pi} d\phi' \int_0^{2\pi} \exp\left[\frac{V(\cos \phi - \cos \phi')}{2}\right] \int_0^{4F\theta / [(\cos \phi - \cos \phi')^2 + (\sin \phi - \sin \phi')^2]} \frac{1}{\eta} \exp\left[-\frac{1}{\eta} - \frac{V^2[(\cos \phi - \cos \phi')^2 + (\sin \phi - \sin \phi')^2]\eta}{16}\right] d\phi d\eta \quad (3.36)$$

$$\overline{\Theta}_{a,c,f} = \frac{1}{16\pi^2 \cdot 2\pi} \int_0^{2\pi} d\phi' \int_0^{2\pi} d\phi \int_0^{Fo} \frac{dFo'}{(Fo - Fo')} \exp \left\{ -\frac{[\cos \phi - \cos \phi' - V(Fo - Fo')]^2 + (\sin \phi - \sin \phi')^2}{4(Fo - Fo')} \right\} \left\{ \operatorname{erfc} \left(\frac{Z - H_2}{2\sqrt{Fo - Fo'}} \right) - \operatorname{erfc} \left(\frac{Z - H_1}{2\sqrt{Fo - Fo'}} \right) - \operatorname{erfc} \left(\frac{Z + H_1}{2\sqrt{Fo - Fo'}} \right) + \operatorname{erfc} \left(\frac{Z + H_2}{2\sqrt{Fo - Fo'}} \right) \right\} \quad (3.37)$$

The temperature response trends are given by the calculated results of Equations (3.36) and (3.37). The geometric conditions, such as the values of H_1 , H_2 and H , are the same as those of pure conduction models. Four examples: infinite model, $H = 10$, $H = 50$ and $H = 100$ are selected; the temperature responses with the time when groundwater flows through them are shown in Figure 3.6.

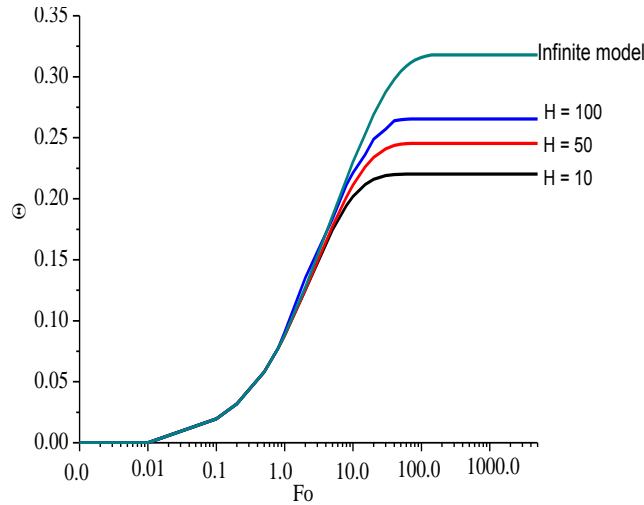


Figure 3.6 Temperature responses of solid cylindrical heat source seepage models with the time

It is clear that all temperature responses reach stability finally even if the model is infinite. The conclusions in section 3.4.2.3.2 illustrates that the ground boundary effect restrains the ever-increasing temperature response to the finite model when there is only pure conduction, while no such restraint limitation is imposed to the infinite model. However, groundwater advection relieves the heat accumulation induced by conduction so that heat transfer effect of energy pile is improved. There is no doubt that the constant

temperature of the ground boundary promotes the trends of reaching steady states, and now groundwater seepage is another stimulated factor causing stable state. Accordingly, the temperature response even for an infinite heat source must reach stability if there is groundwater seepage.

Since groundwater seepage restricts the rising temperature response no matter for infinite or for finite pure conduction model, a balance between heat accumulation and heat alleviation is eventually reached and the temperature response is stable at that time. In addition, the difference of these models' temperature responses decreases as a result of groundwater seepage and becomes smaller than those of pure conduction. The greater the velocity of groundwater flow, the clearer the difference of temperature responses. Figure 3.6 only shows the temperature responses when only one value is endowed to velocity. The temperature responses' curves of different models are displayed in Figure 3.7. It is clear that the response differences reduce with the increase of groundwater velocity.

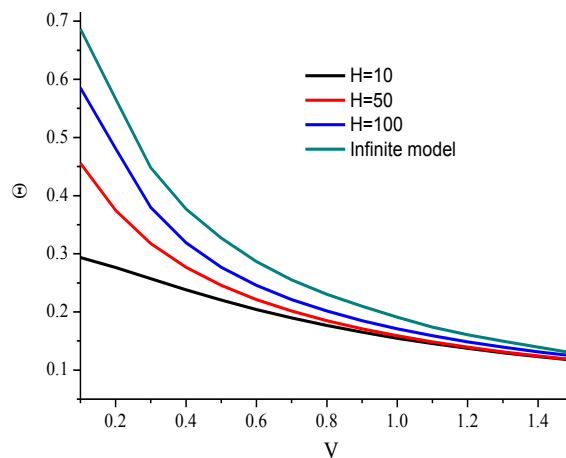


Figure 3.7 The differences of temperature responses with the velocity

The aim of Figure 3.7 is to show that conduction plays the dominant role if

groundwater velocity is small during the heat transfer. For pure conduction models, the size of a GHE has an important influence on thermal response, and the corresponding differences are clear when the conduction role is larger than that of advection. However, groundwater advection shows greater influence if the velocity increases sufficiently, because the temperature response is effectively restrained; for this reason, the conduction which is relevant to the size of heat source cannot act powerfully, the decrease of temperature responses' difference also occur if the advection is significant.

The convection role rests with the value of groundwater velocity if time is constant. Thus, it is worthwhile to study how the temperature responses of the same model vary with the seepage velocity at different times. Selecting the case of $H = 50$ and of course other cases are still feasible. The temperature responses are shown in Figure 3.8

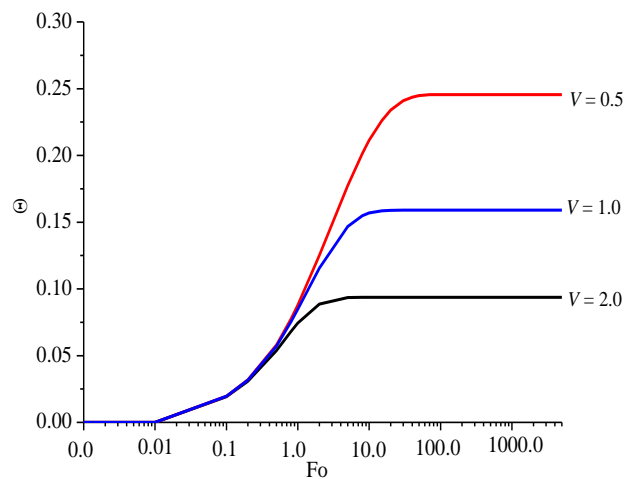


Figure 3.8 The temperature responses with the time while different velocities are adopted

The information in Figure 3.8 certifies that the time of arriving at stable states of non-dimensional temperatures reduces with the groundwater velocity, and that heat convection can greatly relieve the heat accumulation especially when the velocity attains

sufficient magnitude. The need to study the combined conduction / convection model is thus clear.

3.4.3.3.3 Comparisons of temperature responses of representative locations

The center line of the solid cylindrical heat source is located at z -axis and groundwater flows along the positive direction of x -axis. The intersection angle between x -axis' positive direction and any point on the same horizontal plane represented in polar coordinate is denoted as φ . The places on the surface of pile with the greatest temperature and the least temperature are respectively given by $\varphi = 0$ and $\varphi = \pi$ due to groundwater advection (Su et al., 2004). The reason is that groundwater first passes the location $\varphi = \pi$ where is exerted direct advection impact and then moves along the x -axis until it passes through the location $\varphi = 0$, a certain quantity of heat is delivered to $\varphi = 0$ and thereby the corresponding temperature rises obviously.

When the cylindrical coordinate is used, the polar radius and angle of any point are set as r and φ , respectively; the radius of the cylindrical source is r_0 and the dimensionless polar radius $R_D = r / r_0$. It is evident that all the points locating at $\varphi = 0$ of the surface are in possession of $R_D = 1.0$, meanwhile the points with $\varphi = \pi$ are provided with $R_D = -1.0$. The surface's temperature responses to the heat source can be shown when $R_D = 1.0$ and $R_D = -1.0$ are selected. The finite cylindrical model can be employed as it is representative of an actual pile (Shi et al., 2010). According to Equation (3.33), temperature responses are provided when two different assumptions are employed. One case is that the groundwater velocity is constant while the time is varied, and another case is that the time is fixed and the velocity is varied. The location of $R_D = -1.0$ is first

analyzed according to calculation and investigation, and the corresponding information is given in Figure 3.9.

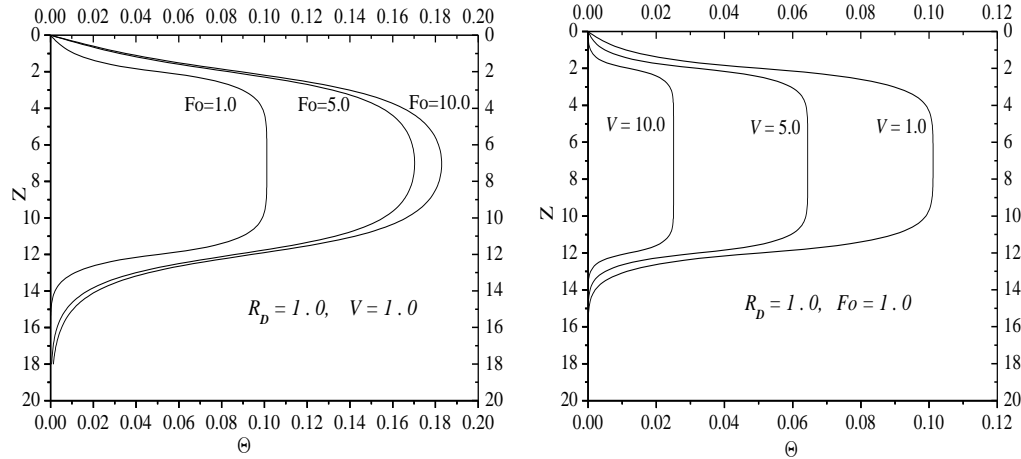


Figure 3.9 Isotherms down z-axis at different time and velocities respectively when $\varphi=0$

In addition, the temperature response' distribution of $R_D = -1.0$ is obtained by means of similar calculation procedure as that of $R_D = 1.0$, and are shown in Figure 3.10:

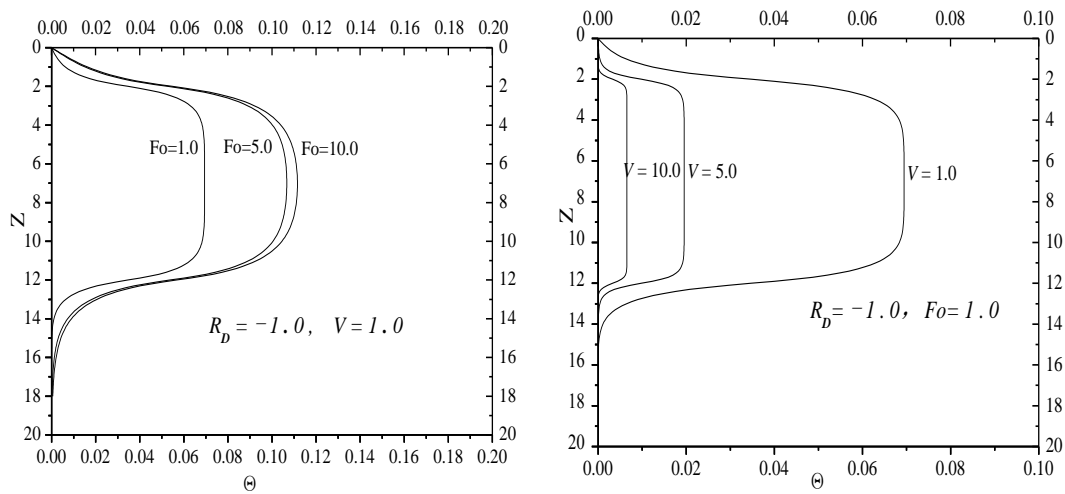


Figure 3.10 Isotherms down z-axis at different time and velocities respectively when $\varphi = \pi$

By analyzing the thermal responses of these two typical angles, it can be seen that the convection effect of groundwater should not be neglected especially when the time is

long or the velocity is large. Thus, groundwater plays an important role in the heat exchange process. According to Figures 3.9 and 3.10, temperature alleviation is evident, where the flow first exerts impact on the pile surface, demonstrating that convection improves the heat exchange efficiently. Briefly, temperature relief becomes clear gradually with the continuance of time when groundwater velocity keeps constant or at any particular time as velocity of flow increases.

3.5 Comparisons between pure conduction models and combined models

In this chapter, emphasis is put on the groundwater advection and explicit analytical solutions are obtained for combined solid cylindrical heat source models. It is necessary to compare the differences between pure conduction and combined heat transfer models to emphasize the contribution of groundwater (Chiasson, 1999). The finite models are employed as the reference objects since the depth of any actual energy pile is finite. Thus, it pays to implement corresponding discussions aiming at these two heat transfer modes, the correlative calculations and programming are based on equations above.

For solid cylindrical pure conduction model, the temperature responses around the pile surface perimeter at any horizontal plane are equal. The integration along circumference of the pile provides the mean response of any fixed horizontal plane for solid cylindrical combined models. Furthermore, an added integration along the pile's depth direction is needed to obtain the whole average temperature response. Therefore, another integral should be added to Equations (3.24) and (3.37); inevitably making the calculation more complex. For this reason, the weighted average method is employed,

whereby a number of locations along the z direction are selected, and their mean value, acquired using weighted average method, is expressed as:

$$\Theta_{ave} = \sum_i^n \Theta_i / n \quad (3.38)$$

Here Θ_i denotes the mean dimensionless temperature of the circle with specific z value at the pile surface no matter for pure conduction or for combined model. The dimensionless temperature ratios of two heat transfer models can directly reveal the influence of groundwater flow, and it changes with the time for different selected h / r_0 values. In the case of constant velocity, the changing trends of ratios are shown in Figure 3.11. The issue of interest is how the enhanced degree of heat exchange rates when groundwater flow exists, the superiority of heat transfer can be calculated according to the relevant expressions above. The ratios of heat transfer rates of two heat transfer modes when velocity is invariable are shown in Figure 3.12

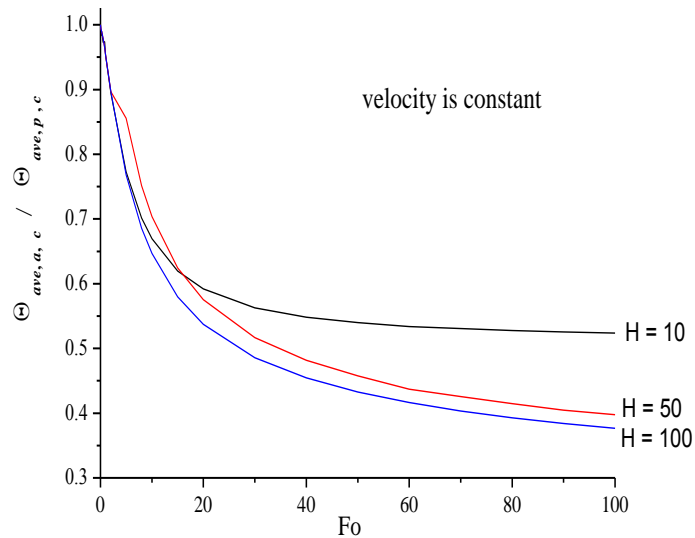


Figure 3.11 The ratios of temperature responses of two heat transfer modes with the time

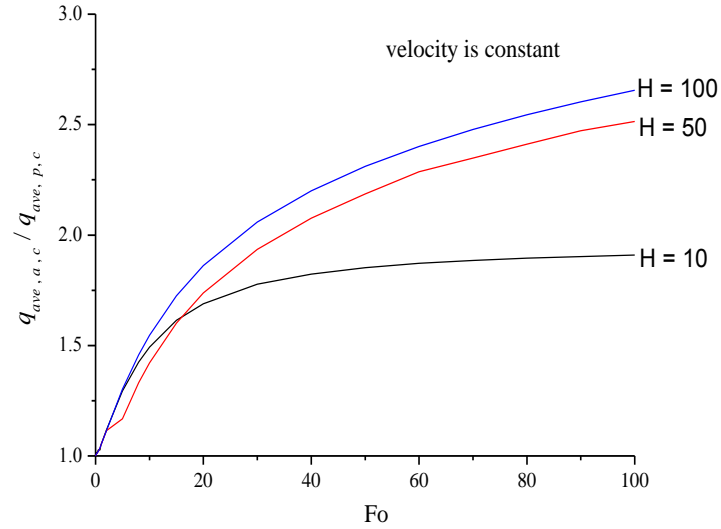


Figure 3.12 The ratios of heat exchange rates of two heat transfer modes with the time

Figures 3.11 and 3.12 show that heat transfer performance can be indeed improved if groundwater flows through energy pile, and the advection effect is particularly beneficial in the initial period on the assumption of constant velocity. For different ratios of length to radius of energy pile, the advantages of groundwater seepage are not much evident at first, but become gradually obvious over the time. Specifically, the larger the ratio, the clearer the heat transfer superiority due to groundwater flow. As stated above, the convection velocity is a critical factor affecting the heat transfer performance when operating energy pile because groundwater carries away the surrounding heat accumulation. Accordingly, at particular time, the influence of velocity is shown following a similar analysis as those underlying in Figures 3.11 and 3.12. Then, the non-dimensional temperatures' ratios and heat exchange rates' ratios if the time maintains constant, can vary with the velocity, and the detailed curves are illustrated in Figures 3.13 and 3.14, respectively.

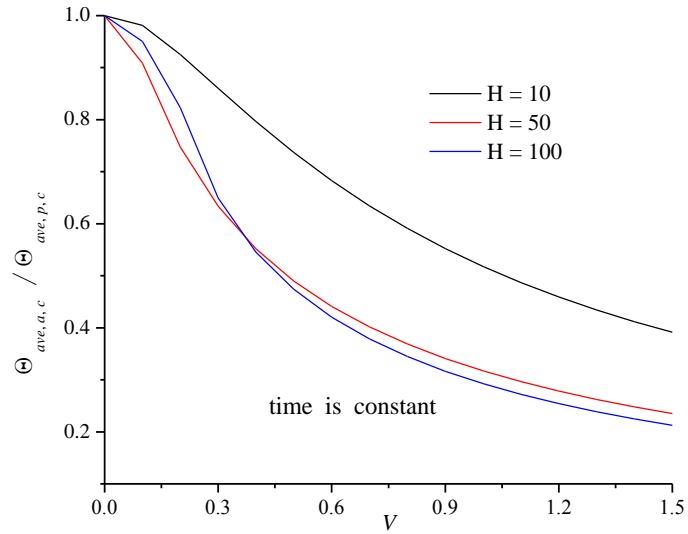


Figure 3.13 The ratios of temperature responses of two heat transfer modes with the velocity

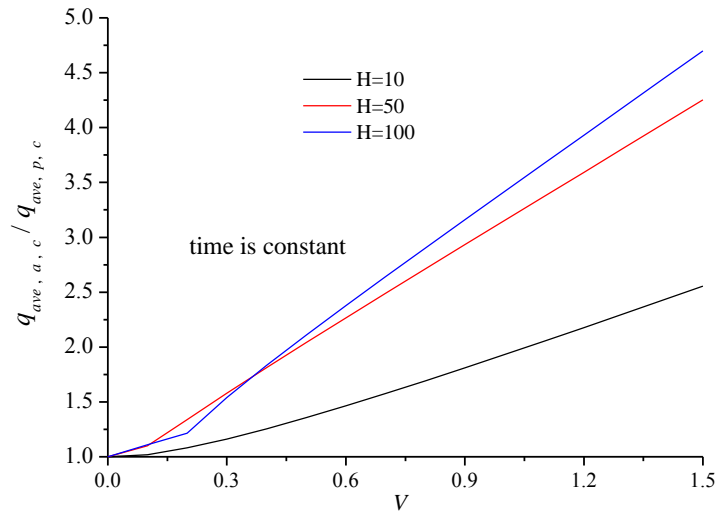


Figure 3.14 The ratios of heat exchange rates of two heat transfer modes with the velocity

The heat transfer superiority is gradually manifested with the increase of groundwater velocity and is also enhanced by a larger ratio of length to radius. The significance of groundwater flow is depicted by the graphs above, the role of groundwater becomes more obvious over a long enough period or if a large velocity exists. It is universally acknowledged that groundwater is significant not only for academic researches but also

for engineering projects, because more air-conditioning load can be undertaken by energy piles due to the improved heat exchange performance induced by groundwater flow.

3.6 Summary

The configuration features of an energy pile indicate that the line heat source and the hollow cylindrical heat source models are not applicable. The solid cylindrical heat source model is a significant help in investigating pile foundation GHEs due to its suitability for simulation. In recent years, researches on the pure conduction of energy pile have made progress, and the influences which groundwater advection exerts on borehole GHEs have been well explored. However, there has been a regrettable lack of theoretical models for the analysis of heat transfer for pile foundation in the presence of groundwater advection. In view of this, the role of groundwater has not been studied. It should be admitted that the required simulation models are hard to establish, and groundwater advection, therefore, is often ignored. The solid cylindrical seepage models analyzed above have clearly demonstrated the favorable effect of groundwater seepage.

Based on both pile conduction models and the combined heat transfer models of borehole GHEs, a proposed methodology for the study of solid cylindrical heat source seepage models including both the infinite and finite cases has been explored, and the characteristics involved in it are theoretically investigated. The influence which every parameter exerts on temperature response has been illuminated. Comparisons made between pure conduction and combined heat transfer, highlighting the specific role of groundwater seepage and proving its importance.

Admittedly, the solid cylindrical model is not the most accurate one, but it does take into account the heat transfer both inside and outside pile, and the basic configuration characteristics of an energy pile have been embodied. The models explored above represent positive progress towards understanding the effects of groundwater advection on practical energy piles. The solid cylindrical heat source seepage models above can be employed in circumstances where very accurate analysis is not required. The above analyses for the solid cylindrical heat source seepage models provide a firm basis on which to build more accurate models.

CHAPTER 4 COMBINED THERMAL EXCHANGE MODLS WHILE GROUNDWATER FLOWS THROUGH RING- COIL HEAT SOURCES

4.1 Introduction

Significant theoretical innovation resulted from the establishment of the solid heat source seepage models described and analyzed in Chapter 3. These models, however, are only approximate in that the spiral coils actually used are not expressed accurately. Heat exchange pipes are placed along the z -axis and structured as a spiral line. Points located at the coils have their own individual position angles. At least the pitch of coils should be represented to express the arrangement of pipes (Ali and Zaidi, 1980). Unfortunately, solid cylindrical models as in Chapter 3, only represents the spiral coils set at the interior surface of pile as a continuous cylindrical heat source. This cylindrical model does not take into account the discontinuity of the heat source in the longitudinal direction, and thus the temperature differences along the length of pile are blurred. Solid cylindrical model is useful if the requirement for calculation accuracy is not high because the interval of coils is ignored.

As groundwater flows through the spiral coils inside the pile foundation GHE, it is necessary to establish more approximate seepage models, as in Chapter 3, to represent the advection role. Improvements are described in this chapter. Such improvements better approximate the spiral coil, with the ring-coil model as shown in Figure 4.1. All

coils buried in the pile are deemed to be a series of separated coils with the same central axis, and a certain pitch between every two adjacent coils exists. The ring radius is assumed equal to that of the pile to make full use of the interior pile space.

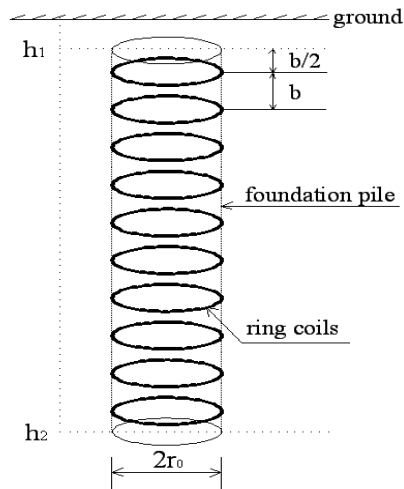


Figure 4.1 Schematic diagram of ring-coil heat source model

Figure 4.1 shows that the pile extends vertically from the starting position h_1 to the end position h_2 and therefore the length is $h_2 - h_1$. Spiral coils with the pitch of b run vertically down the pile. The separated coils begin at the distance of $b / 2$ from h_1 . Advanced from the solid cylindrical heat source model, all coils are not treated as a whole uniform cylindrical heat source but assigned with interval on the surface. The spiral angles are not represented in this model, but the pitch and temperature differences of coils can be approximated. Thus, the ‘ring-coil’ model is more appropriate for describing pile foundation GHEs because its configuration is closer to the profile of spiral coils (Cui et al, 2011). The ring-coil model, will enable more accurate analysis of the temperature distribution around energy pile with or without groundwater advection. The pure conduction models described below, are only concerned with the thermal response to the ring-coil heat source. The combined models emphasize the total

influence exerted by both the heat diffusion of coils and groundwater advection. The content of this chapter chiefly examines the effect of groundwater seepage to emphasize the contribution of the ring-coil heat source seepage models.

4.2 Pure conduction of ring-coil models

4.2.1 The methodology adopted

Most of the preconditions are the same as those of section 3.4, but the pitch b is a new fixed parameter. The spiral tube is represented by a series of separated coils with the radius r_0 . The Green's function is still the basis of obtaining the analytical solutions; both the infinite and the finite models are studied in relation to ring-coil pure conduction. For the infinite model, every spiral pipe is considered as an infinite number of coils set along the z -axis in an infinite medium. For the finite case, the pile depth coordinate is set from h_1 to h_2 along the z -axis in a semi-infinite medium and thus there are a limited number of ring coils. Each ring source emits heat at the intensity of $q_1 b$, therefore the expression of temperature response of any point (x, y, z) in the infinite or the semi-infinite medium except the heat source itself can be gained using the relevant integrals based on the Green function; this is because one ring coil is the gather of an infinite number of points, therefore the total thermal response can be obtained by the superposition of all coils. There is no denying the fact that the finite ring-coil model approximates the actual energy pile.

The Green's function for an infinite homogeneous medium is the most essential and most useful in the heat conduction theory and its expression in the Cartesian coordinates is given by the Equation (4.1):

$$G(x, y, z, \tau; x', y', z', \tau') = \frac{1}{8[\sqrt{\pi a(\tau - \tau')}]^3} \exp\left[-\frac{(x-x')^2 + (y-y')^2 + (z-z')^2}{4a(\tau - \tau')}\right] \quad (4.1)$$

Any coil that contains $z = z'$ can be looked upon as a ring heat source with the heat intensity of $q_l b$, the corresponding conversion from Cartesian coordinates to cylindrical coordinates are written as: $x' = r' \cos \phi'$, $y' = r' \sin \phi'$, $z' = z$, $x = r \cos \phi$, $y = r \sin \phi$, $z = z$. The excess temperature $\theta = t - t_0$ is used to define the temperature response of any point in the medium except heat source itself. The value of θ caused by ring coils continuously releasing heat is obtained by integrating Green function, and the corresponding expression is:

$$\theta_{\text{ring}} = \frac{q_l b}{2\pi\rho c} \int_0^\tau d\tau' \int_0^{2\pi} G d\phi' = \frac{q_l b}{8\rho c} \int_0^\tau \frac{1}{[\pi a(\tau - \tau')]^{3/2}} \exp\left[-\frac{r^2 + r_0^2 + (z - z')^2}{4a(\tau - \tau')}\right] I_0\left[\frac{r r_0}{2a(\tau - \tau')}\right] d\tau' \quad (4.2)$$

4.2.2 Infinite ring-coil heat source model

In the infinite domain, the z coordinate of every coil is expressed as: $z' = \pm(n+0.5)b$, $n = 0, 1, 2, 3, \dots$. This distribution takes ground as the symmetrical plane and countless coils exist in infinite space. The total temperature response produced by all coils heating with a certain intensity is:

$$\begin{aligned} \theta_{p,r,i} &= \frac{q_l}{2\pi\rho c} \sum_{n=-\infty}^{\infty} \int_0^\tau d\tau' \int_0^{2\pi} G(z' = nb + 0.5b) d\phi' \\ &= \frac{q_l b}{8\rho c} \sum_{n=-\infty}^{\infty} \int_0^\tau \frac{1}{[\pi a(\tau - \tau')]^{3/2}} \exp\left[-\frac{r^2 + r_0^2 + (z - nb - 0.5b)^2}{4a(\tau - \tau')}\right] I_0\left[\frac{r r_0}{2a(\tau - \tau')}\right] d\tau' \end{aligned} \quad (4.3)$$

Equation (4.3) can be turned into relatively direct and short formula such as:

$$\theta_{p,r,i} = \frac{q_1 b}{8 \rho c} \int_0^\tau \frac{1}{[\pi a (\tau - \tau')]^{3/2}} I_0 \left[\frac{r r_0}{2a(\tau - \tau')} \right] \cdot \exp \left[-\frac{r^2 + r_0^2}{4a(\tau - \tau')} \right] \cdot \sum_{n=0}^{\infty} \left\{ \exp \left[-\frac{(z - nb - 0.5b)^2}{4a(\tau - \tau')} \right] + \exp \left[-\frac{(z + nb + 0.5b)^2}{4a(\tau - \tau')} \right] \right\} d\tau' \quad (4.4)$$

To simplify Equation (4.4), non-dimensional parameters are given: $Fo = a \tau / r_0^2$, $\Theta = k \theta / q_1$, $Z = z / r_0$, $R = r / r_0$ and $B = b / r_0$. For this, Equation (4.4) is transformed into:

$$\Theta_{p,r,i} = \frac{B}{8} \int_0^{Fo} \frac{1}{[\pi (Fo - Fo')]^{3/2}} I_0 \left[\frac{R}{2(Fo - Fo')} \right] \cdot \exp \left[-\frac{R^2 + 1}{4(Fo - Fo')} \right] \cdot \sum_{n=0}^{\infty} \left\{ \exp \left[-\frac{(Z - nB - 0.5B)^2}{4(Fo - Fo')} \right] + \exp \left[-\frac{(Z + nB + 0.5B)^2}{4(Fo - Fo')} \right] \right\} dFo' \quad (4.5)$$

4.2.3 Finite ring-coil heat source model

The semi-infinite domain consists of the homogenous medium with a ground surface kept at a constant temperature; finite heat source emits heat at the invariable positive heating rate of q_1 . In view of this, the virtual heat source method can be employed to obtain the analytical solution of temperature response. That is to say, the virtual heat sink with a negative heating rate $-q_1$ was set symmetrically to the heat source because the ground boundary exists. The temperature of ground surface, $t = t_0$, is necessary as heat source and virtual sink are symmetrical. The thermal response of any point except the heat source in the underground medium can be obtained by summing up the effects of all heat sources and sinks. According to Figure 4.1, there are $\text{int} [(h_2 - h_1)/b]$ ring coils heat sources. The corresponding thermal response is shown in Equation (4.6).

$$\begin{aligned}
\theta_{p,r,f} &= \frac{q_1 b}{2\pi\rho c} \int_0^\tau d\tau' \left[\sum_{n=0}^{m-1} \int_0^{2\pi} G(z' = h_1 + nb + 0.5b) d\phi' - \sum_{n=0}^{m-1} \int_0^{2\pi} G(z' = -h_1 - nb - 0.5b) d\phi' \right] \\
&= \frac{q_1 b}{8\rho c} \int_0^\tau \frac{1}{[\pi a(\tau - \tau')]^{3/2}} I_0 \left[\frac{r r_0}{2a(\tau - \tau')} \right] \cdot \exp \left[-\frac{r^2 + r_0^2}{4a(\tau - \tau')} \right] \cdot \\
&\quad \sum_{n=0}^{m-1} \left\{ \exp \left[-\frac{(z - h_1 - nb - 0.5b)^2}{4a(\tau - \tau')} \right] - \exp \left[-\frac{(z + h_1 + nb + 0.5b)^2}{4a(\tau - \tau')} \right] \right\} d\tau'
\end{aligned} \tag{4.6}$$

The finite model is deemed as the focus objective since energy pile in practice has finite depth. Most of dimensionless parameters are equal to those of the infinite model, and the non-dimensional starting and end locations' coordinates of coils along the z -axis should be given as $H_1 = h_1 / r_0$ and $H_2 = h_2 / r_0$, respectively. Thus, the non-dimensional analytical solution of the temperature response of the finite ring-coil heat source seepage model is obtained in Equation (4.7). The thermal response of any point except the heat source itself in the semi-infinite underground space is the result of a limited number of separated coils, and the virtual heat source method can be applied.

$$\begin{aligned}
\Theta_{p,r,f} &= \frac{B}{8\pi^{3/2}} \int_0^{Fo} \frac{1}{(Fo - Fo')^{3/2}} I_0 \left[\frac{R}{2(Fo - Fo')} \right] \cdot \exp \left[-\frac{R^2 + 1}{4(Fo - Fo')} \right] \cdot \\
&\quad \sum_{n=0}^{m-1} \left\{ \exp \left[-\frac{(Z - H_1 - nB - 0.5B)^2}{4(Fo - Fo')} \right] - \exp \left[-\frac{(Z + H_1 + nB + 0.5B)^2}{4(Fo - Fo')} \right] \right\} dFo'
\end{aligned} \tag{4.7}$$

4.2.4 The presentation for temperature responses

4.2.4.1 The trends of temperature responses with the time

The whole thermal transmission of energy pile can be described as consisting of several steps; firstly, the heat is delivered by circulating fluid circulating in the spiral tubes to the inner wall of the tubes by convection; secondly, conduction transmits heat to the tubes' outer wall; the heat is then conducted through grout material inside the pile and arrives at the pile's surface; finally, heat is further conducted to the surrounding

underground medium (Li et al, 2011).

For pure conduction models, heat transfer is conducted in all radial directions to the same degree while z is assumed constant. The underground medium receives uninterrupted pulse thermal load from the ring-coil source; the temperature responses around the energy pile show evident feedback especially in the initial period. The infinite ring-coil model infinitely consists of a number of separated coils and every one emits heat pulses continuously, with the result that temperature response cannot attain the stable state. However, the constant temperature of ground boundary does limit the temperature response to the finite ring-coil model, and all cases reach stable temperatures after a long enough time. The temperature responses with the time of both the infinite and the finite ring-coil models are shown in Figure 4.2. The parameter H is the ratio of length to radius of heat source, that is, $H = (h_2 - h_1) / r_0$. It is clear that the time of attaining stable state depends on the model's dimensionless length, i.e. the ratios of length to radius. The greater the ratio, the longer the time needed to reach stability.

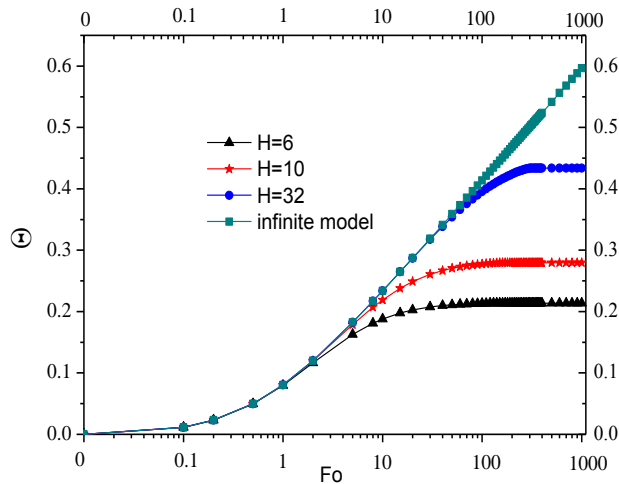


Figure 4.2 The temperature responses of ring-coil pure conduction models

For pile foundation GHEs with a series of separated coils, the temperature response to the infinite model is affirmatively higher than that to the finite model at all times if other conditions are the same. Another conclusion to emphasize is that the temperature response of the infinite model has no upper limit with the time because the constant temperature of ground boundary is not taken into account.

4.2.4.2 Temperature distribution around the ring-coil heat source

The isothermals around coils can give expression to the thermal responses at different positions. For the finite model, the case that is more reasonable to be used because of the finite length of pile. The calculation and programming are conducted based on the Equation (4.7) and the isothermals on the XOY and XOZ planes are shown in Figure 4.3. The thermal responses are symmetrically about the central axis for this only pure conduction exists.

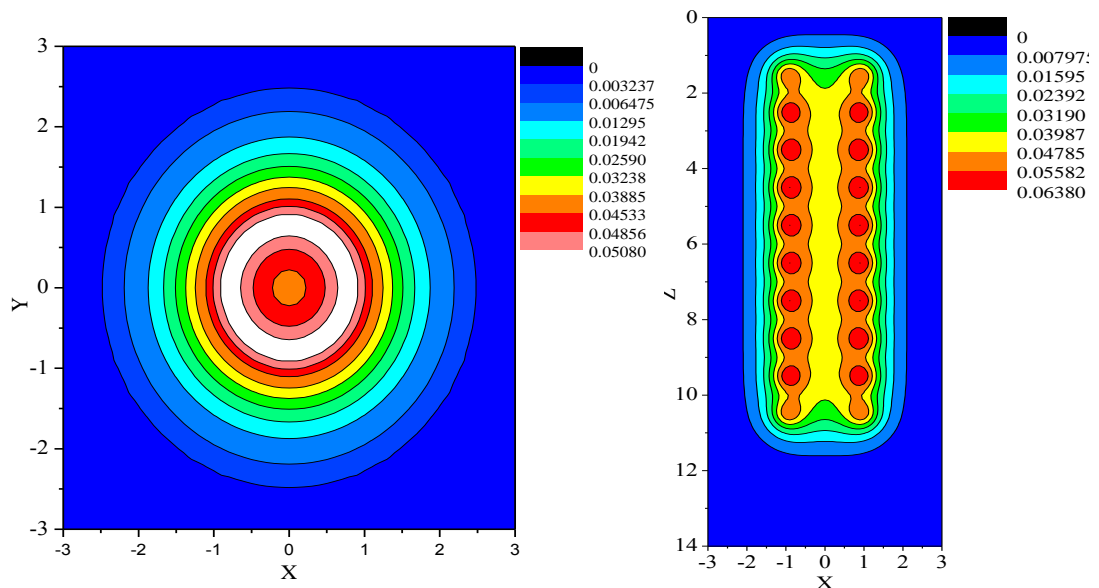


Figure 4.3 The isothermals of ring-coil pure conduction model

The thermal responses near the ring-coil sources are clearly stronger than those relatively further away from the heat sources at the same plane.

4.3 Combined thermal exchange of ring-coil models

4.3.1 The methodology adopted

The heat transfer of ring-coils when groundwater seepage exists is also complicated and unsteady. Compared with those studies in the past, the heat transfer models are proposed while groundwater flows through a series of separated coils, therefore the investigation on ring-coil combined models is novel. The groundwater seepage has the time scale of several months, even years. The groundwater velocity is the most significant parameter defining the advection strength. Since the underground medium is treated as the homogeneous porous medium to simplify the problem, the heat energy equation of both conduction and convection in the porous medium can be described by Equation (3.11), and the equivalent speed $U = \rho_w c_w u / \rho c$.

The important idea can be derived from Equation (3.11), namely, a instantaneous point heat source with stationary location when groundwater flows past it, can be thought of as a moving instantaneous point heat source at (x', y', z') emitting heat at time τ' , leading to a temperature response at any point (x, y, z) at time τ except heat source itself. Green's function theory is employed again to solve the seepage problem and its new expression including the groundwater factor is given by Equation (4.8) is defined based on the existing knowledge (Zhang et al., 2014).

$$M(x, y, z, \tau; x', y', z', \tau') = \frac{1}{8[\pi a(\tau - \tau')]^{3/2}} \exp \left\{ -\frac{[x - x' - U(\tau - \tau')]^2 + (y - y')^2 + (z - z')^2}{4a(\tau - \tau')} \right\} \quad (4.8)$$

Equation (4.8) and the prerequisites are almost the same as those appeared in chapter 3, as far as every coil with radius r_0 is concerned, because it begins to emit heat from $\tau = \tau'$ at a constant heat intensity $q_1 b$. The energy equation and the corresponding conditions are demonstrated as:

$$\begin{cases} \frac{\partial \theta}{\partial \tau} + U \frac{\partial \theta}{\partial (r \cos \varphi)} = a \left(\frac{\partial^2 \theta}{\partial r^2} + \frac{1}{r} \frac{\partial \theta}{\partial r} + \frac{\partial^2 \theta}{\partial z^2} \right) + \frac{q \delta(r - r_0, z - z')}{2\pi r_0 \rho c}, \text{ for } 0 < r < \infty, -\infty < z < \infty, \tau > \tau' \\ \frac{\partial \theta}{\partial r} = 0, \text{ for } r = 0, -\infty < z < \infty, \tau > \tau' \\ \theta = 0, \text{ for } 0 < r < \infty, -\infty < z < \infty, \tau = \tau' \\ \theta = 0, \text{ for } r \rightarrow \infty, -\infty < z < \infty, \tau > \tau' \end{cases} \quad (4.9)$$

where $r_0 = \sqrt{x'^2 + y'^2}$ and $r = \sqrt{x^2 + y^2}$.

An alternative expression of the M function in cylindrical coordinate is:

$$M(r, \varphi, z, \tau; r_0, \varphi', z', \tau') = \frac{1}{8[\pi a(\tau - \tau')]^{3/2}} \exp \left\{ -\frac{[r \cos \varphi - r_0 \cos \varphi' - U(\tau - \tau')]^2 + (r \sin \varphi - r_0 \sin \varphi')^2 + (z - z')^2}{4a(\tau - \tau')} \right\} \quad (4.10)$$

The temperature response induced by a single coil which emits heat continuously is:

$$\theta_{\text{ring}} = \frac{q_1 b}{2\pi \rho c} \int_0^{2\pi} M(r' = r_0) d\varphi' \int_0^{\tau} d\tau' = \frac{q_1 b}{4\pi^{5/2} k} \int_0^{2\pi} \exp \left[\frac{U(x - r_0 \cos \varphi')}{2a} \right] \cdot f(\varphi') d\varphi' \quad (4.11)$$

where

$$f(\varphi') = \frac{1}{R} \int_{R/\sqrt{2a\tau}}^{\infty} \exp \left(-\psi^2 - \frac{U^2 R^2}{16a^2 \psi^2} \right) d\psi = \frac{\sqrt{\pi}}{4R} \left[\exp \left(-\frac{UR}{2a} \right) \operatorname{erfc} \left(\frac{R - U\tau}{2\sqrt{a\tau}} \right) + \exp \left(\frac{UR}{2a} \right) \operatorname{erfc} \left(\frac{R + U\tau}{2\sqrt{a\tau}} \right) \right]. \quad (4.12)$$

And here $R = \sqrt{(x - r \cos \varphi')^2 + (y - r \sin \varphi')^2 + (z - z')^2} = \sqrt{r^2 + r_0^2 - 2rr_0 \cos(\varphi - \varphi') + (z - z')^2}$

4.3.2 Infinite ring-coil heat source model

As for the infinite model, there are an infinite number of ring coils with the z

coordinates of $z' = \pm(n + 0.5)b$, $n = 0, 1, 2, 3, \dots$. The heat transfer along z-direction is ignored when groundwater passes these countless separated coils with a certain pitch. The temperature response at any point except the heat source itself in the medium can be obtained by summing up the functions of all coils and the detailed expression is given in Equation (4.13).

$$\theta_{a,r,i} = \frac{q_l b}{2\pi\rho c} \sum_{n=-\infty}^{\infty} \int_0^{\tau} d\tau' \int_0^{2\pi} M(z' = nb + 0.5b) d\phi' = \frac{q_l b}{4\pi^{5/2}k} \sum_{n=-\infty}^{\infty} \int_0^{2\pi} \exp\left[\frac{U(x - r_0 \cos\phi')}{2a}\right] \cdot f(\phi') d\phi' \quad (4.13)$$

Because R is expressed as $\sqrt{r^2 + r_0^2 - 2rr_0 \cos(\varphi - \phi') + (z - nb - 0.5b)^2}$, Equation (4.13) can be shown in a more detailed manner in case it is combined with Equation (4.12), and a more detailed expression is:

$$\theta_{a,r,i} = \frac{q_l b}{4\pi^{5/2}k} \sum_{n=-\infty}^{\infty} \int_0^{2\pi} \exp\left[\frac{U(x - r_0 \cos\phi')}{2a}\right] \cdot \frac{\sqrt{\pi} d\phi'}{4\sqrt{r^2 + r_0^2 - 2rr_0 \cos(\varphi - \phi') + (z - nb - 0.5b)^2}} \left[\exp\left(-\frac{U\sqrt{r^2 + r_0^2 - 2rr_0 \cos(\varphi - \phi') + (z - nb - 0.5b)^2}}{2a}\right) \operatorname{erfc}\left(\frac{\sqrt{r^2 + r_0^2 - 2rr_0 \cos(\varphi - \phi') + (z - nb - 0.5b)^2} - U\tau}{2\sqrt{a\tau}}\right) \right. \\ \left. + \exp\left(\frac{U\sqrt{r^2 + r_0^2 - 2rr_0 \cos(\varphi - \phi') + (z - nb - 0.5b)^2}}{2a}\right) \operatorname{erfc}\left(\frac{\sqrt{r^2 + r_0^2 - 2rr_0 \cos(\varphi - \phi') + (z - nb - 0.5b)^2} + U\tau}{2\sqrt{a\tau}}\right) \right] \quad (4.14)$$

Equation (4.14) is so complex that the necessity of adopting a dimensionless approach is logical, reducing the number of parameters and showing the analytical solutions concisely. The non-dimensionless parameters introduced in section 4.2 are again employed, together with an additional one, i.e. dimensionless ground velocity $S = u r_0 / a$. The dimensionless analytical solution of temperature response induced by an infinite ring-coil heat source seepage model is given by Equation (4.15).

$$\Theta_{a,r,i} = \frac{B}{4\pi^{5/2}} \sum_{n=-\infty}^{\infty} \int_0^{2\pi} \exp\left[\frac{S \cdot (X - \cos \phi')}{2}\right] \cdot \frac{\sqrt{\pi} d\phi'}{4\sqrt{R^2 + 1 - 2R \cos(\phi - \phi') + (Z - nB - 0.5B)^2}} \left[\exp\left(-\frac{S \cdot \sqrt{R^2 + 1 - 2R \cos(\phi - \phi') + (Z - nB - 0.5B)^2}}{2}\right) \operatorname{erfc}\left(\frac{\sqrt{R^2 + 1 - 2R \cos(\phi - \phi') + (Z - nB - 0.5B)^2} - S \cdot Fo}{2\sqrt{Fo}}\right) \right. \\ \left. + \exp\left(\frac{S \cdot \sqrt{R^2 + 1 - 2R \cos(\phi - \phi') + (Z - nB - 0.5B)^2}}{2}\right) \operatorname{erfc}\left(\frac{\sqrt{R^2 + 1 - 2R \cos(\phi - \phi') + (Z - nB - 0.5B)^2} - S \cdot Fo}{2\sqrt{Fo}}\right) \right] \quad (4.15)$$

4.3.3 Finite ring-coil heat source model

The exploration of the infinite model implies that the two-dimensional (2-D) combined heat transfer has preliminarily announced the influence of groundwater advection. And that, the three-dimensional (3-D) one, i.e. the finite model, adds heat transfer along the z-axis to the thermal transmission of the 2-D model. Because real energy piles are of limited length, study of the 3-D model is more significant. The image method is again suggested because of the boundary role of the ground surface, therefore the temperature of ground boundary contains constant in the whole process and the finite number of coils is $\text{int} [(h_2 - h_1)/b]$. The temperature response of the finite ring-coil model is provided by Equation (4.16), and the contributions of all heat sources and sinks are comprehensively included in it.

$$\theta_{a,r,f} = \frac{q_l b}{16\pi^{5/2} k} \sum_{n=0}^{m-1} \int_0^{2\pi} d\phi' \int_0^{\tau} \exp\left[-\frac{[x - r_0 \cos \phi' - U(\tau - \tau')]^2 + (y - r_0 \sin \phi')^2}{4a(\tau - \tau')}\right] \cdot \left\{ \exp\left[-\frac{(z - h_1 - nb - 0.5b)^2}{4a(\tau - \tau')}\right] - \exp\left[-\frac{(z + h_1 + nb + 0.5b)^2}{4a(\tau - \tau')}\right] \right\} \frac{d\tau'}{\sqrt{a}(\tau - \tau')^{3/2}} \quad (4.16)$$

The non-dimensional expression is obtained by means of transformation based on Equation (4.16) and the new one is generated as:

$$\Theta_{a.r.f} = \frac{B}{16\pi^{5/2}} \sum_{n=0}^{m-1} \int_0^{2\pi} d\varphi' \int_0^{Fo} \exp \left[-\frac{[X - \cos \varphi' - S \cdot (Fo - Fo')]^2 + (Y - \sin \varphi')^2}{4(Fo - Fo')} \right] \cdot \left\{ \exp \left[-\frac{(Z - H_1 - nB - 0.5B)^2}{4(Fo - Fo')} \right] - \exp \left[-\frac{(Z + H_1 + nB + 0.5B)^2}{4(Fo - Fo')} \right] \right\} \frac{dFo'}{(Fo - Fo')^{3/2}} \quad (4.17)$$

4.3.4 The presentation for temperature responses

4.3.4.1 The trends of temperature responses with the time

The impact of the pulse thermal load is lessened once groundwater seepage influences the heat transfer because advection alleviates the heat build-up around heat sources, therefore thermal response in the ground is weakened. The temperature response of the combined heat transfer can reach steady state no matter whether the model is infinite or finite because the underground medium accepts the synthetic actions of two types of heat exchange. For the infinite model, heat accumulation and relief reach balanced condition eventually and thus the temperature fluctuates little from that time. For the finite model, temperature responses definitely attain stable states even when there is only conduction, therefore the response trends must become finally stable in the presence of groundwater advection. Since the isothermals around coils are not symmetrical about the z -axis, the mean temperature response is acquired by integral average method. The integration is executed around the pile perimeter to obtain the average dimensionless temperature. For this, the average values of the infinite and the finite models are respectively shown in Equation (4.18) and (4.19).

$$\overline{\Theta}_{a,r,i} = \frac{B}{16\pi^2} \cdot \frac{1}{2\pi} \sum_{n=-\infty}^{\infty} \int_0^{2\pi} d\varphi \int_0^{2\pi} \exp\left[\frac{S \cdot (R \cos \varphi - \cos \varphi')}{2}\right] \cdot \frac{d\varphi'}{\sqrt{R^2 + 1 - 2R \cos(\varphi - \varphi') + (Z - nB - 0.5B)^2}}$$

$$\left[\exp\left(-\frac{S \cdot \sqrt{R^2 + 1 - 2R \cos(\varphi - \varphi') + (Z - nB - 0.5B)^2}}{2}\right) \operatorname{erfc}\left(\frac{\sqrt{R^2 + 1 - 2R \cos(\varphi - \varphi') + (Z - nB - 0.5B)^2} - S \cdot Fo}{2\sqrt{Fo}}\right) \right. \quad (4.18)$$

$$\left. + \exp\left(\frac{S \cdot \sqrt{R^2 + 1 - 2R \cos(\varphi - \varphi') + (Z - nB - 0.5B)^2}}{2}\right) \operatorname{erfc}\left(\frac{\sqrt{R^2 + 1 - 2R \cos(\varphi - \varphi') + (Z - nB - 0.5B)^2} + S \cdot Fo}{2\sqrt{Fo}}\right) \right]$$

$$\overline{\Theta}_{a,r,f} = \frac{B}{16\pi^{5/2}} \cdot \frac{1}{2\pi} \sum_{n=0}^{m-1} \int_0^{2\pi} d\varphi \int_0^{2\pi} d\varphi' \int_0^{Fo} \exp\left[-\frac{[\cos \varphi - \cos \varphi' - S \cdot (Fo - Fo')]^2 + (\sin \varphi - \sin \varphi')^2}{4(Fo - Fo')}\right] \cdot \quad (4.19)$$

$$\left\{ \exp\left[-\frac{(Z - H_1 - nB - 0.5B)^2}{4(Fo - Fo')}\right] - \exp\left[-\frac{(Z + H_1 + nB + 0.5B)^2}{4(Fo - Fo')}\right] \right\} \frac{dFo'}{(Fo - Fo')^{3/2}}$$

Based on Equations (4.18) and (4.19), the corresponding calculations and programming are conducted. The temperature responses with the time are shown in Figure 4.4. When compared with Figure 4.2, it is evident that the combined models' temperature responses are lower than those of the pure conduction models.

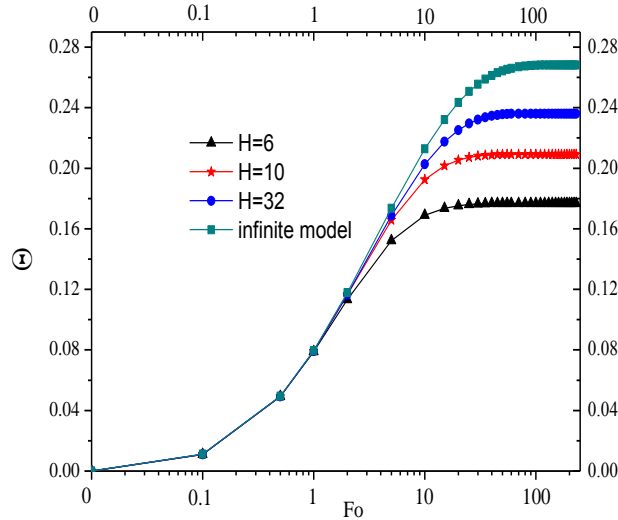


Figure 4.4 The temperature responses of ring-coil combined heat transfer models

Also, the time required to attain stability is shortened and even the infinite model can eventually achieve stability. The same summary applies for both the pure conduction

and the combined models, that is, the infinite model give rises to the maximum response, and the thermal responses vary from weak to strong with the increase of dimensionless lengths if time and velocity are both constant.

4.3.4.2 The temperature distribution around ring-coil heat source

Any pile foundation GHE has limited length, thus the finite combined heat transfer model is again employed to exhibit the temperature distribution around those separated coils as groundwater flows past them. The corresponding isothermals on the XOY and the XOZ planes are shown in Figure 4.5. Figure 4.5 illustrates that the temperature field is asymmetry about the axis as groundwater seepage exists. Thermal responses of the right side are higher than those of the left side because groundwater flows in the positive direction of the X-axis.

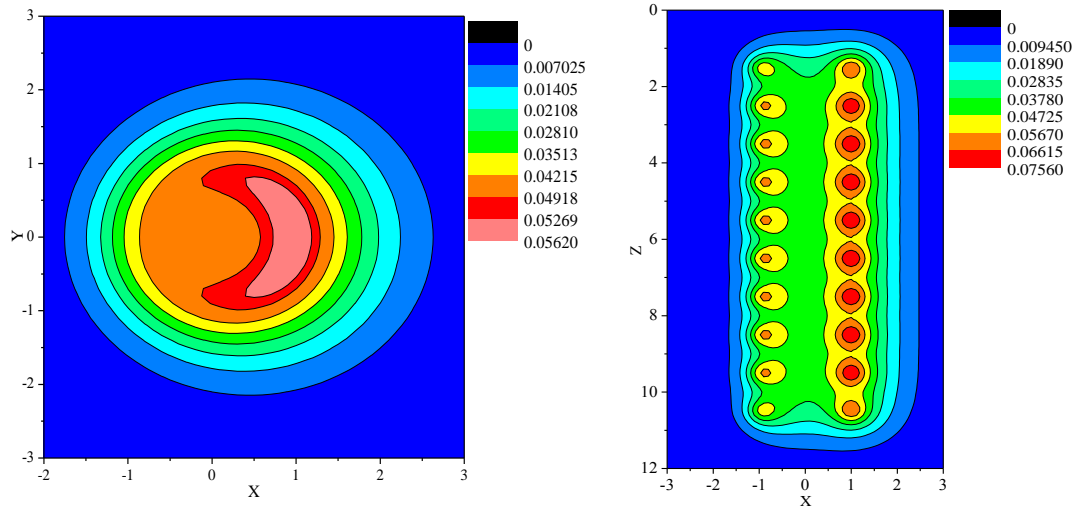


Figure 4.5 The isothermals of ring-coil combined heat transfer model

4.3.5 The characteristics of finite ring-coil seepage model

Now that the finite model approximates to the actual pile foundation GHEs with

spiral coils, it is worth examining the characteristics revealed by the model. The impacts of some factors such as groundwater velocity, coil pitch and so on should be explored to reveal their roles.

4.3.5.1 The thermal responses at locations with different radial distances from ring-coil heat source

In consideration of the asymmetric temperature profile, the integral average method is employed to obtain the mean temperature response of any circle regarding z -axis as central line at different XOY cross sections. The mid depth of the model along the z -axis is chosen, i.e. $Z = (H_1 + H_2) / 2$. Taking the case of $H = 10$ for example, there are three values of R and the temperature responses with the time are given in Figure 4.6. Constant values $S = 0.5$ and $B = 1.0$ are respectively set for velocity and coil pitch. Figure 4.6 makes clear that response strength radially changes from strong to weak. The excess temperature is zero at infinite distance from the ring-coil heat source, which conforms with the prerequisites of combined models.

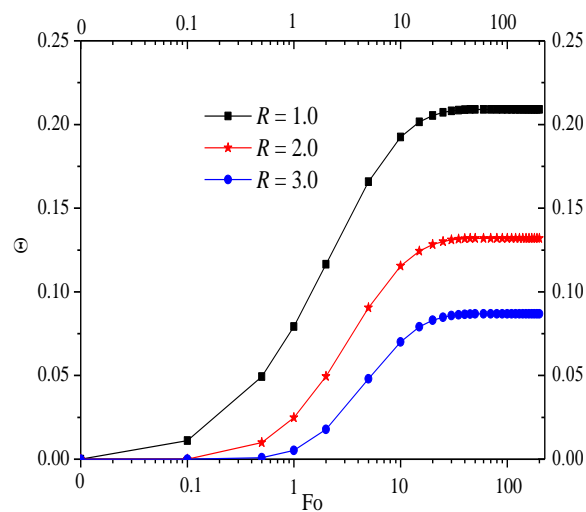


Figure 4.6 The temperature responses of positions with different R values

The groundwater velocity is assumed to flow along the forward direction of x -axis. The upstream and downstream sides show different thermal responses because the groundwater first makes contact with the position ($\varphi = \pi$) and then flows through the place ($\varphi = 0$) of energy pile. From the perspective of alleviating heat accumulation, the side $\varphi = \pi$ is affected to a greater degree by groundwater advection and the heat delivered by groundwater convection unfavorably influences the downstream thermal transfer. However, the heat build-up around pile GHEs is mitigated by the groundwater advection at last (Fan et al, 2007b). R values of 0.5, 1.0 and 1.5 are applied and the time and the velocity are kept constant. The temperature profiles along the z -axis for cases of $\varphi = 0$ and $\varphi = \pi$ are shown in Figure 4.7.

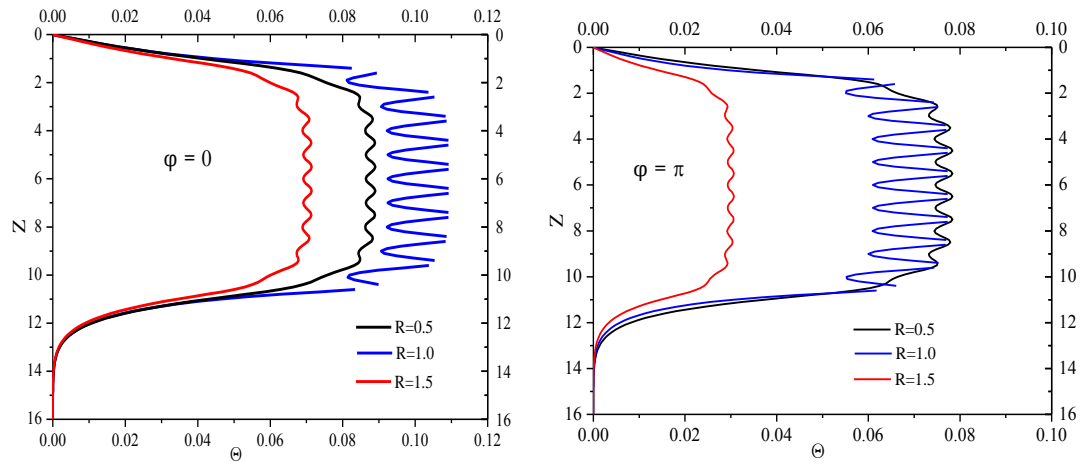


Figure 4.7 Temperature profiles along z -axis when φ adopts 0 and π respectively

The oscillating curves prove that the coils arrangement does affect the temperature distribution. The maximum values of temperature responses appear on those planes which contain a ring-coil, and the wave valleys occur at the mid distance between coils. The position is just right on the point of coils if the value of R is 1.0 at the horizontal planes with coils, thus the corresponding temperature responses of these positions are

infinite according to the Fourier law. What is more, the temperature responses of positions where $\varphi = \pi$ are significantly less than those with $\varphi = 0$ because of groundwater flow.

4.3.5.2 The role of groundwater velocity

The critical factor of groundwater seepage is the velocity because its value determines the degree of convection influence. Heat can be easily removed from the surrounding of coils if the velocity attains a certain level. Groundwater then takes the accumulated heat caused by ring-coil heat sources away to the far distances; this is helpful to improve the heat transfer between heat sources and the surrounding medium. However, groundwater advection cannot contribute superior function to whole heat transfer if the velocity value is small or even close to zero. In such a situation, pure conduction plays a dominant role and the heat build-up around pile becomes more and more serious; this leads to poor heat exchange performance because the temperature difference between pile GHEs and the surrounding underground medium is small and continuous heat dissipation is slowed. The middle depth $(H_1 + H_2) / 2$ is still chosen as the object when $R = 1.0$. The temperature responses with the time if velocity adopts different values are given in Figure 4.8, meanwhile pile foundation GHEs have a fixed length H and a fixed coils pitch.

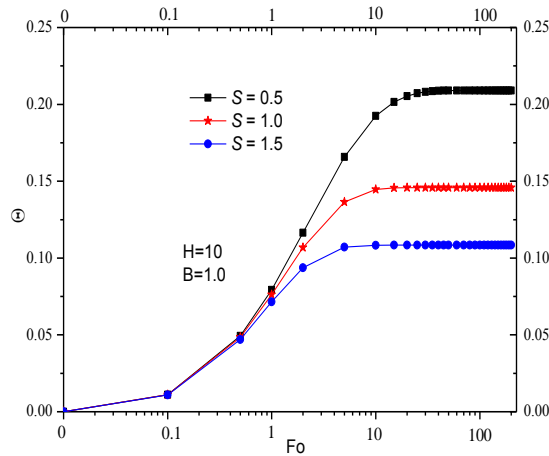


Figure 4.8 The temperature responses with the time when velocity adopts different values

Based on the Darcy's law, the value of groundwater velocity in the porous medium depends on the local underground hydraulic gradient and hydraulic conductivity (Wang, 1986). Three cases with corresponding velocities are compared and the temperature responses are illustrated in Figure 4.8. Figure 4.8 indicates that the time needed for arriving at steady state decreases and the ultimate temperature response is smaller if the velocity is larger, that is, the thermal stability is easier reached when the seepage is strong, therefore the heat exchange can be improved. Accordingly, it is vital to understand the local hydraulic gradient before conducting calculation and analysis.

4.3.5.3 The effects of coil pitch

Spiral coils with a definite pitch are installed in an energy pile, and the temperature responses induced by the coils are affected by the pitch when coils' radius and depth are confirmed. Pitch reflects the denseness of the coils arrangement along the z-axis, defining the number of coil heat sources with the same heating rate. Coil pitch must has a considerable effect on the temperature responses of the models.

The fluid passes by much pipeline if there is a dense arrangement occurs, thus the

heat transfer rate can be high. However, extra cost and the inconvenience in construction and fabrication of energy pile are caused. Another problem is that thermal interferences among coils are certainly serious, which is disadvantageous to the performance of energy pile. In addition, the temperature responses in the surrounding medium are enhanced quickly, thus reaching the steady state takes longer.

But, the tube surface area available for heat exchange becomes small when a sparse arrangement appears if the pitch is large, causing the pile space inefficiently utilized. Too big a pitch defeats the purpose of using a spiral tube, the significance of which is to provide a large total surface area. As stated in chapter 1, the spiral tube has a higher heat transfer coefficient because more area is available for heat exchange.

In fact, the choice of pitch for an energy pile should take account of the actual situation. Taking $H = 10$ for example, four different pitch values are set, i.e. $B = 0.2, 1.0, 2.5,$ and 5.0 when groundwater velocity is constant. The corresponding numbers of ring coils are 50, 10, 4 and 2, respectively. The temperature responses at mid depth when $R = 1.0$ are shown in Figure 4.9.

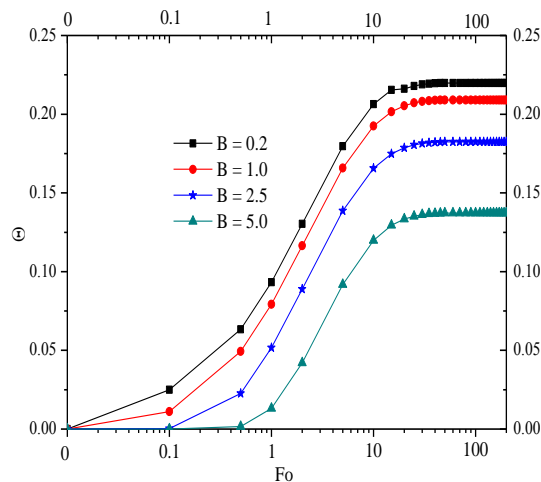


Figure 4.9 The temperature responses with the time when coils pitch adopts different values

Figure 4.9 indicates that temperature responses vary from high to low when B varies from small to big. From another perspective, when H and R are still respectively 10 and 1.0, the temperature response changes with the velocity at any fixed time. Four values are again set as 0.2, 1.0, 2.5, and 5.0 for B . The temperature responses are different as B takes different values, but all decrease with the velocity, and the detailed information is depicted in Figure 4.10.

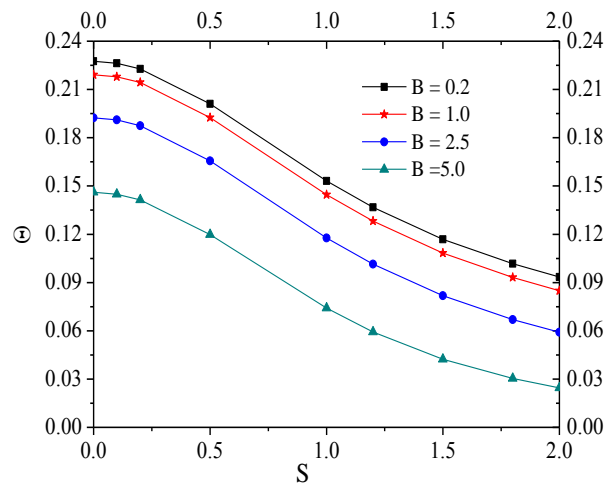


Figure 4.10 The temperature responses with the velocity when coil pitch adopts different values

4.3.5.4 Comparisons of temperature responses at different distances along z-axis from ring-coils

The ring-coil models take approximate account of non-continuity of the heat source along z -axis. The coil radius is assumed equal to that of the pile in order to maximize the length of the heat exchange tube. At the time of $R = 1.0$, temperature responses fluctuate at all positions along the z -axis except at the coils themselves, due to the pulse thermal load. These responses differ because every position (except the coils) is at a particular distance from each coil, and the distances between any fixed coil and each position except coil itself are all different.

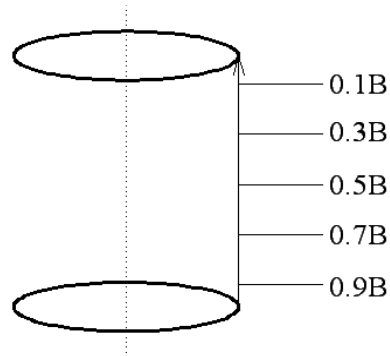


Figure 4.11 Two adjacent coils and different positions between them

For the example of $H = 10$ with 10 ring coils spaced along z -direction ($B = 1.0$), the fifth and the sixth coils as well as their interval are displayed in Figure 4.11 showing five different positions. The temperature response of each position with the time is indicated in Figure 4.12 when the groundwater velocity keeps constant. The points $0.1 B$ and $0.9 B$ show the strongest thermal responses because they are closest to the coils. In contrast, the position $0.5 B$ has the least thermal response value because it is relatively far from any of two coils. The temperature responses at $0.3 B$ and $0.7 B$ attain the intermediate levels.

There are four coils above the fifth coil and another four below the sixth coil. The fifth and the sixth coils and their interval are selected for detailed study because they are situated near the mid depth of the pile. As the sum of distances from every coil to any particular position in the medium remains constant and all coils provide the equal thermal pulse load, the temperature response of any position between the fifth and the sixth coils depends on the distance from the adjoining coil.

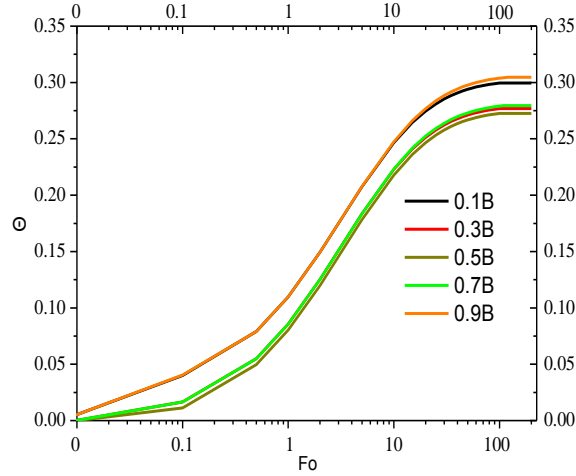


Figure 4.12 The temperature responses of different positions between adjacent coils

4.3.5.5 The alternative method for simplifying calculation

As mentioned in section 4.2.4.2, isothermals distributions are not symmetrical owing to the seepage influence and thus the mean temperature response at any horizontal cross section should be obtained by the integral average method. However, this increases the number of integrations, causing excessive complexity. The temperature response at the energy pile's external surface is a good judgment index to check the heat exchange performance. For a constant value of z , the temperature responses of $\varphi = 0$ and $\varphi = \pi$ when $R = 1.0$ can be discussed. If the average value of these two cases is used to substitute for result obtained by the integral average method, what would be the error? If ER denotes the error rate (Huang et al, 2004), Θ_{ave} and Θ_{be} are respectively the integral mean value and the mean value of $\varphi = 0$ and $\varphi = \pi$, then the expression of error rate can be defined as:

$$ER = (\Theta_{ave} - \Theta_{be}) / \Theta_{ave} \quad (4.20)$$

The middle depth $(H_1 + H_2) / 2$ when $R = 1.0$ is selected as the object and three

different values are used for H . For one thing, errors of temperature responses do change with the time when coil pitch B and velocity L remain stable. For another, groundwater velocity leads to the errors with different degrees if time Fo and coil pitch B keep constant. Figure 4.13 shows the graphs corresponding to these two conditions.

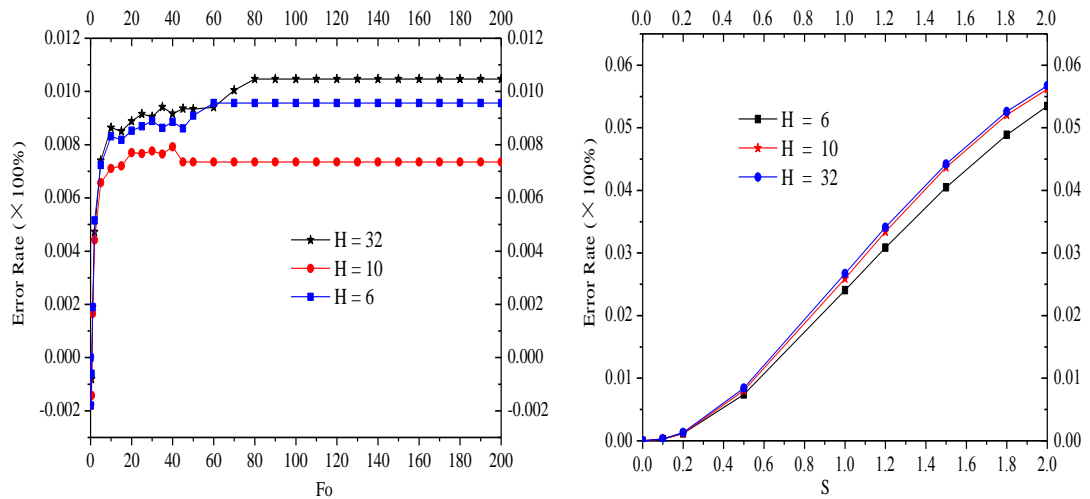


Figure 4.13 The errors of two calculation methods while H adopts different values

Another train of thought is to calculate errors of temperature response arising from different values set for B . Firstly, the errors over the time can be deduced supposing that both length H and velocity S are constant. Secondly, with respect to confirmed length H and time Fo , the errors with the velocity S can be presented. The variation trends are shown in Figure 4.14.

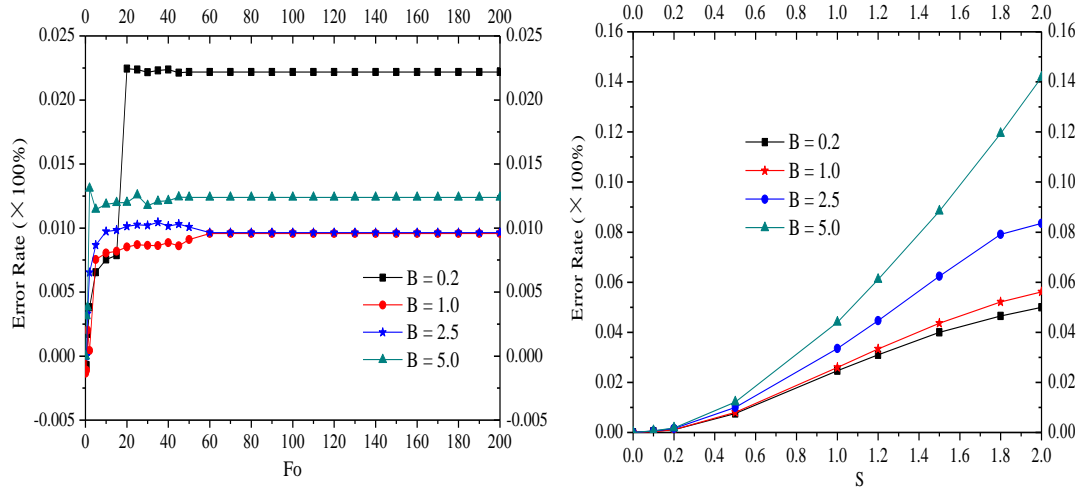


Figure 4.14 The errors of two calculation methods when B takes different values

According to Figure 4.14, the error ranges are so minor that the average value of $\varphi = 0$ and $\varphi = \pi$ can be utilized to substitute for that obtained by the integral average method. The calculation process is considerably simplified by this approach especially when accuracy requirements are not strict.

4.4 Comparisons between pure conduction and combined heat transfer

A ring-coil heat source with groundwater seepage produces a temperature field different from that of the pure conduction model under the influence of advection. Because the heat transfer efficiency of the combined ring-coil model is improved over that of pure conduction, comparisons between the two models identify the significance of studying ring-coil heat source seepage models. Fo represents the time scale over which groundwater effects are realized and S represents the strength of seepage, and these two critical parameters are the independent variables. The heat exchange between ring coils and the surrounding medium expresses the performance characteristics of the model. The ring-coil heat source behaves as if it “add flowers to embroidery” when

groundwater flows through it. The diameter of the ring-coil is equal to that of the pile to employ the most of the available space in providing heat exchange area. The mid depth of the model is selected as a typical location for the comparisons. First of all, for the different values of H , assuming that the seepage velocity is stable, the temperature response ratios and the corresponding heat transfer rates' ratios with the time are indicated in Figure 4.15, where the subscripts 1 and 2 respectively denote the combined heat transfer and pure conduction.

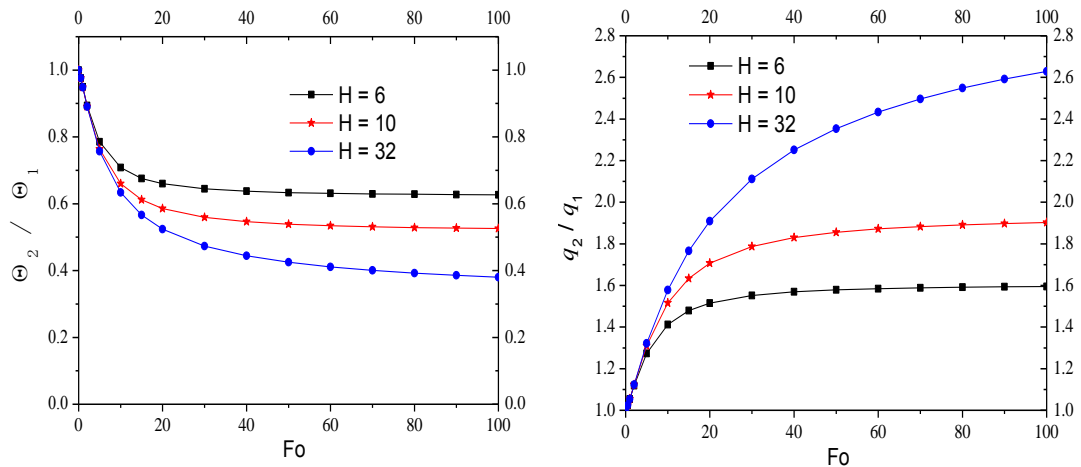


Figure 4.15 The temperature responses ratios and heat transfer rates' ratios with the time while the velocity is constant

These two ratios can change with the groundwater velocity when the time is constant. The corresponding curves are given in Figure 4.16, Figures 4.15 and 4.16 prove that the role of groundwater flow is indeed important. The effect of seepage may be initially very small, but its effect unfolds gradually over the time if the velocity is fixed, and the impact is obvious after a long time. Similarly, the seepage effect on the ring-coil heat source is becoming increasingly evident as velocity of groundwater flow increases at any fixed time. The seepage influence is clearer for those ring-coil sources with larger

ratios of length to radius. In summary, groundwater seepage strengthens heat transfer rates and improves heat transfer performance of the ring-coil heat source. This performance is encouraging regarding prospective ability to cope with a larger air-conditioning load. Those regions with abundant groundwater resources and/or with strong hydraulic head are important potential areas for improving heat transfer performance of energy pile.

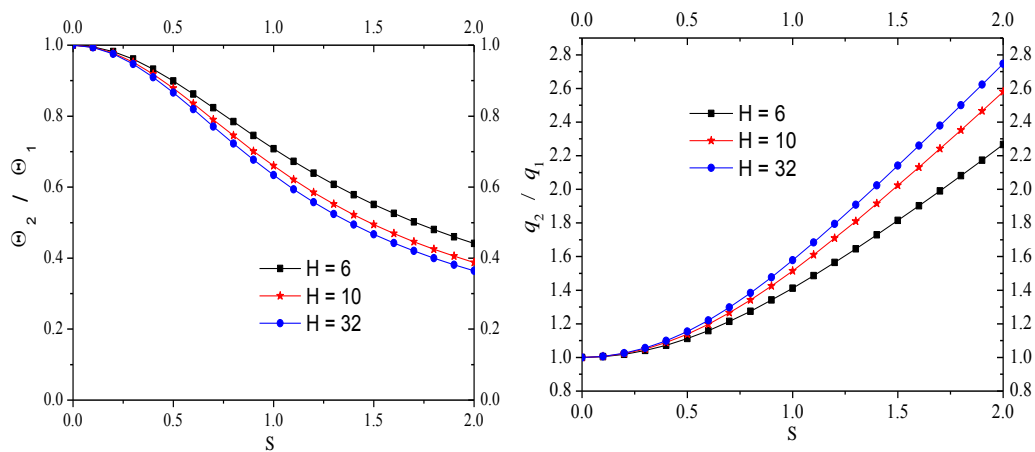


Figure 4.16 The temperature responses ratios and heat transfer rates' ratios with the velocity while the time is constant

4.5 Summary

Explained and analyzed in the chapter are the ring-coil seepage models for pile foundation GHE. Both the infinite (2-D) and the finite (3-D) models have been explored. Because the pitch of the coils has been taken into consideration, a feature which previously has never been focused is the discontinuity of the heat source down the pile. The effects of this discontinuity on the temperature response in the surrounding medium have been calculated and the potential behaviour of energy piles are now better understood. This understanding applies to the case of pure conduction when there is no

groundwater seepage and also the case when there is flowing groundwater. The mathematics underpinning the establishment of the seepage models is identified and the equations were developed for various conditions. The characteristics of ring-coil seepage models were explored, and performance comparisons between pure conduction and combined heat transfer were made. The influence of groundwater advection on the ring-coil heat source should be drawn attention especially when the time or the velocity becomes sufficient to improve the heat transfer performance of energy pile. The ring-coil seepage model is a theoretical research innovation and it lays a firm foundation for the study of more complex models or even engineering projects. Since the groundwater flows across the ring coils within the energy pile, the research on the whole heat transfer process including conduction and groundwater advection is a new research area. The novel components of this chapter are the modeling of the ring-coil heat source in an underground medium with groundwater seepage. Account is taken of both conduction and convection when groundwater flows through the energy piles.

CHAPTER 5 SPIRAL HEAT SOURCE MODELS WITH GROUNDWATER FLOW

5.1 Introduction

The investigations reported in Chapters 3 and 4 on the solid cylindrical and ring-coil heat source seepage models brought forth novel theoretical simulations of the heat transfer for the energy pile with groundwater advection. However, deficiencies still exist in that the solid cylindrical model only assumes its surface as a whole homogeneous heat source and there is no attempt to model the pitch of the actual coils. The ring-coil model is a significant advance because the spiral tube is represented as a series of separated coils, but spiral configuration of the heat source tube is still simplified as there is no connection between adjacent coils. Thus, at this point, the most accurate model has not yet been proposed. Further, improvements should be explored and a model incorporating the genuine spiral heat source is examined and reported in this chapter. The convection of groundwater flow will be included in the simulations. The heat exchange tube, this time, is represented as a spiral line, thereby ignoring the thickness dimension of tube for both pure conduction and combined one involving conduction and groundwater advection. Since the spiral seepage model is close to being realistic, the effects of groundwater advection should be more realistic. As the same as previous chapters, the spiral line heat source seepage models are classified into the infinite and the finite cases.

Strictly, the first step is to analyze the infinite-length model in an infinite

homogenous medium to obtain the 2-D analytical solutions. Secondly, it is necessary to include the effect of ground surface for the finite-length energy pile especially under the condition of long-term performance of heat transfer. The heat transfer behaviour of the finite-length spiral seepage model in a semi-infinite medium is regarded as the emphatic research objective, and the corresponding characteristics will be studied. The schematic diagram of the finite spiral heat source is shown in Figure 5.1.

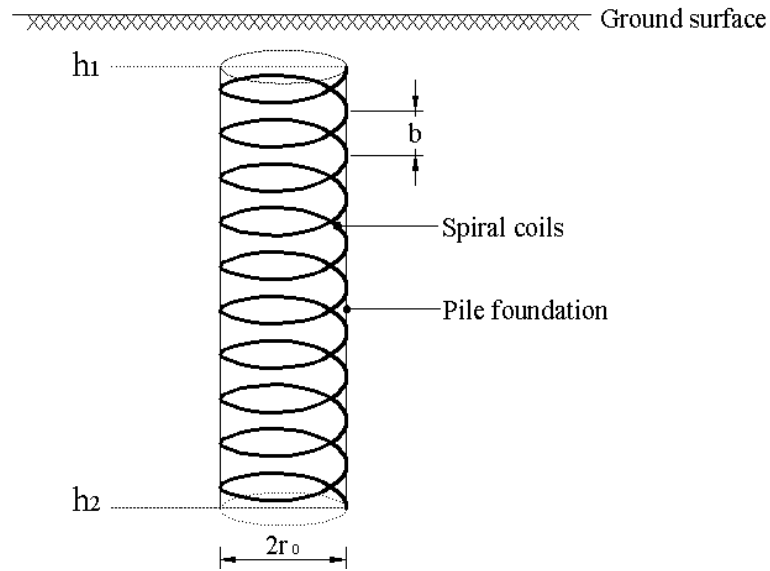


Figure 5.1 The geometry of the spiral heat source inside the pile foundation GHE

Figure 5.1 illustrates the spiral coils installed in the pile. The radius of coil is the same as that of the pile, and all coils are no longer separated ones but a successive spiral lines with a certain pitch b . The grout or concrete is poured into the pile becoming integral with spiral tube once it has hardened. Groundwater is assumed to flow through the GHE for the purpose of mathematical modeling equations, which is a simplification, since this would not be completely the real case for a hardened energy pile.

5.2 The spiral-coil models without considering groundwater seepage

5.2.1 The research technique

As in chapters previously, Green's function is employed to give the temperature response induced by any instantaneous heat point source in the infinite homogeneous medium. The spiral coil is deemed as a gathering of an infinite number of spirally arranged points. Thus, the integral with respect to relevant variables, can be conducted to obtain the total contribution of the whole spiral line (Zhang et al., 2013b). The analytical solution of the temperature response at any point in the medium except heat source in rectangular and cylindrical coordinates have been respectively listed in Equations (3.1) and (3.3), where (x', y', z') and (x, y, z) are respectively the coordinates of the point heat source and any other point in the medium; τ' and τ respectively denote the start time of emitting heat and any subsequent time. The conversion relationships between the two coordinate systems are: $x' = r' \cos \varphi'$, $y' = r' \sin \varphi'$, $z' = z'$ and $x = r \cos \varphi$, $y = r \sin \varphi$, $z = z$, and the distance from the point heat source (x', y', z') to any point (x, y, z) in the medium is given as:

$$R = \sqrt{(x - x')^2 + (y - y')^2 + (z - z')^2} = \sqrt{r^2 + r'^2 - 2rr' \cos(\varphi - \varphi') + (z - z')^2} \quad (5.1)$$

Green's function is the fundamental tool for solving such unsteady heat conduction problems. For the pile foundation GHE, the buried spiral tube is simplified as a series of continuous coils with the pitch of b . The thickness dimension of the tube can be neglected with a little loss of accuracy, (r', z', φ') are the coordinates of points on the spiral lines and the corresponding expressions are $r' = r_0$ and $z' = b \varphi' / (2\pi)$ (Li., 2011). To analyze the spiral line models, it is assumed that the underground medium is homogeneous and its thermal properties are constant, and the GHE emits heat at the intensity of $q_1 b$ per unit length from time $\tau' = 0$, the initial temperature and temperatures at

other times are expressed as t_0 and t , respectively. The excess temperature $\theta = t - t_0$ is the temperature response at any point in the underground medium except heat source itself. The preconditions or assumptions are almost the same as those listed in chapter 3 and 4. The governing equation and the corresponding conditions for the infinite and the finite transient heat conductions are shown in Equation (5.2):

$$\left. \begin{aligned}
 \frac{\partial \theta}{\partial \tau} &= a \left(\frac{\partial^2 \theta}{\partial r^2} + \frac{1}{r} \frac{\partial \theta}{\partial r} \right) + \frac{q \delta(r-r_0, z-z', \phi-\phi')}{2\pi r_0 \rho c}, \text{ for } 0 < r < \infty, \phi' = 2\pi z' / b, -\infty < z' < +\infty, \tau > 0, \text{ (infinite model)} \\
 \frac{\partial \theta}{\partial \tau} &= a \left(\frac{\partial^2 \theta}{\partial r^2} + \frac{1}{r} \frac{\partial \theta}{\partial r} + \frac{\partial^2 \theta}{\partial z'^2} \right) + \frac{q \delta(r-r_0, z-z', \phi-\phi')}{2\pi r_0 \rho c}, \text{ for } 0 < r < \infty, \phi' = 2\pi z' / b, h_1 < z' < h_2, \tau > 0, \text{ (finite model)} \\
 \theta &= 0, \text{ for } 0 < r < \infty, \tau = 0 \\
 \frac{\partial \theta}{\partial r} &= 0, \text{ for } r = 0, \tau > 0 \\
 \theta &= 0, \text{ for } r \rightarrow \infty, \tau \geq 0
 \end{aligned} \right\} \text{ (for infinite and finite models)} \quad (5.2)$$

5.2.2 Infinite spiral heat source model

A spiral line with unlimited length takes the place of the ring-coil tube in an infinite medium. The cylindrical coordinates of the points on the spiral line are given by $r' = r$ and $z' = b\phi' / (2\pi)$. The solution of this two dimensional (2-D) problem becomes:

$$\begin{aligned}
 \theta_{p, s, i} &= \frac{q_l b}{2\pi \rho c} \int_0^\tau d\tau' \int_{-\infty}^{\infty} G(z' = b\phi' / 2\pi) d\phi' = \frac{q_l b}{16\pi \rho c} \int_0^\tau d\tau' \int_{-\infty}^{\infty} \frac{1}{[\pi a(\tau - \tau')]^{3/2}} \\
 &\quad \exp \left[-\frac{r^2 + r_0^2 - 2rr_0 \cos(\phi - \phi') + (z - b\phi' / 2\pi)^2}{4a(\tau - \tau')} \right] d\phi'
 \end{aligned} \quad (5.3)$$

Or

$$\theta_{p, s, i} = \frac{q_l b}{8\pi^2 k} \int_{-\infty}^{\infty} \frac{1}{R_s} \cdot \operatorname{erfc} \left(\frac{R}{2\sqrt{a\tau}} \right) d\phi' \quad (5.4)$$

where $R_s = \sqrt{r^2 + r_0^2 - 2rr_0 \cos(\varphi - \varphi') + (z - b\varphi'/2\pi)^2}$.

Corresponding non-dimensional parameters are introduced to reduce the number of parameters and simplify the calculation as follows: $Fo = a\tau / r_0^2$, $\Theta_{p,s,i} = k\theta / q_1$, $Z = z / r_0$, $R = r / r_0$ and $B = b / r_0$. The dimensionless temperature responses of the infinite spiral pure conduction model are given in Equations (5.5) or (5.6).

$$\Theta_{p,s,i} = \frac{B}{16\pi^{5/2}} \int_0^{Fo} \frac{1}{(Fo - Fo')^{3/2}} \cdot \int_{-\infty}^{\infty} \exp\left[-\frac{R^2 + 1 - 2R\cos(\varphi - \varphi') + (Z - B\varphi'/2\pi)^2}{4(Fo - Fo')}\right] dFo' d\varphi' \quad (5.5)$$

$$\Theta_{p,s,i} = \frac{B}{8\pi^2 R_m} \int_{-\infty}^{\infty} \operatorname{erfc}\left[\frac{R_m}{2\sqrt{Fo}}\right] d\varphi' \quad (5.6)$$

where $R_m = \sqrt{R^2 + 1 - 2R\cos(\varphi - \varphi') + (Z - B\varphi'/2\pi)^2}$ and erfc is the complementary error function.

5.2.3 Finite spiral heat source model

A finite-length spiral line in a semi-infinite medium is next considered. The spiral starts at $z' = h_1$ or $\varphi' = 2\pi h_1 / b$, and ends at $z' = h_2$ or $\varphi' = 2\pi h_2 / b$. Therefore, the solution may be expressed as:

$$\begin{aligned} \theta_{p,s,f} &= \frac{q_1 b}{2\pi\rho c} \int_0^{\tau} d\tau' \left[\int_{2\pi h_1/b}^{2\pi h_2/b} G(z' = b\varphi'/2\pi) d\varphi' - \int_{2\pi h_1/b}^{2\pi h_2/b} G(z' = -b\varphi'/2\pi) d\varphi' \right] \\ &= \frac{q_1 b}{16\pi\rho c} \int_0^{\tau} \frac{d\tau'}{[\pi a(\tau - \tau')]^{3/2}} \cdot \exp\left[-\frac{r^2 + r_0^2}{4a(\tau - \tau')}\right] \\ &\quad \int_{2\pi h_1/b}^{2\pi h_2/b} \exp\left[\frac{2rr_0 \cos(\varphi - \varphi')}{4a(\tau - \tau')}\right] \left\{ \exp\left[-\frac{(z - b\varphi'/2\pi)^2}{4a(\tau - \tau')}\right] - \exp\left[-\frac{(z + b\varphi'/2\pi)^2}{4a(\tau - \tau')}\right] \right\} d\varphi' \end{aligned} \quad (5.7)$$

Or

$$\theta_{p,s,f} = \frac{q_l b}{8\pi^2 k} \int_{2\pi h_1/b}^{2\pi h_2/b} \left[\frac{1}{R_1} \cdot \operatorname{erfc}\left(\frac{R_1}{2\sqrt{a\tau}}\right) - \frac{1}{R_2} \cdot \operatorname{erfc}\left(\frac{R_2}{2\sqrt{a\tau}}\right) \right] d\phi' \quad (5.8)$$

where $R_1 = \sqrt{r^2 + r_0^2 - 2rr_0 \cos(\varphi - \varphi') + (z - b\varphi'/2\pi)^2}$

$$R_2 = \sqrt{r^2 + r_0^2 - 2rr_0 \cos(\varphi - \varphi') + (z + b\varphi'/2\pi)^2} \text{ .}$$

The non-dimensional parameters of section 5.2.2 are again adopted, and another two letters $H_1 = h_1 / r_0$ and $H_2 = h_2 / r_0$ are respectively made use of to express the dimensionless starting and end positions of the spiral line. In such a way, Equations (5.7) and (5.8) can be changed into Equations (5.9) and (5.10), respectively.

$$\Theta_{p,s,f} = \frac{B}{16\pi^{5/2}} \int_0^{Fo} \frac{1}{(Fo - Fo')^{3/2}} \cdot \exp\left[-\frac{R^2 + 1}{4(Fo - Fo')}\right] \cdot \int_{2\pi H_1/B}^{2\pi H_2/B} \exp\left[\frac{2R \cos(\varphi - \varphi')}{4(Fo - Fo')}\right] \cdot \left\{ \exp\left[-\frac{(Z - B\varphi'/2\pi)^2}{4(Fo - Fo')}\right] - \exp\left[-\frac{(Z + B\varphi'/2\pi)^2}{4(Fo - Fo')}\right] \right\} d\varphi' dFo' \quad (5.9)$$

$$\Theta_{p,s,f} = \frac{B}{8\pi^2} \int_{2\pi H_1/B}^{2\pi H_2/B} \left[\frac{1}{NR_1} \cdot \operatorname{erfc}\left(\frac{NR_1}{2\sqrt{Fo}}\right) - \frac{1}{NR_2} \cdot \operatorname{erfc}\left(\frac{NR_2}{2\sqrt{Fo}}\right) \right] d\varphi' \quad (5.10)$$

where $NR_1 = \sqrt{R^2 + 1 - 2R \cos(\varphi - \varphi') + (Z - B\varphi'/2\pi)^2}$

$$NR_2 = \sqrt{R^2 + 1 - 2R \cos(\varphi - \varphi') + (Z + B\varphi'/2\pi)^2}$$

5.3 Heat transfer comparisons between pile foundation GHE and borehole GHE

As the diameter of the pile is thicker than that of the borehole, the interior heat capacity of the pile itself becomes significant and should be taken into consideration. Spiral tubes possess better heat transmission ability than the single U-tube or the double

U-tubes installed into the borehole, therefore a pile foundation GHE has a better heat transfer performance. Comparisons between these two types of GHE are made below to emphasize the heat transfer superiority of the energy pile; these comparisons show the application of energy piles to be of a better class. The diameter of a borehole is from 130mm to 150mm while that of a pile is over 400mm. For comparison purposes below, the borehole diameter is set as 150mm and piles 400mm, 600mm, 800mm and 1000mm. The finite spiral model is studied and its analytical solution of temperature response reveals the temperature variations aligned with the ground. The integral averaging method with regard to the parameter Z is performed to obtain the mean temperature response of the borehole's or energy pile's surface. Thereby, the corresponding expressions of the line source and the spiral source are respectively expressed by Equations (5.11) and (5.12):

$$\Theta_{ave,p,l,f} = \frac{1}{4\pi} \cdot \frac{1}{H} \int_0^H \int_0^H \left\{ \frac{erfc \left[\frac{\sqrt{R^2 + (Z - Z')^2}}{2\sqrt{Fo}} \right]}{\sqrt{R^2 + (Z - Z')^2}} - \frac{erfc \left[\frac{\sqrt{R^2 + (Z + Z')^2}}{2\sqrt{Fo}} \right]}{\sqrt{R^2 + (Z + Z')^2}} \right\} dZdZ' \quad (5.11)$$

$$\Theta_{ave,p,s,f} = \frac{B}{16\pi^{5/2}} \cdot \frac{1}{H_2 - H_1} \cdot \frac{1}{2\pi} \int_{H_1}^{H_2} \int_0^{2\pi} \int_0^{Fo} \frac{1}{(Fo - Fo')^{3/2}} \cdot \exp \left[-\frac{R^2 + 1}{4(Fo - Fo')} \right] \cdot \int_{2\pi H_1/B}^{2\pi H_2/B} \exp \left[\frac{2R \cos(\varphi - \varphi')}{4(Fo - Fo')} \right] \cdot \left\{ \exp \left[-\frac{(Z - B\varphi' / 2\pi)^2}{4(Fo - Fo')} \right] - \exp \left[-\frac{(Z + B\varphi' / 2\pi)^2}{4(Fo - Fo')} \right] \right\} dZd\varphi d\varphi' dFo' \quad (5.12)$$

where Equation (5.11) refers to the mean surface temperature responses of the borehole GHE and Equation (5.12) refers to that of pile foundation GHE.

The running time of the GCHP system is usually from several hours to hundreds or even thousands of hours. Accordingly, one month of simulated time, i.e.720 hours, is

chosen for the simulation. Firstly, the temperature response ratios of the pile foundation GHE with different diameters to the borehole GHE can be calculated based on Equations (5.11) and (5.12). As shown in Figure 5.2, these ratios increase with the time.

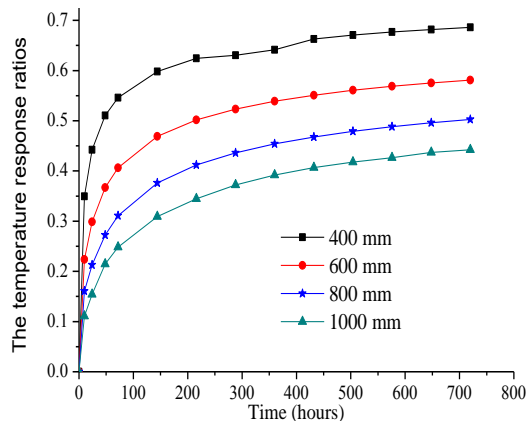


Figure 5.2 The temperature response ratios of pile foundation GHE to borehole GHE

Figure 5.2 shows clearly that the temperature response ratios reduce with the increase of pile diameter, assuming that other preconditions are constant; this is because the interior heat capacity is allowed for. The larger the diameter, the greater the heat ‘soaking’ ability of the energy pile and the smaller the temperature responses at the outside surface of GHE.

The particular concern is the degree of heat exchange advantage. Thus, the heat transfer rates’ ratios of pile foundation GHEs to the borehole GHE are revealed in Figure 5.3. The heat transfer rate is gradually improved as the pile diameter becomes large; the reason is that the spiral tubes are set along the interior surface of pile so its diameter is nearly equal to that of the pile. The larger the pile diameter, the better the heat transfer performance, at any constant time. Figure 5.3 explains that the energy pile’s ability to cope with the air-conditioning load is initially particularly good. At first, the heat transfer rate of a pile foundation GHE is equivalent to that of several meters’

borehole GHE, but the degree of equivalence reduces gradually with the running time of the heat pump system.

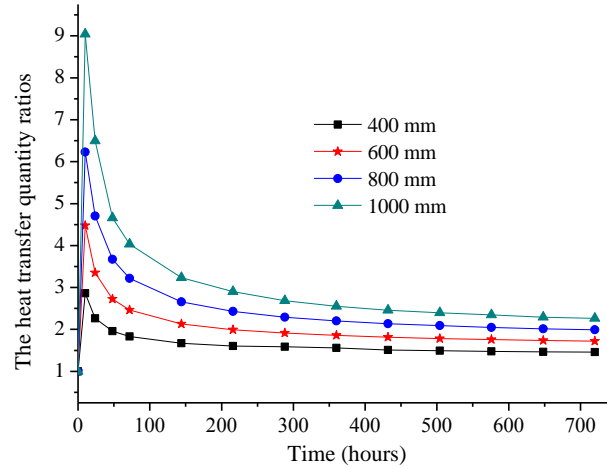


Figure 5.3 The heat transfer rates' ratios of pile foundation GHE to borehole GHE

Figure 5.3 shows that the heat transfer superiority of the pile foundation GHE is obvious especially for those with large diameters, and heat transfer ability is very excellent in the initial running period. Theoretical research on the most accurate mathematical model of energy pile is therefore vital. The influence of groundwater on the energy pile can be investigated accurately as long as the simulation model is sufficiently reasonable.

5.4 New models with groundwater seepage

5.4.1 The research technique

Groundwater seepage is a common phenomenon especially in the coastal areas or others with rich groundwater sources. The underground medium can be regarded as a homogeneous porous medium, in which the energy pile's heat transfer process consists of conduction by solid matrix and liquid (water) in its pores and convection by the

moving groundwater. This is the first time to propose the simulation models describing the influence that groundwater advection exerts on spiral line heat source, and these contents are different with those appeared in the references. It is assumed that the velocity u of groundwater flow is uniform over the whole domain and its direction is in the x -coordinate positive direction. The energy equation and the new Green's function under the conditions of groundwater transfusion have been given in section 3.2.2 and 3.2.3. The advection problems can be formulated in the same manner as that of the moving source problem. As a result, the analytical solutions may also be obtained by means of the Green's function when groundwater flows through spiral coils. For the spiral seepage model, preconditions or assumptions except for the configuration of the spiral coils, are the same as those described in Chapter 3 or 4. Accordingly, the energy governing equation and the corresponding conditions are represented by Equation (5.13).

$$\left. \begin{aligned}
 \frac{\partial \theta}{\partial \tau} + u \frac{\partial \theta}{\partial (r \cos \varphi)} &= a \left(\frac{\partial^2 \theta}{\partial r^2} + \frac{1}{r} \frac{\partial \theta}{\partial r} \right) + \frac{q \delta(r-r_0, z-z', \varphi-\varphi')}{2\pi r_0 \rho c}, \text{ for } 0 < r < \infty, -\infty < z' < +\infty, \varphi' = 2\pi z' / b, \tau > 0, \text{ (infinite model)} \\
 \frac{\partial \theta}{\partial \tau} + u \frac{\partial \theta}{\partial (r \cos \varphi)} &= a \left(\frac{\partial^2 \theta}{\partial r^2} + \frac{1}{r} \frac{\partial \theta}{\partial r} + \frac{\partial^2 \theta}{\partial z'^2} \right) + \frac{q \delta(r-r_0, z-z', \varphi-\varphi')}{2\pi r_0 \rho c}, \text{ for } 0 < r < \infty, \varphi' = 2\pi z' / b, h_1 < z' < h_2, \tau > 0, \text{ (finite model)} \\
 \theta &= 0, \text{ for } 0 < r < \infty, \tau = 0 \\
 \frac{\partial \theta}{\partial r} &= 0, \text{ for } r = 0, \tau > 0 \\
 \theta &= 0, \text{ for } r \rightarrow \infty, \tau \geq 0
 \end{aligned} \right\} \text{(for infinite and finite models)} \quad (5.13)$$

5.4.2 Infinite spiral heat source model

Coils are considered as a spiral line source in an infinite medium with groundwater advection. The spiral source is regarded as a collection of an infinite number of point sources with cylindrical coordinates of $r' = r_0, z' = b\phi' / (2\pi)$. The length of the spiral line is infinite and only heat transfer along x and y directions are considered. The temperature response can also be written straightforwardly as:

$$\theta_{a, s, i} = \frac{q_l b}{2\pi\rho c} \int_0^{\tau} d\tau' \int_{-\infty}^{\infty} M(r' = r_0, z' = b\varphi'/2\pi) d\varphi = \frac{q_l b}{4\pi^{5/2}k} \int_{-\infty}^{\infty} \exp\left[\frac{U(x - r_0 \cos \varphi')}{2a}\right] f(\varphi') d\varphi' \quad (5.14)$$

where $R = \sqrt{r^2 + r_0^2 - 2rr_0 \cos(\varphi - \varphi') + (z - b\varphi'/2\pi)^2}$ in the function f .

Equation (5.14) can be further transformed into Equation (5.15) to express the temperature response in detail.

$$\theta_{a, s, i} = \frac{q_l b}{2\pi\rho c} \int_{-\infty}^{\infty} d\varphi' \int_0^{\tau} \frac{1}{8[\pi a(\tau - \tau')]^{3/2}} \cdot \exp\left[-\frac{[x - r_0 \cos \varphi' - u(\tau - \tau')]^2 + (y - r_0 \sin \varphi')^2 + (z - b\varphi'/2\pi)^2}{4a(\tau - \tau')}\right] d\tau' \quad (5.15)$$

Equation (5.15) is so long and tedious that non-dimensional expression is once again utilized for simplification. The relevant dimensionless parameters consist of $Fo = a \tau / r_0^2$, $\Theta_{a, s, i} = k \theta / q_l$, $Z = z / r_0$, $R = r / r_0$, $B = b / r_0$ and $S = u r_0 / a$. Thus, Equation (5.15) is transformed as follows.

$$\Theta_{a, s, i} = \frac{B}{16\pi^{5/2}} \int_0^{Fo} \frac{1}{(Fo - Fo')^{3/2}} \int_{-\infty}^{\infty} \exp\left[-\frac{[X - \cos \varphi' - S(Fo - Fo')]^2 + (Y - \sin \varphi')^2 + (Z - B\varphi'/2\pi)^2}{4(Fo - Fo')}\right] dFo' d\varphi' \quad (5.16)$$

5.4.3 Finite spiral heat source model

A finite-length spiral line in a semi-infinite medium is next considered. The spiral line starts at $z^2 = h_1$ or $\varphi' = 2\pi h_1 / b$, and ends at $z^2 = h_2$ or $\varphi' = 2\pi h_2 / b$. Two additional non-dimensional parameters $H_1 = h_1 / r_0$ and $H_2 = h_2 / r_0$ are used. Again the images are set symmetrically about the ground boundary that keeps constant temperature, the depth of spiral line is finite and therefore heat transfer along x, y and z directions are all thought over, and the solution is obtained as:

$$\begin{aligned}\theta_{a,s,f} &= \frac{q_l b}{2\pi\rho c} \int_0^\tau d\tau' \left[\int_{2\pi h_1/b}^{2\pi h_2/b} M(z' = b\varphi'/2\pi) d\varphi' - \int_{2\pi h_1/b}^{2\pi h_2/b} M(z' = -b\varphi'/2\pi) d\varphi' \right] \\ &= \frac{q_l b}{4\pi^{5/2} k} \int_{2\pi h_1/b}^{2\pi h_2/b} \exp\left[\frac{U(x-r_0 \cos \varphi')}{2a}\right] \cdot [f(R_1, \varphi') - f(R_2, \varphi')] d\varphi'\end{aligned}\quad (5.17)$$

$$R_1 = \sqrt{r^2 + r_0^2 - 2rr_0 \cos(\varphi - \varphi') + (z - b\varphi'/2\pi)^2} \text{ and } R_2 = \sqrt{r^2 + r_0^2 - 2rr_0 \cos(\varphi - \varphi') + (z + b\varphi'/2\pi)^2}.$$

After corresponding transformation, Equation (5.17) can be changed into:

$$\begin{aligned}\theta_{a,s,f} &= \frac{q_l b}{16\pi^{5/2} \rho c} \int_{\varphi_1}^{\varphi_2} d\varphi' \int_0^\tau \exp\left[-\frac{[x - r_0 \cos \varphi' - u(\tau - \tau')]^2 + (y - r_0 \sin \varphi')^2}{4a(\tau - \tau')}\right] \\ &\quad \left\{ \exp\left[-\frac{(z - b\varphi'/2\pi)^2}{4a(\tau - \tau')}\right] - \exp\left[-\frac{(z + b\varphi'/2\pi)^2}{4a(\tau - \tau')}\right] \right\} \cdot \frac{d\tau'}{[a(\tau - \tau')]^{3/2}}\end{aligned}\quad (5.18)$$

There are a large number of parameters in Equation (5.18), making it seemed complicated. In view of this, the non-dimensional equation is used for deriving corresponding analytical solutions. The dimensionless parameters are almost the same as those involved in the infinite spiral source, in addition, H_1 and H_2 are two additional dimensionless parameters denoting denote dimensionless starting and end locations of spiral line, respectively. Thus, the expression of temperature response of the finite spiral source model with groundwater seepage is:

$$\begin{aligned}\Theta_{a,s,f} &= \frac{B}{16\pi^{5/2}} \int_0^{Fo} \frac{1}{(Fo - Fo')^{3/2}} \int_{2\pi H_1/B}^{2\pi H_2/B} \exp\left[-\frac{[X - \cos \varphi' - S(Fo - Fo')]^2 + (Y - \sin \varphi')^2}{4(Fo - Fo')}\right] \\ &\quad \left\{ \exp\left[-\frac{(Z - B\varphi'/2\pi)^2}{4(Fo - Fo')}\right] - \exp\left[-\frac{(Z + B\varphi'/2\pi)^2}{4(Fo - Fo')}\right] \right\} d\varphi' dFo'\end{aligned}\quad (5.19)$$

5.5 Characteristics of spiral heat source seepage models

5.5.1 The regular pattern of temperature responses

5.5.1.1 The temperature responses with the time

5.5.1.1.1 Pure conduction models

The infinite model, as explained in chapters above, has a temperature response that continuously increases with the time. Whereas, the finite model, with a constant temperature of ground boundary, raises the underground temperature until the maximum stable values are reached. The trends of temperature responses can be expressed as the differences between infinite and finite models (Man et al, 2013), and Figure 5.4 gives the corresponding temperature responses with the time. The values of H are set as 2, 10 and 50 for the finite model.

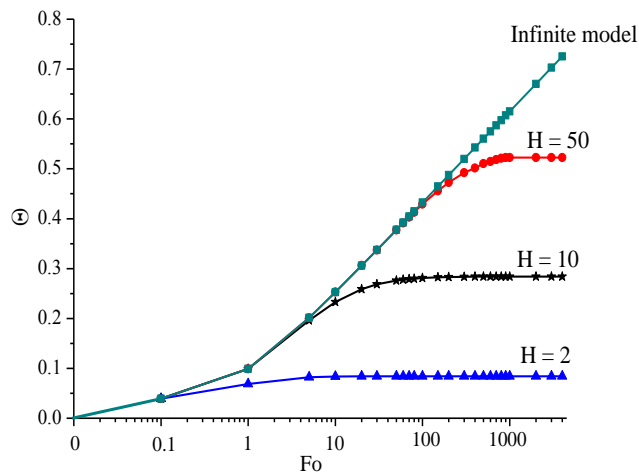


Figure 5.4 The temperature responses of spiral pure conduction models with the time

Notably, the basic regular patterns of temperature responses are all progressively increase with the time, and the differences between infinite and finite models are shown at last. Furthermore, an increase of H reinforces the temperature response for the same time period. In addition, the differences of all temperature responses are a little initially but then become more and more obvious with the time.

5.5.1.1.2 Heat transfer models with groundwater seepage

For GHEs with different dimensions, the thermal responses of points on the same horizontal circle, with the z -axis as center line, are different because of the configuration of spiral heat source and the groundwater seepage, that is, the temperature distributions around the z -axis on any horizontal plane when Z is not zero and R is constant are dissimilar. It is necessary to understand the asymmetry of temperature distribution. For the infinite model, another integral is conducted with respect to parameter φ to obtain the mean temperature response value of the circle with the same R at any horizontal plane, and the expression is shown as follows:

$$\begin{aligned}\overline{\Theta}_{a,s,i} &= \frac{B}{16\pi^{5/2}} \int_0^{Fo} \frac{1}{(Fo - Fo')^{3/2}} \frac{1}{2\pi} \int_0^{2\pi} \int_{-\infty}^{\infty} \exp \left[-\frac{[R \cos \varphi - \cos \varphi' - S(Fo - Fo')]^2 + (R \sin \varphi - \sin \varphi')^2 + (B\varphi'/2\pi)^2}{4(Fo - Fo')} \right] dFo' d\varphi' \\ &= \frac{B}{32\pi^{7/2}} \int_0^{Fo} \frac{1}{(Fo - Fo')^{3/2}} \int_0^{2\pi} \int_{-\infty}^{\infty} \exp \left[-\frac{[R \cos \varphi - \cos \varphi' - S(Fo - Fo')]^2 + (R \sin \varphi - \sin \varphi')^2 + (B\varphi'/2\pi)^2}{4(Fo - Fo')} \right] dFo' d\varphi d\varphi'\end{aligned}\quad (5.20)$$

For the finite model, the analytical solutions of the mean temperature response of the circle located on any horizontal plane is achieved by integrating with respect to the parameter φ , i.e.

$$\begin{aligned}\overline{\Theta}_{a,s,f} &= \frac{B}{32\pi^{7/2}} \int_0^{Fo} \frac{1}{(Fo - Fo')^{3/2}} \int_0^{2\pi} \int_{2\pi H_1/B}^{2\pi H_2/B} \exp \left[-\frac{[R \cos \varphi - \cos \varphi' - S(Fo - Fo')]^2 + (R \sin \varphi - \sin \varphi')^2}{4(Fo - Fo')} \right] \\ &\quad \left\{ \exp \left[-\frac{(Z - B\varphi'/2\pi)^2}{4(Fo - Fo')} \right] - \exp \left[-\frac{(Z + B\varphi'/2\pi)^2}{4(Fo - Fo')} \right] \right\} d\varphi' d\varphi dFo'\end{aligned}\quad (5.21)$$

The temperature responses, when both the velocity and the coil pitch keep constant, of both the infinite and the finite models with the time are shown in Figure 5.5. It is clear that all responses finally reach stable states no matter whether the model is infinite or finite as long as the groundwater flow exists. This new model confirms that the temperature response can be stable when the heat accumulation induced by conduction

and the heat alleviation produced by groundwater advection arrive at a heat balance.

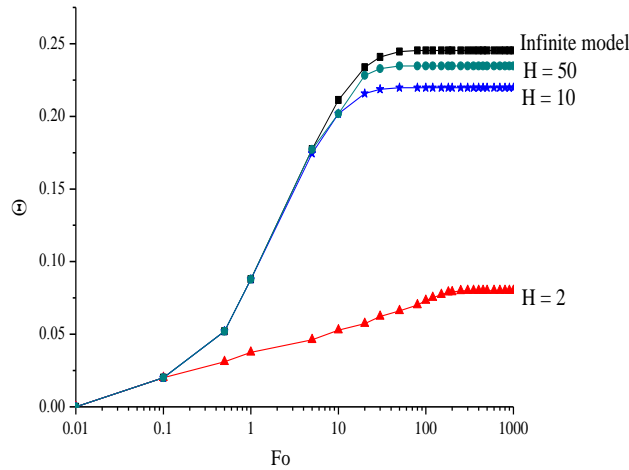


Figure 5.5 The temperature responses of spiral combined heat transfer models with the time

Figure 5.5 demonstrates that the thermal response of the infinite model is stronger than those of the finite models. For the finite model, the response becomes strong gradually with the increase of H .

The spiral combined model is more accurate compared with the solid cylindrical and ring-coil combined models, and the differences of them can be obtained by means of the corresponding temperature responses with the time or the velocity. For example, the finite model is employed because any energy pile has the finite depth, the temperature responses of three different models increase with the time while velocity is constant, and these responses drops with the velocity if the time is constant; Figure 5.6 show the detailed curves when the value of pitch B is 1.0. The relative errors from spiral to ring-coil models and from spiral to solid cylindrical models are respectively is -8.5% and 11%. However, the values of errors decrease with the increase of groundwater velocity because the convection occupies the absolute predominance gradually. It is suggested that the value of pitch B should be less than 1.0 if solid and ring-coil models are

employed for calculation.

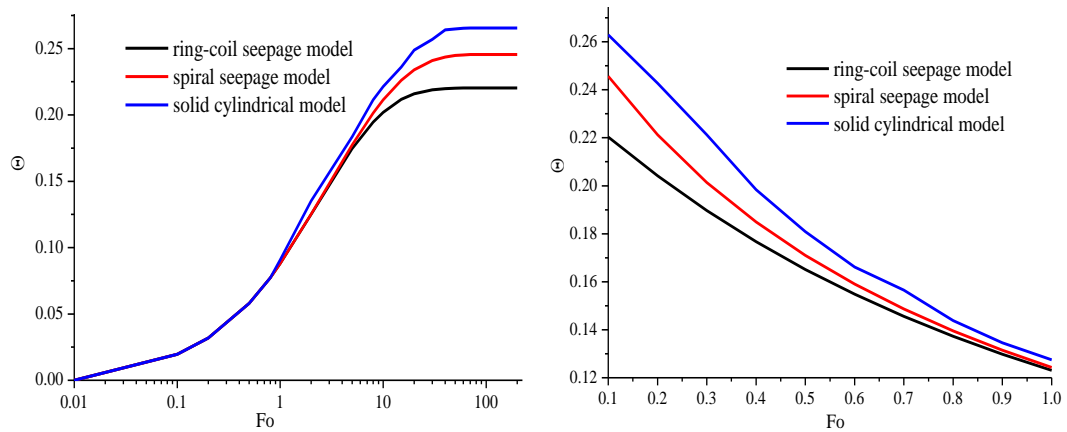


Figure 5.6 The temperature responses of different combined models with the time and the velocity

5.5.1.2 The temperature distribution around spiral coils

5.5.1.2.1 Pure conduction models

The isothermals diagram giving temperature distribution around a spiral heat source for an energy pile of limited length, assuming only pure conduction plays a role. According to the calculation and analysis based on Equation.(5.9) or (5.10) when Fo and B are fixed. The isothermals at vertical XOZ and horizontal XOY planes are both presented in Figure 5.7. Since the heat exchange tube is a spiral line, the temperature field is not symmetrical about the coordinate axis. Positions close to the heat source can show stronger thermal responses as expected. With the constant thermal transmission, it is inevitable that the heat accumulates in the medium and therefore the heat exchange between the GHE and its surrounding medium is unfavourably affected, and the heat transfer performance of the energy pile deteriorates.

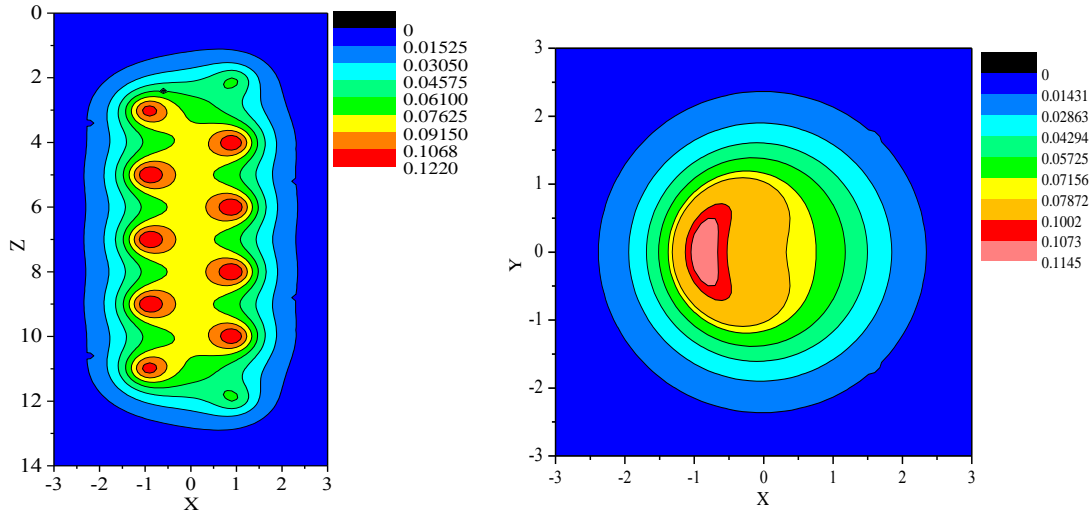


Figure 5.7 Isotherms induced by spiral pure conduction model

5.5.1.2.2 Heat transfer models with groundwater seepage

The isotherms of vertical and horizontal planes when calculation and analysis are conducted based on Equation (5.19), are shown in Figure 5.8.

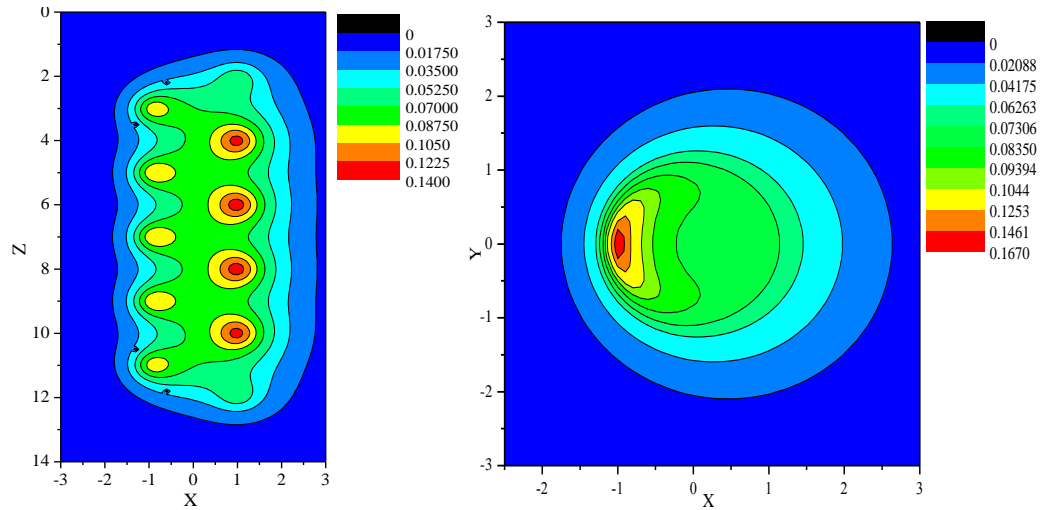


Figure 5.8 Isotherms of the spiral combined heat transfer model

The intuitive temperature distributions are intuitively reflected in this case involving groundwater transfusion. Most noticeable is that temperature responses at the right side are larger than at the left side due to the groundwater flow. Because the groundwater

flows along the positive direction of the x-axis and the corresponding heat dissipation from the spiral coils heat source has a certain shifting to the right, leading to the result of Figure 5.8.

5.5.2 The temperature responses of locations with different radial distances from the heat source

The temperature responses differences of those points around the energy pile are discussed below. Three conditions containing $R = 1.0$, $R = 2.0$ and $R = 3.0$ are assumed for the case of $H=10$ and the position $Z = (H_1+H_2) / 2$ is selected for examination. The calculation results based on Equation (5.21) appear in Figure 5.9, which further demonstrates that the temperature responses are stable at any point in the underground medium except for the heat source itself.

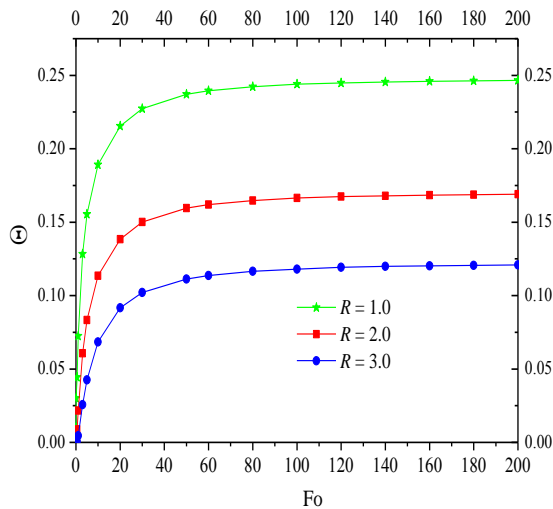


Figure 5.9 The temperature responses with the time when R adopts different values

Figure 5.8 indicates that the temperature response reduces with the increase of the radial distance from the spiral heat source. More specifically, the nearer to the heat source, the more intensive the temperature response.

5.5.3 The role of groundwater velocity

As stated in previous chapters, the velocity of groundwater transfusion is associated with the local hydraulic gradient. This parameter determines the strength of advection. Temperature responses tend to be stable when the heat dissipation by conduction and heat alleviation by convection arrive at a balance. To assume a constant heat exchange rate of a pile foundation GHE and a fixed configuration of the spiral coils, which means the role of heat source must be immobile and the effect of groundwater advection must relate to the groundwater velocity. If the velocity S becomes large, the time needed to attain a steady state is reduced, and the opposite is true when the velocity is small. Taking the case of $H = 10$ as a example when three values are set for S , the temperature responses of the spiral seepage models with unchanged pitch B are shown in Figure 5.10.

As expected, the temperature responses drop with the rise of velocity, because the stronger the groundwater seepage, the greater the ability to carry away heat. Thus, the heat accumulation can be efficiently alleviated by convection, gradually lessening the thermal responses.

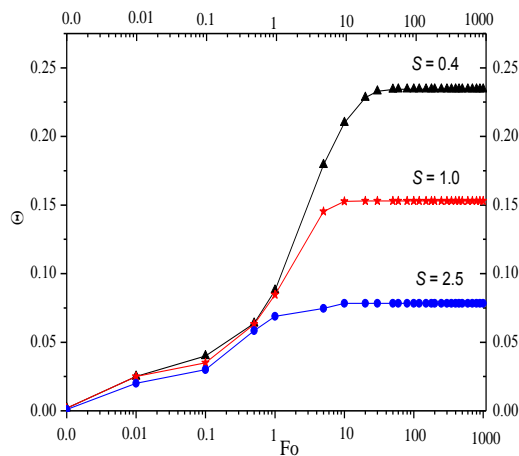


Figure 5.10 The temperature responses with the time while S adopts three different values

Furthermore, the temperature field around the GHE shows clear variations for different values of velocity S . Figure 5.11 illustrates the distribution change caused by the increase of groundwater velocity.

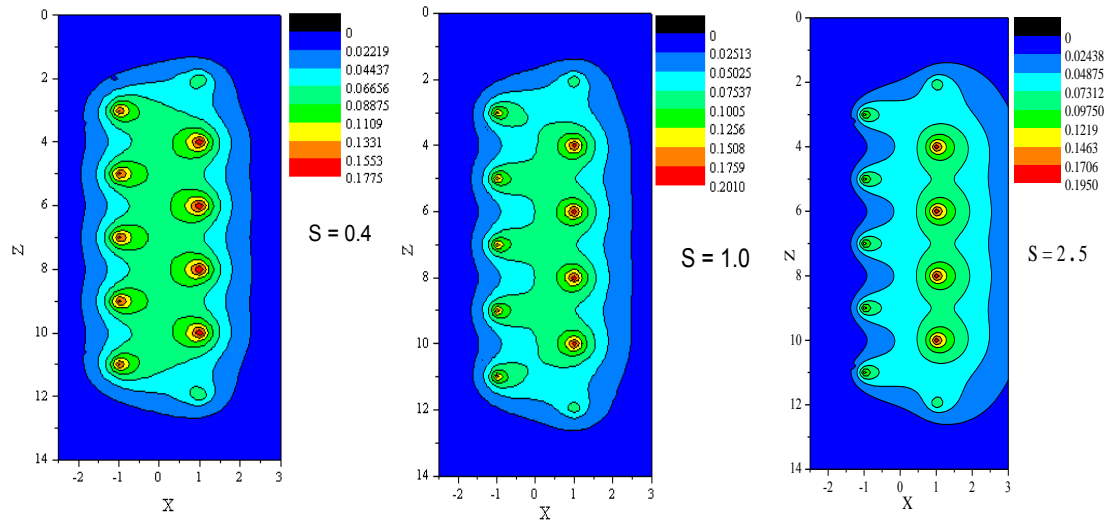


Figure 5.11 Temperature fields with different velocities of groundwater flow

Groundwater seepage makes the degree of asymmetry of the isotherms increasingly evident because the role of groundwater becomes gradually pronounced with the increase of velocity.

5.5.4 Influence of pitch B of spiral coils

As in chapter 4, where the effect of the ring-coil model's pitch B was reported, similar consideration was given to the spiral model's pitch B denoting the density of the coils along the z -axis (Mishra and Gupta, 1979). Given that the start-stop positions of the coils are fixed, a small value of B represents a short distance between adjacent coils and therefore there are more coils in total. The heat transfer capacity per meter GHE is boosted, but the thermal interference occurring among coils unavoidably becomes worse. The temperature responses of the surrounding underground medium rise rapidly, adverse

to continuous heat transfer. Another shortcoming is that difficulties in engineering construction are increased. In contrast, a large value of B reduces the heat transfer capacity, leading to undesirable heat transfer effects and the reduction in the GHE capacity to meet the heating or cooling load. Briefly, in the design, it is important to weigh the advantages and the disadvantages and therefore, on this basis, the pitch of spiral coils should be chosen to fit the need of the actual situation. The temperature responses with the time are shown in Figure 5.12 for different values of pitch B .

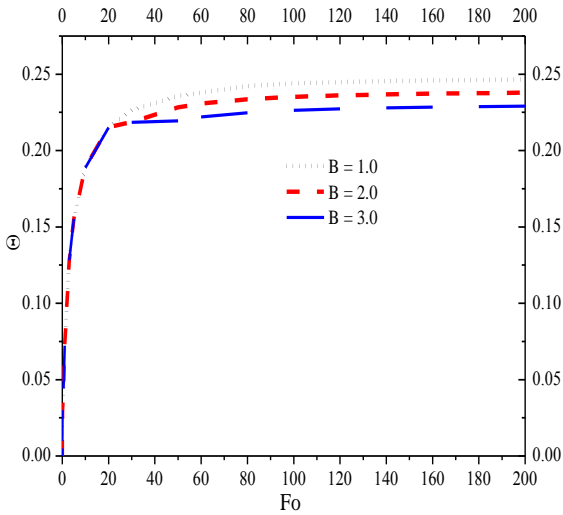


Figure 5.12 The temperature responses with the time while B adopts different values

The isothermals distributions for $B = 1.0$, $B = 2.0$ and $B = 3.0$ are displayed in Figure 5.13.

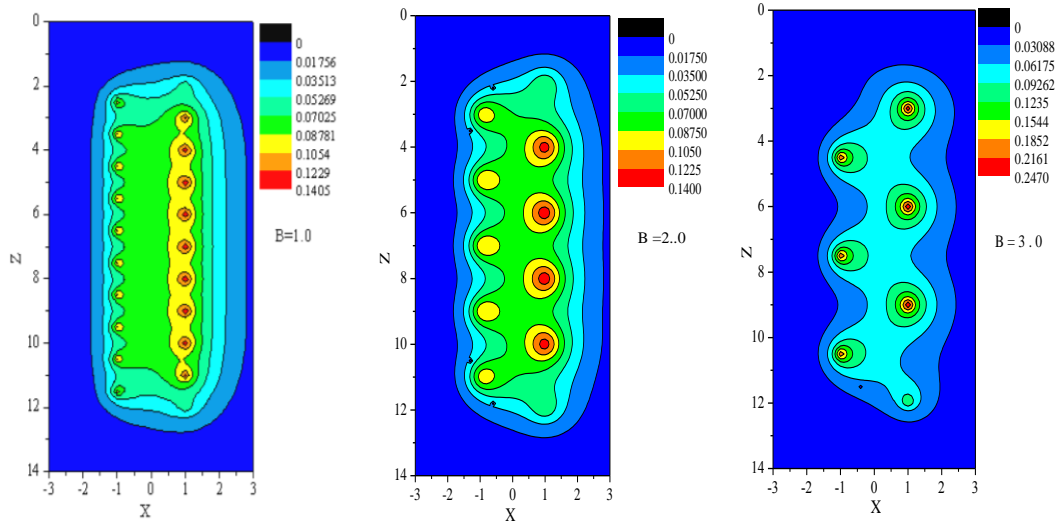


Figure 5.13 The temperature fields when B adopts different values

5.5.5 The alternative simplified calculation method

The finite spiral model can approximately represent the actual energy pile, and is therefore more appropriate than the solid and the ring-coil models. It can be employed to show the temperature responses of energy pile's surface during the process of heat dissipation. Equation (5.19) contains double integrals giving the analytical solution of the temperature response. By adding an additional integral is added to Equation (5.19), the mean temperature response can be obtained at the energy pile's surface at any horizontal plane along the z -axis. The new expression is given by Equation (5.21) with R set as 1.0. A further integral, with respect to z , can be added to Equation (5.21) making a total of four integrals, to generate the total mean temperature response, not only around the circumference of the pile but also along the depth direction. The expression of mean average temperature response is obtained as follows:

$$\overline{\Theta}_{a,s,f} = \frac{B}{32\pi^{7/2}} \int_0^{Fo} \frac{1}{(Fo - Fo')^{3/2}} \int_{H_1}^{H_2} dZ \int_0^{2\pi H_2/B} \int_0^{2\pi H_1/B} \exp\left[-\frac{[R\cos\varphi - \cos\varphi' - S(Fo - Fo')]^2 + (R\sin\varphi - \sin\varphi')^2}{4(Fo - Fo')}\right] \left\{ \exp\left[-\frac{(Z - B\varphi' / 2\pi)^2}{4(Fo - Fo')}\right] - \exp\left[-\frac{(Z + B\varphi' / 2\pi)^2}{4(Fo - Fo')}\right] \right\} d\varphi' d\varphi dFo' \quad (5.22)$$

However, this calculation will be more complicated. To simplify the calculation, five different points along the z-axis are selected with the aim of obtaining the mean temperature response when R is 1.0, and the comparisons between the results respectively obtained by two different methods can be made. The mean values with the time and the velocity are both shown in Figure 5.14, and the most accurate result obtained by the quadruple integrals approach is compared with the mean of temperature responses of five different selected positions.

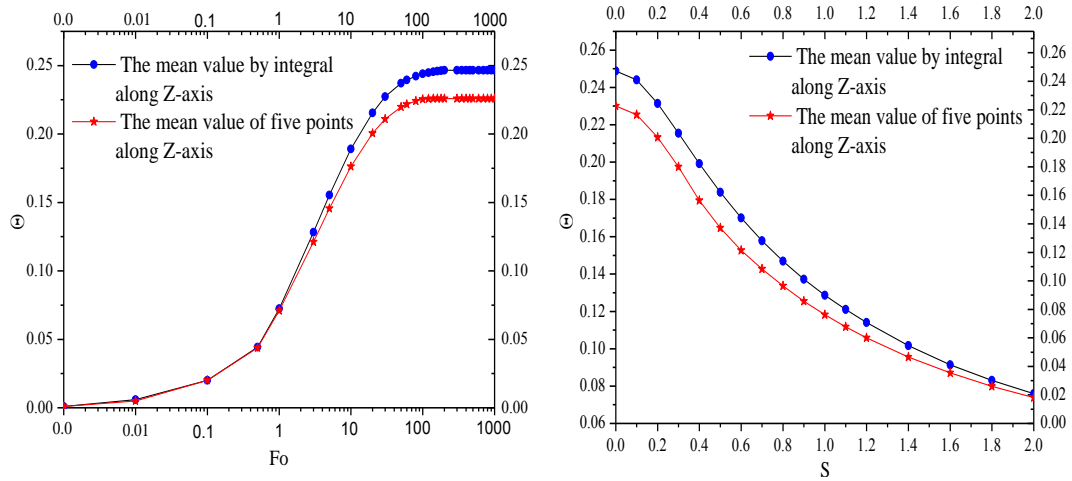


Figure 5.14 The temperature responses of two calculation methods with the time and with the velocity respectively

The relative errors of the simplified approach increase with the time and with the velocity. In the case of a very long time or a very large velocity, the error can reach 10%, which means the error, in general, is not great. Therefore, the method by way of five different positions' mean can be used especially for some engineering projects, because

the requirement for the computational accuracy is not too high.

5.5.6 Comparison between the temperature responses of $\varphi = 0$ and $\varphi = \pi$

Groundwater flows along the positive direction of the x-axis, and first contacts the left side of the GHE where $\varphi = \pi$ and alleviates the heat emitted from the spiral coils. Afterwards, groundwater continues to flow and then passes the position $\varphi = 0$, i.e. the right side. Despite the fact that groundwater advection relieves thermal response no matter for $\varphi = \pi$ or for $\varphi = 0$ finally, the benefits of them are achieved in the order, or even one side is disadvantageously influenced by another one in a given period. To be more specific, the heat is removed when the groundwater goes through the position $\varphi = \pi$. This heat, however, is carried across with unfavorable effects to the position $\varphi = 0$ during a time interval; there is no doubt that the heat around $\varphi = \pi$ and $\varphi = 0$ can both be removed at last. In order to compare the responses of these two sides of the pile surface, an integration is performed along the z-axis based on Equation (5.19). The temperature responses at $\varphi = 0$ and $\varphi = \pi$ when R is 1.0 are given by Equations (5.23) and (5.24) respectively.

$$\Theta_{a,s,f,\varphi=0} = \frac{B}{16\pi^{5/2}} \frac{1}{H_2 - H_1} \int_0^{Fo} \frac{1}{(Fo - Fo')^{3/2}} \int_{H_1}^{H_2} dZ \int_{2\pi H_1/B}^{2\pi H_2/B} \exp \left[-\frac{[1.0 - \cos \varphi' - S(Fo - Fo')]^2 + (0.0 - \sin \varphi')^2}{4(Fo - Fo')} \right] \left\{ \exp \left[-\frac{(Z - B\varphi' / 2\pi)^2}{4(Fo - Fo')} \right] - \exp \left[-\frac{(Z + B\varphi' / 2\pi)^2}{4(Fo - Fo')} \right] \right\} d\varphi' dFo' \quad (5.23)$$

$$\Theta_{a,s,f,\varphi=\pi} = \frac{B}{16\pi^{5/2}} \frac{1}{H_2 - H_1} \int_0^{Fo} \frac{1}{(Fo - Fo')^{3/2}} \int_{H_1}^{H_2} dZ \int_{2\pi H_1/B}^{2\pi H_2/B} \exp \left[-\frac{[-1.0 - \cos \varphi' - S(Fo - Fo')]^2 + (0.0 - \sin \varphi')^2}{4(Fo - Fo')} \right] \left\{ \exp \left[-\frac{(Z - B\varphi' / 2\pi)^2}{4(Fo - Fo')} \right] - \exp \left[-\frac{(Z + B\varphi' / 2\pi)^2}{4(Fo - Fo')} \right] \right\} d\varphi' dFo' \quad (5.24)$$

The results are plotted in Figure 5.15, and it is apparent that the response value at the side of $\varphi = 0$ is stronger than that of the side $\varphi = \pi$.

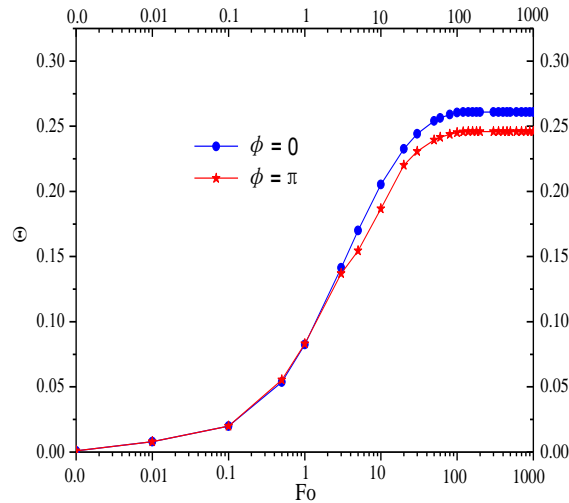


Figure 5.15 The temperature responses of the sides $\varphi = 0$ and $\varphi = \pi$

5.5.7 The influence which groundwater seepage exerts on a pile group

The temperature responses caused by a single spiral heat source in the presence of groundwater seepage and the corresponding analytical solutions have become understood. Any engineering project would have an array of energy piles supporting the whole building. The temperature response at any point except the heat sources themselves is the sum of contributions mad by each energy pile. Equation (5.19) gives the expression produced by one spiral heat sources while groundwater flows through it, and the total result taking account of all piles and their coordinates under the condition of groundwater seepage is expressed by Equation (5.25).

$$\Theta_{to, a, s, f} = \sum_{i=1}^n \Theta_{i, a, s, f} = \sum_{i=1}^n \frac{B}{16\pi^{5/2}} \int_0^{Fo} \frac{1}{(Fo - Fo')^{3/2}} \int_{2\pi H_1/B}^{2\pi H_2/B} \exp \left[-\frac{[X - X_i - \cos \varphi' - S(Fo - Fo')]^2 + (Y - Y_i - \sin \varphi')^2}{4(Fo - Fo')} \right] \left\{ \exp \left[-\frac{(Z - B\varphi' / 2\pi)^2}{4(Fo - Fo')} \right] - \exp \left[-\frac{(Z + B\varphi' / 2\pi)^2}{4(Fo - Fo')} \right] \right\} d\varphi' dFo' \quad (5.25)$$

where X_i and Y_i are respectively the X and Y coordinates of the axis center of every energy pile at the horizontal plane.

The depths of all piles are assumed the same and the tops and bottoms of all spiral heat sources are at the same levels, and the geometry of the energy piles with the corresponding spiral heat sources is identical.

For example, an engineering project with a total of 15 energy piles is employed as the reference object. The piles are arrayed in the form of a 3X5 matrix, and a plane of the pile group array is shown in Figure 5.16.

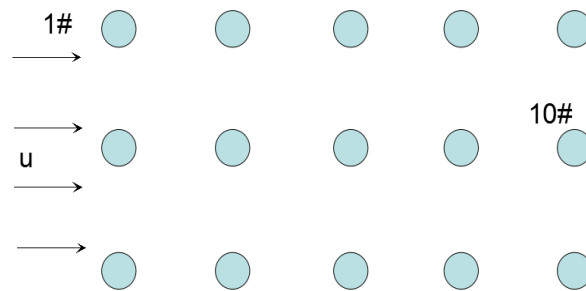


Figure 5.16 The distribution pattern of pile group

The temperature distribution of the whole energy pile group can be realized with the aid of Equation (5.25), and is shown in Figure 5.17. In the event of groundwater seepage which is along the positive direction of X , the temperature responses of the left area of pile group are lower than those on the right. The closer to the left boundary, the weaker the temperature response, making obvious the degree of influence that groundwater seepage exerts. In contrast, the temperature responses rise gradually when the distance to the right boundary of pile group becomes increasingly short.

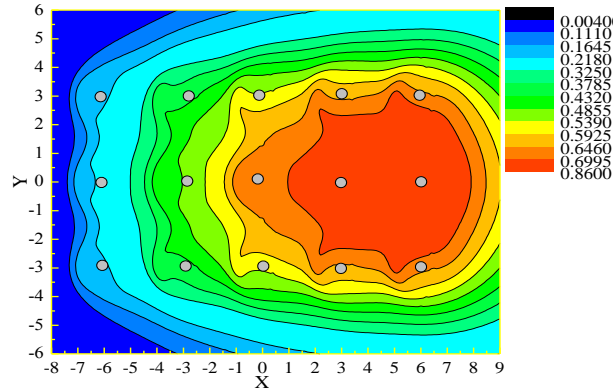


Figure 5.17 The temperature distribution of pile group with groundwater advection

In addition, temperature responses near pile 1# and 10 # are depicted in Figure 5.18, and the difference is shown clearly. Pile 1# is located at the position which is least to the left when passed by groundwater, therefore experiencing the severest cooling impact, and the thermal disturbances from other energy piles are the weakest case. Accordingly, the heat transfer performance of this pile and its near area is improved with the most favorable degree. However, the heat taken away to the right by the groundwater has an adverse impact on the heat transfer performance of pile 10 # and its surrounding medium in a certain period. For this reason, the largest temperature responses can be found in the locations near pile 10 # .

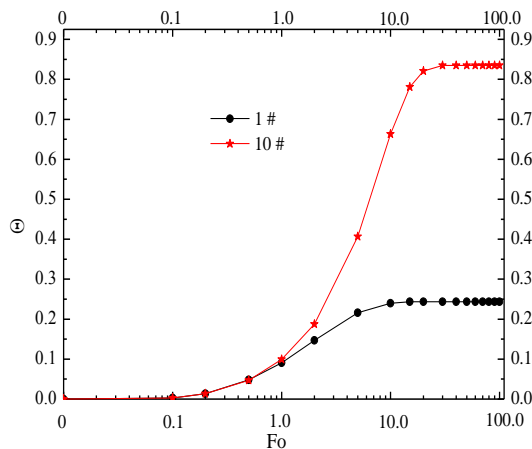


Figure 5.18 The temperature responses of places near pile 1# and pile 10#

The above confirms the evidence of previous chapters in showing that groundwater seepage advantageously improves the heat transfer performance energy piles with spiral coils. Thus, the whole underground heat accumulation over the area of pile group can be alleviated in this way. It should be admitted that the investigations on influence which groundwater advection exerts on not only single energy pile but also a group of energy piles are novel and original.

5.6 Comparisons between models without and with groundwater seepage

The spiral heat transfer models for pure conduction and combined conduction and advection are compared to highlight the role of groundwater seepage. The readers are reminded that the finite model is the one to be considered for this purpose whether pure conduction or combined heat transfer is considered because of the limited length of actual pile foundation GHEs. Equation (5.22) gives the whole mean temperature response of the finite spiral seepage model; in addition, the corresponding expression for the pure conduction model is represented by Equation (5.26).

$$\overline{\Theta}_{p,s,f} = \frac{B}{16\pi^{5/2}} \frac{1}{H_2 - H_1} \frac{1}{2\pi} \int_0^{Fo} \frac{1}{(Fo - Fo')^{3/2}} \cdot \exp\left[-\frac{R^2 + 1}{4(Fo - Fo')}\right] \cdot \int_{H_1}^{H_2} dZ \int_0^{2\pi} d\varphi \int_{2\pi H_1/B}^{2\pi H_2/B} \exp\left[\frac{2R\cos(\varphi - \varphi')}{4(Fo - Fo')}\right] \cdot \left\{ \exp\left[-\frac{(Z - B\varphi' / 2\pi)^2}{4(Fo - Fo')}\right] - \exp\left[-\frac{(Z + B\varphi' / 2\pi)^2}{4(Fo - Fo')}\right] \right\} d\varphi' dFo' \quad (5.26)$$

There is a striking contrast in Figure 5.19 which displays the comparisons. Firstly, the temperature responses with the time are provided when seepage velocity is constant. Secondly, the temperature responses change with the groundwater velocity given that the time is fixed. Obviously, temperature response of the model with groundwater

transfusion is lower than without groundwater transfusion, and the differences of temperature responses become larger and larger with the time or with the velocity. It is increasingly clear that groundwater flow is a significant contributor to energy pile effectiveness, after some time has elapsed or if the flow velocity is sufficiently large.

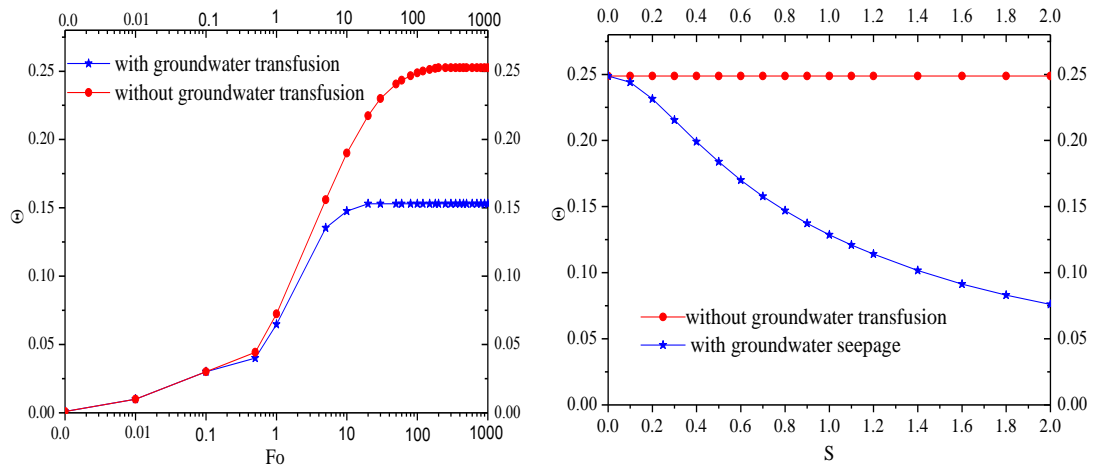


Figure 5.19 The temperature responses of pure conduction and combined heat transfer

Q_p and Q_a are the heat transfer rates of spiral pure conduction and combined heat transfer, respectively. The most important significance of groundwater transfusion is the enhancement of the heat transfer ability. Figure 5.20 shows how the ratios of heat transfer rates change with the velocity and with the time. It can be seen that the heat transfer ability gradually improves with the velocity or with the time. This proves the importance of the existence of groundwater transfusion, a phenomenon which should be exploited especially when the velocity is large or the time is sufficiently long. Groundwater transfusion improves the performance of pile foundation GHEs by strengthening the heat exchange quantity, enabling pile foundation GHEs to meet more heating load or cooling load. By embedding the heat exchange tubes within the piles, holes for which have in any case to be drilled, the expense of drilling boreholes

dedicated to solely to the GHE is decreased, which means the initial cost of the engineering projects can be reduced. Basically the pile is conducting two jobs at the same time: 1. supporting the building and 2. acting as part of the building cooling or heating.

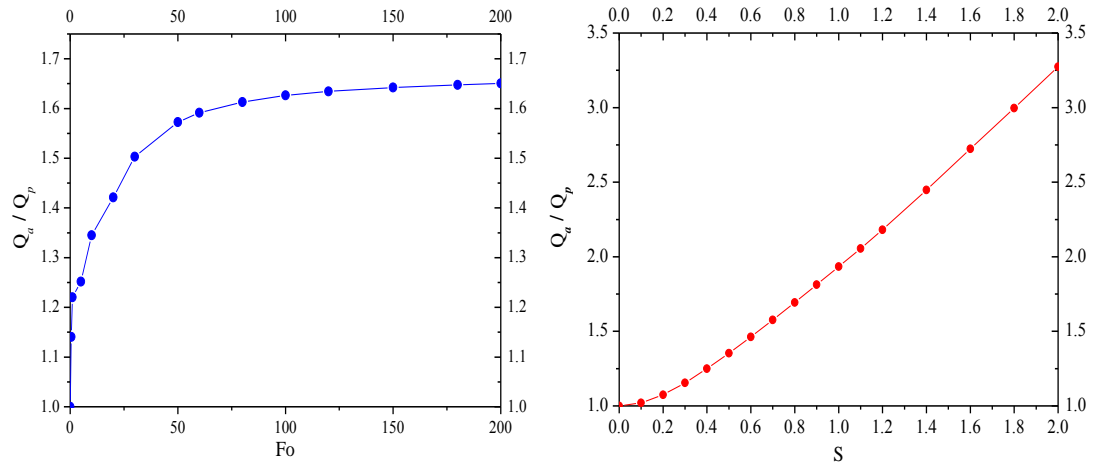


Figure 5.20 The heat transfer rates' ratios of two heat transfer modes with the time and with the velocity

5.7 Summary

Explored in this chapter is the spiral heat source seepage models first including conduction aspect and then the added effects of groundwater advection for pile foundation GHEs. Both the infinite and the finite models are formulated and discussed, and the corresponding analytical solutions are obtained. The spiral model is more representative of the actual spiral heat exchange tube, and the shortcomings of existing models such as solid cylindrical and ring-coil models can be improved. The finite model constitutes the research focus because real pile foundation GHE must be limited in length. The influences exerted by many parameters on temperature response have been

studied to better demonstrate the versatility and power of analytical solutions. For an engineering project in practice, the initial cost can be dropped if the energy pile technology is employed because the expense on drilling boreholes GHEs can be reduced. Furthermore, the heat transfer ability of an energy pile has been shown to be very marked when comparing borehole GHEs with energy piles. The simulations for spiral heat source seepage model show that groundwater flow has a beneficial influence on the heat transfer performance of the pile foundation GHE; the greater the transfusion, the more effective the heat transfer. Thus, a bigger heating or cooling load can be coped with if using the pile foundation GHEs, and the initial investment can be further reduced. This exploration about spiral models with groundwater transfusion provides sufficient theoretical guidance for engineering projects, and potentially boosts the continuous development of energy pile technology.

CHAPTER 6 THERMAL TRANSMISSION EXPERIMENTS OF ENERGY PILES

6.1 Introduction

The most accurate models of pile foundation GHE with groundwater advection have been proposed in chapter 5. The seepage models can be indirectly verified if the corresponding pure conduction models are validated by on-site experiments. It is unfortunate that there are no test rigs on which to conduct groundwater advection experiments. Groundwater velocity is so small that the experimental simulation is extremely difficult. In addition, the period needed for observing any obvious effect of groundwater advection is too long. For these reasons, the pure thermal transmission experiments of energy pile can be firstly tried and this can provide reliable basis for seepage test rigs in the future.

The pile foundations of an office building have spiral coils installed, enabling the energy piles to transmit heat to the surrounding underground medium. Some parameters including temperatures, flow rate of circulating liquid, power of equipments and so on were recorded over time. The significant findings could be obtained based on these parameters recorded during the experiments. Theoretical models are then employed using some data and geometric parameters of GHE to calculate the results. Finally, comparisons between experimental data and theoretical results indicate the degree of reliability of the mathematical model. Thus, the seepage model can be indirectly

certified provided that the pure conduction model is proven to be correct.

6.2 Presentation on energy piles of building employing the GCHP system

6.2.1 Characteristics of pile foundation GHE

The engineering project is located in Jinan, Shandong of China, the office building of new energy develop center of Shandong Coalfield Geology Bureau. Both pile foundation and borehole GHEs are employed for GCHP system. Some piles are used to bury spiral heat exchange tubes for taking on a certain proportion of air conditioning load, this helps to reduce the initial cost of drilling boreholes.

All pile foundations of the building lie in the place 1m below the ground boundary. There are totally 52 piles acting as the energy piles. Because spiral coils are installed in the pile, the diameter of which is a little larger than that of coils. For this project, the pile and spiral coil diameters are 800mm and 750mm, respectively; the pile length is approximately 26m and the spiral coils length nearly 25m as the pile must be a little longer to hold the spiral tube. The coil pitch is 200mm and the material is high-density polyethylene (HDPE), which has high thermal conductivity and good corrosion resistance (WIKIPEDIA, 2014). The heat transfer coefficient of a spiral tube is higher than that of a straight tube. The spiral tube is fixed into a precast hollow steel cage and the assembly is then lowered into the pile. Afterwards concrete is poured to fill the hole to form the complete energy pile as shown in Figure 6.1.

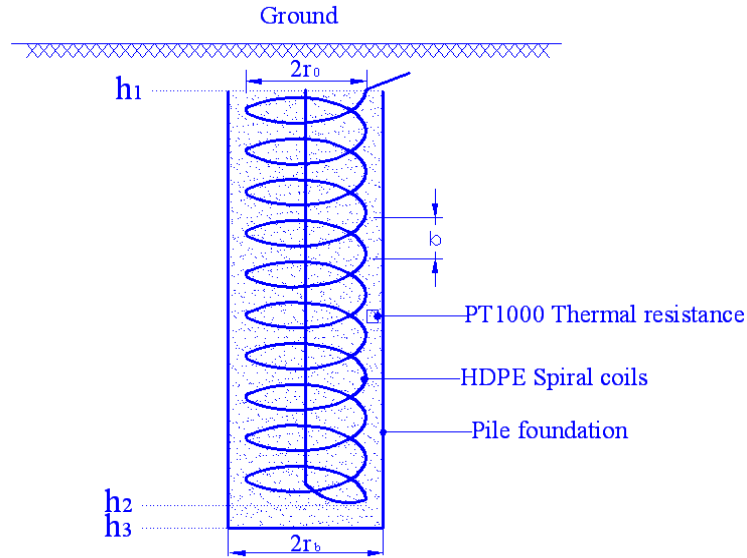


Figure 6.1 Schematic diagram of on-site energy pile

The parameters h_1 , h_2 and h_3 are various distances of parts of the energy pile from the ground as shown 1m, 26m and 27m respectively; and b is the coils pitch. $h_2 - h_1$ is the spiral coil length of 25m, $h_3 - h_1$ is the pile depth at 26m. Circulating liquid flows through the spiral coils to transfer heat to the surrounding underground medium.

6.2.2 The local underground thermal properties

Because some underground parameters are included in the mathematical model, their values must be measured to achieve the calculation accuracy. A rock and soil thermophysical tester developed by Shandong Jianzhu University is employed to measure the local ground thermal properties. The underground medium, thermal conductivity, volume specific heat and initial temperature were all obtained by testing (IGSHP SHJU, 2012). The detailed information is shown in Table 6.1 and a photograph of the testing machine is shown in Figure 6.2. The tests must be made in advance of construction because the design size of the GHEs depends on knowing the parameters'

values.

Table 6.1 Introduction of underground medium

Underground medium	Thermal conductivity	Volume specific heat	Initial temperature
Red mud and rock layer	1.301w/(m ·°C)	1.945×10 ⁶ J/(m ³ ·°C)	14.9 °C



Figure 6.2 The photo of thermophysical tester

6.3 Description and analysis about experiments

6.3.1 Experimental procedures

The thermal exchange consists of the heat release from the circulating liquid and therefore it is unnecessary to consider the freezing problem (Michopoulos et al., 2007), the pure water without anti-freeze fluid is employed to transmit heat to the underground medium. Two equipments, with constant heating powers, are employed for heating the circulating water and measuring temperatures and flow rate at time interval, they were self-developed by Shandong Coalfield Geology Bureau. Each equipment consists of circulating pump, electric heater, flow meter and thermal resistor (Zhang, 2010). The inlet and outlet temperatures of the circulating water were recorded on entering and leaving each instrument over time, and the power supplied for heating and the flow rate

of circulating liquid were continuously kept at regular interval.

In addition, PT1000 thermal resistors were installed at the mid depth of the spiral tubes, because their precisions are high (HMIL, 2009). The underground original temperature is known and the temperature response at the mid depth of pile over time is recorded by these experimental resistors. A schematic diagram of the heat transfer experiments is shown in Figure 6.3.

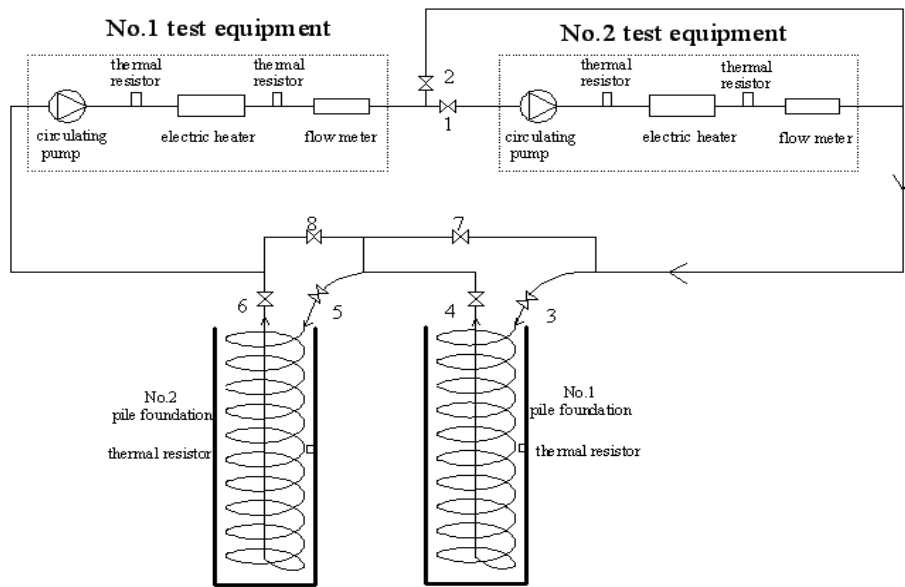


Figure 6.3 Schematic diagram of heat transfer experiment of pile foundation GHEs

There are two groups of experiments involving two energy piles. For the first experiment, only one equipment is used and another one is closed. Circulating liquid flows only through the spiral tube of No.1 pile, and all relevant data with the time are recorded. Both equipments are next employed to enhance the heating power because they are connected in series, but on this occasion, only No.2 pile receives the circulating water in accordance with the experimental design as the temperature field around No.1 pile has been disturbed in the first experiment. The sizes of No.1 and No.2, their layouts

and spiral tubes are identical no matter whether inside or outside the piles.

Specifically, No.1 equipment and No.1 pile were utilized in the first experiment, and at that time valves 1, 5, 6 and 7 are closed and valves 2, 4, 6 and 8 open. After that, No.1 and No.2 equipments were connected in series while No.2 pile and not No.1 pile was included in the circuit according to the experimental design. During the second experiment, valves 2, 3, 4 and 8 were closed while valves 1, 5, 6 and 7 were opened. The flow rate and temperatures of the circulating water were doubly checked as each equipment has its own flow meter and thermal resistors. Figure 6.4 shows some on-site photographs of the experiments.



Figure 6.4 The on-site photos of heat transfer experiments of energy piles

6.3.2 The analysis on recorded data

6.3.2.1 The first experiment

The heating powers of the two equipments are unequal. One set has low power and one high. The No.1 equipment with low power was first used to heat the circulating liquid, and the inlet and outlet temperatures increased gradually with the time, and the corresponding data is shown in Figure 6.5. It took about 70 hours to finish the first experiment, the temperature difference between inlet and outlet temperatures of circulating water rises sharply at first before quickly becoming approximate stable within the range of from 2.5 °C to 3.0 °C.

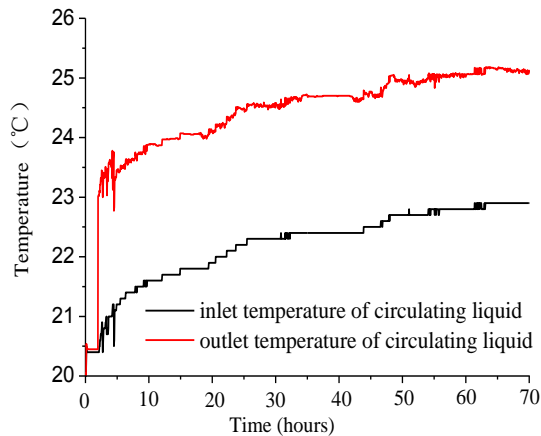


Figure 6.5 The inlet and outlet temperatures of the circulating liquid in the first experiment

The flow rate fluctuated slightly as shown in Figure 6.6, the unit is liters per minute and the value is from 11.5L/min to 12.5L/min..

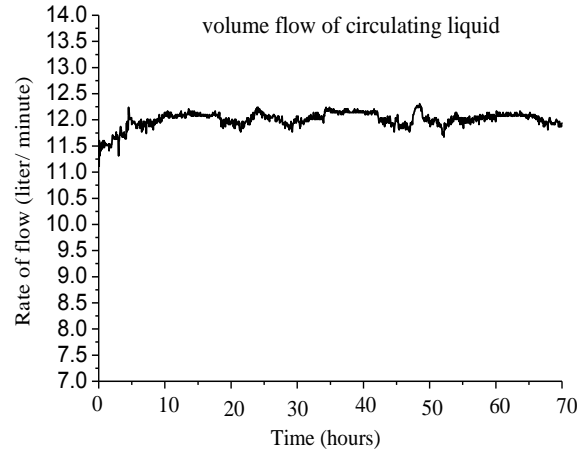


Figure 6.6 The flow rate of the circulating liquid in the first experiment

To calculate the heat transfer rate of an energy pile, one method is to use the formula $q = C_p \times (t_{out} - t_{in}) \times m_{li} / h_{st}$ (Jalaluddin and Miyara, 2012), where C_p is the specific heat capacity of circulating liquid (4.2 kJ / (kg. °C)) since it is pure water; t_{out} and t_{in} are respectively outlet temperature and inlet temperature, m_{li} and h_{st} respectively denote the volume flow and the length of the spiral tube. The values of temperatures and volume flow were recorded over time, and h_{st} is 25m as in section 6.2. Another method is to make use of the heating power of No.1 equipment, because the circulating water is heated by equipment's electric heater to raise its temperature before it flows through spiral tube to release heat to the surrounding underground medium. The power is denoted by P and the heat transfer rate is given by $q = P / h_{st}$. The value of P is shown in Figure 6.7. The power, P , remained stable during the nearly 70 hours of the first experiment, although some slight degree of fluctuations was apparent. The mean value can be selected when calculating q .

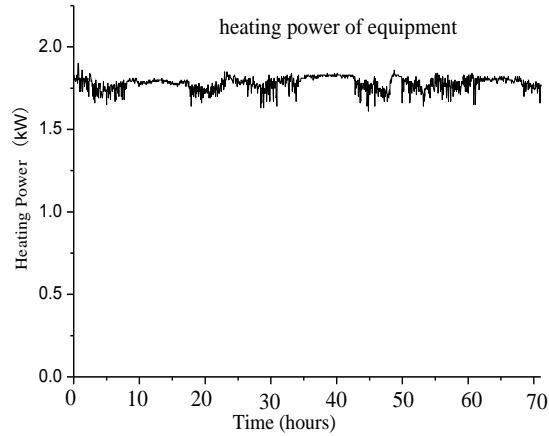


Figure 6.7 The heating power of the No.1 instrument in the first experiment

As a rule, the heat transfer rates obtained by two different methods should be equal, but the local environment and other interference lead to some data deviations. Figure 6.8 describes the heat transfer rates obtained by the two methods. On the whole, the results are similar but the values deduced from the inlet and the outlet temperatures are higher than those derived based on heating power. This is because some heat is also indirectly provided by instruments such as water pumps during the experiment. The method based on the inlet and the outlet temperatures is more accurate and this approach should be adopted for calculating the heat exchange rate of the energy pile.

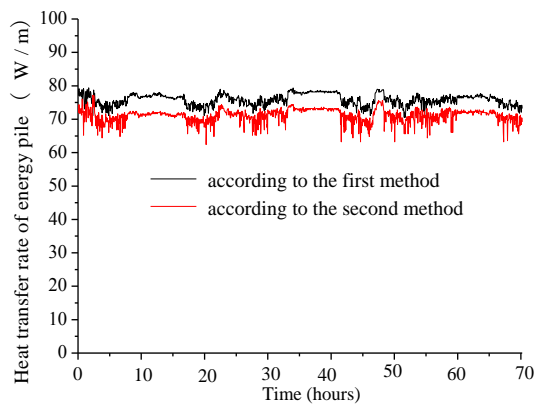


Figure 6.8 The heat transfer rates according to two different methods in the first experiment

The mean output of the whole experiment was nearly 75.91W/m, and this value can be used when validating the mathematical model. Because the thermal resistors were set at fixed locations inside the piles, the temperature response can be recorded at regular time interval. As a consequence, the experimental data can be compared with the mathematical results to check the performance of the simulation models.

6.3.2.2 The second experiment

As the heat transfer rate of the energy pile is small in the first experiment, the thermal response was not intense enough. To better check the temperature responses induced by an energy pile when heat transfer between the GHE and the underground medium occurs, the second experiment was conducted, and this time the high heating power was supplied. For the second experiment, two equipments were connected in series to increase the heating power; accordingly the heat transfer capability was strengthened. The circulating water first flows through the No.1 equipment and is heated by the low power electric heater, and then flows through the No.2 one with high heating power. The No.1 pile had been used in the first experiment and thus the original temperature around the pile was disturbed to a certain degree, therefore the temperatures were now not in accordance with the preconditions of the mathematical model and the comparisons between the experimental data and the calculated results will lose meaning. Thus, the No.2 pile was substituted for the No.1 pile. In the same way, the inlet and the outlet temperatures of the circulating water are given as follows:

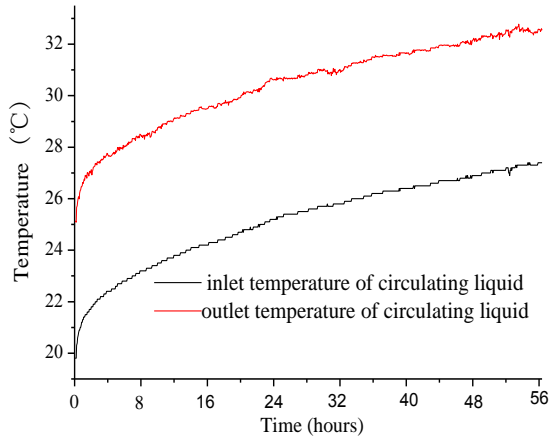


Figure 6.9 The inlet and outlet temperatures of the circulating liquid in the second experiment

It is obvious that the temperature difference between inlet and outlet temperatures is larger than that of the first experiment, because the heat transfer quantity is greater in view of the enhanced heating power. The heat transfer ability becomes more evident due to the stronger temperature response, the experimental effect is clearer. Therefore, the experimental time was shortened to 55 hours at which time the inlet and outlet temperatures difference was nearly stable.

The flow rate of the circulating water with the time is shown in Figure 6.10, with values between 13.5L/min and 14L/min.

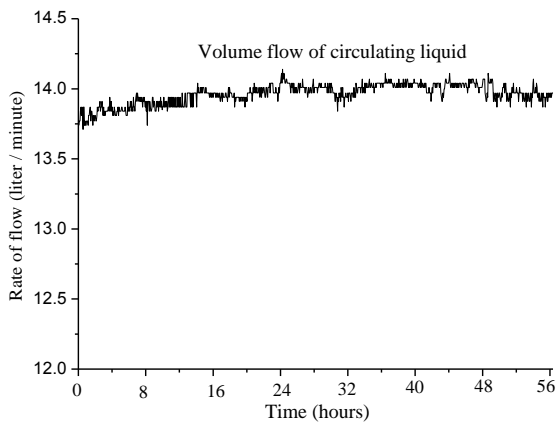


Figure 6.10 The flow rate of the circulating liquid in the second experiment

The total heating power of the two equipments with the time is depicted in Figure 6.11 and clearly larger than that of only one equipment, and almost twice that of the first experiment.

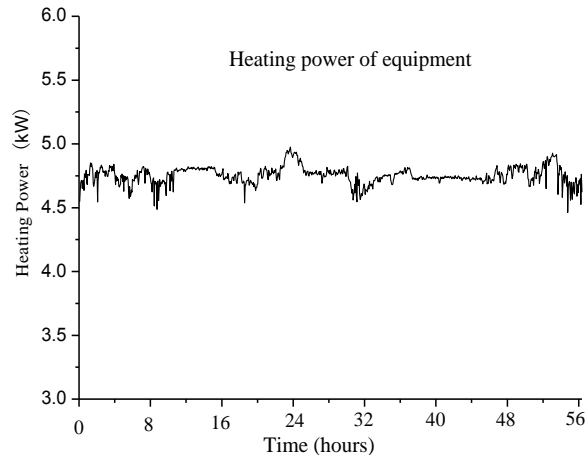


Figure 6.11 The total heating power of the No.1 and the No.2 instruments in the second experiment

The two different methods used in the first experiment, for assessing heat supply to the fluid, are applied again to calculate the value of q , and the corresponding values are provided in Figure 6.12,

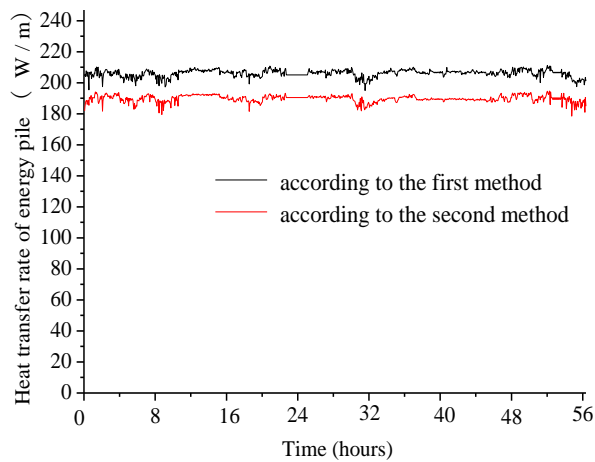


Figure 6.12 The heat transfer rates according to two different methods in the second experiment

The result obtained by the first method remains higher than that with the help of the second method, thus the mean value of heat transfer rate during the experimental period was around 206.52W/m.

6.4 The comparisons between mathematical model results and experimental findings

The equations of the analytical solution for the temperature response induced by the energy pile, require the values of the experimental parameters to be incorporated. Equation (6.1) is the expression of the finite spiral heat source model of pile foundation GHE.

$$\begin{aligned} \theta &= \frac{q_l b}{2\pi\rho c} \int_0^\tau d\tau' \left[\int_{2\pi h_1/b}^{2\pi h_2/b} G(z' = b\phi'/2\pi) d\phi' - \int_{2\pi h_1/b}^{2\pi h_2/b} G(z' = -b\phi'/2\pi) d\phi' \right] \\ &= \frac{q_l b}{16\pi\rho c} \int_0^\tau \frac{d\tau'}{[\pi a(\tau - \tau')]^{3/2}} \cdot \exp\left[-\frac{r^2 + r_0^2}{4a(\tau - \tau')}\right] \cdot \\ &\quad \int_{2\pi h_1/b}^{2\pi h_2/b} \exp\left[\frac{2rr_0 \cos(\phi - \phi')}{4a(\tau - \tau')}\right] \left\{ \exp\left[-\frac{(z - b\phi'/2\pi)^2}{4a(\tau - \tau')}\right] - \exp\left[-\frac{(z + b\phi'/2\pi)^2}{4a(\tau - \tau')}\right] \right\} d\phi' \end{aligned} \quad (6.1)$$

The diameter of spiral coils is 750mm and therefore the radius r_0 is 750mm / 2 = 375mm, and the spiral coil's pitch b is 200mm.

Thermal resistors continuously measured temperatures at their locations at all times and the initial temperature is known, therefore the temperature response θ can be acquired; and the corresponding thermal properties were obtained using the approximate tests. As a consequence, the formula $\Theta = k \theta / q_l$ was applied to obtain the experimental non-dimensional temperature response. To obtain the simulation model's results, dimensionless parameters were introduced as: $Fo = a \tau / r_0^2$, $\Theta = k \theta / q_l$, $R = r / r_0$, $Z = z$

$/ r_0, H_1 = h_1/ r_0, H_2 = h_2/ r_0$ and $B = b / r_0$. The thermal resistors were set at the locations of $r = r_0$ and thus R is 1.0. The actual parameters and the corresponding dimensionless values are given in Table 6.2.

Table 6.2 The actual parameters and corresponding dimensionless values

b , B	200mm , 0.54
h_1 , H_1	1.0m , 2.67
h_2 , H_2	26.0 m, 69.33
h , H	25.0m, 66.67
r , R	375mm, 1.0

Based on Equation (6.1), the non-dimensional expression is given.

$$\Theta = \frac{B}{16\pi^{5/2}} \int_0^{Fo} \frac{1}{(Fo - Fo')^{3/2}} \cdot \exp\left[-\frac{R^2 + 1}{4(Fo - Fo')}\right] \cdot \int_{2\pi H_1/B}^{2\pi H_2/B} \exp\left[\frac{2R \cos(\varphi - \varphi')}{4(Fo - Fo')}\right] \cdot \left\{ \exp\left[-\frac{(Z - B\varphi' / 2\pi)^2}{4(Fo - Fo')}\right] - \exp\left[-\frac{(Z + B\varphi' / 2\pi)^2}{4(Fo - Fo')}\right] \right\} d\varphi' dFo' \quad (6.2)$$

The location of thermal resistor was at $z = 13.5$ so the value of the corresponding dimensionless value Z is 36. The comparisons between the calculated results of the mathematical model and the findings of the first experiment are described in Figure 6.13. To clearly show the process of experiment, the horizontal coordinate represents the actual time i.e. the unit is hour, and the vertical coordinate is non-dimensional temperature. It is seen that two curves are very similar in shape and only a small difference exists between them at all times.

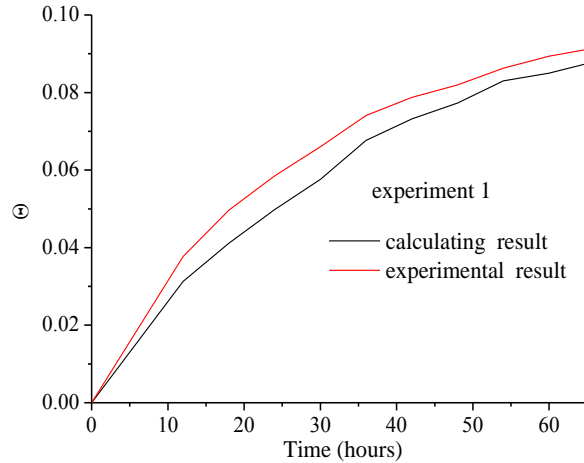


Figure 6.13 Comparisons between calculated results and experimental findings of the first experiment

The next step was to check the temperature response of the second experiment against the mathematical model. In this experiment, the heat supplied to the circulating fluid was much greater to enhance the heat transfer ability of energy pile. The temperature responses with the time are shown in Figure 6.14.

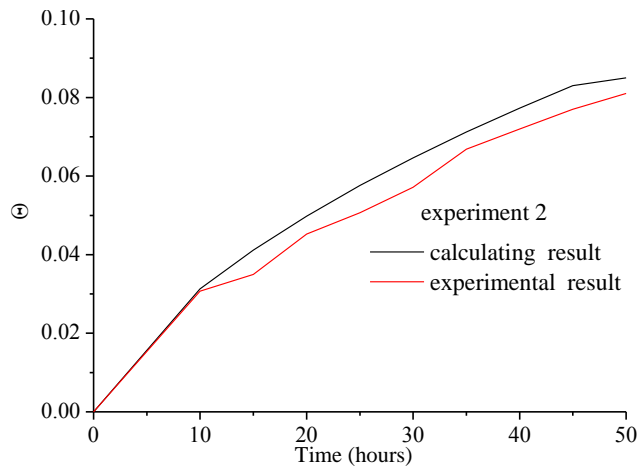


Figure 6.14 Comparisons between calculated results and experimental findings of the second experiment

According to Figures 6.13 and 6.14, in the first experiment, the experimental

temperature responses were slightly greater than those calculated by the model; but the opposite was the case for the second one. Thus, the degree of boosting temperature response in the second experiment was less than the degree of boosting the heat supplied to the circulating fluid. The comparisons do show that the temperature responses of both model and experiments are very similar and the differences between them are quite minor. It can justifiably be claimed that the spiral mathematical model of pile foundation GHE has been validated by the experiments, and this model can be applied to analyze thermal responses in other cases, no matter for academic research or for when designing a real engineering scheme.

6.5 Summary

The spiral heat source is the most accurate model for describing the behaviour of a pile foundation GHE, and can be employed for the design or thermal analysis of an energy pile because its validity has been checked against the heat exchange experiments of energy piles. Two heat transfer experiments were conducted to check the rationality and logicity of the model, and the theoretical research underpinning the model has been vindicated in practice. Comparisons between experimental and calculated results were made under both low heat transfer rate and large heat transfer rate conditions.

It is difficult to establish an experiment rig to measure the impacts of groundwater seepage on energy piles. It is argued, however, that the combined model of pure conduction and groundwater advection is fundamentally the same problem as evidenced by the mathematical expressions, since the experiments confirmed the mathematical model in the case of pure conduction, there is no good reason to suppose that the model would not be confirmed in the case of conduction with groundwater advection.

The fundamental principles of pure conduction and combined heat transfer are the same, and Green's function is made full use of to analyze the temperature response induced by the heat source if both conduction and advection exists. The static heat source, in the latter advection case, can be regarded as a moving heat source while groundwater flows through energy pile, thereby the groundwater seepage models are obtained exactly according to the corresponding conduction models.

In conclusion, given that the heat transfer model has been experimentally verified when there is no groundwater, the models which also allow for groundwater advection can be said to have been indirectly confirmed. Accordingly, the experiments described in this chapter are particular valuable.

CHAPTER 7 BACK CALCULATION METHOD BASED ON THE LINE HEAT SOURCE SEEPAGE MODELS TO OBTAIN GROUNDWATER VELOCITY

7.1 Introduction

According to all investigations in previous chapters, the groundwater advection is important especially when the seepage intensity is large enough. The influence that groundwater exerts on the heat transfer process cannot always be ignored. For the most frequently used borehole GHEs, the heat transfer performance and economic efficiency can both be improved if groundwater seepage is taken into account. It is important to know approximately what the velocity might be before conducting studies on groundwater influence. Figure 7.1 provides the schematic diagram of the groundwater that passes borehole GHE.

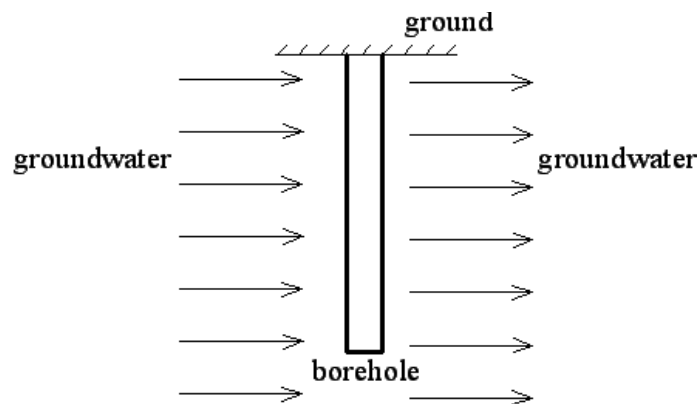


Figure 7.1 The groundwater flowing through borehole GHE

The value and the orientation of groundwater velocity vary with the locations as hydraulic gradients are never constant. If the velocity, only is well understood then the influence of groundwater seepage can be controlled. However, it is difficult to obtain an accurate velocity without special measures because groundwater is obviously below ground. At present, engineering projects simply ignore groundwater to simplify calculations. This will inevitably lead to errors especially when groundwater seepage is at a high level. Sometimes there have been attempts to measure groundwater velocity, but the work involved is troublesome and difficulties arise in achieving a accurate measure as the order of magnitude of seepage velocity is too small and the underground geological structure is usually complex (Ni et al, 2009). Consequently to this day, there is no solution to assessing groundwater velocity at a given location in any simple practical manner. The object of this chapter is to explore a methodology based on the line heat source seepage models for obtaining the groundwater velocity.

As a rule, pile foundation GHEs cannot cope with the heating or cooling load for the whole building. Energy piles and borehole GHEs together function as the elements responsible for releasing and extracting underground heat. As described above, the geometry of a borehole is simpler than that of a pile and therefore a borehole GHE is usually fitted with a line heat source. Accordingly, the line heat source seepage models are employed to ‘back analyze’ the local groundwater velocity. After that, the groundwater influence on pile foundation GHEs can be investigated. Because analytical solutions for the borehole GHE under the influence of groundwater are ready-made expressions, the velocity can be deduced with the help of the inverse algorithm if on-site temperature responses at chosen locations have been recorded. Details of the back

calculation method and the necessary supporting measures are demonstrated step by step in this chapter.

7.2 The influence that groundwater seepage exerts on a borehole GHE

It is necessary to stress the advantageous role played by groundwater prior to the introduction of the back calculation method, because the significance for obtaining the groundwater velocity can be emphasized by this way.

7.2.1 The analytical solutions of line heat source models with groundwater advection

The expressions of line heat source seepage models were given in section 3.3, but these analytical solutions for both infinite and finite models are repeated to remind their reliabilities.

7.2.1.1 Infinite line heat source seepage model

The analytical solution for the infinite line heat source seepage model is given in Equation (7.1) where q_1 denotes the heat transfer rate of borehole GHE.

$$\theta_{a,t,i} = \frac{1}{4\pi} \int_0^{\tau} \frac{1}{(\tau - \tau')} \exp \left[-\frac{[r \cos \beta - u \cos \varphi(\tau - \tau')]^2 + [r \sin \beta - u \sin \varphi(\tau - \tau')]^2}{4a(\tau - \tau')} \right] d\tau' \quad (7.1)$$

where $\theta_i = t - t_0$, t and t_0 are respectively transient temperature and initial temperature. β is the intersection angle from the x-axis's positive direction to the point location in question, r is the radial radius of the point from the borehole center.

To reduce the number of parameters and simplify the expression, non-dimensional parameters are introduced such as: $\Theta_i = k \theta_i / q_1$, $S = u r / a$, $Fo = a\tau / r^2$. Then the

dimensionless form is displayed as:

$$\Theta_{a,l,i} = \frac{1}{4\pi} \int_0^{Fo} \frac{1}{(Fo - Fo')} \exp \left[-\frac{[\cos \beta - S \cos \varphi(Fo - Fo')]^2 + [\sin \beta - S \sin \varphi(Fo - Fo')]^2}{4(Fo - Fo')} \right] dFo' \quad (7.2)$$

7.2.1.2 Finite line heat source seepage model

The temperature response of the finite heat source model while groundwater seepage exists is given in Equation (7.3).

$$\theta_{a,l,f} = \frac{q_l}{8\pi k} \int_0^{\tau} \frac{d\tau'}{\tau - \tau'} \cdot \exp \left[-\frac{[r \cos \beta - u \cos \varphi(\tau - \tau')]^2 + [r \sin \beta - u \sin \varphi(\tau - \tau')]^2}{4a(\tau - \tau')} \right] \cdot \left\{ \operatorname{erfc} \left[\frac{z-h}{2\sqrt{a(\tau - \tau')}} \right] - \operatorname{erfc} \left[\frac{z-0}{2\sqrt{a(\tau - \tau')}} \right] - \operatorname{erfc} \left[\frac{z+0}{2\sqrt{a(\tau - \tau')}} \right] + \operatorname{erfc} \left[\frac{z+h}{2\sqrt{a(\tau - \tau')}} \right] \right\} \quad (7.3)$$

where r and β respectively have the same meanings as those of the infinite model, the line stretches from the ground boundary to the depth h . Equation (7.3) is converted as follows:

$$\Theta_{a,f,l} = \frac{1}{8\pi} \int_0^{Fo} \frac{dFo'}{Fo - Fo'} \cdot \exp \left[-\frac{[\cos \beta - S \cos \varphi(Fo - Fo')]^2 + [\sin \beta - S \sin \varphi(Fo - Fo')]^2}{4(Fo - Fo')} \right] \cdot \left\{ \operatorname{erfc} \left[\frac{Z-H}{2\sqrt{Fo - Fo'}} \right] - 2 \cdot \operatorname{erfc} \left[\frac{Z}{2\sqrt{Fo - Fo'}} \right] + \operatorname{erfc} \left[\frac{Z+H}{2\sqrt{Fo - Fo'}} \right] \right\} \quad (7.4)$$

where $H = h/r$, the dimensionless depth of the line heat source.

7.2.2 Comparisons between temperature responses of with and without groundwater seepage

The value of velocity S gives expression to the advection strength. An increase of S , causes the groundwater seepage's contribution to the whole heat transfer process to become increasingly outstanding, resulting in smaller and smaller temperature response.

The temperature responses of the finite line source with the time and with the velocity are both illustrated in Figure 7.2, where the temperature responses of the seepage model are the mean values. Pure conduction leads to larger temperature response than that of combined heat transfer at the time of constant S , proving that seepage indeed improves the heat transfer performance of a borehole GHE. There is no velocity for the pure conduction model, and the final temperature response remains constant when the time is fixed. However, the temperature response drops with seepage strength if groundwater advection is included in the heat transfer model.

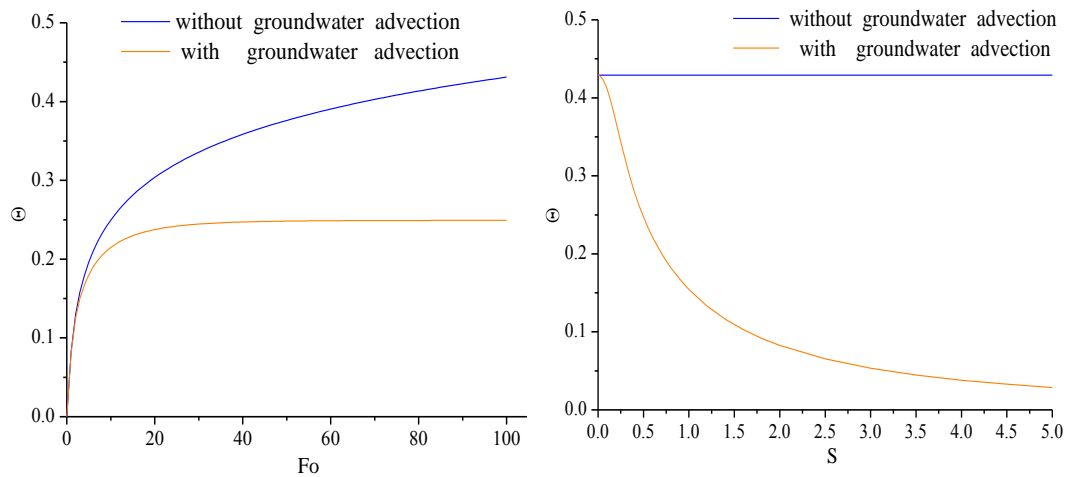


Figure 7.2 Temperature responses of with and without groundwater seepage

7.2.3 The temperature field while groundwater seepage exists

7.2.3.1 The influence of seepage angles

The orientation of groundwater seepage is also from -180° to 180° and the temperature field around a borehole GHE is determined by the seepage direction if velocity value is constant. The following figures give a brief picture of the differences in temperature fields as orientation of flow changes. For the three orientations: 0° , 45° and 90° , the

diagrams and the corresponding temperature distributions are respectively listed in Figures 7.3 and 7.4.

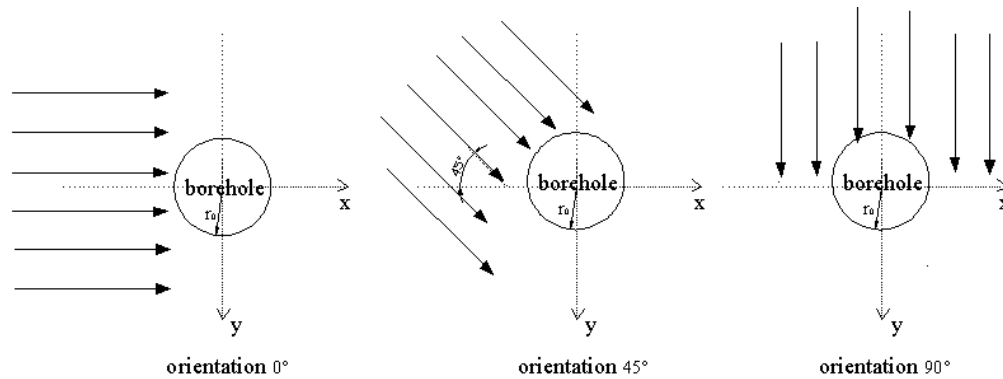


Figure 7.3 The diagram of different groundwater orientations

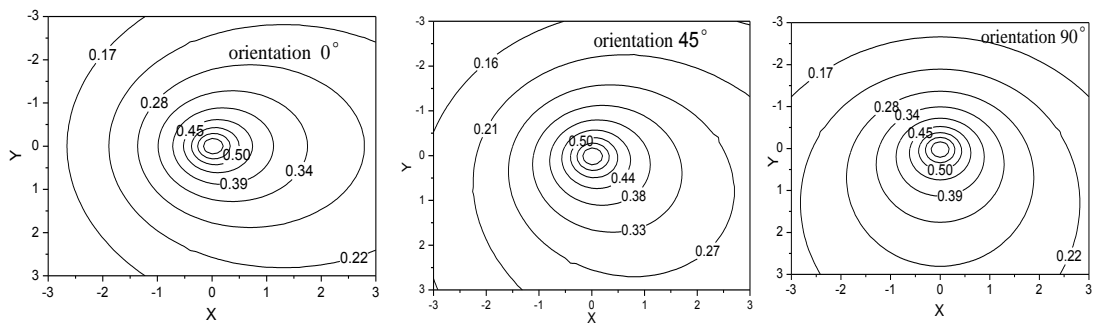


Figure 7.4 The temperature fields when groundwater orientation takes different angles

According to Figures 7.3 and 7.4, the temperature distribution around the borehole GHE does varies with seepage directions, proving the importance of groundwater orientation.

7.2.3.2 The influences of seepage's intensity and time

Based on analyses in section 7.2.2, the seepage's intensity and duration can bring about different thermal responses. A borehole GHE is regarded as a line heat source with the constant heating rate q_1 ; and the surrounding medium experiences changing temperature distributions with velocity value or time if groundwater seepage exists. The

temperature distribution is shown when the orientation is 0° , which means groundwater flows along the positive direction of the X -axis at this time. Isotherms can be plotted as Fo and S change. Firstly, the temperature field varies with the velocity value while Fo is kept fixed. The graphs are shown below:

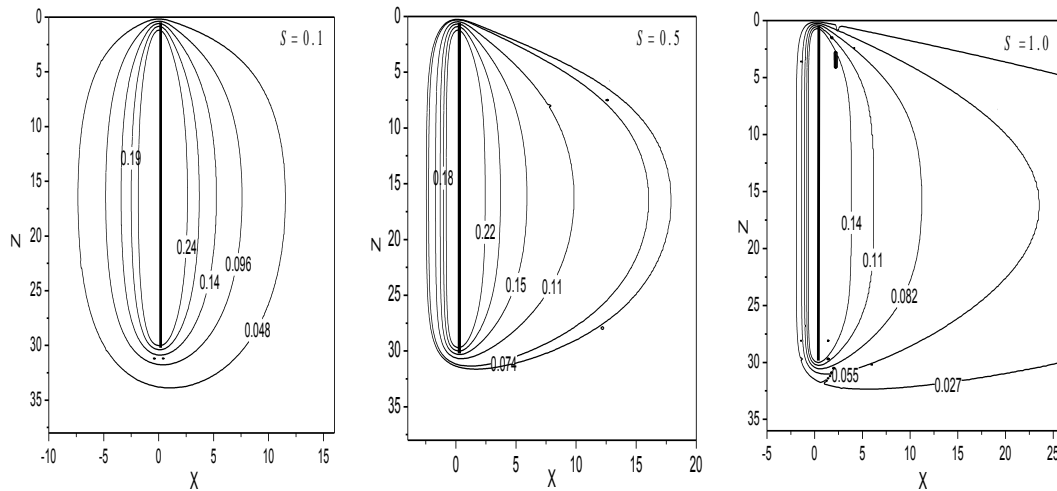


Figure 7.5 The isotherms with the increase of S

There is a delicate asymmetry of temperature distribution when S is small, because it seems that pure conduction plays the predominant role in the heat exchange process. The seepage effect, however, becomes more obvious as S increases. Isotherms depict the advection role and the gradually more noticeable temperature asymmetry with the velocity value S . Figure 7.6 shows that temperature responses of both sides of Z -axis present different distributions with the time when S is constant, illustrating how the seepage effect is affected by time.

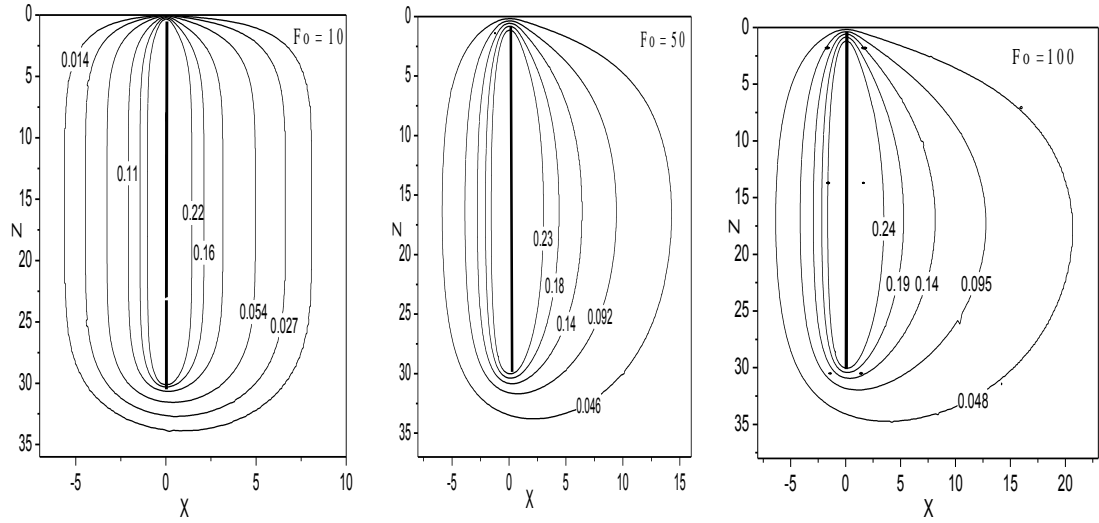


Figure 7.6 The isotherms with the increase of Fo

7.2.3.3 The change regulation of mean temperature

A hydraulic gradient's direction differs between regions or areas; the intersection angle between the positive x -axis direction and the seepage direction varies from -180° to 180° . If the velocity value is constant, that is, seepage intensity maintains stable, therefore the temperature response at the same location changes with the seepage directions. However, the mean calculated temperature responses explain that they are all nearly equal. Equations (7.2) and (7.4) are analytical solutions of temperature responses respectively induced by infinite and finite models. Since the seepage orientation is usually two-dimensional, the integral average method can be utilized to acquire the mean temperature responses for every model. With another integral, added to Equations (7.2) and (7.4), the respective expressions become as shown in Equations (7.5) and (7.6), both of which are double integrals.

$$\overline{\Theta}_{ave, a, l, i} = \frac{1}{2\pi} \cdot \frac{1}{4\pi} \int_{-\pi}^{\pi} \int_0^{Fo} \frac{1}{(Fo - Fo')} \exp \left[-\frac{[\cos \beta - S \cdot \cos \varphi (Fo - Fo')]^2 + [\sin \beta - S \cdot \sin \varphi (Fo - Fo')]^2}{4(Fo - Fo')} \right] dFo' d\beta \quad (7.5)$$

$$\overline{\Theta}_{ave, a, l, f} = \frac{1}{8\pi} \cdot \frac{1}{2\pi} \int_{-\pi}^{\pi} \int_0^{Fo} \frac{d\beta dFo'}{Fo - Fo'} \cdot \exp \left[-\frac{[\cos \beta - S \cdot \cos \varphi (Fo - Fo')]^2 + [\sin \beta - S \cdot \sin \varphi (Fo - Fo')]^2}{4(Fo - Fo')} \right] \cdot \left\{ \operatorname{erfc} \left[\frac{Z - H}{2\sqrt{Fo - Fo'}} \right] - 2 \cdot \operatorname{erfc} \left[\frac{Z}{2\sqrt{Fo - Fo'}} \right] + \operatorname{erfc} \left[\frac{Z + H}{2\sqrt{Fo - Fo'}} \right] \right\} \quad (7.6)$$

Regarding intersection angles, some typical cases were chosen for study. Exploring whether the mean temperature response of medium surrounding the borehole GHE is related to the groundwater velocity or not. Mean temperature responses with the time are obtained using the finite heat source seepage model. Figure 7.7 provides a clear explanation of the corresponding information. Results were calculated for many angles with very little impact on the mean temperature response.

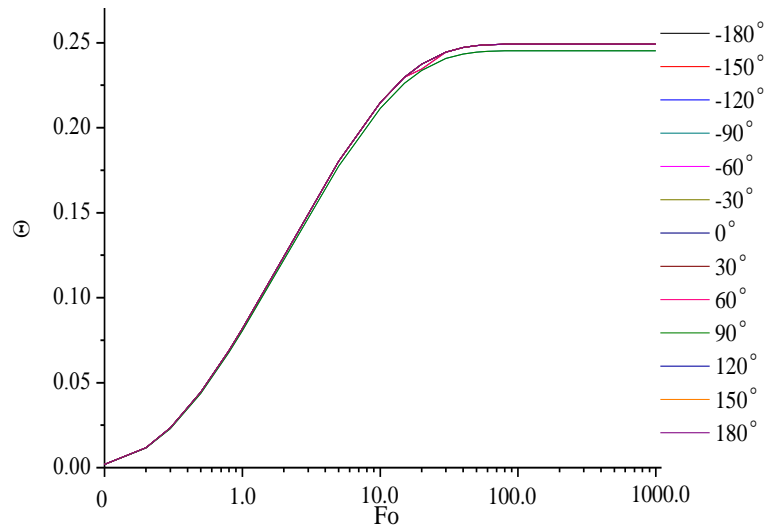


Figure 7.7 The mean temperature responses with the time when φ adopts different angles

Another case is the relationship between groundwater velocity value and mean temperature response. Figure 7.8 shows that no matter what the velocity value is, the mean temperature responses when seepage orientation employs different angles are nearly equal if S keeps constant. The larger the S , the smaller the temperature responses.

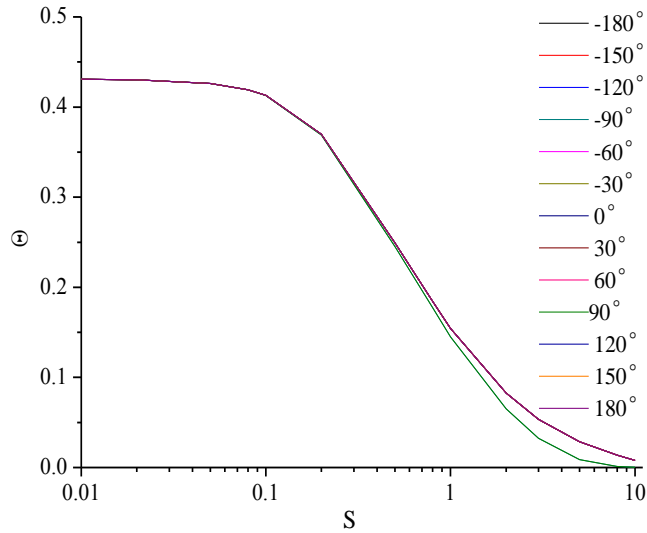


Figure 7.8 The mean temperature responses with S when φ adopts different values

7.3 Description of the back calculation method

7.3.1 The arrangement of test points on the horizontal plane

As stated in section 7.1, to estimate the velocity of seepage is a difficult problem with which engineers and scholars have to deal. This is a subject of research in its own right. Novel methods are needed for a breakthrough. With limited trial temperature data and a borehole GHE, however, a methodology entitled “back calculation” based on the line heat source seepage models is proposed. Both the value and the orientation of the groundwater velocity influencing the temperature responses can be deduced with the help of reverse reasoning algorithm.

Flowing orientation is determined by the hydraulic gradient’s direction, and the greater the gradient, the larger the velocity intensity. Groundwater can sometimes flow in a three-dimensional fashion or even in a rough-and-tumble manner, but in general the flow is approximately planar or two-dimensional (Zhang et al, 2007), so that two-

dimensional seepage is assumed in this analysis. To fulfill the reverse-reasoning, at least three points with the same radius r regarding the borehole center as circle center are distributed around a borehole GHE, and the 120-degree intersection angle between every two adjacent points is defined to ensure an even-distribution. Admittedly, the reverse reasoning effect would be more accurate if there are more than three well-distributed points around the borehole, but calculation complexity is increased and the temperature response difference between adjacent points would be small. Accordingly, the procedure can be demonstrated with only three points to check the reverse-calculation effect. Figure 7.9 depicts the basis for the back calculation demonstration.

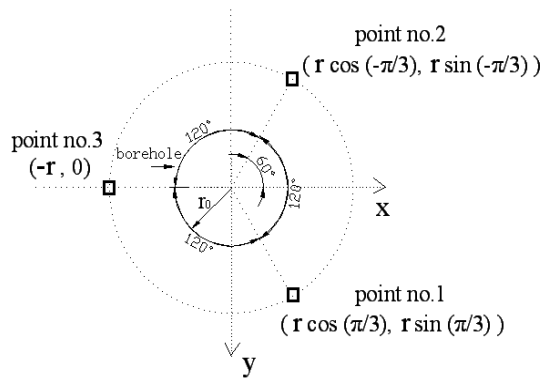
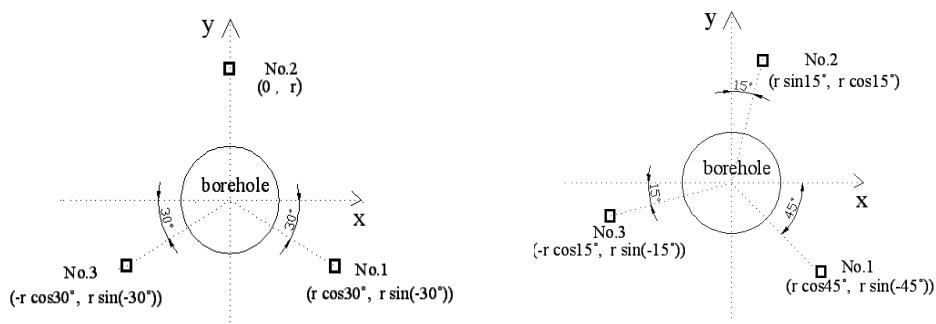


Figure 7.9 The schematic diagram of three evenly-distributed points around borehole GHE

Figure 7.9 displays one mode of distributing the three points; some other examples are depicted as:



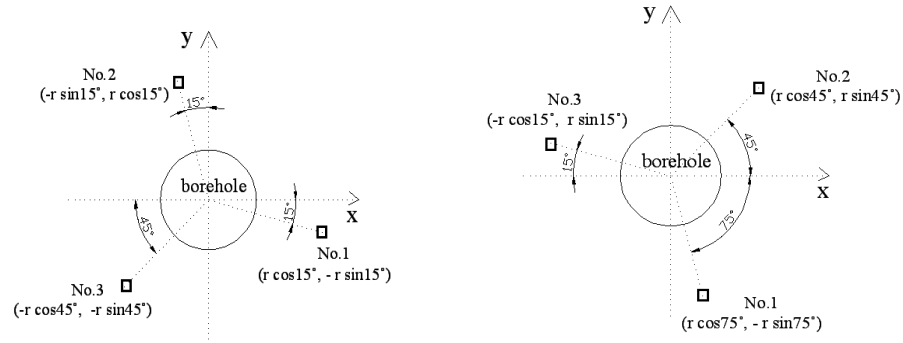


Figure 7.10 Some other distributing modes for three points around borehole GHE

In addition, Figure 7.11 shows the examples where there are four, five and six evenly-distributed points.

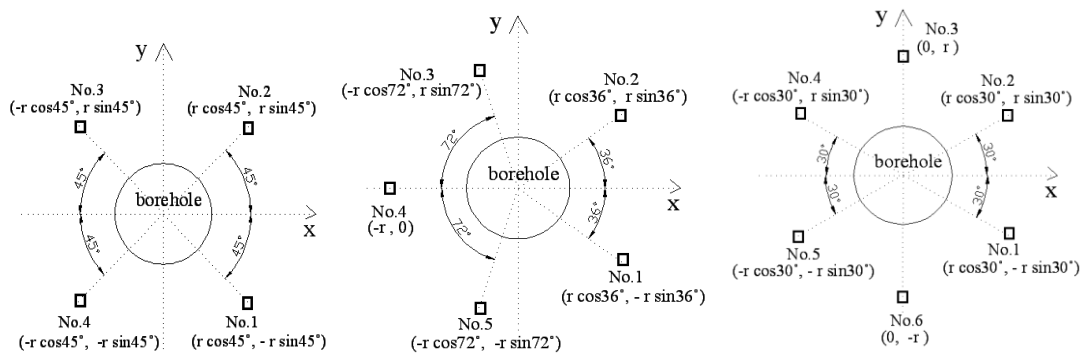


Figure 7.11 The distributing diagram while there are different numbers of points

The calculation difficulty is unavoidably increased though added points can improve the back calculation effect. For this reason, the mode employing three evenly-distributed points is preferentially taken into account, only if the calculated result using three points is deemed unsatisfactory would it be desirable to test a larger number of points.

7.3.2 The depth location of distributed points

If the infinite line heat source seepage model is employed for the reverse reasoning algorithm, the depth of the three points would be irrelevantly but the depth must be decided upon in case of the finite model.

The graphs in section 7.3.1 only describe the horizontal distribution of points at a particular depth. The differences of the temperature responses of different depths are evident. The mean temperature responses based on Equation (7.6) are calculated for different values of Z , and the corresponding temperature responses in the Z -axis direction or the depth direction for different values of S are shown in Figure 7.12. It is evident that the temperature responses, higher up and lower down are weaker than those at intermediate depths with the middle positions showing the highest temperature response. Accordingly, the set points are positioned at mid height of borehole GHE.

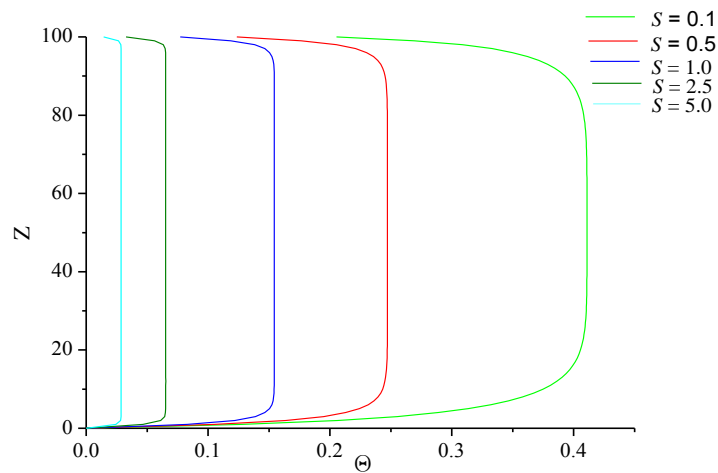


Figure 7.12 The mean temperature responses of the finite model along Z -axis

7.3.3 The principles of back calculation

7.3.3.1 The objective function

The temperature responses with the time can be recorded after setting points (Gehlin and Hellstrom, 2003). Because the specific velocity is unknown, the velocity ranges need to be chosen for value and orientation. For example, the velocity range is usually set from 10^{-6} m /s to 10^{-2} m /s according to the local geological information. The angle can be defined from -180° to 180° , the complete range of possibilities, in the absence of

any local physical information. As the test data are recorded at regular intervals, the continuous iterations across the value and orientation ranges are performed in the process of back calculation. Given that the differences between test findings and calculated results are at the minimum, when the calculated temperature responses equal the measured data, the corresponding value and orientation must be the actual groundwater parameters (Yu and Fang, 2002). The objective function is expressed in Equation (7.7).

$$T = \sum_{j=1}^n (\Theta_{cal,j} - \Theta_{rec,j})^2 \quad (7.7)$$

where $\Theta_{cal,j}$ and $\Theta_{rec,j}$ denote the non-dimensional temperatures obtained respectively by models and by recorded data. Because $\Theta_{rec,j} = k\theta_j / q_1 = k(t - t_0) / q_1$, the non-dimensional value can be acquired if the transient temperature, the initial temperature, thermal conductivity and heat transfer rate are all measured in advance. The initial temperature can be noted before operating the GHEs, and the transient temperature can be recorded at regular time intervals. Obviously, there are many groups of three values for the three points concerned. Thermal conductivity k and q_1 are respectively obtained by thermal test equipment and by calculated results.

Three points are set around the borehole and thereby three objective functions should be established. In the case when all three achieve the minimum, the corresponding value and orientation are the actual cases. To be more specific, every point has own objective function, the value and orientation cannot be determined if only one function achieves the minimum. It could happen that all meet their minimum requirements but at slightly different values and orientations in each case. When the velocity ranges between the

three are acceptably small, the intersection of the three ranges can produce the chosen single velocity estimate.

In addition to the objective function shown in Equation (7.7), another way is to establish the total sum of the squared deviations between calculated and measured values, i.e. Equation (7.8).

$$T = \sum_{j=1}^n (\Theta_{cal,j,1} - \Theta_{rec,j,1})^2 + (\Theta_{cal,j,2} - \Theta_{rec,j,2})^2 + (\Theta_{cal,j,3} - \Theta_{rec,j,3})^2 \quad (7.8)$$

However, only one function is displayed in Equation (7.8), thus the possibility of producing error may be higher than that in the case of three functions above. Furthermore, the ranges of three points can help to verify each other if functions are respectively established. Thus, the intersection is more accurate than the result would be for only one function. For this reason, it is suggested that three functions should be established.

The flow chart of the iteration process is shown in Figure 7.13, the corresponding calculations and programmes are conducted according to this illustration.

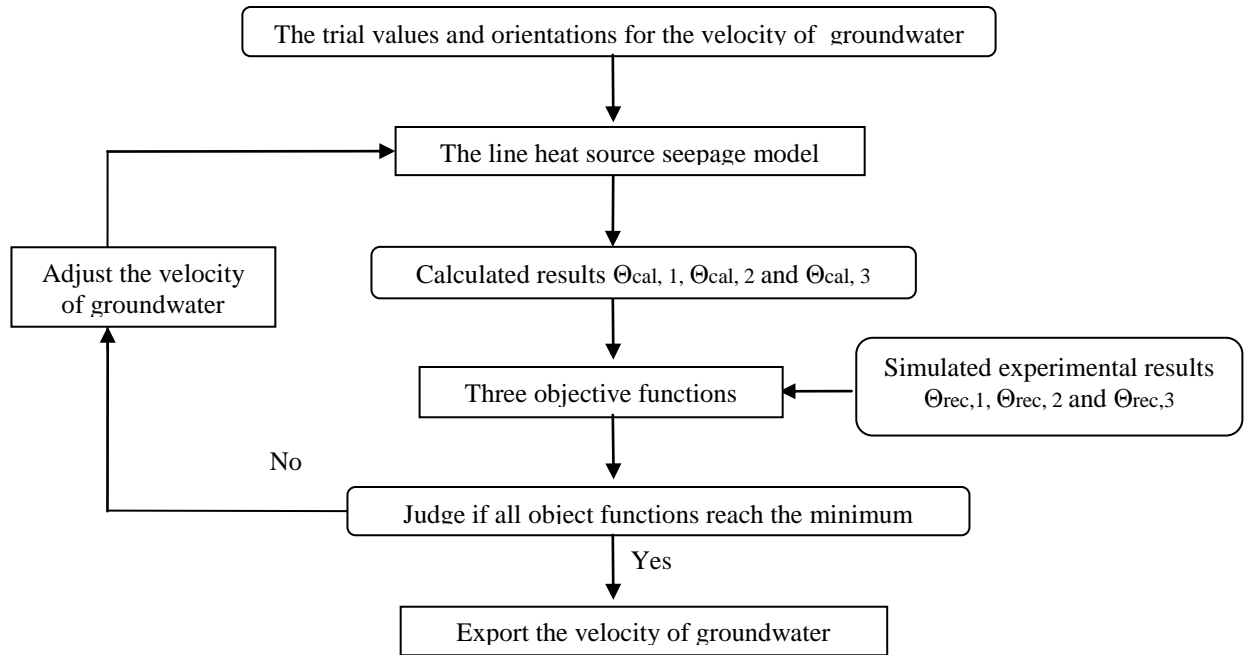


Figure 7.13 The flow chart of the iteration process for obtaining groundwater velocity

7.3.3.2 The partial derivatives

Section 7.3.3.1 has demonstrated that the actual S and φ can be confirmed if all objective functions achieve the minimum. No matter whether the infinite or the finite model is considered, the analytical solutions of temperature responses are binary functions with two independent variables S and φ . In case T makes the first order partial derivatives respectively with respect to parameters S and φ , the corresponding signs can be indicated respectively by $T^{\Delta,S}$ and $T^{\Delta,\varphi}$, and the necessary conditions for realizing the minimum of T are concluded as (Ye and Shen, 2006):

$$\begin{cases} T^{\Delta,S} = 0 \\ T^{\Delta,\varphi} = 0 \end{cases} \quad (7.9)$$

Because both S and φ are discrete variables rather than continuous variables, it cannot be guaranteed that the values of $T^{\Delta,S}$ and $T^{\Delta,\varphi}$ must be zero. However, the minor values

which are next to zero can be endowed respectively to $T^{\Delta,S}$ and $T^{\Delta,\varphi}$, and the values can be adjusted according to the calculation process to respectively limit S and φ into a smaller and smaller range, and the best findings are that a single S and a single φ can be determined at last.

7.3.3.2.1 Derivative formulas of infinite line heat source seepage model

Velocities fulfilling Equation (7.9) are named as stationary points (Xu, 1999). The stationary points which simultaneously satisfy the Equation (7.9) of three object functions maybe the unique one or may cover a small range. The detailed expressions for $T^{\Delta,S}$ and $T^{\Delta,\varphi}$ are respectively demonstrated in Equation (7.10) and (7.11).

$$T^{\Delta,S} = 2 \sum_{j=1}^n (\Theta_{\text{cal},j} - \Theta_{\text{rec},j}) \Theta_{\text{cal},j}^{\Delta,S} = 2 \sum_{i=1}^n \left\{ \frac{1}{4\pi} \int_0^{Fo_j} \frac{1}{(Fo_j - Fo')} \exp \left[-\frac{[X - S \cos \varphi (Fo_j - Fo')]^2 + [Y - S \sin \varphi (Fo_j - Fo')]^2}{4(Fo_j - Fo')} \right] dFo' - \Theta_{\text{rec},j} \right\} \cdot \frac{1}{4\pi} \int_0^{Fo_j} \frac{1}{(Fo_j - Fo')} \exp \left[-\frac{[X - S \cos \varphi (Fo_j - Fo')]^2 + [Y - S \sin \varphi (Fo_j - Fo')]^2}{4(Fo_j - Fo')} \right] \cdot \frac{2 \cdot [X - S \cos \varphi (Fo_j - Fo')] \cdot \cos \varphi (Fo_j - Fo') + 2 \cdot [Y - S \sin \varphi (Fo_j - Fo')] \cdot \sin \varphi (Fo_j - Fo')}{4(Fo_j - Fo')} dFo' \quad (7.10)$$

$$T^{\Delta,\varphi} = 2 \sum_{j=1}^n (\Theta_{\text{cal},j} - \Theta_{\text{rec},j}) \Theta_{\text{cal},j}^{\Delta,\varphi} = 2 \sum_{j=1}^n \left\{ \frac{1}{4\pi} \int_0^{Fo_j} \frac{1}{(Fo_j - Fo')} \exp \left[-\frac{[X - S \cos \varphi (Fo_j - Fo')]^2 + [Y - S \sin \varphi (Fo_j - Fo')]^2}{4(Fo_j - Fo')} \right] dFo' - \Theta_{\text{rec},j} \right\} \cdot \frac{1}{4\pi} \int_0^{Fo_j} \frac{1}{(Fo_j - Fo')} \exp \left[-\frac{[X - S \cos \varphi (Fo_j - Fo')]^2 + [Y - S \sin \varphi (Fo_j - Fo')]^2}{4(Fo_j - Fo')} \right] \cdot \frac{-2 \cdot [X - S \cos \varphi (Fo_j - Fo')] \cdot S \sin \varphi (Fo_j - Fo') + 2 \cdot [Y - S \sin \varphi (Fo_j - Fo')] \cdot S \cos \varphi (Fo_j - Fo')}{4(Fo_j - Fo')} dFo' \quad (7.11)$$

7.3.3.2.2 Derivative formulae for finite line heat source seepage model

Detailed expressions of the first order partial derivatives can be expressed, firstly the formula of $T^{\Delta,S}$ is given by Equation (7.12).

$$\begin{aligned}
T^{\Delta, S} &= 2 \sum_{j=1}^n (\Theta_{\text{cal},j} - \Theta_{\text{rec},j}) \cdot \Theta_{\text{cal},j}^{\Delta, S} = 2 \sum_{j=1}^n \left\{ \frac{1}{8\pi} \int_0^{F_{o_j}} \frac{1}{(F_{o_j} - Fo')} \exp \left[-\frac{[\cos \beta - S \cos \varphi(F_{o_j} - Fo')]^2 + [\sin \beta - S \sin \varphi(F_{o_j} - Fo')]^2}{4(F_{o_j} - Fo')} \right] \cdot \right. \\
&\quad \left. \left\{ \operatorname{erfc} \left[\frac{Z-H}{2\sqrt{F_{o_j} - Fo'}} \right] - 2^* \operatorname{erfc} \left[\frac{Z}{2\sqrt{F_{o_j} - Fo'}} \right] + \operatorname{erfc} \left[\frac{Z+H}{2\sqrt{F_{o_j} - Fo'}} \right] \right\} dFo' - \Theta_{\text{rec},j} \right\} \quad (7.12) \\
&\cdot \frac{1}{8\pi} \int_0^{F_{o_j}} \frac{1}{(F_{o_j} - Fo')} \exp \left[-\frac{[\cos \beta - S \cos \varphi(F_{o_j} - Fo')]^2 + [\sin \beta - S \sin \varphi(F_{o_j} - Fo')]^2}{4(F_{o_j} - Fo')} \right] \cdot \\
&\quad \left\{ \operatorname{erfc} \left[\frac{Z-H}{2\sqrt{F_{o_j} - Fo'}} \right] - 2^* \operatorname{erfc} \left[\frac{Z}{2\sqrt{F_{o_j} - Fo'}} \right] + \operatorname{erfc} \left[\frac{Z+H}{2\sqrt{F_{o_j} - Fo'}} \right] \right\} \cdot \\
&\quad \frac{2 \cdot [\cos \beta - S \cos \varphi(F_{o_j} - Fo')] \cdot \cos \varphi(F_{o_j} - Fo') + 2 \cdot [\sin \beta - S \sin \varphi(F_{o_j} - Fo')] \cdot \sin \varphi(F_{o_j} - Fo')}{4(F_{o_j} - Fo')} dFo'
\end{aligned}$$

Secondly, the formula for $T^{\Delta, \varphi}$ is shown as:

$$\begin{aligned}
T^{\Delta, \varphi} &= 2 \sum_{j=1}^n (\Theta_{\text{cal},j} - \Theta_{\text{rec},j}) \cdot \Theta_{\text{cal},j}^{\Delta, \varphi} = 2 \sum_{j=1}^n \left\{ \frac{1}{8\pi} \int_0^{F_{o_j}} \frac{1}{(F_{o_j} - Fo')} \exp \left[-\frac{[\cos \beta - S \cos \varphi(F_{o_j} - Fo')]^2 + [\sin \beta - S \sin \varphi(F_{o_j} - Fo')]^2}{4(F_{o_j} - Fo')} \right] \cdot \right. \\
&\quad \left. \left\{ \operatorname{erfc} \left[\frac{Z-H}{2\sqrt{F_{o_j} - Fo'}} \right] - 2^* \operatorname{erfc} \left[\frac{Z}{2\sqrt{F_{o_j} - Fo'}} \right] + \operatorname{erfc} \left[\frac{Z+H}{2\sqrt{F_{o_j} - Fo'}} \right] \right\} dFo' - \Theta_{\text{rec},j} \right\} \quad (7.13) \\
&\cdot \frac{1}{8\pi} \int_0^{F_{o_j}} \frac{1}{(F_{o_j} - Fo')} \exp \left[-\frac{[X - S \cos \varphi(F_{o_j} - Fo')]^2 + [Y - S \sin \varphi(F_{o_j} - Fo')]^2}{4(F_{o_j} - Fo')} \right] \cdot \\
&\quad \left\{ \operatorname{erfc} \left[\frac{Z-H}{2\sqrt{F_{o_j} - Fo'}} \right] - 2^* \operatorname{erfc} \left[\frac{Z}{2\sqrt{F_{o_j} - Fo'}} \right] + \operatorname{erfc} \left[\frac{Z+H}{2\sqrt{F_{o_j} - Fo'}} \right] \right\} \cdot \\
&\quad \frac{-2 [\cos \beta - S \cos \varphi(F_{o_j} - Fo')] \cdot S \sin \varphi(F_{o_j} - Fo') + 2 [\sin \beta - S \sin \varphi(F_{o_j} - Fo')] \cdot S \cos \varphi(F_{o_j} - Fo')}{4(F_{o_j} - Fo')} dFo'
\end{aligned}$$

7.3.3.2.3 Determine the velocity after using partial derivatives

For each objective function, the values of $T^{\Delta, S}$ and $T^{\Delta, \varphi}$ are zeros or nearly zeros, that means two limitations are set for achieving the minimum for each function. Totally, there are six conditions to be satisfied while the three functions simultaneously fulfill the requirements of the minimum. Normally, the number of conditions is the reason for setting three points rather than only one. Although if an accurate velocity cannot be

determined in such a way, the six conditions can only be met by a small range of velocities, those remaining velocities will then be put into Equation (7.7) one by one for comparison. In this way, the single velocity can be discovered because this velocity Equation (7.7) can find the minimum.

7.4 Characteristics involved in the infinite line heat source seepage model

7.4.1 The relationship between points' radius and velocity value

The distance from the points to the borehole center is worth discussing because this parameter needs to be employed during the back calculation. How to determine the radial radius to the borehole center line depends on the velocity. For example, studies of this relationship can be conducted while the three points are distributed as in Figure 7.8. Because the angle of groundwater seepage is from -180° to 180° , some angles within this range are picked for investigation. A 15° interval was set and therefore the angles such as -180° , -165° and so on were employed. A significant finding is that the value of dimensionless velocity should be from 0.1 to 3.0 according to the analysis. With regard to the non-dimensional velocity $S = ur / a$, the product of actual velocity value and radial radius of the point is within the range $0.1a$ to $3a$.

On the one hand, the differences of three points' temperature responses maybe very small when S is less than 0.1, which is unfavourable for the back calculation. On the other hand, the temperature response may be too weak if S is greater than 3.0. This range is proven suitable for all directions of groundwater seepage if only the corresponding angle is from -180° to 180° . Thereby, this relationship is not only applicable for all

layouts of Figure 7.9 and 7.10, but also feasible for other distributions of three points which are evenly-distributed around the borehole GHE.

To show the temperature responses with time, two extreme values of S , i.e. 0.1 and 3.0, are picked to depict the corresponding curves shown in Figure 7.14. The correct circumstances are certainly between these two conditions while S adopts other values. Emphasizing again, the relationship between point's radial distance and velocity value is that their product must lie in the range $0.1a$ to $3.0a$.

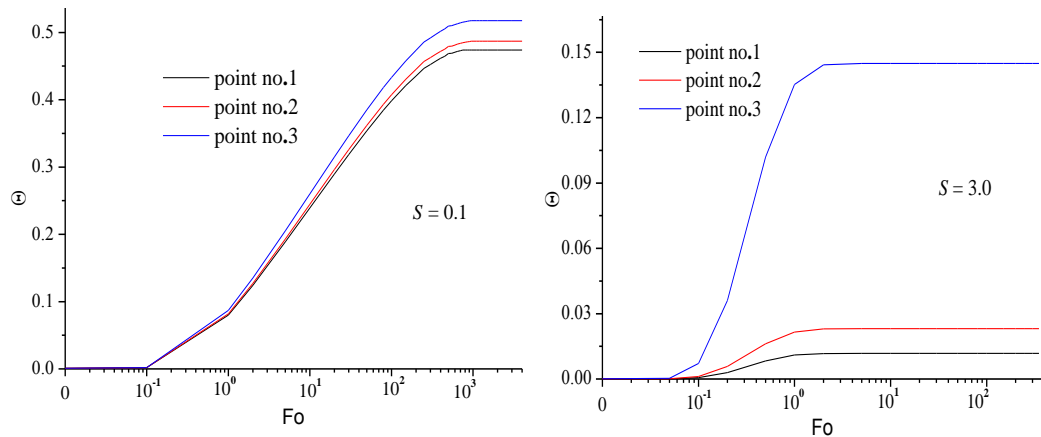


Figure 7.14 The temperature responses of three points when S adopts two extreme values

7.4.2 The research on inflection points of the temperature response curves

Figure 7.14 illustrates that the temperature responses curves of three points first possess an increasing slope and then a continuously decreasing slope until the stable states are reached. The inflection points are significant, as they mark the change from one stage to the other. From the mathematical standpoint, the so-called inflection point is the concave-convex transition point on function curves (TUDM, 2007). If the second derivative of a function with respect to an independent variable is positive, the curve is concave in shape and if negative, it is convex. The location at which the second order

derivative equal to zero is known as an inflection point. Equation (7.2) takes into account the relationship between the inflection point and its corresponding time of occurrence. The parameter Fo is an independent variable and $\Theta_{cal, j}$ the corresponding function value. The first derivative with respect to Fo is calculated using the corresponding formula:

$$\Theta_{cal, j}^{\Delta, Fo} = \frac{1}{4\pi} * \frac{1}{Fo} * \exp \left[-\frac{(\cos \beta - S * \cos \varphi * Fo)^2 + (\sin \beta - S * \sin \varphi * Fo)^2}{4Fo} \right] \quad (7.14)$$

After that, the second derivative is found from Equation (7.15) based on Equation (7.14).

$$\Theta_{cal, j}^{\Delta\Delta, Fo} = -\frac{1}{4\pi} \cdot \frac{1}{Fo^2} \cdot \exp \left[-\frac{(\cos \theta - S \cdot \cos \varphi \cdot Fo)^2 + (\sin \theta - S \cdot \sin \varphi \cdot Fo)^2}{4Fo} \right] + \frac{1}{16\pi} \cdot \frac{1}{Fo} \cdot \exp \left[-\frac{[\cos \theta - S \cdot \cos \varphi \cdot Fo]^2 + [\sin \theta - S \cdot \sin \varphi \cdot Fo]^2}{4Fo} \right] \cdot \left[\frac{2S \cdot \cos \varphi \cdot Fo \cdot (\cos \theta - S \cdot \cos \varphi \cdot Fo) + (\cos \theta - S \cdot \cos \varphi \cdot Fo)^2}{Fo^2} + \frac{2S \cdot \sin \varphi \cdot Fo \cdot (\sin \theta - S \cdot \sin \varphi \cdot Fo) + (\sin \theta - S \cdot \sin \varphi \cdot Fo)^2}{Fo^2} \right] \quad (7.15)$$

Sometimes Fo cannot fulfill the zero value of the second derivative. In this case, the method of bisection is utilized at the positive and negative boundaries of the second derivative, thereby acquiring an approximate Fo . Exploration on the time of arriving at the inflection points of three points was conducted. The Fo coordinate of inflection point is only related to the velocity value S and is hardly affected by the seepage angle φ . This conclusion is the same no matter which of the three points around the borehole is used for analysis. Figure 7.15 demonstrates that the time Fo when the inflection point is reached changes with the velocity value S . To conveniently and clearly reveal the correlation between Fo and S , $Lg(S)$ is used for the horizontal coordinate and Fo for the longitudinal coordinate. The Fo of the inflection point remains nearly constant at low

velocities and drops rapidly as S becomes larger.

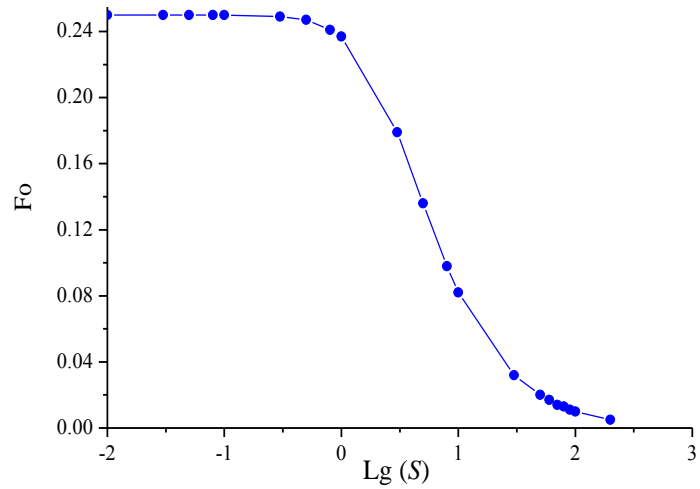


Figure 7.15 The changing trend that Fo is along with $Lg(S)$

For the inflection point, another significant correlation is that L , the product of the S and Fo , can vary with the velocity value S , as shown in Figure 7.16. L increases with S until the stable state is reached. The slope firstly increases and then decreases until L is stable. Thereby, Fo of the inflection point is inversely proportional to S when the groundwater velocity attains enough intensity of flow.

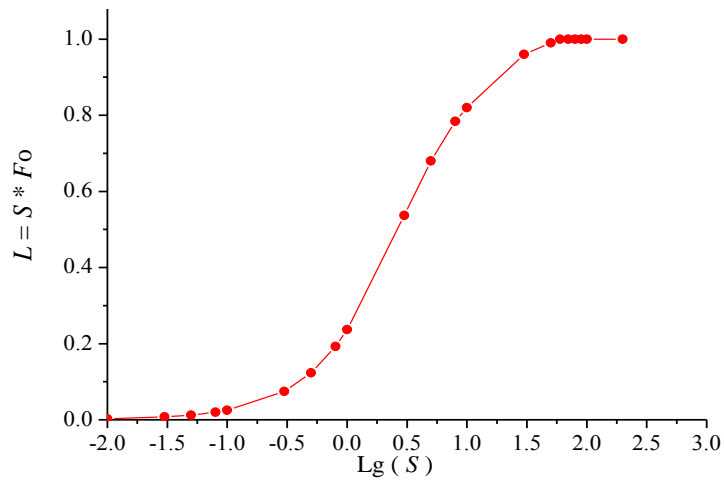


Figure 7.16 The curve which product of S and Fo changes with $Lg(S)$

7.4.3 The relationship between the time needed for reaching half of the stable temperature response and the velocity value

The groundwater seepage causes convection and the temperature response reaches a stable state eventually. When the stable state is reached, the corresponding temperature responses values depend on the velocity strength. According to the curves, temperature response increases gradually in the early period at an increasing rate and the corresponding change of temperature response at set internal are evident. For this reason, the data of this stage is more useful than the later for conducting the back calculation. The clearer the differences of the data recorded at different times for any point, the better the back calculation effect.

On the whole, the half value of stable temperature response can be selected to observe the corresponding time, because the data recorded up the half maximum temperature point is more valuable for the reverse reasoning purpose. The time needed to halfway attain the stable temperature response is far less than that required to achieve the remaining half. Figure 7.17 describes the relationship between time of arriving at the half of stable values and the corresponding velocity value.

The calculations and explorations for three points when different seepage angles are assigned to the groundwater have all been conducted, it should be noted that halfway Fo is related only with velocity value and is hardly affected by the seepage angles or points' locations.

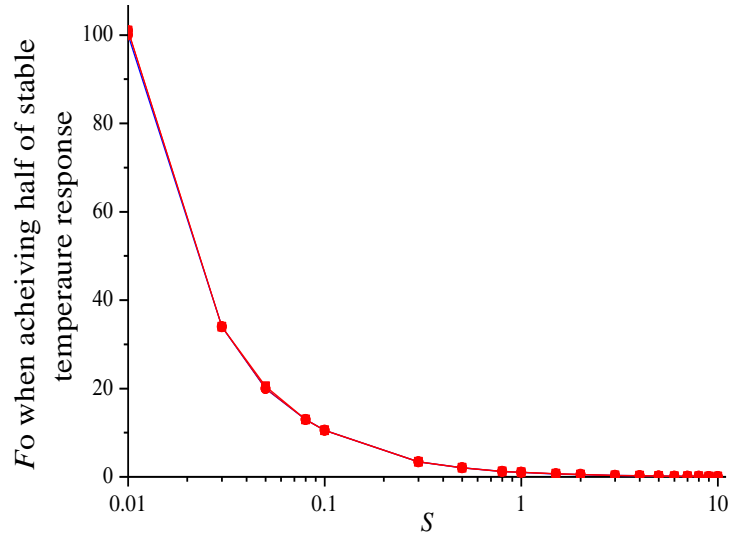


Figure 7.17 The change trend of Fo of reaching the half stable temperature response with S

7.4.4 Preliminary judgment on orientation of groundwater flow

Before conducting a reverse reasoning algorithm, it is necessary to make a brief judgment on the range of orientations although the accurate angles are not known at that time. Since there are three points distributed around the borehole, the differences in the temperature responses are sufficiently employed to allow a rough estimate of the orientation. The three temperature responses vary as groundwater orientation changes, because the influence of groundwater advection at each point also changes if the orientation is adjusted. Figure 7.18 reveals the temperature difference between every two points when the flow takes different orientations.

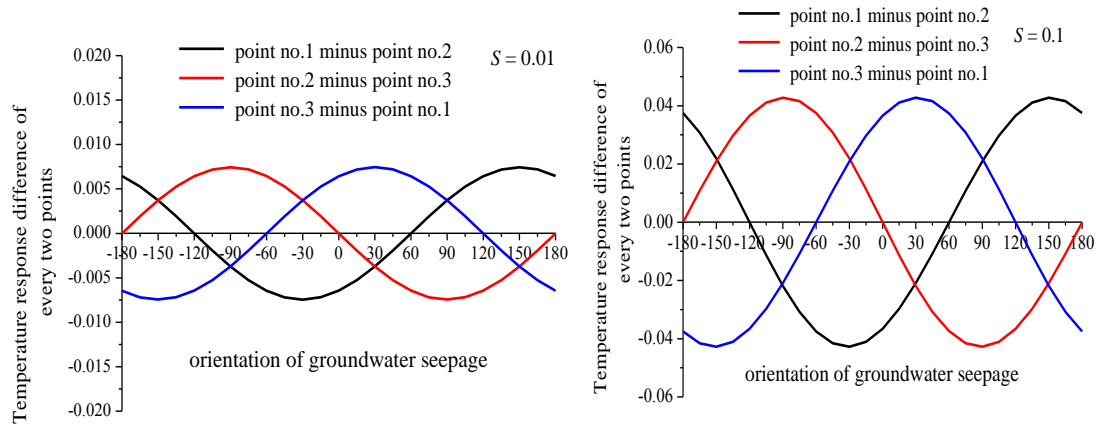


Figure 7.18 The influence that groundwater orientation exerts on temperature difference of every two points

According to Figure 7.18, differences in temperature responses are determined to some extent by the orientation of groundwater seepage; this effect becomes increasingly obvious with the increase of velocity value. In this way, the range of orientations can be preliminarily judged, helping the back calculation process.

7.4.5 The estimation of velocity value based on the ratio of the maximal response to the minimal response

The orientation and the value of groundwater velocity have obvious impacts on the temperature response of every point. Thus, the differences of three points' temperature responses depend on the velocity. The difference between the maximum and the minimum responses reflects the seepage intensity in the case of a constant orientation. Thus, the ratio of the maximum to the minimum is a significant parameter for estimating the velocity value. After detailed calculation, the ratio is hardly influenced by the variation of seepage angles, but it does increase with the enhancing of velocity intensity. The curves indicating the relationship between the ratios and the velocity values are

shown in Figure 7.19.

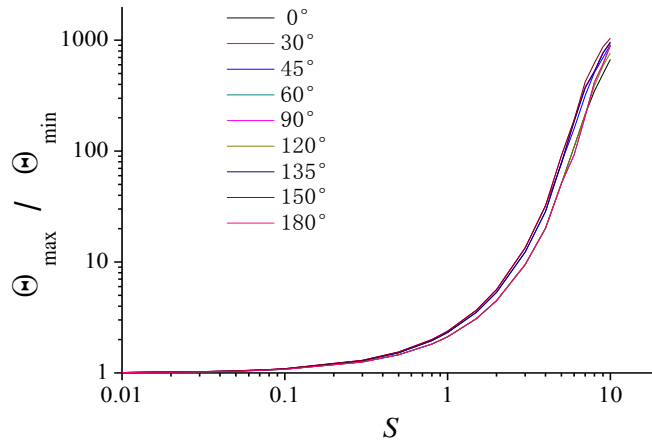


Figure 7.19 The ratios of the maximum to the minimal responses with S

The three points are fixed in the corresponding positions and the orientation ranges between -180° and 180° , therefore the ranges -180° to 0° and 0° to 180° are symmetrical in terms of their influences on the three points' temperature responses. Accordingly, the analysis based on the range 0° and 180° can sufficiently prove the problem. Angles such as 0° , 30° , 45° and so on were chosen. A clear fitting formula, i.e. Equation (7.16), is summarized to report the relationship between ratio and S , where Pr means the ratio.

$$Pr = 0.31776 + 0.87555S + 1.06117 S^2 + 0.58003 S^3 + 0.11425 S^4 \quad (7.16)$$

7.5 Characteristics involved in the finite line heat source seepage model

7.5.1 The influence that orientation exerts on the comparisons of three points' temperature responses

The first arrangement of three points in Figure 7.10 is randomly selected for analysis; the same research ideas apply even if other arrangements are adopted. The temperature

responses of three points rise with time when S and ϕ are given confirmed values, and one example is shown in Figure 7.20.

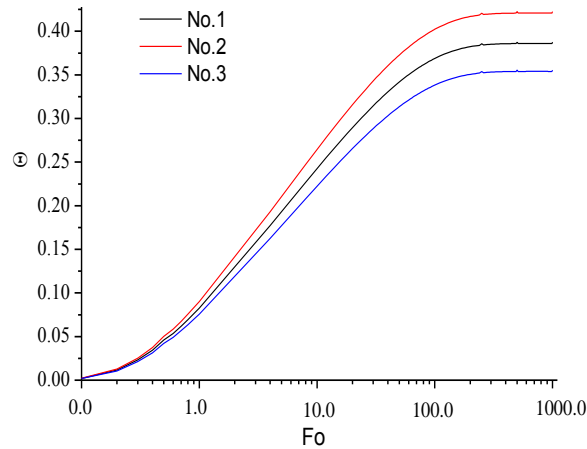


Figure 7.20 The temperature responses of three points with the time

Groundwater seepage incites the temperature responses at points, and the influence degrees are certainly determined by the velocity. All temperature responses reduce with the increase of S . As investigated above, in the case of the infinite heat source seepage model, the seepage orientation plays a significant role in affecting the temperature responses at three points. What is the reaction of the finite model if seepage orientation changes? Studies were conducted and a similar summary to that of the infinite model was obtained. Carefully noted, the temperature response at every point fluctuates ceaselessly with the seepage orientation when time and velocity value are constant. The temperature responses rather than their differences are directly given in Figure 7.21. It is clear that the relative sizes of the three temperature responses vary with the seepage orientation.

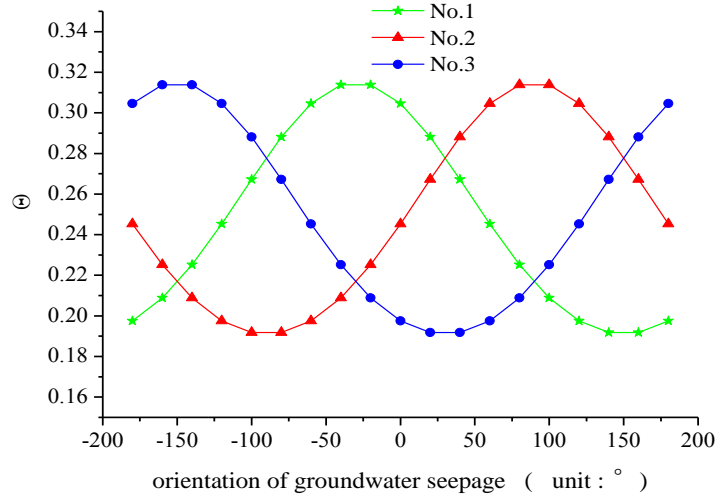


Figure 7.21 The temperature responses of three points with the seepage orientation

7.5.2 The slopes of the temperature responses with the time

Figure 7.20 interprets that the temperature responses increase with the time until they achieve the stable states. The complete trends are the same as those of the infinite model, whereby temperature responses first go through a stage of continuous increase in slope, followed by a period of slope that keeps decreased, and finally all the curves can arrive at stable states.

Equation (7.4) represents the temperature response of any point except heat source itself, thereby the slope of temperature response with time can be calculated using the first order derivative of Θ with respect to Fo . The alternate variable m is introduced, where $m = Fo - Fo'$. Equation (7.4) is transformed into:

$$\Theta_{a,f,t} = \frac{1}{8\pi} \int_0^{Fo} \frac{dm}{m} \cdot \exp \left[-\frac{(\cos \beta - S \cdot m \cdot \cos \varphi)^2 + (\sin \beta - S \cdot m \cdot \sin \varphi)^2}{4m} \right] \cdot \left\{ \operatorname{erfc} \left[\frac{Z-H}{2\sqrt{Fo-Fo'}} \right] - 2\operatorname{erfc} \left[\frac{Z}{2\sqrt{Fo-Fo'}} \right] + \operatorname{erfc} \left[\frac{Z+H/2}{2\sqrt{Fo-Fo'}} \right] \right\} \quad (7.17)$$

And the first order derivative of Θ with respect to Fo is given by Equation (7.18).

$$\Theta_{a,f,l}^{\Delta, Fo} = \frac{1}{8\pi} \cdot \frac{1}{Fo} \cdot \exp\left[-\frac{(\cos \beta - S \cdot Fo \cdot \cos \varphi)^2 + (\sin \beta - S \cdot Fo \cdot \sin \varphi)^2}{4Fo}\right] \cdot \left\{ \operatorname{erfc}\left[\frac{Z-H}{2\sqrt{Fo-Fo'}}\right] - 2\operatorname{erfc}\left[\frac{Z}{2\sqrt{Fo-Fo'}}\right] + \operatorname{erfc}\left[\frac{Z+H/2}{2\sqrt{Fo-Fo'}}\right] \right\} \quad (7.18)$$

The curves applying to the three points' slopes with the time while S and φ remain constant are displayed in Figure 7.22.

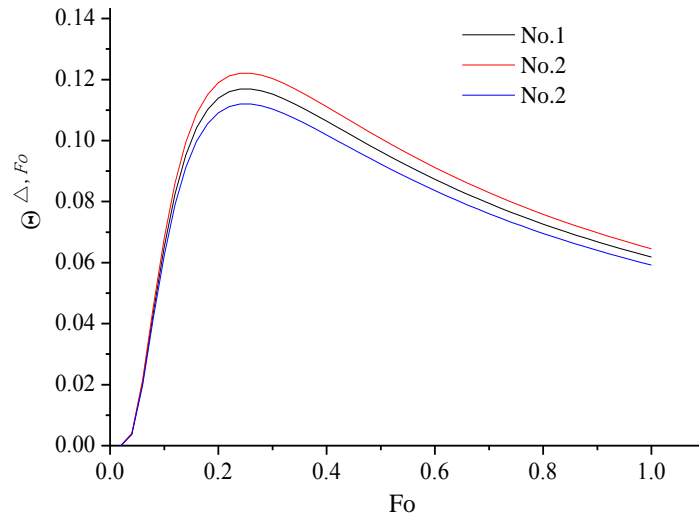


Figure 7.22 The variation trends of slopes of three points while S and φ remain changeless

Figure 7.22 illustrates that when the slopes applying to the three points stop rising, they begin to decrease at nearly equal times. Because the changing trends of slopes of all points present the same regular pattern and the corresponding times are nearly equal, any one point can be chosen to explore the slope trends when orientation and value of groundwater velocity change. Meanwhile, the influence of the velocity intensity on the slope trend of any one point can be studied if the orientation is fixed. Figure 7.23 describes the corresponding conclusions.

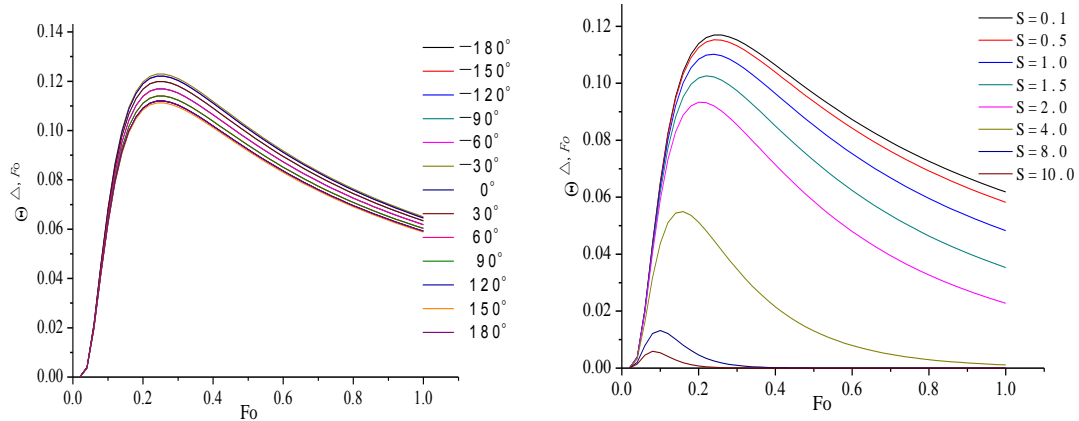


Figure 7.23 The slopes with the time when orientation and velocity value respectively change

Figure 7.23 shows that the change of orientation slightly alters the slope but has no effect on the slope's regular pattern. The time when the slopes start to decrease does not change with the orientation. In addition, an increase of velocity value gives rise to variation of slope curves in terms of not only the extent but also the pattern. The slope reduces with enhancement of velocity, and the time when the curve peaks becomes earlier and earlier.

7.6 The trials of back calculation

The principles of back calculation for obtaining groundwater velocity are summarized. There are no actual experimental data, but those simulated for the three points' temperature responses can be used to validate the back calculation procedure. If S and φ are known beforehand, their values can be put into theoretical model Equation (7.2) or (7.4) and the temperature responses can then be obtained by calculation. As a rule, the use of actual experimental data will result in some deviations from the model results. Accordingly, random disturbances can be added to the model results to simulate the experimental data.

7.6.1 Trials based on the infinite line heat source seepage model

S and φ were first respectively set randomly as 0.1 and 45° ; the temperature responses of three points with time could then be obtained. Based on the results obtained using Equation (7.2), the random errors are added to the theoretical values. The theoretical and simulated experimental temperature responses of the three points are shown in Figure 7.24.

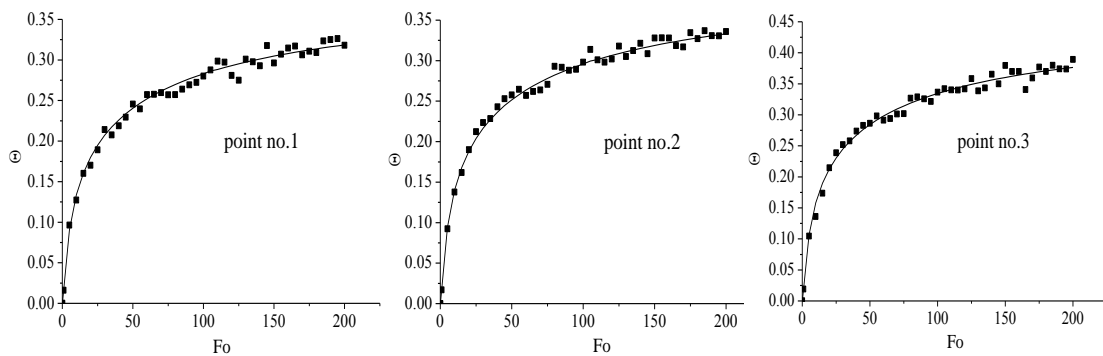


Figure 7.24 The theoretical temperature responses versus simulated experimental data

$$(S = 0.1, \varphi = 45^\circ)$$

The different discrete times were put into Equation (7.2) and therefore the theoretical results could be achieved by use of this analytical solution. Given that software produced random errors were then imposed on the theoretical temperature responses of the three points, the discrete scattergrams of three points denoting the simulated experimental data could be obtained as shown in Figure 7. 24. There are no actual experimental data as stated above, but these simulated discrete data are similar in form and values to the real experimental data with time, which means this is a valid approach to the testing of the reverse reasoning algorithm. As long as the simulated experimental time is long enough for the real data to be representative, the accuracy of back

calculation method is satisfied. According to this reverse reasoning analysis, Equation (7.7) achieves the minimum when $S = 0.1$ and $\varphi = 42^\circ, 43^\circ, 44^\circ, 45^\circ$ and 46° . The exact orientation cannot be determined but an accurate value of velocity is acquired. Nevertheless, the orientation range is determined by the procedure within a narrow range of possibilities, which means the error is only small. The median should be selected to diminish the estimation error when a unique orientation angle cannot be confirmed; thus the value of 44° is defined as the actual orientation.

A further example, based on 0.5 and 60° respectively set or S and φ , produced the results shown in Figure 7.25.

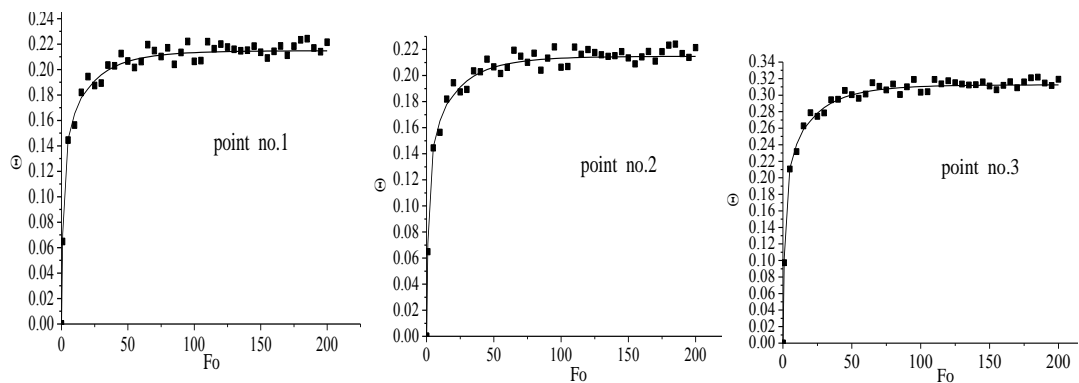


Figure 7.25 The temperature responses of theoretical results and simulated experimental data

$$(S = 0.5, \varphi = 60^\circ)$$

Figure 7.25 reveals larger derivations induced by random error and this simulation is closer to the actual experiment. This example indicates that the accurate unique value can be achieved after making full use of back calculation procedures, which means the results are $S=0.5$ and $\varphi =60^\circ$. These trials can prove the validity and the practicality of the back calculation method, providing a sufficient theoretical basis for predicting groundwater velocity given measured temperatures over a sufficiently long time period

at three well chosen points in the ground at the same radial distance from the pile centre. Thus, back calculation can be used in support of the design of engineering projects of pile foundation GHEs.

7.6.2 Trials based on the finite line heat source seepage model

Similar trials to those above based on the infinite model were also conducted. Specifically, errors were set randomly and then added to the model results to generate simulated experimental data.

Firstly, both the model results and the simulated experimental data of three points are all illustrated in Figure 7.26. S and φ were set respectively as 0.2 and 60° in this example.

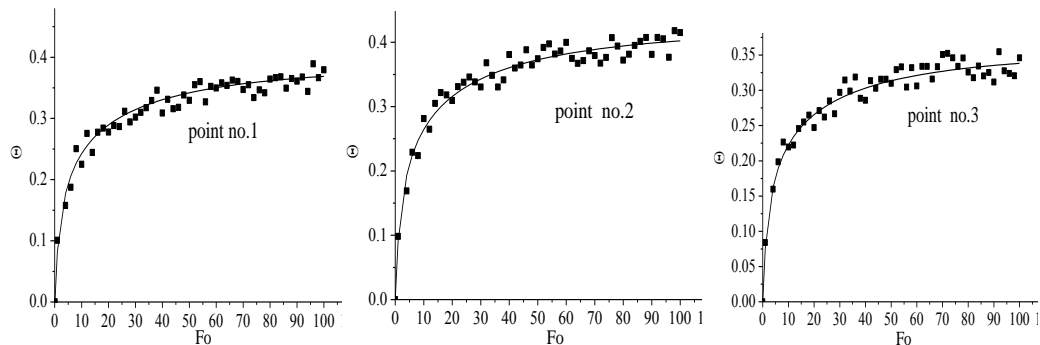


Figure 7.26 The temperature responses of theoretical results and simulated experimental data

$$(S = 0.2, \varphi = 60^\circ)$$

Having used the back calculation procedure as above, the accurate velocity value S and orientation φ can be determined.

$S = 1.0$ and $\varphi = 30^\circ$ were then set and the final effect again shows that the back calculation method is convincing for obtaining groundwater velocity. The corresponding figures are shown in Figure 7.27.

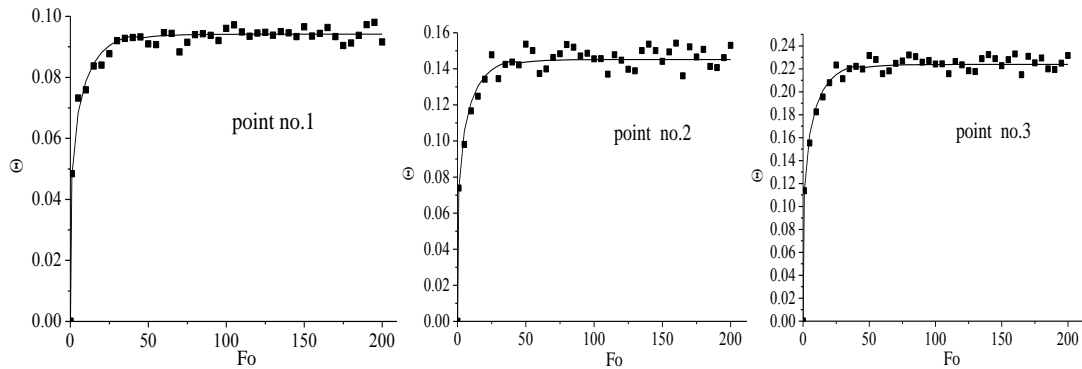


Figure 7.27 The temperature responses of theoretical results and simulated experimental data

$$(S = 1.0, \varphi = 30^\circ)$$

It is explicit that the random errors are larger than those of the first example. In such a way, a reverse reasoning algorithm was further validated and several results finally obtained. There are five suitable matches for S and φ , namely, $(S=1.0, \varphi=30^\circ)$, $(S=1.01, \varphi=29^\circ)$, $(S=1.01, \varphi=30^\circ)$, $(S=1.01, \varphi=31^\circ)$ and $(S=1.02, \varphi=29^\circ)$. Single values of S and φ cannot be confirmed, but the differences in the five matches are minor, therefore the accurate velocity can be basically determined. The median values of S and of φ are respectively 1.01 and 30° . It follows that the outcomes of the back calculation are nearly equal to the actual values.

7.7 Summary

This chapter gives a detailed reverse reasoning algorithm methodology for obtaining the groundwater velocity. It is suggested that three or more points at which temperature responses are measured, are evenly-distributed around a borehole GHE. According to the line heat source seepage model, which describes the temperature response to a borehole GHE under conditions of groundwater seepage, objective functions of every point can be established and then combined with the extremum method of a multivariate

function. The partial derivatives are used in seeking the accurate velocity, and the corresponding characteristics of groundwater water seepage are investigated based on the temperature responses of three points. The differences in temperature responses of three points due to the influences of velocity and direction are explored in detail.

Ranges in the directions and the values of groundwater velocity can be initially confirmed on a preliminary base, which is helpful to further discussion; and to some extent the validity of the reverse-reasoning process can be checked. More suitably distributed points around the borehole can produce better calculation results, but many such points would not only increase the effort in their physical establishments in actual engineering projects, but also leads to a more complex calculation procedure. Trials were employed to verify the back calculation method, and successive attempts using different examples were made. No matter for the infinite or for the finite model, the reverse reasoning algorithm was proved feasible when S and φ values were set.

Three points proved enough to ensure the validity of the back calculation method if they are evenly-distributed around the borehole GHE. Appropriate random errors, to simulate the randomness expected of real experiment data, were imposed on the theoretically calculated results. It is noted that no actual experiment was made and that such work must follow. The content of this chapter provides a theoretical basis for future experiment. It is worth obtaining the values of S and φ of the groundwater velocity, so that the way in which groundwater seepage influences the heat transfer performance of GHE can be understood.

CHAPTER 8 CONCLUSIONS AND RECOMMENDATIONS FOR FUTURE WORK

The study has investigated the heat transfer of pile foundation GHE with groundwater advection. This process is more complex than that of pure conduction because thermal exchange consists of conduction and convection. Based on the existing research related to both combined heat transfer of borehole GHEs and pure conduction of energy piles, this work focused on the development of novel simulation models for pile foundation GHE with groundwater advection, and the proposed models ranged from simple to complicated. The pure conduction experiments of pile foundation GHEs were conducted to check the heat transfer ability and then to be used to verify the corresponding models. The groundwater seepage experiments have not been actualized, but the analytical solutions of the combined heat transfer models were derived from those of pure conduction. Therefore, it is certain that seepage models can be verified indirectly in case pure conduction models are validated by actual experiments. Making use of the experimental data to prove the reasonability of simulation model is a significant progress in the study of energy pile technology.

In addition, groundwater velocity containing orientation and value is determined by local hydraulic gradient. Because velocity gives expression to the essence and strength of groundwater seepage, how to obtain the velocity is the vital precondition of investigating groundwater advection's influence. In view of the complexity of underground structure, it is hard to achieve the velocity by means of direct test. An

important methodology entitled “back calculation” was proposed and then taken advantage of to obtain the groundwater velocity, and this is favorable to explore the impact of groundwater flow. The detailed conclusions are as the following descriptions.

8.1 The existing research work

Borehole GHE has also been the main research area because it is most widely used in conventional GCHP system, the corresponding mathematical models and experiments have been conducted, such as the line heat source models and numerical simulations, and heat transfer experiments with and without groundwater advection. These contents were summarized in chapter 2, this thesis focuses on the analytical solutions of models and therefore the corresponding characteristics involved in the line heat sources' analytical solutions were laid emphasis.

Due to the high initial cost caused by borehole GHEs, the exploration on new kind of GHE to reduce expense is an inexorable trend. The application of energy pile technology drives scholars or experts to propose theoretical knowledge or to implement experiments. It is reported that the pure conduction research for pile foundation GHEs have made obvious progress, and this can advocate the application of pile foundation GHEs. Since the diameter of pile is large meanwhile the depth is not as long as that of borehole, line heat source or hollow cylindrical heat source are not suitable for it. Therefore, solid cylindrical heat source model and other models with corresponding analytical solutions were suggested. Much research has been conducted to investigate groundwater impact on borehole GHEs, however, heat transfer models for pile foundation GHE with groundwater flow have not been investigated. In this regard, and based on the new form of Green function and the energy pile's pure conduction models, the corresponding

seepage models were explored.

8.2 The simulation models of pile foundation GHE with groundwater advection

To show the geometry of pile foundation and the influence of groundwater seepage, simulation models embodying heat dissipation with groundwater advection were introduced one by one, and the ensuing combined heat transfer exhibited a greater degree of accuracy. Each type of simulation model includes both infinite and finite models, the significant difference between them concerns whether or not the ground boundary is taken into account.

Solid cylindrical heat source seepage models were firstly proposed, and further simplifications were adopted to conveniently depict the circumstance of energy pile with groundwater flow. The whole surface was regarded as a cylindrical heat source with a uniform heating rate, however, the pitch of spiral coils was not considered. The interior heat capacity of the pile was not ignored and the internal space of the pile is backfilled with the material identical to that of outside the pile. The solid cylindrical heat source emits heat as the groundwater flows through it. The models and the corresponding conditions were thus established and thereafter analytical solutions of infinite and finite models were obtained. The corresponding demonstrations were given in chapter 3, showing that this model is obviously progressive compared with line and hollow heat source seepage models.

The ring-coil heat source seepage models were then studied to express the configuration of spiral coils. In this model, the spiral heat exchange tube inside the pile

is not a continuous cylindrical source but a series of separated coils, arranged along the depth direction of the pile, which means the pitch impact was paid attention. This model is not the most accurate type but its proposal is a landmark. Simulation models and the expressions of temperature responses as well as the corresponding characteristics were all investigated, as shown in chapter 4.

Lastly, as regards the spiral heat source models with groundwater advection, the corresponding research was conducted in chapter 5. All coils are considered as a spiral line rather than separated coils. Therefore, spiral coils inside the pile under the impact of groundwater were illustrated by spiral line with groundwater flow. Chapter 5 describes the detailed information related to the establishment of the models together with analytical solutions were given. The characteristics different from those of other models were discussed. It is concluded that this model is the most accurate type for simulating the heat transfer of pile foundation GHE with groundwater advection.

The spiral heat source seepage model is the optimal choice from the perspective of academic research, but the corresponding calculation and analysis is very complicated. Even though the research process is relatively effortless in the study of the other models, the calculation precision is lower than that required for the spiral seepage model. It can be concluded that the choice of model should be in line with the practical situation being considered. As a rule, the most accurate model is always employed in academic research and theoretical analysis, whereas the simple models can be put to use for engineering projects to reduce the calculation difficulty, because the requirements for engineering projects are not so high or strict as those involved are not interested in further developing the models, but in using them for practical purpose.

8.3 The heat transfer experiments of pile foundation GHEs

It is of great value to employ energy piles for conducting heat transfer experiments because the heat exchange ability can be observed. In addition, pure conduction models can be verified by means of comparisons with experimental data and model results. Energy piles were part of the existing engineering project, heat transfer quantity, temperature response of certain locations and other parameters were timely recorded. The on-site operations of heat transfer experiments, aided by the assistance of on-site construction personnel, were described in chapter 6. The effects of the experiments were shown to be satisfactory. To some extent, the experiments can be regarded as simulations of the actual working state of pile foundation GHEs. The most accurate model was found to be the spiral heat source, and the corresponding seepage model's analytical solutions were deduced based on those of the pure conduction models. Thereby, the spiral heat source seepage model can be indirectly proven if the corresponding pure conduction model is verified by experiments.

8.4 The back calculation method for obtaining groundwater velocity

By way of setting points around borehole GHE and establishing corresponding objective functions, the groundwater velocity including orientation and value can be obtained by reverse reasoning algorithm; the whole procedures of achieving this aim were summarized in chapter 7; the characteristics involved in the back calculation were studied. Infinite and finite heat source seepage models were respectively employed to check their corresponding methodologies, the actual velocity can be realized according to the reverse deduction. Some examples were attempted to verify the rationality of this

methodology, and it is certain that the methodology is a novel investigation which provides the necessary basis for the study of the influence exerted by groundwater advection on pile foundation GHE.

8.5 Recommendations for future work

The seepage models of pile foundation GHEs are novel and favorable for the exploration of the combined heat transfer including conduction and groundwater advection. Because groundwater movement can alleviate heat accumulation around GHEs and further promote heat transfer, the significance of studying the impact of groundwater advection is evident. It should be noted that although the results of the presented research outlined in this thesis is affirmative, some defects and deficiencies still exist and the future work is recommended.

This study focuses on a single pile foundation GHE and a pile group with matrix arrangement, but, quite obviously, there are different arrangements for piles of buildings. For this reason, it is necessary to investigate the influence that groundwater exerts on a pile group with different arrangements. Then, the influence of groundwater on energy piles should be discussed when the seepage direction varies rather than only assuming it to be along the positive direction of x -axis.

The thermal properties of underground mediums inside and outside the pile are assumed identical in the process of studying the combined heat transfer of energy piles. The next stage in the work is to conduct a novel investigation on the influence of groundwater advection given that the thermal property of inside the pile differs from that of outside the pile.

Additionally, in this study, the pure conduction experiments were conducted to check the heat transfer ability and to verify the simulation model of pile foundation GHE. Although the seepage model can be indirectly validated, this is not the ultimate research goal. Therefore, the experiment rig will be established to enable the heat transfer experiments of pile foundation GHE passed which by groundwater.

In further summary, the research about groundwater flow has attracted more and more attentions due to the favorable effect of advection. The valid combination of energy piles and groundwater seepage is a novel research area, and this can promote further investigation about GHEs to a new research peak and advocate the further development of GSHP technology.

REFERENCES

- Ali S., Zaidi A.H., 1980. Pressure Drop and Stability of Flow in Negative Logarithmic Spiral Tube Coils. *Industrial & Engineering Chemistry Process Design and Development*, 19(1): 75-80
- Brent R.P., 1977. Computation of the regular continued fraction for Euler's constant. *Mathematics of Computation*, 31(139): 771-777.
- Bear J, 1983. Dynamics of fluids in porous media. Li Jingsheng, Chen Chongxi, translation. Beijing: China Architecture & Building Press.
- Bose J.E., Parker J. D., McQuison F. C., 1985. Design / data manual for closed-loop ground-coupled heat pump systems, Atlanta: ASHRAE.
- Carslaw H.S., Jaeger J.C., 1959. Heat conduction in solids. 2th ed. Clarendon Press, Oxford.
- Chang Y.P., Kang C. S., Chen D. J., 1973. The use of fundamental Green's functions for the solution of problems of heat conduction in anisotropic media. *International Journal of Heat and Mass Transfer*, 16(10): 1905-1918.
- Chiasson A.D., 1999. Advances in modeling of ground-source heat pump systems, Master Thesis, Oklahoma State University.
- Chiasson A.D., Rees S. J., Spitler J. D., 2000. A preliminary assessment of the effects of groundwater flow on closed-loop ground-source heat pump systems, *ASHRAE Transactions*, 106(1): 380-393.

- Choi J.C., Park J., Lee S. R., 2013. Numerical evaluation of the effects of groundwater flow on borehole heat exchanger arrays, *Renewable Energy*, 52:230-240.
- Cui P., Yang H.X., Fang Z.H., 2006. Heat transfer analysis of ground heat exchangers with inclined boreholes, *Applied Thermal Engineering*, 26: 1169-1175.
- Cui P., Li X., Man Y., Fang Z.H., 2011. Heat transfer analysis of pile geothermal heat exchangers with spiral coils, *Applied Energy*, 88: 4113-4119.
- Deerman J.D., Kavanaugh S.P., 1991. Simulation of vertical U-tube ground-coupled heat pump systems using the cylindrical heat source solution. *Ashrae Transactions*, 01: 287-294.
- Diao N.R., Li Q.Y., Fang Z.H., 2004. Heat transfer in ground heat exchangers with groundwater advection. *International Journal of Thermal Sciences*. 43: 1203-1211.
- Diao N.R., Fang Z.H., 2006. *Ground-coupled heat pump technology*, 1st ed, Beijing: Higher Education Press.
- Dupray F., Laloui L., Kazangba A., 2014. Numerical analysis of seasonal heat storage in an energy pile foundation, *Computers and Geotechnics*, 55: 67-77.
- Eckert E.R.G., 1976. The ground used as energy source, energy sink, or for energy storage, *Energy*, 1(3): 315-323.
- Eskilson P., 1987. *Thermal analysis of heat extraction boreholes*, Doctoral Thesis, University of Lund, Department of mathematical Physics, Lund, Sweden.
- Fan R., Ma Z.L., Yao Y., Li B., 2007a. Experimental research on influence of groundwater advection on performance of GHE, *Acta Energetica Sinica*, 28(8):

874-880.

Fan R., Jiang Y.Q., Yao Y., Deng S.M., Ma Z.L., 2007b. A study on the performance of a geothermal heat exchanger under coupled heat conduction and groundwater advection, *Energy* 32: 2199-2209.

Feng C.C., Wang F.H., Zhang X., Jiang Y.G., Wang X.K., 2011. Experiment on the Factors that Ground Water Flow Influence the Performance of the Heat Exchanger, *Refrigeration and Air Conditioning*, 25(4): 05.

Fujii H., Itoi R., Fujii J., Uchida Y., 2005. Optimizing the design of large-scale ground-coupled heat pump systems using groundwater and heat transport modeling, *Geothermics*, 34: 347-364.

Gao J., Zhang X., Liu J., Li K.S., Yang J., 2008. Thermal performance and ground temperature of vertical pile-foundation heat exchangers: a case study, *Applied Thermal Engineering*, 28: 2295-2304.

Gashti E.H.N., Malaska M., Kujala K., 2014. Evaluation of thermo-mechanical behavior of composite energy piles during heating/cooling operations. *Engineering Structures* 75: 363-373.

GB 50155-2003 Terminology of heating ventilation and air conditioning, 2003. Beijing: China Architecture & Building Press.

Gehlin S.E.A., Hellstrom G., 2003. Influence on thermal response test by groundwater flow in vertical fractures in hard rock, *Renewable Energy*, 28: 2221-2238.

Go G.H., Lee S.R., Yoon S., Kang H.b., 2014. Design of spiral coil PHC energy pile considering effective borehole thermal resistance and groundwater advection effects,

- Applied Energy,125: 165-178.
- Hamada Y., Saitoh H., Nakamura M., Kubota H., Ochifuji K., 2007. Field performance of an energy pile system for space heating, *Energy and Buildings*, 39: 517-524.
- Hassani Nezhad Gashti E., Uotinen V.M., Kujala K., 2014. Numerical modelling of thermal regimes in steel energy pile foundations: A case study, *Energy and Buildings*, 69: 165-174.
- Healy P.F., Ugursal V.I., 1997. Performance and economic feasibility of ground source heat pumps in cold climate, *International Journal of Energy Research*, 21(10): 857-870.
- Hellstrom G., 1991. Ground heat storage, Thermal analysis of duct storage systems. Doctoral Thesis, Department of Mathematical Physics, University of Lund, Sweden.
- HMIL, 2009. Jin Hu, Jiang Su, Thermal resistance indexing table of PT1000, Huasheng Measuring Instrument Ltd.
<<http://www.hsybs.net/6696505-Article-11901/>>
- Huang J.H., Shi X.Y., Tang Z.W., 2004. Pseudo 3D model of ground heat exchangers for GSHP, *Journal of China Agricultural University*, 9(5): 51-54.
- IGSHP SHJU, 2012. Test report of thermal response on rock soil, Institute of Ground Source Heat Pump, Shandong Jianzhu University.
- Ingersoll, L.R., Zobel, O.J., Ingersoll, A.C., 1954. *Heat Conduction with Engineering, Geological and Other Applications*. McGraw-Hill, New York, p. 325.
- Jalaluddin, Miyara A., Tsubaki K. Inoue S., Yoshida K., 2011. Experimental study of

- several types of ground heat exchanger using a steel pile foundation, *Renewable Energy*, 36: 764-771.
- Jalaluddin, Miyara A., 2012. Thermal performance investigation of several types of vertical ground heat exchangers with different operation mode, *Applied Thermal Engineering*, 33-34: 167-174.
- Kavanaugh S.P., Rafferty K., 1997. Ground-source heat pumps: Design of geothermal systems for commercial and institutional buildings, ASHRAE (American Society of Heating, Refrigerating and Air-Conditioning Engineers, Inc.), Atlanta, Georgia.
- KAYANE I., TANIGUCHI M., SANJO K., 1985. Alteration of the groundwater thermal regime caused by advection. *Hydrological sciences journal*, 30(3): 343-360.
- Kelvin, Sir W.T., 1882. cited by Ingersoll, et al., 1954. *Mathematical and Physical Papers*, II, p.41, ff., K.Morino, T.Oka, Study on heat exchanged in soil by circulating water in a steel pile,
- Konecny F., Fürst J., 2010. The generation of 2-D random velocity fields of groundwater flows via stream functions, *Computers & Geosciences*, 36(5) :598- 604.
- Lalouin L., Nuth M., Vulliet L., 2006. Experimental and numerical investigations of the behavior of a heat exchanger pile, *International Journal for Numerical and Analytical Methods in Geomechanics*, 30: 763-781.
- Langley B.C., 1989. Heat pump technology: system design, installation, and troubleshooting, Englewood Cliffs, NJ: Prentice Hall.
- Lee C.K., Lam H.N., 2012. A modified multi-ground -layer model for borehole ground heat exchangers with an inhomogeneous ground water flow, *Energy*, 47: 378-387.

- Lee C.K., Lam H.N., 2013. A simplified model of energy pile for ground-source heat pump systems, *Energy*, 55: 838-845.
- Lee J.U., Kim T., Leigh S.B., 2015. Applications of building-integrated coil-type ground-coupled heat exchangers – Comparison of performances of vertical and horizontal installations, *Energy and Buildings*, 2015, 93: 99-109.
- Li H., Nagano K., Lai Y.X., 2012. A new model and solutions for a spiral heat exchanger and its experimental validation, *International Journal of Heat and Mass Transfer*, 55: 4404-4414.
- Li M., Lai A.C.K, 2012. New temperature response functions (G functions) for pile and borehole ground heat exchangers based on composite-medium line-source theory, *Energy*, 38: 255-263.
- Li X., Fang L., Zhao Q., Fang Z. H., 2011. Coil heat source model for embedded spiral tube based geothermal heat exchangers and its analytical solutions, *Journal of Engineering for Thermal Energy and Power*, 26(4): 475-479.
- Li X., 2011. The heat transfer and study and engineering application of energy piles, Master Thesis, Shandong Jianzhu University.
- Liu H., Jin H., Xing S.Y., Duan Y., Hao X.Y., 2012. Influence of groundwater seepage on GHE temperature field, *Water Resources and Power*, 30 (12): 117-119.
- Liu J., Zhang X., Gao J., Li K.S., 2009. Heat transfer performance test and numerical simulation of pile-pipe ground source heat pump system, *Acta Energetica Sinica*, 30(6): 727-731.
- Lund J.W., 2006. Present utilization and future prospects of geothermal energy

- worldwide. Proceeding of the Renewable Energy 2006 Conference, Makuhari Messe, Chiba, Japan, 47-52.
- Man Y., Yang H.X., Diao N.R., Liu J.H., Fang Z.H., 2010. A new model and analytical solutions for borehole and pile ground heat exchangers, *International Journal of Heat and Mass Transfer*, 53: 2593-2601.
- Man Y., Yang H.X., Diao N.R., Cui P., Lu L., Fang Z.H., 2011. Development of spiral heat source model for novel pile ground heat exchangers, *HVAC & Research*, 17(6):1075-1088.
- Man Y., Yang H.X., Fang Z.H., Qu Y.X., 2013. Analytical Thermal Analysis of Novel Foundation Pile Ground Heat Exchanger with Spiral Coils. *Proceedings of the 8th International Symposium on Heating, Ventilation and Air conditioning*, Xi'an, China, Oct , 653-663.
- Mei V.C., 1986. Horizontal ground coil heat exchanger theoretical and experimental analysis, Oak Ridge National Laboratory / CON193.
- Michopoulos A., Bozis D., Kikidis P., Papakostas K., Kyriakis N.A., 2007. Three-years operation experience of a ground source heat pump system in Northern Greece. *Energy and Buildings*, 39(3): 328-334.
- Mikhailov G.A., 1978. Numerical construction of a random field with given spectral density, *Doklady Akademia Nauk SSR* 238(3): 793-795.
- Miller W.A., 1987. Laboratory examination and seasonal analysis of frosting and defrosting for an air-to-air heat pump. *ASHRAE Trans*, 93(1): 1474-1489.
- Mishra P., Gupta S.N., 1979. Momentum transfer in curved pipes.1.Newtonian fluids,

- Industrial & Engineering Chemistry Process Design and Development, 18(1): 130-137.
- Modaressi H., Laloui L., Aubry D., 1991. Numerical modelling of thermal consolidation. 2nd European Speciality Conference on Numerical Methods in Geotechnical Engineering, Santander, 1: 280–292.
- Molina-Giraldo N., Blum P., Zhu K., Bayer P., Fang Z.H., 2011. A moving finite line source model to simulate borehole heat exchangers with groundwater advection, International Journal of Thermal Science, 50: 2506-2513.
- Morino K., 1994. Study on heat exchanged in soil by circulating water in a steel pile, Energy and Buildings, 21: 65-78.
- Neuman S.P., Witherspoon P.A., 1970. Finite element method of analyzing steady seepage with a free surface. Water Resources Research, 6(3): 889-897.
- NHBC (National House Building Council), 2010. Efficient Design of Piled Foundations for Low Rise Housing, Design Guide, NHBC Foundation, Milton Keynes, UK.
- Ni C.F., Li, S. G., P.E., ASCE F., 2009. Approximate analytical solution to groundwater velocity variance in unconfined trending aquifers in the presence of complex sources and sinks, Journal of Hydrologic Engineering, 14(10): 1119-1125.
- Park S., Lee D., Choi H.J., Jung K., Choi H., 2015. Relative constructability and thermal performance of cast-in-place concrete energy pile: Coil-type GHEX (ground heat exchanger), Energy, 2015, 81: 56-66.
- Patterson B.M., Annable M.D., Bekele E.B., Furness A.J., 2010. On-line groundwater velocity probe: laboratory testing and field evaluation, Journal of contaminant

- hydrology, 117(1): 109-118.
- Ramamoorthy M., Jin H., Chiasson A.D., Spitler J.D., 2001. Optimal sizing of hybrid ground-source heat pump systems that use a cooling pond as a supplemental heat rejecter--a system simulation approach / Discussion, ASHRAE transactions, 107:26.
- Sanner B., 2001. Shallow Geothermal Energy, Geo-Heat Center Bulletin, 22(3): 19-25.
- Shi L., Zhang F.F., Lin Y., Li X., Fang Z.H., 2010. The 2-D thermal analysis of the coil ground heat exchanger inside piles, Journal of Shandong Jianzhu University, 25(2): 177-183.
- Su D.C., Diao N.R., Fang Z.H., 2004. An analytical solution of the temperature response in ground heat exchangers with groundwater advection, The 6th International Symposium of Heat Transfer, Beijing, 112.
- Tang D.Y., 2000. Analysis and Treatment for an Accident of Driven Cast-in-place Pile Foundation, Building Structure, 05.
- TUDM, 2007. Advanced Mathematics, 6th ed, Beijing, Higher Education Press, Tongji University, Department of Mathematics.
- Wang D.C., 1986. General Hydrogeology, 2nd ed, Beijing: Geological Publishing House.
- Wei H.P., 1987. Application of optimal technology, Shanghai Tongji University Press.
- Wang H.J., Qi C.Y., Du H.P., Gu J.H., 2009. Thermal performance of borehole heat exchanger under groundwater flow: A case study from Baoding, Energy and Buildings, 41: 1368-1373.
- WIKIPEDIA, 2014. High-density polyethylene.

< http://en.wikipedia.org/wiki/High-density_polyethylene >

Xu L.Z., 1999. Modern Mathematics Handbook, 1st ed, Wuhan: Huazhong University of Science & Technology Press.

Ye Q.X., Shen Y.H., 2006. Handbook of Applied Mathematics, 2nd ed, Beijing, Science Press.

You S., Cheng X.H., Guo H.X., Yao Z.Q., 2014. In-situ experimental study of heat exchange capacity of CFG pile geothermal exchangers, Energy and Buildings, 79: 23-31.

Yu M.Z., Fang Z.H., 2002. A method for in situ determining the thermal properties of deep ground, Journal of Engineering Thermodynamics, 23(3): 354-356.

Yu M.Z., Peng X.F., Fang Z. H., Li X. D., 2007. Method for determining deep thermal properties accounting for water advection, Journal of Basic Science and Engineering, 15(2): 196-201.

Yuill G.K., Mikler V., 1995. Analysis of the effect of induced groundwater flow on heat transfer from a vertical open-hole concentric-tube thermal well. American Society of Heating, Refrigerating and Air-Conditioning Engineers, Inc., Atlanta, GA (United States).

Zanchini E., Lazzari S., Priarone A., 2012. Long-term performance of large borehole heat exchanger fields with unbalanced seasonal loads and groundwater flow, Energy, 38: 66-77.

Zeng H.Y., Diao N.R., Fang Z.H., 2002. A finite line-source model for boreholes in

- geothermal heat exchanges, *Heat Transfer-Asian Research*, 31(7):558-567.
- Zeng H.Y., Diao N.R., Fang Z.H., 2003. A model of finite-length linear heat source for the vertical embedded pipe of a ground-source heat pump, *Journal of Engineering for Thermal Energy & Power*, 18(2): 166-169.
- Zhang M.Y., 2010. Technical discussion and analysis on rock-soil thermal parameter tester, *China Ground Source Heat Pump Net*.
< <http://www.ccgshp.com/news/view.php?id=4172>>
- Zhang S.F., Li Q., Gao P.L., 2007. Natural difference for groundwater seepage, *Chinese Journal of Computational Physics*, 24(3): 307-312.
- Zhang W.K., Yang H.X., Lu L., Fang Z.H., 2013a. The analysis on solid cylindrical heat source model of foundation pile ground heat exchangers with groundwater flow, *Energy* 55: 417- 425.
- Zhang W.K., Yang H.X., Fang Z.H., Diao N.R., 2013b. Analytical Solutions of Combined Heat Transfer on Spiral Tubes in Energy Piles, *The 12th International Conference on Sustainable Energy Technologies*, Hong Kong, China.
- Zhang W.K., Yang H.X., Lu L., Cui P., Fang Z.H., 2014. The research on ring-coil heat transfer models of pile foundation ground heat exchangers in the case of groundwater seepage. *Energy and Buildings*, 71:115-128.
- Zheng Z.Y., 1998. *Application of Heat Pump Technology in Air-conditioning*, Beijing: China Machine Press.
- Zhong Z., Tang Z.W., 2007. Energy pile geothermal heat pump system and its application, *Renewable Energy Resources*, 25(2): 94-96.